Copyright

by

Anthony Frederick Bentivegna

2012

**The Dissertation Committee for Anthony Frederick Bentivegna Certifies that this is the approved version of the following dissertation:**

# Multi-Scale Characterization, Implementation, and Monitoring of Calcium Aluminate Cement Based-Systems

**Committee:**

Kevin J. Folliard, Supervisor

Jason H. Ideker, Co-Supervisor

Maria C.G. Juenger

David W. Fowler

Harovel G. Wheat

# Multi-Scale Characterization, Implementation, and Monitoring of Calcium Aluminate Cement Based-Systems

**by**

**Anthony Frederick Bentivegna, B.S.C.E., M.S.E.**

**Dissertation**

Presented to the Faculty of the Graduate School of

The University of Texas at Austin

in Partial Fulfillment

of the Requirements

for the Degree of

**Doctor of Philosophy**

**The University of Texas at Austin**

**May 2012**

# Dedication

To the ladies of my life (Karla, Mom, and Michelle) for your support and encouragement through the years.

# Acknowledgements

First, I would like to thank Dr. Kevin Folliard for his guidance and support over the last five years. You have been a great mentor, colleague and friend. I can never repay you for everything you have given me. I look forward to continue working with you in the future.

I would like to thank Dr. Jason Ideker for his support and guidance over the last five years. You have been an amazing friend from day one at the lab. I appreciate everything you have done for me and truly consider you a great friend.

Thank you to Dr. David Fowler, Dr. Maria Juenger, and Dr. Harovel Wheat for agreeing to serve on my dissertation committee and providing your guidance over the alst three years.

Thank you to Michael Rung and Sherian Williams for all of your support throughout the project. Sherian, thank you for approving, organizing and managing our finances and accounting this project had a lot of subcontractors and challenging situations, I greatly appreciate all of your help. Mike, I appreciate all of your computer and technology input on the project.

I would like to thank Dr. Thano Drimalas for his continued support throughout the project. You were always there in the clutch times when I needed you. Sorry, for giving you such a hard time when you were writing your dissertation. If I only knew what was to come five years ago, I wouldn't have given you such a hard time. Thanks for being a great mentor and friend. I look forward to working together in the future and more importantly going fishing together.

Thanks to Federico “Fred” Aguayo and Jose Zuniga, you were the best undergraduate research assistants I could have ever asked for. You truly did amazing work and I wish you both all the success in the future. You are great friends and I look forward to working with you in the future.

Thank you to the graduate students who helped me over the last five years. I want to thank: Chris Clement, Philip Pesek, Evan Wehrle, Alex Garde, Travis Lowe, and Many Others. Chris, I can never repay you for your knowledge you have imparted on me in all aspects of life. I greatly appreciate all of the time and effort. Thano and Evan you guys were there when I needed you most. Thank all of you for being great friends, I hope that we continue to travel together and become better friends in the future.

Last but certainly not least, I would like to thank Karla, my mom, and sister. Karla, thank you for reading this entire dissertation and preventing me from looking like an absolute fool because of my horrible writing. I love you and look forward growing old together. Mom and Michelle, thank you for all of your love and support throughout my graduate degrees.

May 3, 2012

# Multi-Scale Characterization, Implementation, and Monitoring of Calcium Aluminate Cement Based-Systems

Anthony Frederick Bentivegna, Ph.D.

The University of Texas at Austin, 2012

Supervisor: Kevin J. Folliard and Jason H. Ideker

Calcium aluminate cement (CAC) is a rapid hardening cementitious material often used in niche concrete repairs where high early-age strength and robust durability are required. This research project characterized the implications of the additions of various mineral and chemical admixtures to plain CAC to mitigate strength reductions associated with conversion, an inevitable strength reduction associated with the densification of metastable hydrates ($CAH_{10}$ and $C_2AH_8$) to stable hydrates ($C_3AH_6$ and $AH_3$). The effect of these admixtures on early-age strength development, volume change, and the correlation to macro-scale performance were reported in this dissertation. Various mixtures of CAC were investigated including: pure CAC, binary blends of CAC with fly ash (Class C) or $CaCO_3$, and ternary blends of CAC with slag and silica fume. Characterization of the influence of these admixtures on hydration was completed using x-ray diffraction, isothermal calorimetry, and chemical shrinkage. Investigations on the implications of early-age volume change were conducted for autogenous deformation. In addition to laboratory testing, the final phase of the project was to correlate and elucidate the data generated in the laboratory to real-world field performance. Field trials were conducted to evaluate and monitor the behavior of CAC systems and investigate the link between laboratory generated research and actual large scale behavior.

# Table of Contents

List of Tables ..... xvi

List of Figures ..... xviii

Chapter 1: Introduction ..... 1

1.1 Background ..... 1

1.2 Scientific Network ..... 2

1.3 Objectives ..... 3

1.4 Content ..... 4

Chapter 2: Literature Review ..... 6

2.1 Calcium Aluminate Cement Introduction ..... 6

2.2 CAC History ..... 6

2.2 Raw Materials, Chemistry, Manufacturing, and Physical Characteristics of CAC ..... 7

2.3 CAC Hydration and Conversion ..... 11

2.3.1 Microstructural Development ..... 11

2.3.2 Heat of Hydration ..... 14

2.3.3 Chemical Shrinkage ..... 17

2.4 Properties of CAC Concrete ..... 19

2.4.1 Properties of Fresh CAC Concrete ..... 19

2.4.1.1 Setting Time ..... 20

2.4.1.2 Workability ..... 21

2.4.2 Properties of Hardened CAC Concrete ..... 22

2.4.2.1 Conversion and Strength Development ..... 22

2.4.2.2 Plastic Shrinkage ..... 24

2.4.2.3 Autogenous Deformation ..... 25

2.4.2.4 Drying Shrinkage ..... 26

2.4.3 Durability of CAC Concrete ..... 27

2.4.3.1 Sulfate Resistance ..... 28

2.4.3.2 Corrosion ..... 29

2.4.3.3 Chloride Diffusion ....29
2.3.3.4 Carbonation....30
2.4.3.3 Alkaline Hydrolysis ....31
2.4.3.5 Freeze-Thaw ....33
2.5 Influence of Admixtures on CAC ....33
2.5.1 Accelerators and Retarders ....33
2.5.1.1 Accelerators ....34
2.5.1.2 Retarders ....35
2.5.3 Water Reducers....35
2.5.4 Latex and Polymer Resins ....37
2.6 Blended Systems....38
2.6.1 Portland Cement....38
2.6.2 Slag ....41
2.6.3 Silica Fume ....41
2.6.4 Ternary Blended - Slag and Silica Fume ....42
2.6.5 Fly Ash....43
2.6.6 Fillers ....45
2.7 Applications, Assessment, and Specifications of CAC Concrete....46
2.7.1 Applications of CAC Concrete ....46
2.7.1.1 Rapid Hardening ....47
2.7.1.2 Abrasion and Impact Resistance....48
2.7.1.3 Pipes....48
2.7.1.4 Refractory Resistance ....49
2.7.2 Assessment of Existing CAC Concrete ....49
2.7.3 Current Specifications for Use of CAC ....53
2.8 Summary....55
Chapter 3: Experimental Materials and Procedures....56
3.1 Materials ....56
3.1.1 Cementitious Materials ....56
3.1.2 Chemical Admixture Characteristics ....57

3.2 Mixture Proportions and Procedures .....59
3.3 Procedures .....59
3.3.1 Isothermal Calorimetry .....59
3.3.2 Qualitative X-Ray Diffraction .....60
3.3.3 Chemical Shrinkage .....60
3.3.4 Autogenous Deformation .....64
3.4 Nomenclature .....69

Chapter 4: Characterization and Development of a Paste and Mortar Isothermal Calorimeter for Calcium Aluminate Cements .....71
4.1 Introduction .....71
4.2 Grace AdiaCal Isothermal Calorimeter .....74
4.3 Repeatability of PC Mortar and Paste .....78
4.4 Influence of Sample Size Variability of PC Paste and Mortar .....82
4.5 Initial Evaluation of CAC Paste and Mortar .....86
4.6 Development of CAC Isothermal Calorimeter .....90
4.6.1 Physical Modifications .....90
4.6.2 Improved Temperature Control System .....92
4.6.3 Altered PID Algorithm .....92
4.6.4 Calibration System .....93
4.6.5 Summary .....97
4.7 Sample Size Variability CAC Paste and Mortar .....98
4.8 Repeatability of CAC Paste and Mortar .....102
4.9 Calorimetry Analysis Techniques .....107
4.9.1 Heat Flow (mW/g) .....107
4.9.2 Cumulative Heat Release (J/g) .....109
4.10 Discussion .....110
4.11 Conclusions .....113

Chapter 5: Hydration and Early-age Volume Deformation of Plain CAC .....115
5.1 Hydration of CAC at 20°C .....116
5.1.1 Influence of LSA at 20°C .....116

5.1.2 Influence of HRWR at 20°C ..... 120
5.1.3 Influence of Combined LSA and HRWR at 20°C ..... 125
5.1.3.1 Isothermal Calorimetry at 20°C ..... 125
5.1.3.2 Qualitative XRD at 20°C ..... 127
5.1.3.3 Chemical Shrinkage at 20°C ..... 130
5.1.3.4 Autogenous Deformation at 20°C ..... 134
5.2 Hydration of CAC at 38°C ..... 135
5.2.1 Influence of LSA at 38°C ..... 135
5.2.2 Influence of HRWR at 38°C ..... 137
5.2.3 Influence of Combined LSA and HRWR at 38°C ..... 138
5.2.3.1 Isothermal Calorimetry ..... 139
5.2.3.2 Qualitative XRD at 38°C ..... 140
5.2.3.3 Chemical Shrinkage at 38° C ..... 147
5.2.3.4 Autogenous Deformation at 38° C ..... 151
5.3 Conclusions ..... 152

Chapter 6: Influence of Chemical Admixtures, SCMs, and Fillers on CAC Hydration and Early-age Volume Deformation ..... 154
6.1 Influence of Ternary Blended CAC with Slag and Silica Fume ..... 154
6.1.1 Hydration of TCAC at 20°C ..... 155
6.1.1.1 Influence of TCAC on Isothermal Calorimetry and Qualitative XRD at 20°C ..... 155
6.1.1.2 Influence of TCAC on Chemical Shrinkage at 20°C ..... 161
6.1.1.3 Influence of TCAC on Autogenous Deformation at 20°C 163
6.1.2 Hydration of TCAC at 38°C ..... 164
6.1.2.1 Influence of TCAC on Isothermal Calorimetry and Qualitative XRD at 38°C ..... 165
6.1.2.2 Influence of TCAC on Chemical Shrinkage at 38°C ..... 169
6.1.2.3 Influence of TCAC on Autogenous Deformation at 38°C 172
6.1.3 Summary ..... 173
6.2 Influence of Limestone ..... 174
6.2.1 Hydration of CAC-LF at 20°C ..... 174

6.2.1.1 Influence of CAC-LF on Isothermal Calorimetry at 20°C174
6.2.1.2 Influence of CAC-LF on Chemical Shrinkage at 20°C 176
6.2.1.3 Influence of CAC-LF on Autogenous Deformation at 20°C .....178
6.2.2 Hydration of CAC-LF at 38°C.....179
6.2.2.1 Influence of CAC-LF on Isothermal Calorimetry at 38°C179
6.2.2.2 Influence of CAC-LF on Chemical Shrinkage at 38°C 181
6.2.2.3 Influence of CAC-LF on Autogenous Deformation at 38°C .....183
6.2.3 Summary.....184
6.3 Influence of High-Calcium Fly Ash .....186
6.3.1 Hydration of CAC-FA at 20°C .....186
6.3.1.1 Influence of CAC-FA on Isothermal Calorimetry at 20°C186
6.3.1.2 Influence of CAC-FA on Chemical Shrinkage at 20°C188
6.3.1.3 Influence of CAC-FA on Autogenous Deformation at 20°C .....190
6.3.2 Hydration of CAC-FA at 38°C .....191
6.3.2.1 Influence of CAC-FA on Isothermal Calorimetry at 38°C191
6.3.2.2 Influence of CAC-FA on Chemical Shrinkage at 38°C193
6.3.2.3 Influence of CAC-FA on Autogenous Deformation at 20°C .....194
6.3.3 Summary.....196
6.4 Influence of Chemical Admixtures.....197
6.4.1 Influence of Citric Acid .....197
6.4.1.1 Influence of Citric Acid on Isothermal Calorimetry at 20°C .....197
6.4.1.2 Influence of Citric Acid on Isothermal Calorimetry at 38°C .....199
6.4.2 Influence of Latex.....201
6.4.2.1 Influence of Latex on Isothermal Calorimetry at 20°C 201
6.4.2.2 Influence of Latex on Chemical Shrinkage at 20°C .....203
6.4.2.3 Influence of Latex on Autogenous Deformation at 20°C205

6.4.2.4 Influence of Latex on Isothermal Calorimetry at 38°C 206
6.4.2.5 Influence of Latex on Chemical Shrinkage at 38°C .....208
6.4.2.6 Influence of Latex on Autogenous Deformation at 38°C210
6.4.3 Summary .....211
6.5 Results .....212
6.5.1 Hydration .....212
6.5.2 Early-age Volume Deformation .....216
Chapter 7: Large Scale Field Investigations of Rapid Repair Materials .....218
7.1 Introduction and Background .....219
7.1.1 Construction Techniques .....220
7.1.2 Materials .....221
7.1.3 Shrinkage .....222
7.1.4 Summary .....222
7.2 Existing CAC Field Repairs .....223
7.2.1 Full-depth CAC Repair .....223
7.2.2 Bonded Concrete Overlay .....225
7.2.3 Interstate 290: Full-depth Repair .....226
7.2.4 Bridge Thin-bonded Concrete Overlay .....227
7.2.5 Partial Depth Bridge Deck Repair .....228
7.2.6 Summary .....229
7.3 CSA Bonded Overlay Repair .....229
7.3.1 Project Background .....230
7.3.2 Bridge Deck Preparation and Concrete Removal .....231
7.3.3 Repair Placement and Curing .....234
7.3.4 Summary .....236
7.4 UT Austin Bonded CAC and CSA Repair .....237
7.4.1 Introduction .....237
7.4.2 Base Slab Construction .....240
7.4.3 Surface Preparation .....246
7.4.4 Overlay Formwork and Instrumentation .....248

7.4.5 CSA Overlay Placement ....253
7.4.6 CAC Toppling Slab Placement ....258
7.4.7 Slab Performance ....261
7.4.7.1 Hydration/Curing Temperatures ....261
7.4.7.2 Strength Development ....266
7.4.7.3 Volume Change ....271
7.4.7.4 Visual Observations and Crack Mapping ....272
7.4.7.5 Drying Shrinkage ....278
7.4.8 Discussion ....280
7.5 Summary ....283
7.6 Conclusions ....285

Chapter 8: Conclusions and Recommendations ....286
8.1 Conclusions ....286
8.1.1 Hydration and Micro-structural Development ....286
8.1.2 Early-age Volume Deformation and Large Scale Field Performance 288
8.2 Future Work ....289

Appendix A: Material Certificates ....290

Appendix B: Characterization of Grace AdiaCal Isothermal Calorimeter ....295
Appendix B.1: Repeatability of PC Mortar ....295
Appendix B.2: Repeatability of PC Paste ....296
Appendix B.3: Influence of Sample Size Variability on PC Mortar ....298
Appendix B.4: Influence of Sample Size Variability on PC Paste ....300
Appendix B.5: PR-59 Temperature Controller Specifications ....302
Appendix B.6: Thermoelectric Heater-Cooler Specifications ....303
Appendix B.7: Influence of Sample Size Variability on CAC Mortar ....305
Appendix B.8: Influence of Sample Size Variability on CAC Paste ....306
Appendix B.9: Repeatability of CAC Mortar ....308
Appendix B.10: Repeatability of CAC Paste ....310

Appendix C: Hydration and Early-age Volume Deformation of TCAC systems313

Appendix D: Hydration and Early-age Volume Deformation of CAC-LF systems324

Appendix E: Hydration and Early-age Volume Deformation of CAC-FA Systems329

Appendix F: Strain and Temperature Data Logging Equipment Specifications .332

References.....339

# List of Tables

Table 1: Chemical composition and origins of Production for range of calcium aluminate cements currently available (Campas, 1998) .....8

Table 2: Heats of hydration of CAC and OPC (kJ/kg) (Campas, 1998).....14

Table 3: Summary of chemical shrinkage testing results at varying temperatures (mL $H_2O$/g cement) (Ideker, 2008).....18

Table 4: Setting times of CAC and portland cement paste (Campas, 1998) .....20

Table 5: Effect of Various Chemical Admixtures on CAC Setting (Campas, 1998). .....34

Table 6: Strength development of CAC – fly ash mortars (Fernandez-Carrasco, 2008) .....44

Table 7: XRF oxide analysis.....57

Table 8: Cement and supplementary cementitious materials nomenclature and replacement ratios by mass of cement .....70

Table 9: Chemical admixture nomenclature and basic composition .....70

Table 10: PC Testing Matrix.....79

Table 11: Portland cement mortar repeatability at various temperatures .....80

Table 12: Portland cement paste repeatability at various temperatures.....81

Table 13: Mixture matrix for the repeatability of PC mortars with variable samples sizes.....83

Table 14: Portland cement mortar repeatability at various temperatures and various sample sizes .....84

Table 15: Mixture matrix for the repeatability of PC pastes with variable samples sizes.....85

Table 16: Portland cement paste repeatability at various temperatures and various sample sizes .....86
Table 17: CAC mortar mixture matrix variability in sample size .....99
Table 18: CAC mortar repeatability at various temperatures and various sample sizes .....100
Table 19: CAC paste mixture matrix variability in sample size.....100
Table 20: CAC paste repeatability at various temperatures and various sample sizes .....101
Table 21: CAC mixture matrix for CAC mortar repeatability.....103
Table 22: CAC mortar repeatability at various temperatures .....104
Table 23: CAC mixture matrix for CAC paste repeatability .....105
Table 24: CAC paste repeatability at various temperatures and various sample sizes .....106
Table 25: Typical bonded overlay concrete mixture proportions (Sprinkel, 2008)221
Table 26: CSA overlay mixture design.....253
Table 27: Final mixture design for CAC overlay .....259
Table 28: Quantified cracking results .....276

# List of Figures

Figure 1: Approximate composition range of CAC, adapted from (Scrivener, 2003) .....9

Figure 2: Schematic diagram of a reverberatory furnace (Campas, 1998) .....10

Figure 3: Schematic indicating the motivation for the hydration and conversion of the stable hydrates and rearrangement of the metastable hydrates (Scrivener, 2003) .....12

Figure 4: Heat flow curve of CAC hydrated at 20°C for different w/c: Top: without $Li_2SO_4$, Bottom: with lithium sulfate (Gosselin C. , 2009) .....15

Figure 5: Isothermal calorimetry of plain CAC at 38°C, with and without $Li_2SO_4$ (Gosselin C. , 2009) .....16

Figure 6: Chemical shrinkage development of CAC and portland cement at different temperatures (Fu, 2011) .....19

Figure 7: Modified Vicat setting time results for CAC systems (Fu, 2011).....21

Figure 8: Schematic strength development curves for calcium aluminate cement concrete at w/c~0.4 and cement content of 400 kg/$m^3$ (Campas, 1998) .....23

Figure 9: Autogenous deformation of two CAC binder systems (Fu, 2011).....26

Figure 10: Effect of demoulding time on drying shrinkage (Lamberet S. F., 2008).27

Figure 11: Compressive strength development of CAC-PC mixtures a) Mixture 100% CAC, b) Mixture 75% CAC – 25% PC, c) Mixture 50% CAC – 50%PC, and d) Mixture 25% CAC – 75% PC (Kirca, 2008) .....40

Figure 12: Heat flow of Fe-low CAC substituted by 30% fly ash, 30% slag, 5% silica fume (Gosselin C. , 2009). .....45

Figure 13: Illustration of the buoyancy method for measuring chemical shrinkage (Sant L. a., 2006).....61
Figure 14: Illustration of the dilatometry method for measuring chemical shrinkage (Kosmatka, 2008).....62
Figure 15: Experimental setup for chemical shrinkage at UT Austin .....63
Figure 16: Example chemical shrinkage at 1 hour and 14 days .....64
Figure 17: Autogenous deformation experimental setup.....66
Figure 18: Example samples for autogenous deformation testing.....67
Figure 19: Example deviation of chemical shrinkage and autogenous deformation69
Figure 20: Example PC paste and mortar isothermal calorimetry heat flow at 23°C and 38°C .....73
Figure 21: Example PC paste and mortar isothermal calorimetry heat flow at 23°C and 38°C .....74
Figure 22: A) External View of the Grace AdiaCal Isothermal Calorimeter B) Internal View of Sample Placement. .....75
Figure 23: Grace AdiaCal TC Sample Holder. .....76
Figure 24: Grace AdiaCal TC GUI. .....77
Figure 25: Heat flow of portland cement mortar at 23°C isothermal .....79
Figure 26: Heat flow of portland cement paste at 23°C isothermal.....81
Figure 27: Heat flow of various PC mortar sample size at 23°C isothermal.....83
Figure 28: Heat flow of various PC paste sample size at 23°C isothermal .....85
Figure 29: Measurement failure due to excessive heat generation of TCAC system at 38°C .....87
Figure 30: Measurement failure due to excessive heat release and ambient temperature variation at 60°C .....88

Figure 31: Excessive heat release and sluggish temperature control.....89
Figure 32: Stainless steel calorimeter chamber .....91
Figure 33: Machined aluminum lids.....91
Figure 34: Typical calibration curve for a TAM Air Calorimeter. .....94
Figure 35: Resistors .....95
Figure 36: Wiring schematic for series circuit for calibration diagram.....95
Figure 37: Calibration curves for CAC at 5°C, 23°C, and 60°C .....97
Figure 38: Repeatability of various CAC mortar sample sizes at 23°C .....99
Figure 39: Repeatability of various CAC paste sample sizes at 23°C.....101
Figure 40: Heat flow of CAC mortar at 23°C isothermal.....104
Figure 41: Heat flow of CAC paste at 23°C .....106
Figure 42: Example heat of hydration of CAC and OPC paste with varying LSA dosages at 23°C.....108
Figure 43: Example cumulative heat release of CAC paste with varying LSA dosages at 23°C .....109
Figure 44: Standard deviation of the time of peak heat of hydration for PC and CAC paste .....111
Figure 45: Standard deviation of the time of peak heat of hydration for PC and CAC mortar.....111
Figure 46: Standard deviation of peak heat of hydration for PC and CAC paste 112
Figure 47: Standard deviation of peak heat of hydration for PC and CAC mortar113
Figure 48: Heat flow of CAC hydrated at 20°C for varying LSA dosages .....116
Figure 49: Cumulative heat release of CAC hydrated at 20°C for varying LSA dosages.....117

Figure 50: Qualitative XRD of CAC with and without 1% LSA hydrated at 20°C, characterizing the formation of $CAH_{10}$ and $C_2AH_8$ and the depletion of CA .....119
Figure 51: Heat flow of CAC hydrated at 20°C for varying HRWR dosages .....121
Figure 52: Cumulative heat release of CAC hydrated at 20°C for varying HRWR dosages .....121
Figure 53: Cumulative heat release of CAC hydrated at 20°C with varying LSA and HRWR dosages added separately .....123
Figure 54: Qualitative XRD of CAC with and without 1% HRWR hydrated at 20°C, characterizing the minimal formation of $CAH_{10}$ and $C_2AH_8$ and the depletion of CA .....124
Figure 55: Heat flow of CAC hydrated at 20°C for varying LSA and HRWR dosages .....126
Figure 56: Cumulative heat release of CAC with varying dosages of LSA and HRWR at 20°C .....126
Figure 57: Qualitative XRD of CAC with 1.0% LSA and 1.0% HRWR hydrated at 20°C, illustrating the formation $C_2AH_8$ and the depletion of CA...128
Figure 58: In-situ temperature of CAC – 1.0% LSA + 1.0% HRWR in isothermal calorimeter at 20°C .....129
Figure 59: Chemical shrinkage of CAC with varying dosages of LSA and HRWR at 20°C .....131
Figure 60: Chemical shrinkage with standard deviation for CAC with varying dosages of LSA and HRWR at 20°C .....131
Figure 61: Comparison of chemical shrinkage with isothermal calorimetry cumulative heat release .....132

Figure 62: Chemical shrinkage as a function of cumulative heat of CAC with varying LSA dosages .....133
Figure 63: Autogenous deformation of CAC with varying dosages of LSA and HRWR at 20°C .....134
Figure 64: Heat flow of CAC hydrated at 38°C for varying LSA dosages .....135
Figure 65: Cumulative heat release of CAC hydrated at 38°C for varying LSA dosages .....136
Figure 66: Heat flow of CAC hydrated at 38°C for varying HRWR dosages .....137
Figure 67: Cumulative heat release of CAC hydrated at 38°C for varying HRWR dosages .....138
Figure 68: Heat flow of CAC hydrated at 38°C with varying dosages of LSA and HRWR.....139
Figure 69: Cumulative heat release of CAC hydrated at 38°C with varying dosages of LSA and HRWR .....140
Figure 70: (Part A) Qualitative XRD of CAC with LSA and HRWR hydrated at 38°C, illustrating the formation $C_2AH_8$ .....142
Figure 71: (Part B) Qualitative XRD of CAC with LSA and HRWR hydrated at 38°C, illustrating the reduction of CA .....144
Figure 72: (Part C) Qualitative XRD of CAC with LSA and HRWR hydrated at 38°C, illustrating conversion.....146
Figure 73: Chemical shrinkage of CAC with varying dosages of LSA and HRWR at 38°C .....148
Figure 74: Chemical shrinkage with standard deviations for CAC with varying dosages of LSA and HRWR at 38°C .....148

Figure 75: Comparison of chemical shrinkage with isothermal calorimetry cumulative heat release ..... 149
Figure 76: Chemical shrinkage as a function of cumulative heat of CAC with varying LSA dosages. ..... 150
Figure 77: Autogenous deformation of CAC with varying dosages of LSA and HRWR at 38°C ..... 151
Figure 78: Heat flow of TCAC hydrated at 20°C for varying LSA and HRWR dosages ..... 155
Figure 79: Cumulative heat release of TCAC hydrated at 20°C for varying LSA and HRWR dosages ..... 156
Figure 80: Cumulative heat release of TCAC hydrated at 20°C for varying LSA dosages ..... 157
Figure 81: Qualitative XRD of plain CAC and TCAC hydrated at 20°C, illustrating the minimal formation of $CAH_{10}$ and $C_2AH_8$ and the depletion of CA158
Figure 82: Qualitative XRD of plain CAC and TCAC with 1% LSA and 1% HRWR hydrated at 20°C, illustrating the minimal formation of $CAH_{10}$ and $C_2AH_8$ and the depletion of CA ..... 160
Figure 83: Chemical shrinkage of TCAC with varying dosages of LSA and HRWR at 20°C ..... 161
Figure 84: Chemical shrinkage as a function of cumulative heat of CAC with varying LSA dosages. ..... 162
Figure 85: Autogenous Shrinkage of TCAC with varying dosages of LSA and HRWR at 20°C ..... 164
Figure 86: Heat flow of TCAC hydrated at 38°C for varying LSA and HRWR dosages ..... 165

Figure 87: Cumulative heat release of TCAC hydrated at 38°C for varying LSA and HRWR dosages .....166
Figure 88: (Part A) Qualitative XRD of TCAC with LSA and HRWR hydrated at 38°C, illustrating the formation $C_2AH_8$ and $C_2AH_8$ .....167
Figure 89: (Part B) Qualitative XRD of TCAC with LSA and HRWR hydrated at 38°C, illustrating formation of some $C_3AH_6$ .....168
Figure 90: Chemical shrinkage of TCAC with varying dosages of LSA and HRWR at 38°C .....169
Figure 91: Early-age chemical shrinkage of TCAC with varying dosages of LSA and HRWR at 38°C .....170
Figure 92: Chemical shrinkage as a function of cumulative heat of CAC with varying LSA dosages. .....171
Figure 93: Autogenous deformation of TCAC with varying dosages of LSA and HRWR at 38°C .....172
Figure 94: Heat flow of CAC-LF hydrated at 20°C for varying LSA and HRWR dosages .....175
Figure 95: Cumulative heat release of CAC-LF hydrated at 20°C for varying LSA and HRWR dosages .....175
Figure 96: Chemical shrinkage of CAC-LF with varying dosages of LSA and HRWR at 20°C .....177
Figure 97: Chemical shrinkage as a function of cumulative heat of CAC-LF with varying LSA dosages. .....178
Figure 98: Autogenous deformation of CAC-LF with varying dosages of LSA and HRWR at 20°C .....179

Figure 99: Heat flow of CAC-LF hydrated at 38°C for varying LSA and HRWR dosages ..... 180
Figure 100: Cumulative heat release of CAC-LF hydrated at 38°C for varying LSA and HRWR dosages ..... 180
Figure 101: Chemical shrinkage of CAC-LF with varying dosages of LSA and HRWR at 20°C ..... 181
Figure 102: Chemical shrinkage as a function of cumulative heat of CAC-LF with varying LSA dosages at 38°C. ..... 182
Figure 103: Autogenous deformation of CAC-LF with varying dosages of LSA and HRWR at 20°C ..... 184
Figure 104: Heat flow of CAC-FA hydrated at 20°C for varying LSA and HRWR dosages ..... 186
Figure 105: Cumulative heat release of CAC-FA hydrated at 20°C for varying LSA and HRWR dosages ..... 187
Figure 106: Chemical shrinkage of CAC-FA with varying dosages of LSA and HRWR at 20°C ..... 188
Figure 107: Chemical shrinkage as a function of cumulative heat of CAC-FA with varying LSA dosages at 20°C. ..... 189
Figure 108: Autogenous deformation of CAC-FA with varying dosages of LSA and HRWR at 20°C ..... 190
Figure 109: Heat flow of CAC-FA hydrated at 38°C for varying LSA and HRWR dosages ..... 191
Figure 110: Cumulative heat release of CAC-FA hydrated at 38°C for varying LSA and HRWR dosages ..... 192

Figure 111: Chemical shrinkage of CAC-FA with varying dosages of LSA and HRWR at 38°C .....193
Figure 112: Chemical shrinkage as a function of cumulative heat of CAC-FA with varying LSA dosages at 38°C .....194
Figure 113: Autogenous deformation of CAC-FA with varying dosages of LSA and HRWR at 38°C .....195
Figure 114: Heat flow of CAC hydrated at 20°C for varying Citric Acid and LSA dosages .....198
Figure 115: Cumulative heat release of CAC hydrated at 20°C for varying Citric Acid and LSA dosages .....198
Figure 116: Heat flow of CAC hydrated at 38°C for varying Citric Acid and LSA dosages .....200
Figure 117: Cumulative heat release of CAC hydrated at 38°C for varying Citric Acid and LSA dosages .....200
Figure 118: Heat flow of CAC with latex hydrated at 20°C with varying LSA and citric acid .....202
Figure 119: Cumulative heat release of CAC with latex hydrated at 20°C with varying LSA and citric acid .....202
Figure 120: Chemical shrinkage of CAC with latex hydrated at 20°C with varying LSA and citric acid .....203
Figure 121: Chemical shrinkage with standard deviation of CAC with latex hydrated at 20°C with varying LSA and citric acid .....204
Figure 122: Chemical shrinkage as a function of CAC with latex hydrated at 20°C with varying LSA and citric acid .....205

Figure 123: Autogenous deformation of CAC with latex with varying dosages of LSA and citric acid at 20°C.....206
Figure 124: Heat flow of CAC with latex hydrated at 20°C with varying LSA and citric acid.....207
Figure 125: Cumulative heat release of CAC with latex hydrated at 20°C with varying LSA and citric acid .....207
Figure 126: Chemical shrinkage of CAC with latex hydrated at 20°C with varying LSA and citric acid .....208
Figure 127: Chemical shrinkage with standard deviation of CAC with latex hydrated at 38°C with varying LSA and citric acid.....209
Figure 128: Chemical shrinkage as a function of CAC with latex hydrated at 20°C with varying LSA and citric acid .....210
Figure 129: Autogenous deformation of CAC with latex with varying dosages of LSA and citric acid at 38°C.....211
Figure 130: 14 Day chemical shrinkage of CAC control mixtures with various SCMs hydrated at 20°C and 38°C .....213
Figure 131: Chemical shrinkage as a function of CAC control mixtures with various SCMs hydrated at 20°C .....214
Figure 132: Chemical shrinkage as a function of CAC control mixtures with various SCMs hydrated at 38°C .....215
Figure 133: Autogenous deformation of CAC control mixtures with various SCMs and latex hydrated at 20°C and 38°C.....216
Figure 134: Full-depth CAC repair in downtown Chicago .....224
Figure 135: a) Emergency entrance ramp to Children's Memorial Hospital, b) cracking, c) scaling .....225

Figure 136: a) Full-depth CAC repair on Interstate 290 in downtown Chicago, IL, b) cracking....226
Figure 137: a) Latex modified CAC bridge deck, b) surface scaling, c) crazing, and d) cracking....227
Figure 138: Repair of the Roosevelt Bridge in downtown Chicago, IL....228
Figure 139: Site location....230
Figure 140: Sunset Beach bridge....230
Figure 141: Milling of bridge deck....232
Figure 142: Setup and calibration of hydro-demolition robot....233
Figure 143: Placement and finishing of repair materials....235
Figure 144: Completed repair section....236
Figure 145: Repair option No. 1 an existing on grade concrete pavement....238
Figure 146: Repair option no. 2 existing elevated bridge decks....239
Figure 147: Repair option no. 3 develop continously reinforced slabs on grade 240
Figure 148: Site layout and elevation of on-grade slabs....240
Figure 149: Initial site grading....241
Figure 150: Construction of the base slab formwork....242
Figure 151: Students marking and placing the steel reinforcement....243
Figure 152: Final steel reinforcement location....244
Figure 153: Casting of the PC concrete base slab....245
Figure 154 a) Remotely controlled hydro-demolition robot, b) water supply power house....246
Figure 155: Hydro-demolition robot in use scarifying the concrete surface....247
Figure 156: Freshly washed concrete surface after hydro-demolition....248
Figure 157: Overlay formwork and data logging station....249

Figure 158: Data logging system .....250
Figure 159: Concrete embedment strain gages .....250
Figure 160: Thermochron i-Button temperature sensor and data loggers .....251
Figure 161: Campbell scientific weather station setup near repair slabs.....252
Figure 162: a) Slab cleaning, b) volumetric mix truck .....254
Figure 163: Volumetric mixture truck prior to casting.....255
Figure 164: Placement of the latex-modified CSA overlay.....256
Figure 165: Three hour wet-cure .....257
Figure 166: Plastic settlement cracking of the concrete surface.....258
Figure 167: Placement of the CAC overlay.....260
Figure 168: CSA concrete slab schematic and time of concrete pour details.....261
Figure 169: Mid-depth CSA 24 hour curing temperatures .....262
Figure 170: Interface of repair slab and base slab 24 hour curing temperatures .262
Figure 171: CAC concrete slab schematic and time of concrete pour details .....264
Figure 172: Mid-depth CAC 24 hour curing temperatures.....265
Figure 173: Interface of repair slab and base slab 24 hour curing temperatures .265
Figure 174: Six hour strength development of CSA and CAC.....267
Figure 175: Semi-adiabatic box .....268
Figure 176: Semi-adiabatic curing temperatures for CAC mixture.....269
Figure 177: Long-term strength development .....270
Figure 178: Shrinkage/expansion of rapid hardening cementitious materials in –situ .....271
Figure 179: CSA slab cracking overview .....273
Figure 180: CAC slab cracking overview.....273
Figure 181: Crazing of CAC slab .....274

Figure 182: a) Typical cracking patter in the CSA slab, b) CAC slab.....274
Figure 183: Crack mapping grid.....275
Figure 184: a) Core location taken to determine depth of cracking, b) Cores with cracks highlighted.....278
Figure 185: Drying shrinkage.....279
Figure 186: Mass change of drying shrinkage specimens.....280
Figure 187: Autogenous deformation of CAC at 20°C and 38°C.....283
Figure 188: Fondu Material Certificate.....290
Figure 189: TCAC Material Certificate.....291
Figure 190: LF Material Certificate.....292
Figure 191: FA Material Certificate.....293
Figure 192: CSA Material Certificate.....294
Figure 193: Heat flow of portland cement mortar at 5°C isothermal.....295
Figure 194: Heat flow of portland cement mortar at 23°C isothermal.....296
Figure 195: Heat flow of portland cement mortar at 38°C isothermal.....296
Figure 196: Heat flow of portland cement mortar at 60°C isothermal.....296
Figure 197: Heat flow of portland cement paste at 5°C isothermal.....297
Figure 198: Heat flow of portland cement paste at 23°C isothermal.....297
Figure 199: Heat flow of portland cement paste at 38°C isothermal.....298
Figure 200: Heat flow of portland cement paste at 60°C isothermal.....298
Figure 201: Heat flow of various PC mortar sample size at 5°C isothermal.....299
Figure 202: Heat flow of various PC mortar sample size at 23°C isothermal.....299
Figure 203: Heat flow of various PC mortar sample size at 38°C isothermal.....300
Figure 204: Heat flow of various PC mortar sample size at 60°C isothermal.....300
Figure 205: Heat flow of various PC paste sample size at 5°C isothermal.....301

Figure 206: Heat flow of various PC paste sample size at 23°C isothermal .....301
Figure 207: Heat flow of various PC paste sample size at 38°C isothermal .....302
Figure 208: Heat flow of various PC paste sample size at 60°C isothermal .....302
Figure 209: Heat flow of various CAC mortar sample size at 5°C isothermal ...305
Figure 210: Heat flow of various CAC mortar sample size at 23°C isothermal .305
Figure 211: Heat flow of various CAC mortar sample size at 38°C isothermal .306
Figure 212: Heat flow of various CAC mortar sample size at 60°C isothermal .306
Figure 213: Heat flow of various CAC paste sample size at 5°C isothermal .....307
Figure 214: Heat flow of various CAC paste sample size at 23°C isothermal ....307
Figure 215: Heat flow of various CAC paste sample size at 38°C isothermal ....308
Figure 216: Heat flow of various CAC paste sample size at 60°C isothermal ....308
Figure 217: Heat flow of CAC mortar size at 5°C isothermal.....309
Figure 218: Heat flow of CAC mortar size at 23°C isothermal.....309
Figure 219: Heat flow of CAC mortar size at 38°C isothermal.....310
Figure 220: Heat flow of CAC mortar size at 60°C isothermal.....310
Figure 221: Heat flow of CAC paste size at 5°C isothermal .....311
Figure 222: Heat flow of CAC paste size at 23°C isothermal .....311
Figure 223: Heat flow of CAC paste size at 38°C isothermal .....312
Figure 224: Heat flow of CAC paste size at 60°C isothermal .....312
Figure 225: Heat flow of TCAC hydrated at 20°C for varying LSA dosages .....313
Figure 226: Cumulative heat release of TCAC hydrated at 20°C for varying LSA dosages.....313
Figure 227: Heat flow of TCAC hydrated at 20°C for varying HRWR dosages 314
Figure 228: Cumulative heat release of TCAC hydrated at 20°C for varying HRWR dosages.....314

Figure 229: Qualitative XRD of TCAC with LSA hydrated at 20°C, illustrating the formation of $CAH_{10}$ and $C_2AH_8$ .....315
Figure 230: Qualitative XRD of TCAC with HRWR hydrated at 20°C, illustrating the formation of $CAH_{10}$ and $C_2AH_8$ .....316
Figure 231: Qualitative XRD of TCAC with LSA and HRWR hydrated at 20°C, illustrating the formation of $CAH_{10}$ and $C_2AH_8$ .....317
Figure 232: Chemical shrinkage with standard deviation for TCAC with varying dosages of LSA and HRWR at 20°C .....318
Figure 233: Heat flow of TCAC hydrated at 38°C for varying LSA dosages.....318
Figure 234: Cumulative heat release of TCAC hydrated at 38°C for varying LSA dosages.....319
Figure 235: Heat flow of TCAC hydrated at 38°C for varying HRWR dosages 319
Figure 236: Cumulative heat release of TCAC hydrated at 38°C for varying HRWR dosages.....320
Figure 237: Qualitative XRD of TCAC with 1% HRWR hydrated at 38°C, illustrating the formation of $C_2AH_8$ and some $C_3AH_6$ .....321
Figure 238: Qualitative XRD of TCAC with 1% LSA and 0.5% HRWR hydrated at 38°C, illustrating the formation of $C_2ASH_8$, $C_2AH_8$ and some $C_3AH_6$322
Figure 239: Chemical shrinkage with standard deviation for TCAC with varying dosages of LSA and HRWR at 38°C .....323
Figure 240: Heat flow of CAC-LF hydrated at 20°C for varying LSA dosages .324
Figure 241: Cumulative heat release of CAC-LF hydrated at 20°C for varying LSA dosages.....324
Figure 242: Heat flow of CAC-LF hydrated at 20°C for varying HRWR dosages325

Figure 243: Cumulative heat release of CAC-LF hydrated at 20°C for varying HRWR dosages .....325
Figure 244: Chemical shrinkage with standard deviation for CAC-LF with varying dosages of LSA and HRWR at 20°C .....326
Figure 245: Heat flow of CAC-LF hydrated at 38°C for varying LSA dosages .326
Figure 246: Cumulative heat release of CAC-LF hydrated at 38°C for varying LSA dosages .....327
Figure 247: Heat flow of TCAC hydrated at 38°C for varying HRWR dosages 327
Figure 248: Cumulative heat release of CAC-LF hydrated at 38°C for varying HRWR dosages .....328
Figure 249: Chemical shrinkage with standard deviation for CAC-LF with varying dosages of LSA and HRWR at 38°C .....328
Figure 250: Heat flow of CAC-FA hydrated at 20°C for varying LSA dosages .329
Figure 251: Cumulative heat release of CAC-FA hydrated at 20°C for varying LSA dosages .....329
Figure 252: Chemical shrinkage with standard deviation for CAC-FA with varying dosages of LSA and HRWR at 20°C .....330
Figure 253: Heat flow of CAC-FA hydrated at 20°C for varying HRWR dosages330
Figure 254: Cumulative heat release of CAC-FA hydrated at 20°C for varying HRWR dosages .....331
Figure 255: Chemical shrinkage with standard deviation for CAC-FA with varying dosages of LSA and HRWR at 38°C .....331
Figure 256**:** CR-10X data logger specifications .....332
Figure 257: AM16/32 multiplexer specifications .....333
Figure 258: 120 ohm terminal input modules .....334

Figure 259: Vishay concrete embedment strain gage .....335
Figure 260: Wiring diagram for concrete embedment strain gages.....336
Figure 261: Strain gage control program written PC 400.....337
Figure 262: Thermochron iButton specifications .....338

# Chapter 1: Introduction

## 1.1 Background

Calcium aluminate cement was invented in the early 1900's and first patented under the name "Ciment Alumineux" in 1908 by Bied. This cement is known now as simply calcium aluminate cement (or abbreviated as CAC) although it has been called over the years high-alumina cement or Ciment Fondu. CAC was developed initially to withstand exposure to sulfate environments but has since been used in a wide range of applications where the following properties are sought (Scrivener, 2003):

- Rapid hardening with setting times similar to those of portland cement
- Resistance to attack by acids and some other chemicals aggressive to portland cement
- Ability to withstand repeated heating to high temperatures
- Ability to withstand low temperatures in placing and use
- Resistance to abrasion and impact with appropriate aggregates
- In mixtures containing portland cement, calcium sulfate or both, the ability to trigger ettringite-induced early strength gain and restrained expansion (when desired for shrinkage compensation)

CAC concrete has been used in a wide range of applications, but it is generally not a direct competition for portland cement because of its higher relative cost. Rather, CAC is used only in cases where special properties, such as rapid hardening for repair applications, are deemed critical. Calcium aluminates hydrate rapidly due to the absence of any diffusion barriers, thereby allowing for continuous and rapid dissolution of calcium and alumina ions and subsequent formation of calcium aluminate hydrates as part of a massive precipitation process which rapidly fills in voids and leads to quick and efficient hardening and strength development. Calcium and aluminate ions readily

dissolve and diffuse throughout a given volume, and at some point, say two to three hours after the cement first contacts the water, solid hydration products begin to rapidly form throughout the emerging microstructure, not just in the local vicinity of dissolving cement grains. The massive precipitation of CAC hydration products generates considerable heat and a concomitant rapid hardening and early strength gain.

The hydration of CAC is also unique in that different reaction products form at different temperatures, and some products that do form are meta-stable and are destined to convert to stable hydration products at some point in time. The latter process is known as conversion, which results in a complete transformation in crystal structure and overall microstructure. The stable hydrates are about twice as dense as the meta-stable hydrates, resulting in a major decrease in the porosity of the system (as the volume of hydrates decreases with increasing solid density) and a parallel reduction in mechanical properties, such as compressive strength and elastic modulus. This reduction in strength can be accommodated provided that adequate structural strength remains after conversion to safely handle the loading on the structure. A detailed review of CAC hydration is provided in Chapter 2 of this dissertation, and only some of key attributes are highlighted here, enough to convey the complexity of CAC hydration and to highlight the global issue of conversion.

### 1.2 SCIENTIFIC NETWORK

The research conducted in this dissertation was funded by Kerneos Aluminate Technologies. Kerneos, Inc. is the largest manufacturer of calcium aluminate cement. In 2004, Kerneos, Inc. developed a scientific network comprised of the top cement and concrete research programs from around the world to further develop fundamental scientific knowledge of this unique cementitious material. The network includes research

directed by Dr. Karen Scrivener at Ecole Polytechnique Federale de Lausanne (EPFL) in Lausanne, Switzerland, where the focus is characterizing the microstructural development of CAC based-systems. Dr. Michael Thomas leads efforts at the University of New Brunswick (UNB) in Fredericton, New Brunswick, Canada centered on characterizing CAC concrete durability. Recently, researchers at Oregon State University in Corvallis, Oregon, under the direction of Dr. Jason Ideker, joined the Scientific Network. They focus on early-age volume deformation of CAC based-systems as well as development of American Society for Testing and Materials (ASTM) standards for the use of calcium aluminate cement. The final group in the Scientific Network is led by Dr. Kevin Folliard at the University of Texas at Austin. His reseach group focuses on the characterization of CAC based-systems hydration, early-age volume deformation and linking behavior to actual field performance. Drs. Kevin Folliard and Jason Ideker are the co-supervisors of this dissertation and research.

### 1.3 OBJECTIVES

The purpose of the research described in this dissertation was to characterize and investigate the link between laboratory performance and field performance of CAC based-systems. Significant emphasis was placed on characterizing the hydration of CAC, in combination with various chemical admixtures, supplementary cementitious materials (SCMs) and inert fillers. Analytical tools, specifically isothermal calorimetry, x-ray diffraction, and chemical shrinkage testing, were implemented to characterize the hydration and micro-structural development of the combinations of materials combinations of materials and develop a database of influences of various materials on CAC hydration and strength development. Another area of emphasis was the characterization and quantification of early-age volume changes of mortar and concrete

containing CAC (in combination with various admixtures, binders, and fillers). Laboratory testing, specifically autogenous deformation and restrained shrinkage testing were performed to characterize the volume change under isothermal conditions. Large-scale field trials consisted of casting thin-bonded overlays on existing pavement slabs.

### 1.4 CONTENT

This dissertation is divided into eight chapters. In Chapter 2, a literature review of calcium aluminate cement, specifically the history, hydration, conversion, and volume deformation, is presented.

Chapter 3 describes the various materials, experimental procedures and equipment used. Chemical analysis and sample preparation procedures are described. A brief background and relevant references for various analytical techniques implemented are given.

In Chapter 4, the results of the characterization of a new paste and mortar isothermal calorimeter are presented. The research delved into a comprehensive study of the repeatability and effect of sample size variability on paste and mortar samples for this equipment. Then, investigations of the use of the calorimeter for rapid repair materials specifically CAC are presented. However, excessive heat release from these materials proved the current calorimeter incapable of maintaining isothermal temperatures during testing. Therefore, a custom designed isothermal calorimeter tailored for the hydration characteristics of these materials was built.

Chapter 5 summarizes the findings of research focusing on the influence of chemical admixtures on plain CAC hydration and early-age volume deformation.

Chapter 6 focuses on the effects of various supplementary cementing materials and fillers on CAC behavior, with focus on the effects on conversion and strength reduction.

Chapter 7 describes a large-scale field project that compared a calcium sulfoaluminate cement-based overlay to a calcium aluminate cement-based overlay.

Chapter 8 summarizes the key findings of this dissertation and recommends areas of research for further investigation.

# Chapter 2: Literature Review

## 2.1 Calcium Aluminate Cement Introduction

CAC is a rapid hardening hydraulic cementitious material that has been used for concrete repair and new construction, refractory applications, sewer pipe linings and the building chemistry market for over 100 years. This chapter is a compilation of published data and research on CAC based-systems with a focus on the history, cement chemistry, hydration, conversion phenomena, and early-age volume change. The aim of this literature review is to provide a broad background on calcium aluminate cements from the microstructural level to the full-scale field performance, thereby laying the groundwork for this dissertation and the work completed within it.

## 2.2 CAC History

In the mid-nineteenth century several researchers found that calcium aluminate powders had cementing properties. In 1888, the first patent for calcium aluminate cement was issued. Much of the research and development was completed by J.J. Bied in Le Teil, France where he worked at the J. & A. Pavin de Lafarge company. His work was prompted by the need for a sulfate-resistant cement. In 1908 his work on the development of a manufacturing process resulted in a patent of the manufacturing process, where bauxite, and other low silica material are fused together with limestone to produce calcium aluminate cement (Campas, 1998). This cement was not only resistant to sulfates, but also possessed the ability to rapidly harden. After several years of increasing production the material first came on the market in 1918 under the trade name of Ciment Fondu Lafarge (CFL). The first applications where the rapid hardening properties of CAC were harnessed were during World War I for the repair and reconstruction of gun replacements and shelters. Also, due to its sulfate resistance the

Paris-Lyon-Marseille (P.L.M.) Railway used CAC to rebuild a tunnel passing through an anhydrite (anhydrous calcium sulfate) mass (Campas, 1998). A more thorough review of the history and case studies of CAC concrete are presented in Section 2.7.2.

## 2.2 RAW MATERIALS, CHEMISTRY, MANUFACTURING, AND PHYSICAL CHARACTERISTICS OF CAC

Limestone and bauxite are the raw components which are fused to manufacture calcium aluminate cement. Bauxite is the only suitable alumina source existing in nature that can be used for calcium aluminate cement manufacturing. CAC typically used for infrastructure applications contain 38-40% $Al_2O_3$, which are made from ferruginous bauxites and contain up to 20% $Fe_2O_3$. Certain grades of CACs have higher alumina contents, specifically used for refractory resistance, which use purer sources of raw bauxites and limestone that contain low iron, and other impurities. CAC produced for these applications typically contain 60 to 80% $Al_2O_3$ (Campas, 1998). Table 1 summarizes the chemical compositions of the various CAC cements available.

Table 1: Chemical composition and origins of Production for range of calcium aluminate cements currently available (Campas, 1998)

| Grade | $Al_2O_3$ | CaO | $SiO_2$ | $Fe_2O_3$ + FeO | $TiO_2$ | MgO | $Na_2O$ | $K_2O$` | Color | Countries of manufacture |
|---|---|---|---|---|---|---|---|---|---|---|
| Standard' low alumina | 36-42 | 36-42 | 3-8 | 12-20 | <2 | ~1 | ~0.1 | ~0.15 | Grey or buff to black | France, Spain, Croatia, USA, India, Eastern Europe |
| Low alumina, low iron | 48-60 | 36-42 | 3-8 | 1-3 | <2 | ~0.1 | ~0.1 | ~0.05 | Light buff or grey to white | France, Usa, India, Korea, Brazil |
| Medium alumina | 65-75 | 25-35 | <0.5 | <0.5 | <0.05 | ~0.1 | <0.3 | ~0.05 | White | France, UK, USA, Japan, China, India, Korea, Brazil |
| High alumina | >80 | <20 | <0.2 | <0.2 | <0.05 | <0.1 | <0.2 | ~0.05 | White | USA, France, Japan, Brazil, Korea |

Figure 1 illustrates the approximate composition range of calcium aluminate cements (Scrivener, 2003). This figure shows a ternary phase diagram of $CaO$-$SiO_2$-$Al_2O_3$ with comparison of composition ranges of ordinary portland cements.

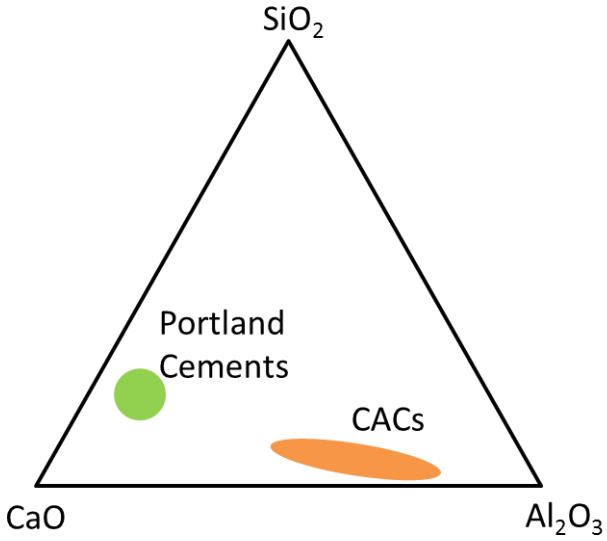


Figure 1: Approximate composition range of CAC, adapted from (Scrivener, 2003)

In CACs with lower alumina content the cementitious phases present can be complex. The principal reactive phase found in CAC is monocalcium aluminate, CA or $CaAl_2O_4$ which makes up roughly 40-60% of the cement. The other key component of anhydrous CAC is $C_{12}A_7$ (manyenite), which is the most reactive calcium aluminate phase and thus responsible for the most rapid increases in setting. The amount of this component is strictly limited to prevent early stiffening or flash setting (Scrivener, 2003).

Reverberatory open-hearth furnaces are used to manufacturer typical grades of calcium aluminate cements for civil engineering applications. Figure 2 illustrates a reverberatory open-hearth furnace used for the manufacturing of CAC.

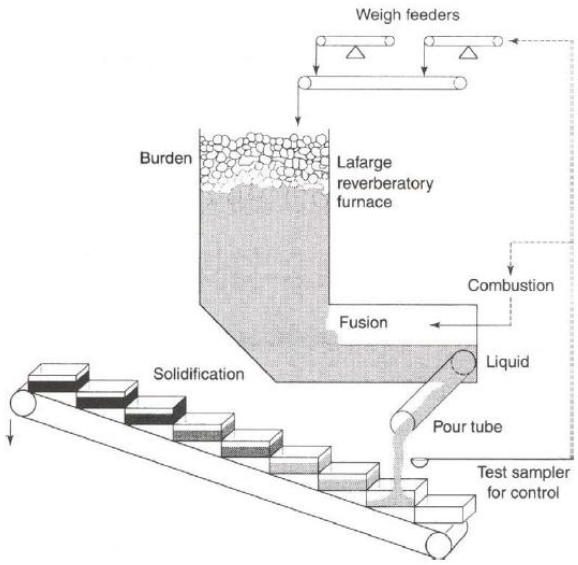


Figure 2: Schematic diagram of a reverberatory furnace (Campas, 1998)

The furnace is charged with raw limestone and bauxite in a vertical stack. Coal or oil is typically used to fire the furnace. Hot gases travel up the stack where water and carbon dioxide are driven off. The materials are melted when they drop from the storage stack into the hearth of the furnace. The molten cement continuously pours from a hole in the furnace into molds and cooled. The temperature of the molten cement exceeds 1450°C (Campas, 1998).

After cooling, the dark, fine-grained clinker is ground using ball mills. CAC clinker is much harder than ordinary portland cements, thus requiring more energy to grind and causing more wear on manufacturing equipment. Also, unlike portland cements, after grinding there is no gypsum or other material addition made to the cement. (Campas, 1998).

Generally, CAC has a specific gravity of 3200-3250 kg/m$^3$, which is slightly higher than portland cements. The specific gravity increases with the increasing iron

content. Standard grades of CAC have a specific surface area (Blaine) of 250-400 $m^2/kg$ with a typical residue of a 5% on a 100 μm sieve (Campas, 1998).

## 2.3 CAC HYDRATION AND CONVERSION

This section describes the hydration of CAC, with emphasis on microstructure and the heat of hydration.

### 2.3.1 Microstructural Development

Unlike portland cements where calcium silicate hydrates (C-S-H) and portlandite (CH) form consistently through most time and temperature histories, calcium aluminate cement hydration is strongly dependent on temperature. The hydration process occurs by a process of dissolution and precipitation. The anhydrous CAC phases dissolve upon contact with water and introduce ions in solution, which then begin to precipitate out of the water solution in new chemical combinations, i.e. $CAH_{10}$, $C_2AH_8$, $C_3AH_6$, and poorly crystalline gel-phases (Scrivener, 2003).

When the phases mix together and recombine in the lowest possible energy state, stable hydrates ($C_3AH_6$ and $AH_3$) form. However, due to the speed of nucleation the formation of the phases in the lowest energy state is difficult and is often preceded by the formation of temporary or metastable hydrates ($CAH_{10}$ and $C_2AH_8$). The energy state of the metastable products is lower than the dissolved ions, thus there is a motivation for the new assemblage, but being that there is still a lower energy state possible, a driving force for these metastable hydrates to recombine to form stable hydrates exists. The transformation of metastable hydrates to the lowest energy state of stable hydration products is known as conversion. Figure 3 illustrates the energy motivation of the phases anhydrous CAC to form the metastable and stable hydrates (Scrivener, 2003).

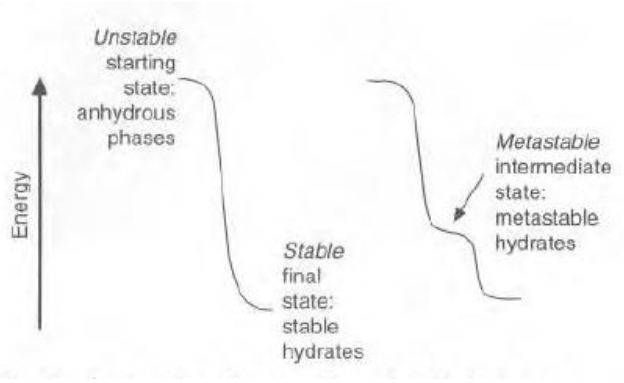


Figure 3: Schematic indicating the motivation for the hydration and conversion of the stable hydrates and rearrangement of the metastable hydrates (Scrivener, 2003)

The stable hydration products are found predominantly when hydration occurs at stable environmental temperatures over 65°C. The hydration of calcium aluminate (CA) to the stable/lowest energy state resulting in the formation of $C_3AH_6$ and $AH_3$ (gibbsite) is shown in Equation 1 (Campas, 1998).

$$3CA + 12H \rightarrow C_3AH_6 + 2AH_3 \quad (1)$$

The stable hydration product $C_3AH_6$ has a compact cubic morphology and gibbsite is a poorly crystalline formless mass (Campas, 1998).

At temperatures below 30°C the first metastable hydration product that forms is $CAH_{10}$. $C_2AH_8$ and $AH_3$ are the primary hydration products that form at temperatures between 35-65°C. Equations 2 and 3 illustrate the hydration of CA (Campas, 1998).

$$CA + 10H \rightarrow CAH_{10} \quad (2)$$

$$2CA + 16H \rightarrow C_2AH_8 + AH_3 \quad (3)$$

When the temporary or metastable hydration products form first, it is inevitable that they will convert to the lowest energy state (stable hydrate assemblages). Equations 4 and 5 demonstrate the conversion reactions of the metastable hydrates. The conversion

of $CAH_{10}$ directly to $C_3AH_6$ is thermodynamically possible; however $C_2AH_8$ usually precedes the formation due to the ease of nucleation (Campas, 1998).

$$2CAH_{10} \rightarrow C_2AH_8 + AH_3 + 9H \quad (4)$$

$$3C_2AH_8 \rightarrow C_3AH_6 + AH_3 + 9H \quad (5)$$

Beyond a transformation in hydration products through solution in hardened concrete, the actual consequences of this phase change has practical implications. When conversion from the metastable hydrates to the stable hydrates occurs there are two implications, which are:

1. There is a densification of hydration products, which results in an increased porosity and a reduction in strength.
2. Water is released, which can hydrate any remaining anhydrous cements particles.

Conversion has the largest impact on CAC concretes made with high water-to-cement ratios (>0.5). These concretes are severely affected by conversion because there is enough water to hydrate nearly all the anhydrous cement and enough space for the less dense metastable hydrates ($CAH_{10}$ and $C_2AH_8$) to form, resulting in artificially and misleading very high early strengths. When conversion to the more dense stable hydrates ($C_3AH_6$ and $AH_3$) eventually occurs there is a significant reduction in volume and increase in porosity resulting in a reduction in strength (Scrivener, 2003).

When the w/c is kept low (<0.4) there is insufficient space and water for all the anhydrous cement to react. Thus, when conversion occurs, water is released as part of the reaction and the remaining anhydrous cement reacts and forms hydrates that fill the pores created by the densification of the existing hydrates during conversion. Therefore, the strength reduction associated with conversion is less significant at these lower w/c (Scrivener, 2003).

### 2.3.2 Heat of Hydration

The heat due to hydration of calcium aluminate cements is rapid compared to portland cements, however the total heat evolved is about the same for the two (~500 kJ/kg). Table 2 shows an example of the total cumulative heat evolution comparison of portland cement and calcium aluminate cement. The majority of the heat evolution from CAC occurs in the first 10 hrs and comes to a halt by 24 hrs, whereas the portland cement continues to generate measureable heat up to 28 days and ever longer when supplementary cementitious materials are used.

Table 2: Heats of hydration of CAC and OPC (kJ/kg) (Campas, 1998)

| Type of Cement | 6 h | 1 day | 5 days | 7 days | 28 days |
|---|---|---|---|---|---|
| Calcium alumiante cement | 340 | 445 | 445 | | |
| Ordinary portland cement | | | | ~ 350 | ~400 |

Heat flow curves generated by isothermal calorimetry for calcium aluminate cement based-systems generally are characterized by an initial peak due to the dissolution of hydration products, followed by an induction period and then a single sharp peak that occurs within the first hours of hydration and demonstrates the massive precipitation of hydrates. The first peak due to dissolution or heat of wetting is neglected and not integrated into curves of total heat evolution. During the dissolution phase the maximum concentration of $Ca^{2+}$ and $Al(OH)_4^-$ ions are in the solution. The length of the induction period is controlled by the presence of nucleation sites occurring from accelerators and/or sand particles (Gosselin C. a., 2008).

In Figure 4, Gosselin shows the heat flow at 20°C of CAC at varying w/c and with a lithium sulfate accelerator.

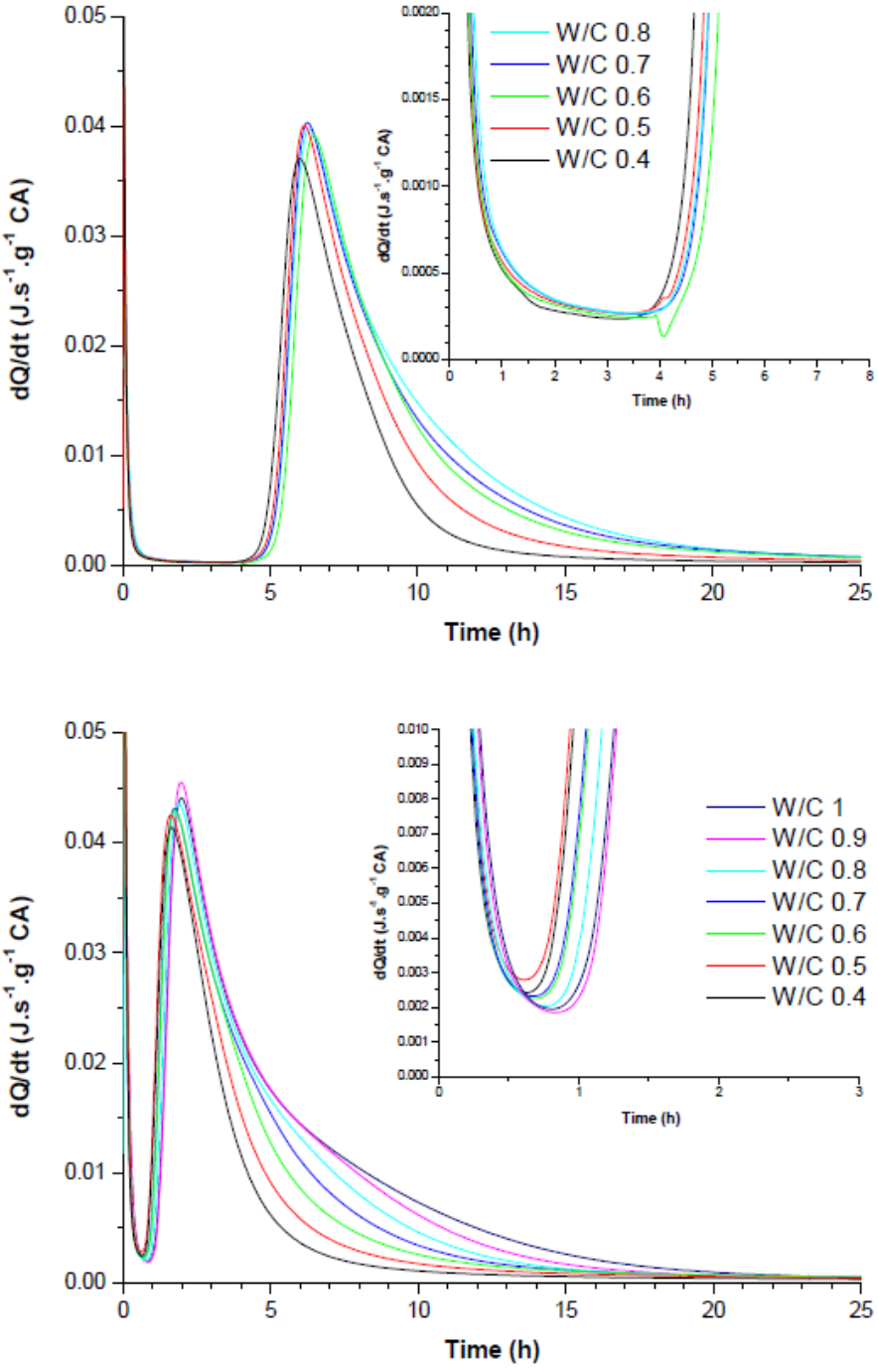


Figure 4: Heat flow curve of CAC hydrated at 20°C for different w/c: Top: without $Li_2SO_4$, Bottom: with lithium sulfate (Gosselin C. , 2009)

From Figure 4, the heat flow of plain CAC with and without the addition of the lithium sulfate accelerator at 20°C was shown. Lower w/cm ratios slightly shorten the duration of the induction period because the critical ion concentration is reached earlier in solution. Gosselin demonstrated that the addition of lithium sulfate accelerator drastically shortens the induction period (2009). Another key point to identify from the heat flow curves is the drastic reduction in heat flow of the lower w/c mixture compared to the mixtures with higher w/c. This rapid deceleration in hydration is believed to be due to the lack of water or space. Lithium sulfate slightly lowers the total heat compared to the mixtures without accelerator.

Figure 5 shows the isothermal calorimetry behavior of CAC systems at 38°C, with and without accelerator.

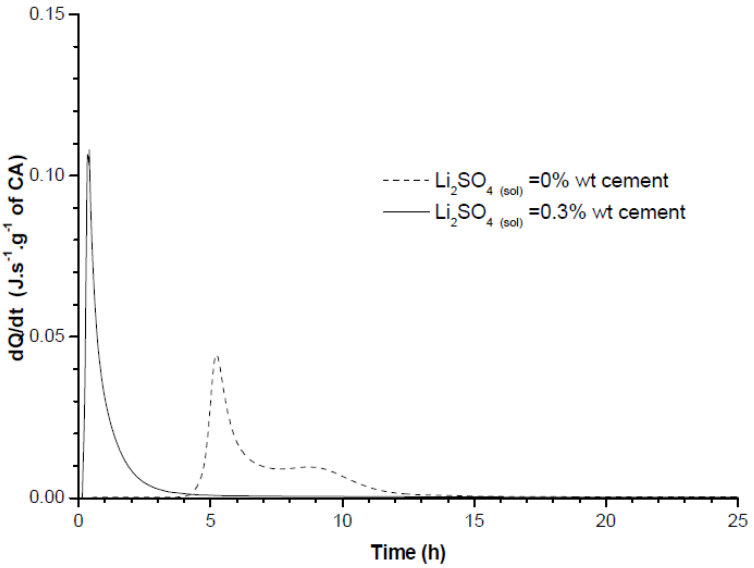


Figure 5: Isothermal calorimetry of plain CAC at 38°C, with and without $Li_2SO_4$ (Gosselin C. , 2009)

At 38°C significantly different behavior is noted for mixtures with and without lithium sulfate accelerator present. With lithium sulfate, a sharp peak occurs rapidly that ends within the first 5 hours. Plain CAC at 38°C has completely different behavior with a main peak occurring followed by a second less intense one over a 9 hr period (Gosselin C. , 2009).

### 2.3.3 Chemical Shrinkage

A more detailed review of chemical shrinkage is presented in Chapter 3, as well as the full description of the testing procedures used in this dissertation. Chemical shrinkage has been defined by Jensen as the "internal volume reduction associated with the hydration reactions in a cementitious material" (2001). The volume change is the result of hydration products occupying less space than the reacting materials in hydrating cement paste. This phenomena was first investigated by Le Chatelier in 1900, when he stated the importance of identifying the difference between *absolute volume* and the *apparent volume* of hardening ordinary portland cement paste, where the absolute volume is a measure of the deformation due to chemical shrinkage and apparent volume means the deformation due to autogenous shrinkage (Jensen O. a., 2001). In 2005, the first standard testing procedure to measure chemical shrinkage of cement pastes was adopted, ASTM C 1608 (2007).

Ideker implemented an automated version of the testing procedure and evaluated chemical shrinkage of CACs for isothermal temperature ranges from 20–55°C. Table 3 summarizes the ultimate chemical shrinkage results of a calcium aluminate cement, named GCX, with and without accelerator as well as a comparison with portland cement. The study showed similar chemical shrinkage properties between CAC with and without accelerator at 20-25°C and from 38-55°C. However, a distinct difference was evident at

30 and 34°C where increased chemical shrinkage was seen in the specimens without accelerator. This was attributed to the formation of more $CAH_{10}$ in the paste without accelerator which contains a higher amount of water compared to the samples with accelerator of which $C_2AH_8$ is the predominant hydration product. It was also shown that the ultimate shrinkage of portland cement was generally not affected by temperature and the ultimate shrinkage ranged from 0.03 to 0.04 mL/g cement which was significantly less than those values seen in calcium aluminate cement paste samples (Ideker, 2008).

Table 3: Summary of chemical shrinkage testing results at varying temperatures (mL $H_2O$/g cement) (Ideker, 2008)

| Temp. | GCX | | GCX + Acc | | OPC | | Duration |
|---|---|---|---|---|---|---|---|
| (°C) | 1 | 2 | 3 | 4 | 1 | 2 | (hr) |
| 20 | 0.078 | - | 0.073 | - | 0.036 | - | 400 |
| 25 | 0.068 | 0.064 | 0.069 | 0.067 | 0.032 | 0.032 | 380 |
| 30 | 0.112 | 0.110 | 0.088 | 0.086 | 0.038 | 0.034 | 380 |
| 34 | 0.115 | 0.112 | 0.080 | 0.074 | 0.033 | 0.031 (82 h) | 200 |
| 38 | 0.121 | 0.113 | 0.116 | 0.113 | 0.035 | 0.035 | 329 |
| 45 | 0.118 | 0.117 | 0.116 | 0.117 | 0.037 | 0.033 | 300 |
| 55 | 0.114 | 0.103 | 0.109 | 0.110 | 0.023 (18 h) | NR | 170 |

Investigations were later continued by Fu (2011) who showed in Figure 6 that different calcium aluminate cements, Fondu and GCX, had 2 to 3 times the chemical shrinkage of portland cement at isothermal temperatures of 38°C. It is also important to note a significant percentage of the shrinkage occurs in the first 24 h highlighting the rapid hydration and early-age strength. Another key discovery of Fu's was the identification of conversion through the use of chemical shrinkage testing. He noted a change in slope of the chemical shrinkage behavior at 4 to 5 days at 38°C and confirmed the transition through complementary x-ray diffraction analysis (Fu, 2011).

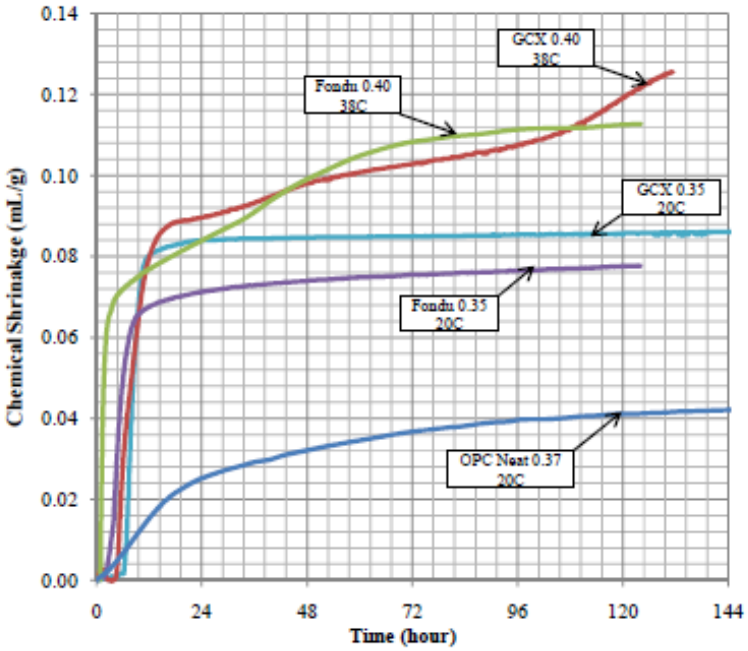


Figure 6: Chemical shrinkage development of CAC and portland cement at different temperatures (Fu, 2011)

## 2.4 Properties of CAC Concrete

This section describes the basic properties of CAC concrete, with emphasis on fresh, hardened, and durability characteristics. The focus is on concrete containing CAC as the sole binder; information on properties of concrete containing CAC in combination with other materials (e.g., portland cement, gypsum, SCMs, etc.) is provided later in this chapter.

### 2.4.1 Properties of Fresh CAC Concrete

The fresh properties of CAC concrete are governed by the same basic parameters, such as w/cm ratio, water content, and cement content, that control portland cement concrete.

#### *2.4.1.1 Setting Time*

The initial setting time of plain CAC is not much different from that of portland cements. However, CAC hardens and loses workability rapidly and the time between initial and final set is brief, around 30 minutes. A typical setting time for CAC cement, without set accelerators or retarders, is 3-5 hours. The setting time is drastically altered by the use of admixtures which is discussed in Section 2.5 Influence of Admixtures on CAC. Table 4 compares the setting time of CAC, OPC and rapid hardening OPC (Campas, 1998).

Table 4: Setting times of CAC and portland cement paste (Campas, 1998)

| Cement | Initial Set, h:min (SD) | Final Set, h:min (SD) |
|---|---|---|
| Calcium Aluminate Cement | 3:55 (±0:35) | 4:10 (±0:35) |
| Rapid-hardening Portland Cement | 2:10 (±1:30) | 2:50 (±1:40) |
| Ordinary Portland Cement | 3:00 (±1:20) | 4:00 (±1:10) |

Setting time is shortened in the temperature ranges from 0-10°C and longer at temperature ranges from 25-30°C. This is attributed to the formation of $C_2AH_8 + AH_3$ from $CAH_{10}$. This maximum time of setting is dependent on the chemical composition of CAC, specifically the ratio of $C_{12}A_7$/CA. The time until setting decreases at temperatures above 30°C (Bushnell-Watson, 1986), (Campas, 1998). It is important to note that these setting behaviors may not be seen in bulk concrete due to the variability or local temperatures due to the heat of hydration; the data presented in Table 4 was from active isothermal curing. These results were confirmed more recently by Fu (2011), his results showed an increase in initial setting time at a higher temperature (38°C) and very short time between initial and final set, less than 20 minutes. He used a modified Vicat testing procedure with varying w/c rather than maintaining consistent flow of the cement paste. The study evaluated two different pure CAC systems, Ciment Fondu ($Al_2O_3$~40%) and the GCX binder ($Al_2O_3$ ~ 50%) with slightly different chemical composition, but showed

a large difference in setting time between the two (2011). Figure 7 presents the setting times of these isothermally cured mixtures.

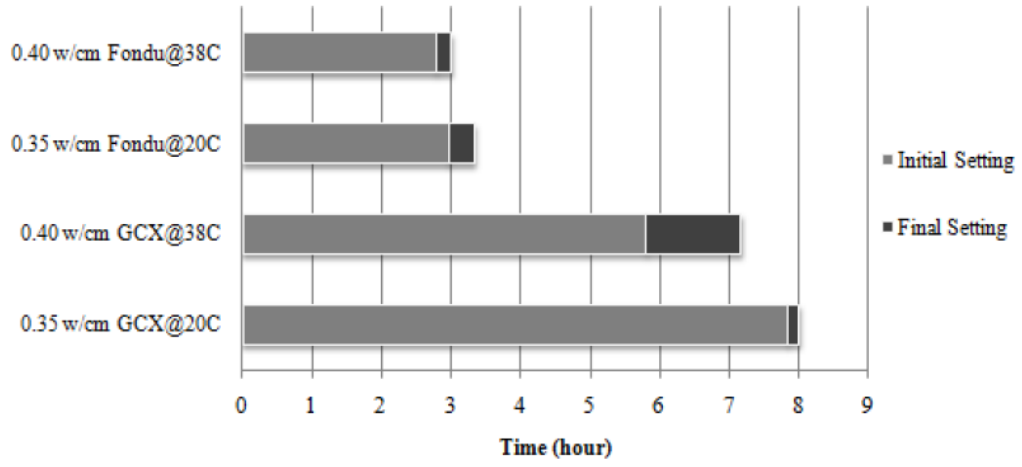


Figure 7: Modified Vicat setting time results for CAC systems (Fu, 2011)

### *2.4.1.2 Workability*

The workability of CAC concrete is similar to that of portland cement concrete at similar w/c without the use of admixtures. The appearance of CAC concretes is "drier" however it flows well under vibration. Before the use of high-range water reducers (superplasticizers) became common, the historical approach to improve workability of CAC concrete at low w/c was to use a higher cement content, usually greater than 400 kg/m$^3$ (Scrivener, 2003). Today there are a variety of plasticizers/water reducing agents available on the market. Section 2.5.3 Water Reducers summarizes the influence of lignosulfate, sulfonated, and polycarboxylate-based admixtures on the workability of CAC concrete.

### 2.4.2 Properties of Hardened CAC Concrete

The most important property of CAC for use in civil engineering applications is its ability to rapidly harden and develop high early-age strength, thereby making it a desirable material for repair applications and fast-track, specialty construction.

#### *2.4.2.1 Conversion and Strength Development*

As stated before, the long-term stable strength of calcium aluminate cements is the result of the stable hydrates, $C_3AH_6$ and $AH_3$. Metastable hydrates, $CAH_{10}$ and $C_2AH_8$, precede the formation of these stable hydrates when hydration occurs in small concrete elements at ambient temperatures. The metastable hydrates consume more water and space than the stable hydrates, thus they rapidly fill the space in a freshly placed matrix and give high early-age strength (Campas, 1998).

During conversion the metastable hydrates "densify" to the stable hydrates, which causes an increase in porosity and a decrease in strength, but also releases water. If the initial w/c is kept low, anhydrous cement remains after the initial hydration. This cement will hydrate with the release of the water from conversion and eventually lead to increase in strength. A typical strength evolution curve is shown in Figure 8 (Campas, 1998).

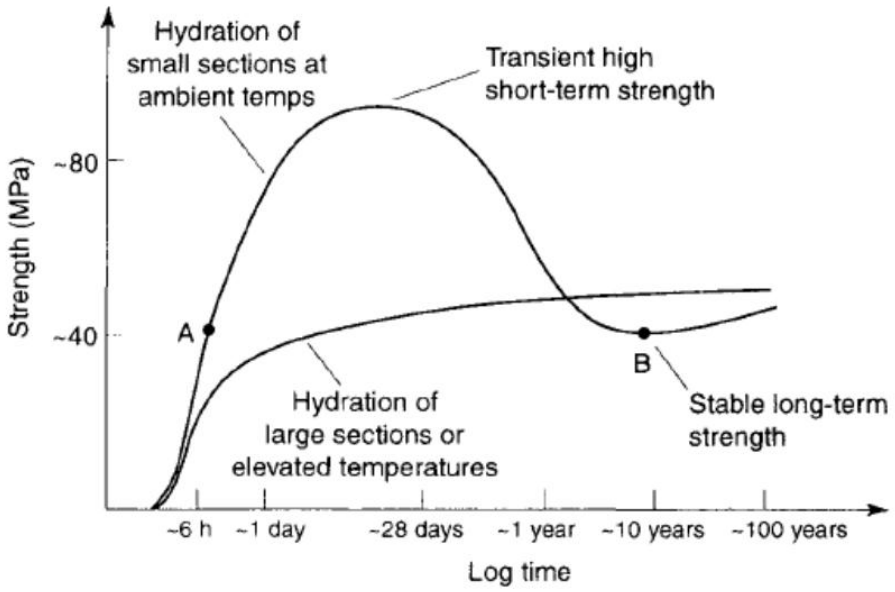


Figure 8: Schematic strength development curves for calcium aluminate cement concrete at w/c~0.4 and cement content of 400 kg/m$^3$ (Campas, 1998)

The process of conversion cannot be prevented in concrete elements that are cured at ambient temperatures. Care must be taken to design for the long-term strength, after the converted microstructure is formed.

The temperature that CAC concrete is exposed to during its lifetime has a large impact on the rate of conversion. It is understood that conversion generally occurs in the first 5-10 years of being in service. Generally, CAC concrete that has been exposed to ambient conditions with w/c near 0.5 have found converted strength >21 MPa which is generally above required design strengths for most applications. If CAC concrete is cured at 38°C immediately after casting the minimum strength occurs within the first 5 days. However, if the concrete is cured at 18°C for 1 day then moved to 38°C the low point in strength development doesn't occur for three months. At temperatures above 70°C, the minimum strength of CAC concrete occurs in the first few hours and a monotonic strength gain after that (Campas, 1998).

Recent work completed by Muller (2010) was aimed at developing a testing procedure that identified the lowest strength of CAC concrete in the first few days after casting. His studies investigated the effect of curing CAC concrete at three different temperature regimes 23, 38, and 50°C. CAC concrete cured at 50°C underwent conversion in the first few hours and had a monotonic strength gain thereafter. The other specimens had rapid strength development that later converted to same strength as the concrete cured at the highest temperature at 90 and 5 days for the 23°C and 38°C curing, respectively (Muller, 2010).

#### *2.4.2.2 Plastic Shrinkage*

Plastic shrinkage occurs as water is lost from the concrete to the environment while the concrete is still plastic (e.g. prior to setting) (116, 2000). It is a combination of chemical and autogenous shrinkage and the rapid evaporation of water from the surface of the concrete (Kosmatka, 2008). Plastic shrinkage cracking can occur in bridge decks or other exposed elements with high surface/volume ratios once the cumulative evaporation from the concrete surface exceeds the cumulative bleeding of the concrete. When cumulative evaporation exceeds cumulative bleeding, water is drawn from within the bulk of the concrete, and the concrete goes into tension (Folliard, 2009). Plastic shrinkage can be prevented by minimizing or slowing the evaporation rate of the bleed water by fogging, wind breaks, shading, plastic sheet covers, wet burlap, spray-on finishing aids (evaporation retarders), and plastic fibers (Kosmatka, 2008). There are no known publications on the plastic shrinkage behavior and resistance to cracking on CAC based-systems. The author believes that for most civil engineering rapid repair applications CAC should not be susceptible to cracking due to the rapid hydration and

strength development, which shortens the time until setting and minimizes the time of the plastic state.

#### *2.4.2.3 Autogenous Deformation*

This section presents a few studies on the autogenous deformation of CAC and more detail on the procedures and mechanisms is presented in Chapter 3. Autogenous deformation is defined as the macroscopic bulk deformation of a closed, isothermal cementitious system that is not subjected to any external forces (Jensen O. a., 2001). The evaluation of autogenous shrinkage of calcium aluminate cement based-systems was considered in this dissertation due to the low w/c, for reasons previously stated, and for the use of CAC for rapid partial-depth repairs of bridge decks. In bridge deck repair, resistance to autogenous shrinkage cracking is essential for long-term durability, due to the fact that early age-cracking may lead to the penetration of harmful chemicals and freeze-thaw deterioration. The remainder of this section reviews the limited data on the autogenous deformation for CAC systems. A more detailed review of the autogenous shrinkage mechanisms and testing protocols is presented in Section 3.3.4 Autogenous Deformation.

Ideker (2008) evaluated the autogenous deformation of CAC in an actively controlled isothermal free deformation frame. The key contribution from his studies revealed that the formation of the metastable hydrates (predominantly $CAH_{10}$) at temperatures below 30°C resulted in an autogenous shrinkage. At temperatures above 30°C, it was observed that stable and metastable hydrates ($C_2AH_8$ and $C_3AH_6$) formed and resulted in an autogenous expansion (Ideker, 2008).

In 2011, Fu investigated the autogenous shrinkage of different pure CAC systems, Fondu and GCX. His research confirmed findings by Ideker (2008) which showed

autogenous expansion at 38°C and shrinkage at 20°C. Figure 9 shows the results of these mixtures with varying w/c and different isothermal curing conditions.

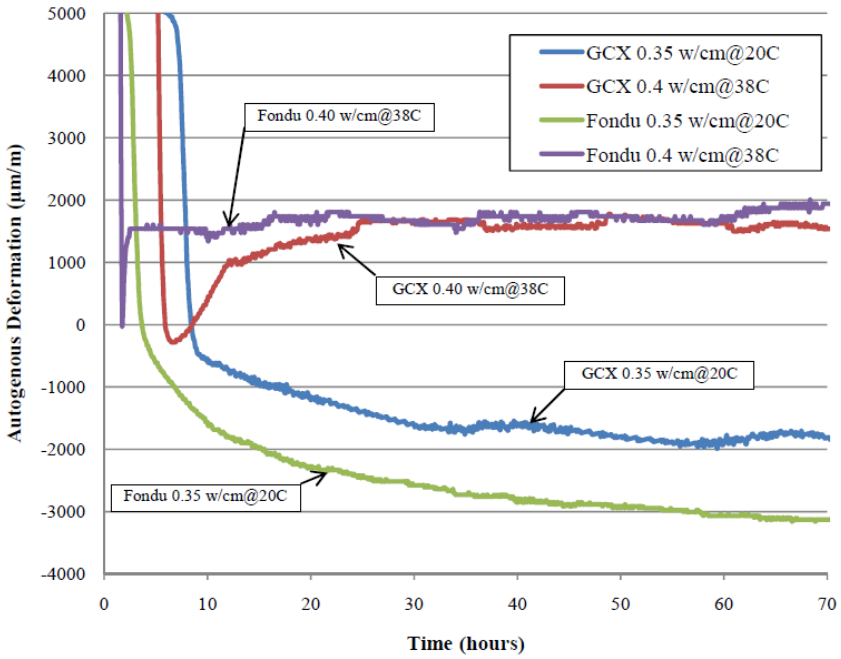


Figure 9: Autogenous deformation of two CAC binder systems (Fu, 2011)

### *2.4.2.4 Drying Shrinkage*

Due to its rapid hydration, CAC concrete exhibits rapid drying and shrinkage, which is completely different from portland cement concrete. The rapid drying is caused by the consumption of the free water. Thus, after the volume change of CAC concrete in the first few days, the long-term drying shrinkage is generally small. Typically half of the drying shrinkage occurs in the first day compared to 7 days for ordinary portland cements (Campas, 1998).

The typical drying shrinkage procedure used is ASTM C 157 for portland cement concrete, which begins measurement at 20°C and 50% RH storage after 28 days of moist

curing (ASTM C 157, 2008). This procedure is well accepted, however is not applicable for CAC due its rapid hardening and hydration. The test does not capture the majority of the shrinkage that occurs in the first few hours after casting. Lamberet et. al. (2008)investigated the effect of different times, the classical time of 24 hours and $T_{off}$, time at which the calcium aluminate cement concrete increases in temperature by 1°C from the initial temperature while still in a fresh state, plus 2 hours, of demolding on the drying shrinkage of two different CAC mortar mixtures. Figure 10 shows the classical procedure underestimates the amount of shrinkage by 2-3 times the ultimate value (2008).

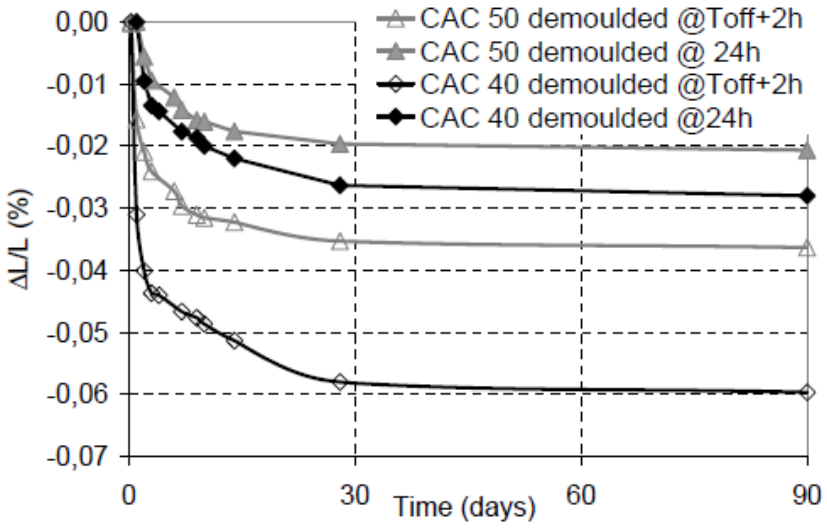


Figure 10: Effect of demoulding time on drying shrinkage (Lamberet S. F., 2008).

### 2.4.3 Durability of CAC Concrete

Calcium aluminate cement was originally developed for use in aggressive environmental conditions where ordinary portland cement concrete had been shown to perform poorly. The long-term performance of CAC concrete is often controlled by the quality of the concrete and the exposure conditions, similar to portland cement. The two

main factors that control the quality of the concrete are the w/c and the cement content. These factors influence the pore structure and determine the ingress of chemicals that may be harmful to the concrete. It has long been stated that to achieve good performance and long-term durability, CAC concrete should have a porosity below 12%, which corresponds to a w/cm of 0.4 or lower (Campas, 1998).

#### *2.4.3.1 Sulfate Resistance*

CAC concretes were originally developed for external sulfate resistance as in the case for the Paris-Lyon-Marseille (P.L.M.) Railway tunnel which was built through anhydrite and gypsum formations (Touche, 1926). Concrete used for this railway has performed excellent to date, with no distress observed in the structure or in companion test specimens immersed in gypsum solution. Similarly, excellent performance in a sulfate environment was reported by Miller and Mason (1933), where CAC concrete exhibited very good durability for over 20 years in the sulfate waters of Medicine Lake, South Dakota. In the same study, portland cement concrete failed completely within in five years, and "sulfate-resistant" portland cement lost nearly half its strength after 10 years.

In the UK in 1970, a comprehensive laboratory and field study was started by the Building Research Establishment (BRE) to investigate the sulfate resistance of concretes, which included CAC concrete. Crammond (1990) reported results after 15 years for concretes with a w/cm that ranged from 0.47 to 0.60. The CAC concrete performed well with only minimal signs of damage. An interesting observation made by BRE researchers and reported by Crammond was that a dense exterior layer was observed on the concrete specimens. The layer was comprised primarily of metastable calcium aluminate hydrates, which may explain the superior performance because the dense

microstructure prevented the ingress of anions in a sulfate-rich environment (Crammond, 1990).

In a more recent study, Dunster (200) looked at the effect of converted and unconverted CAC on sulfate resistance. It is important to note that the concrete used met or exceeded typical current recommendations, unlike the study completed at the BRE, with minimum cement content of 400 kg/m$^3$ and maximum w/c of 0.4. The study showed that unconverted specimens exposed to sulfate solutions for five years had excellent performance and were resistant to attack. However, the converted samples rapidly decayed ettringite and gypsum were present in the system (Dunster A. a., 2001).

#### *2.4.3.2 Corrosion*

Corrosion of reinforcement is the most common form of premature degradation of concrete structures. Corrosion can be initiated by compromising of the passive oxide film that forms on the steel due to the lowering of the internal pH by carbonation or by the ingress of chloride ions. The pH of CAC concrete is lower than portland cement concrete, but is still high enough to sustain the passive layer. For unconverted concrete with metastable hydrates the pH is 12.13, while converted CAC concrete has a pH of 11.97. The controlling factor to the durability of CAC concrete, as with most durability mechanisms, is the permeability of the concrete, which affects the rate of the chloride and carbon dioxide penetration (Scrivener, 2003).

#### *2.4.3.3 Chloride Diffusion*

The corrosion resistance provided to reinforcing steel by the concrete can be divided into two components: first the resistance to the ingress of chlorides and second the protection or resistance of the passive film from breaking down. For CAC concrete, there is no known data on the ingress or rate of ingress of chloride ions into hardened

concrete under laboratory conditions. The only information available highlights the long-term durability of structures exposed to seawater which has shown good performance and minimal penetration of chlorides. A concrete pier in Halifax, Canada was found to have a dense outer layer extending inward 50 mm from the surface which was comprised of AFm phases (Friedel's salt, monosulfate, etc.) and also calcium aluminate hydrates as well as the stable stratlingite hydration product (Campas, 1998). Fryda et. al. (2008) recently did a forensic investigation of a 70 year old bridge in Montrose, Scotland and found identical characteristics with the dense 50 mm surface containing chlorides and sulfates with no signs of corrosion (Fryda H. L., 2008).

A few studies do exist on the breakdown of the passive film and subsequent rate of corrosion in CAC concrete due to excessive chloride concentrations in the pore solution. Andion et al. (2001) and Goni et al. (1991) both found critical chloride threshold concentrations at 1% and found no signs of corrosion at lower concentrations. Friedel's salt was found in specimens; however it was unstable and changed due to the pore solution composition. The decomposition of Friedel's salt is attributed to the liberation of chloride ions in the pore solution which led to the depassivation of steel (Goni, 1991).

#### *2.3.3.4 Carbonation*

The reaction between $CO_2$ and calcium aluminate cement hydration products forms $CaCO_3$ and $AH_3$ regardless of the calcium aluminate hydrates (i.e. stable or metastable). This reaction leads to an increase in strength due to the decreased porosity and formation of new products unless sufficient alkalies are present to cause alkaline hydrolysis, discussed in the next section. As stated before the main concern with

carbonation is the depassivation of the reinforcing steel and potential for corrosion (Campas, 1998).

Dunster (2008) completed a study that investigated the risk of corrosion when carbonation of the cover concrete has occurred and the concrete is subsequently exposed to different internal and external environments. This study investigated CAC concrete with w/c ranging from 0.4 – 0.86 and varying relative humidity. The author showed that the risk of corrosion increases once the carbonation occurs beyond the steel reinforcement. The rate of corrosion was directly related to the internal moisture state of the CAC concrete and the rates of carbonation were the greatest at 65% RH and the slowest when exposed to wetting and drying cycles (Dunster A. , 2008).

Another study characterized the effect of accelerated carbonation on the microstructural development of hardened CAC and the long-term strength. It was shown that carbonation of the CAC resulted in a decreased porosity due to the formation of $CaCO_3$ polymorphs, vaterite and aragonite, in the pores. The decreased porosity led to an increase in the mechanical strength. In addition to forming $CaCO_3$, the conversion process is inhibited due to the preferential carbonation of $CAH_{10}$ (Gaztanaga, 2001).

#### *2.4.3.3 Alkaline Hydrolysis*

Alkaline hydrolysis is a particular form of degradation that only occurs in poor quality CAC concrete and results in the dramatic loss of strength. This form of degradation is caused by the presences of alkalis in concrete, generally from the aggregates, or from external sources. The reaction is believed to be caused by the leaching of the alumina from the calcium aluminate hydrates to form alkaline hydrates which are not well understood. This process is known to be exacerbated when combined with carbonation, which is known to attack calcium hydrates from the calcium aluminate

hydrates to form $CaCO_3$. The carbonation leaves or leaches alkalis in solution making them susceptible for alkaline hydrolysis (Scrivener, 2003).

In these cases, it is believed that the catalytic effect of alkalies tends to increase the solubility of both $CO_2$ and $Al(OH)_3$, leading to a general dissolution and loss of cohesion of the calcium aluminate hydrates. According to Scrivener and Capmas (1998), the following four components must be active in order for alkaline hydrolysis to be a concern:

- High internal porosity
- High humidity (and internal saturation)
- Presence of sufficient quantity of free alkalies
- Presence of sufficient quantity of $CO_2$

Generally, for high quality CAC concrete with w/cm less than 0.40 and cement contents greater than 400 kg/m$^3$, alkaline hydrolysis is not a concern. Also, it is generally quite rare for significant amounts of free alkalies to be present within CAC concrete. However, if alkalies enter into the concrete and concrete is relatively porous and saturated, damage may occur.

In a recent study, Andrade (2001) directly investigated alkali hydrolysis and looked for explanations why in a carbonated aluminous paste, the steel may remain passive without corrosion, but in OPC pastes carbonation always leads to steel corrosion. An unexplainable unique phenomenon was discovered when the CAC mortars became alkaline when wet to passivate the steel and spontaneously changed to neutral when the mortar was dry. Neither scenario provided the conditions to cause corrosion of the reinforcement; it was believed that the formation of the alkaline solid phase when the mortars were dry and its subsequent dissolution when wet may act as a buffering agent to maintain the pH and prevent corrosion (Andrade, 2001).

#### *2.4.3.5 Freeze-Thaw*

Historically, few studies have been completed on the freeze-thaw resistance of CAC concrete, however the data that does exist shows good performance. The main contributing factor to the performance is linked to low porosity of concretes with a maximum w/c of 0.4. CAC concrete has been used in cold climates that experience these cyclical temperatures and no problems have been identified (Scrivener, 2003). The same air-entraining agents used in portland cement concrete (e.g., vinsol resins, gum rosins, synthetics, etc.) have been shown to be suitable for entraining air in CAC concrete (Jolin, 2008).

## 2.5 INFLUENCE OF ADMIXTURES ON CAC

The use of chemical admixtures in CAC concrete mixtures is common and used for the same purpose as in portland cement concrete such as modifying setting time, rheology, strength, and cohesion in the fresh state.

### 2.5.1 Accelerators and Retarders

Generally, alkalis and alkaline compounds shorten the time until setting of CAC while acids delay setting. Many exceptions to this rule exist and can be the reverse of the intended use if low dosages of the admixtures are used (Robson, 1962). The effect of various chemicals have on time of setting of calcium aluminate cement are summarized in Table 5.

Table 5: Effect of Various Chemical Admixtures on CAC Setting (Campas, 1998).

| Accelerators | Retard at low concentrations and accelerate at high concentrations | Retarders |
|---|---|---|
| Lithium hydroxide | Magnesium chloride | Sodium borate |
| Lithium carbonate | Calcium chloride | Sodium chloride |
| Lithium sulfate | Barium nitrate | Potassium sulfate |
| Lithium chloride | Acetic acid | Potassium chloride |
| Lithium nitrate | Calcium sulfate hemihydrate | Barium chloride |
| Calcium hydroxide | Calcium formate | Sodium gluconate |
| Potassium hydroxide | | Sodium citrate |
| Potassium carbonate | | Citric acid |
| Sodium hydroxide | | Hydrochloric acid |
| Sodium carbonate | | Glycerine |
| Sodium sulfate | | Sugar |
| Sulfuric acid (very dilute) | | |

#### *2.5.1.1 Accelerators*

Solutions of sodium, potassium and calcium hydroxides as well as sodium and potassium carbonates are active accelerators of CACs. Common sulfates and nitrates accelerate the set if used in concentrations of 0.5-1% of cement by mass, however they have the opposite of effect if used in dosages below 0.25% (Robson, 1962).

Admixtures containing lithium salts are the most common form of set accelerators used in CAC concretes. Minimal additions (~0.1%) can reduce set times to just a few minutes. A lithium aluminate hydrate forms and serves as a heterogeneous nucleation site that allows for the rapid precipitation (Rodger, 1984).

Gosselin (2008) found that the addition of lithium sulfate under 20°C isothermal conditions leads to the massive precipitation of $CAH_{10}$ and only stops because of the lack of water or space for hydration products. He showed the reduction until the induction period from 9h to 1h with the addition of 0.3% lithium sulfate (Gosselin C. a., 2008).

The addition of portland cement and lime can also accelerate the hydration of CAC. When portland cement is added to CAC in increasing quantities, the setting time becomes quicker until the set becomes almost instantaneous. Combined systems are not typically used in reinforced concrete due to reduced ultimate strength seen with the faster the set times (Robson, 1962).

#### *2.5.1.2 Retarders*

Rodger (1984) found citric acid to be an effective set retarder for CAC concrete. He suggested that an amorphous protective gel coating is presumed to form around the cement grains which complicates the hydrolysis and inhibits the growth of CA hydration products. The gel formation consumes the alumina ions in solution and impedes there use for CA hydration products until the citrate from the citric acid is precipitated (Rodger, 1984).

Robson also found salts of hydroxyl-carboxylic acid, including citric, tartaric, gluconic and carbohydrate salts to be effective. Other effective retarders for CAC include chlorides of sodium, potassium, barium, magnesium, and calcium in small concentrations. When retarders are used with CAC the 1 day strength is often still higher than those cements that are not accelerated and will oftentimes still result in an ultimate strength that is less than no accelerated cements (Robson, 1962).

### 2.5.3 Water Reducers

CAC concretes are generally considered more harsh than portland cement concrete, which makes them more difficult to trowel or float, and they may also bleed excessively. Typical CAC concrete mixtures have a higher fine to coarse aggregate ratio to improve finishability, however this can increase the water/workability demand. The use of very small amounts of surface-active agents is often effective in improving the

workability due to the air entrained in the concrete. When larger doses are used more air becomes entrapped and significantly reduces the strength. Calcium lignosulfonate improves the workability, and does not retard time of setting or entrain much air when used in low dosages (Robson, 1962).

Later, Banfill investigated the use of sulfonated superplasticizers including: sulfonated naphthalene formaldehyde condensate, sulfonated phenol formaldehyde condensate, and sulfonated melamine formaldehyde condensate. He explored the use of these admixtures with a lithium citrate accelerator and a sodium gluconate retarder. The sulfonated superplasticizers were found not to be as effective as with portland cements, however the sulfonated phenol formaldehyde condensate improved the workability of CAC paste and mortar for over 30 minutes at 5 and 20°C (Banfill, 1993).

Fryda investigated the effects of poly-carboxylate based superplasticizers dosages from 0.05% to 0.40%/wt. cement to evaluate the effects on workability and time until the start of the heat of hydration ($t_{off}$). A slump greater than 150mm was achieved in CAC concrete with a w/c 0.3 and 0.1-0.2% dosage of poly-carboxylate superplasticizer. The poly-carboxylate based superplasticizer slightly retarded the time until $t_{off}$, and was offset by addition of lithium carbonate ($Li_2CO_3$) accelerator at dosages from (0.002% - 0.005%/wt. cement) (Fryda H. G., 2000).

Recently, this work was revisited and extended by the investigation of CAC with four poly-carboxylate based superplastizers with varying carboxylate group concentrations. The authors compared the adsorption and zeta potential results of different admixtures and showed that higher zeta potential with corresponding higher absorption values similar to known behavior with portland cements improving the workability. However, there was a negligible effect of the carboxylate concentrations on

these values with CAC which is counter intuitive to known behavior of portland cements (Alonso, 2011).

### 2.5.4 Latex and Polymer Resins

Latex and polymer resins have been used in civil engineering applications for some time. Generally, these materials are added to concrete overlays and flatwork that demands low permeability and improved bonding action to an existing grade. This section briefly summarizes the existing data on the application of this technology with CAC and gives broad overview of applications with portland cements and other rapid hardening cementitious materials.

For CAC, natural and synthetic latex have been successfully used to produce chemically resistant floor toppings for the building chemistry market. In addition, styrene butadiene latex, acrylic polymers, polyvinyl acetate and epoxy resins have been used to improve bonding to substrates for applications such as bridge deck repairs (Campas, 1998). Generally, the latex comprises to 6-15% of the cement mass and can create bond strengths between two concrete surfaces between 550-750 psi (Robson, 1962).

Beyond the two studies mentioned, little information exists on the addition of latex and polymer resins additions to CAC concrete. These materials have been used in combination with portland cements to minimize the time and cost of rehabilitation of distressed concrete pavements by adding the bonding agent to allow for the new overlay concrete on top of the old substrate with a decreased permeability and increased bond strength (Barenberg, 1980) (McCullough B. a., 1995).

A recent study by Yun (2007) characterized the effects of varying dosages of styrene-butadiene polymer on thermal and autogenous shrinkage of very early strength

latex-modified concrete. The study investigated the use of 5% and 15% weight of latex solids – cement ratio on a very early strength calcium sulfoaluminate cement concrete mixtures. The researchers, incorrectly, subtracted the thermal expansion associated with the increased internal temperature due to hydration by applying a static coefficient of thermal expansion factor to the fresh/hydrating cementitious system and then monitoring the autogenous shrinkage after the correction factor had been applied (Viviani, 2006). The application of this factor overestimates the amount of expansion, thus underestimating the amount of shrinkage. In addition, the authors altered the w/c of the mixtures being compared in order to maintain the same slump. This is a cause for error in the comparison of the varying mixtures (Kyong-Ku Yun, 2007).

## 2.6 BLENDED SYSTEMS

Supplementary materials are being added to CAC mixtures in an attempt to improve durability and attempt to mitigate strength reductions associated with conversion. This section presents a summary of published data on the effects of substitutions of various materials (SCMs) and the scientific understanding of their influence on the hydration process.

### 2.6.1 Portland Cement

It has been shown that the addition of CAC to portland cement is an effective way of accelerating the setting time and compensating for shrinkage. However, it has been shown that the substitution may lead to rapid or flash setting over a wide range of replacement levels (from 20-90%). This behavior is dependent on the portland cement composition and the relative amounts of each material. The flash setting is caused by the $C_3A$ in the portland cement and the lack of gypsum which is consumed by the CAC. The rapid setting is also attributed to the formation of ettringite and the acceleration of the

CAC reaction. When portland cement is used in higher rates than the CAC, the main hydration products tend to be calcium silicate hydrates and calcium hydroxide. However, when CAC is used in higher substitution amounts, the main hydration products tend to be $CAH_{10}$, $C_2AH_8$, and $C_3AH_6$ depending on the hydration temperature. With near equal substitution ranges, any form of the hydrates may be found (Campas, 1998). Amathieu (2000) confirmed these findings and elucidated the behavior through the evaluation of various portland cement chemical compositions. The study showed that different calcium sulfate phases and chemical admixtures, accelerators and retarders further complicated hydration, setting and strength development (Amathieu, 2000).

A recent study investigated the strength development of CAC mixtures with 0, 25, 50, and 75% replacement with portland cement. The study also characterized the effect of temperature on the strength development of these mixtures. The authors cured the specimens at static 20, 30, 40, and 50°C as well as initial curing of specimens at 20°C for 28 days then at 30, 40, and 50°C for a total of seven different curing regimes. Figure 11 shows the strength development of the four combinations of CAC mixtures from the seven different curing regimes.

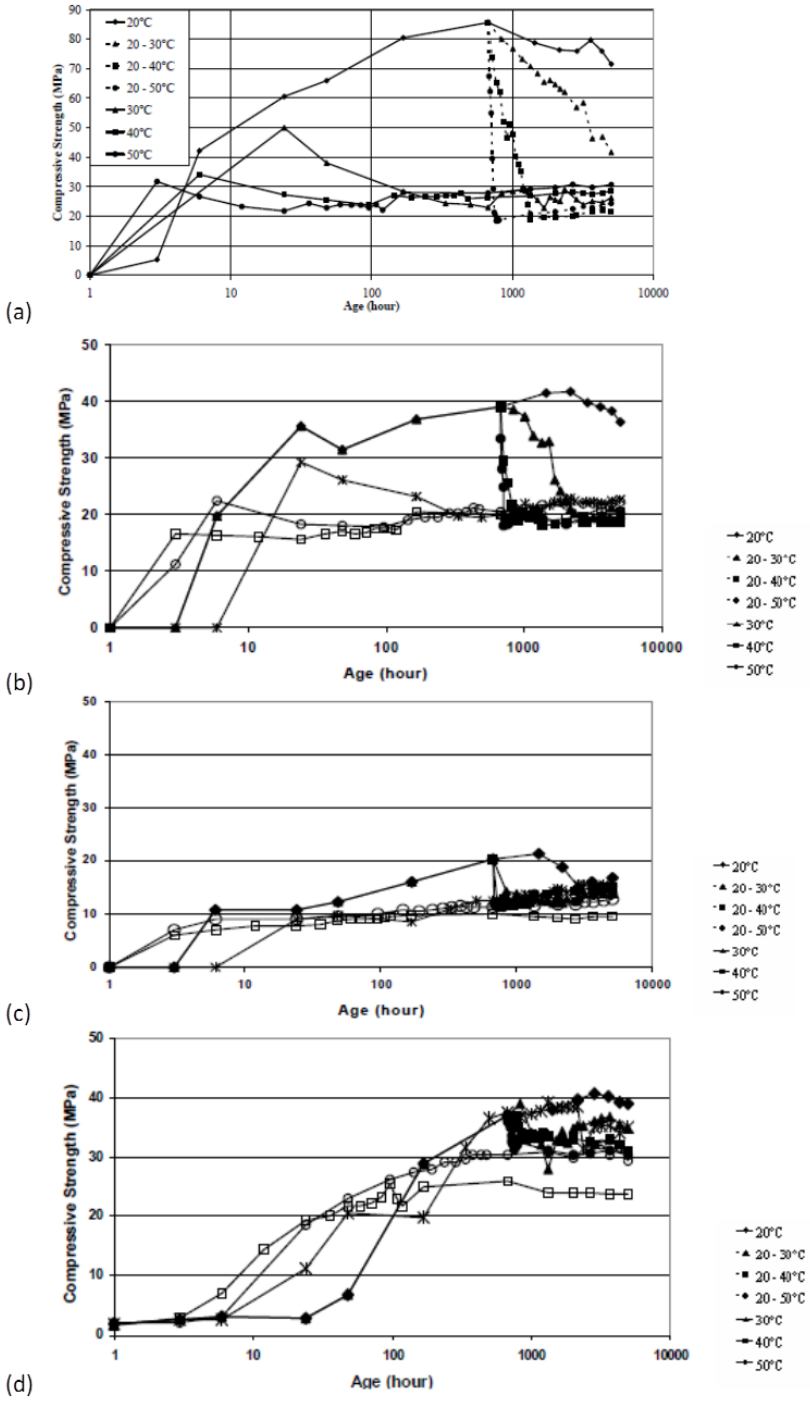


Figure 11: Compressive strength development of CAC-PC mixtures a) Mixture 100% CAC, b) Mixture 75% CAC – 25% PC, c) Mixture 50% CAC – 50%PC, and d) Mixture 25% CAC – 75% PC (Kirca, 2008)

The specimens cured at 20°C for 28 days then moved to higher temperatures had significant delays for conversion compared to those cured at higher temperatures. The CAC-PC binary mixtures behaved similarly to CAC when PC was used in lower substitution percentages and experienced a reduction in strength due to conversion. When PC was used in higher substitution percentages, the amount of calcium aluminate hydrates that formed was reduced and larger percentages of calcium silicate hydrates formed as well as stratlingite ($C_2ASH_8$). Only the mixture containing 75% PC did not experience strength reductions due to conversion (Kirca, 2008).

### 2.6.2 Slag

CAC substitution with up to 50% ground granulated blast furnace slag has been found to form a stable hydrate, stratlingite (also called gehlenite hydrate [$C_2ASH_8$]), up to a temperature of 40°C. Mixtures containing 50/50 slag and CAC have strengths that are about half that of mixtures containing 100% CAC. These mixtures showed continuous strength development for over two years with no minimum in strength associated with conversion (Campas, 1998). Ding (1995) and (1996) investigated a wide range of silica-bearing additives including slag as well as silica fume, fly ash, and sodium silicate on CAC hydration at 38°C. In all studies the addition of sodium salts enhanced the formation of stratlingite and affected strength development. While mixtures containing slag and CAC can be shown to produce long-term stable strengths, the reduction in early-age strength gain may not be a desirable outcome.

### 2.6.3 Silica Fume

Bensted (1990) investigated 30 and 50% replacement of CAC with silica fume. The study showed stratlingite to be the primary hydration product that forms between 20

and 70°C. However, at higher temperature he showed that $C_3AH_6$ had already formed after 1 day (Bensten, 1990).

Collepardi et al. (1995) investigated the replacement of CAC with 15 and 30% silica fume. The use of 15% silica fume prevented strength reductions at 20 and 40°C, due to the formation of gehlenite hydrate ($C_2ASH_8$), a stable hydration product. However, the 30% replacement of silica fume resulted in low overall strengths due to 0.4 water/solids ratio causing an excess of water for hydration of the cement (Collepardi, 1995). Complementary work was completed by Bensted (1996), which hypothesized that the addition of silica fume competes for lime therefore limiting the amount available for conversion (Bensted, 1996).

### 2.6.4 Ternary Blended - Slag and Silica Fume

Recent work completed by Gosselin (2009) and Muller (2010) investigated a ternary blended high-iron CAC with 21.5% slag and 3.5% silica fume. Mixtures cured and stored at 20°C that did not contain an accelerator were found to have a large amount of $CAH_{10}$ and $C_2ASH_8$. However, when 1.2% lithium sulfate accelerator was added to the system, the dominant hydration product was $C_2ASH_8$. At 38°C, mixtures containing 1.2% lithium sulfate formed $C_2AH_8$ and $C_2ASH_8$ at 1 day, but later at 90 days the stratlingite gave way to $AH_3$ and became less distinguishable (Gosselin C. , 2009). Muller showed that the ternary blended system was able to avoid the strength reductions associated with conversion, however the ultimate strength was far below values required for use in most general civil engineering applications (Muller, 2010).

### 2.6.5 Fly Ash

Collepardi et al. (1995) investigated the effect of 20 and 40% replacement of CAC with a low-calcium fly ash. Mixtures with 20% replacement of low-calcium fly ash showed similar strength development properties to control mixtures, however the ultimate strengths were slightly lower and strength reductions associated with conversion were observed. Mixtures containing 40% fly ash showed a drastic reduction in the ultimate strength due to the increase of the relative w/c per gram of CAC. The authors concluded the use of low-calcium fly ash to prevent the densification of hydration products was not advantageous, due to the high replacement levels needed and the low strengths (Collepardi, 1995).

In a more recent study, the replacement of CAC with 0, 10, 25, 40, and 50% with a low-calcium fly ash were explored. Table 6 summarizes the results of the compressive strengths at increasing age of the different mixtures. Fernandez-Carrasco and co-workers (2008) have shown at lower replacement levels, up to 25%, the strength development was similar to the control CAC mixture. As shown by Collepardi et. al. (1995) higher replacement levels, greater than 40%, are required to mitigate strength reductions due to conversion; however, the overall quality of the concrete is poor and not suitable for use (Fernandez-Carrasco, 2008). Thus, concluding the use of low-calcium fly ash is not beneficial for the mitigation of conversion.

Table 6: Strength development of CAC – fly ash mortars (Fernandez-Carrasco, 2008)

| | 2 days | | 28 days | | 180 days | |
|---|---|---|---|---|---|---|
| | Flexural | Compressive | Flexural | Compressive | Flexural | Compressive |
| CAC | 6.9 | 71.3±2.2 | 7.2 | 89.4±4.4 | 5.4 | 80,0±2.1 |
| 10% FA | 8.8 | 70.3±1.3 | 7.4 | 91.0±2.9 | 5.1 | 72.2±2.9 |
| 25% FA | 8.4 | 63.5±1.3 | 5.1 | 70.1±0.9 | 4.3 | 60.6±2.5 |
| 40% FA | 6.4 | 47.0±1.0 | 3.3 | 37.5±1.5 | 3.2 | 39.1±4.3 |
| 50% FA | 5.8 | 31.4±0.4 | 3.0 | 31.4±1.2 | 3.8 | 52.5±1.4 |

Ideker (2008) characterized the effects of the 30% replacement of CAC with a high-calcium fly ash. He found the replacement to have minimal impacts on the isothermal shrinkage behavior seen at 20°C. However, a reduction, proportional to the replacement level, in the early-age expansion seen at 38°C was observed. Parallel isothermal mechanical testing was done with the two previous mixtures, a 30% replacement led to similar strength development to control mixtures and negligible reductions in compressive strength in those specimens cured at 38°C (Ideker, 2008).

Gosselin investigated the heat of hydration and microstructural development of four fly ashes, slag, and silica fume combined with CAC. The heat flow of these binary blended systems is shown in Figure 12. The corresponding CaO percentages are 27.92%, 4.9, 3.73, and 0.23 for FA1, FA2,FA3, and FA4, respectively. A distinct difference in the heat of hydration behavior was seen with the only high calcium fly ash ($CaO = 27.92\%_{wt}$) compared to the control and all other SCMs; however, the cumulative heat was the greatest with this SCM. From this work it was evident that the space is the limiting factor controlling the heat of hydration of the different SCMs. For example, the cumulative heat of the slag mixtures was higher than the mixtures containing fly ash due to the increased density of the slag allowing more room for hydration to occur (Gosselin C. , 2009).

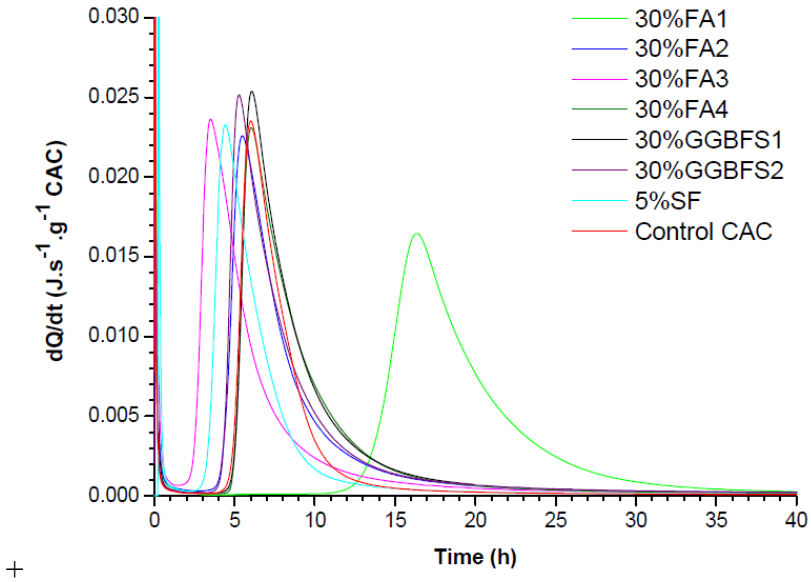


Figure 12: Heat flow of Fe-low CAC substituted by 30% fly ash, 30% slag, 5% silica fume (Gosselin C. , 2009).

### 2.6.6 Fillers

*Fine Grade Quartz Sand*

Gosselin (2009) investigated the addition of fine grained quartz sand as a source of nucleation and growth of hydrates for CAC. The addition of the fillers accelerated the kinetics of hydration by the creation of nucleation sites. The study showed that even without the addition of lithium sulfate accelerator, the increasing addition of sand increased the kinetics. However, when lithium sulfate was used, the induction period was extended when less than 30% of sand was added; but above 30% the induction period was shortened. This was attributed to the absorption of lithium sulfate by the mica mineral present in the filler (Gosselin C. , 2009). It was shown that the addition of fillers has the potential for accelerating the hydration process; however, it can be complicated with addition of other admixtures. Further work is needed to characterize the interaction between certain minerals and chemical admixtures.

*$CaCO_3$*

The use of limestone filler was said to lead to the formation of stable hydration product monocarbonate by Fischer & Kuzel (1982). These results were later confirmed by Bachiorrini (1986) and Trivino (1986) and concluded that strength loss could be avoided with sufficient use of $CaCO_3$. Later, Fentiman had doubts about the long-term stability of these hydration products and said that he found indication of conversion (1985). Later, Kuzel and Baier address the contradictory arguments by finding the addition of $CaCO_3$ to CAC with low $SiO_2$ contents led to the formation of stable hydrates, monocarbonate and gibbsite, up to a temperature of 90°C and under 100% RH. Indications of conversion were found in cements that contained more $SiO_2$, and the amount of conversion was directly proportional to the available amount of $SiO_2$ (Kuzel, 1996).

## 2.7 Applications, Assessment, and Specifications of CAC Concrete

This section is designed to summarize and update existing documentation of common and novel applications of CAC concrete as well as summarize existing literature on the long-term performance. In the final section, a summary of current specifications for CAC and rapid repair materials is presented.

### 2.7.1 Applications of CAC Concrete

As described earlier in this chapter, CAC concrete exhibits several unique characteristics that make it especially suitable for certain specialty applications. The unique properties below are those that make CAC concrete ideal candidates for such specialty applications:

- Rapid hardening with setting times similar to those of portland cement

- Resistance to attack by acids and some other chemicals aggressive to Portland cement
- Ability to withstand repeated heating to high temperatures
- Ability to withstand low temperatures in placing and use
- Resistance to abrasion and impact with appropriate aggregates
- In mixtures containing Portland cement, calcium sulfate or both, the ability to form ettringite which can lead to controllable setting and hardening, shrinkage compensation and combination of free water.

Some key applications that harness the benefits of the above properties are briefly described next.

#### *2.7.1.1 Rapid Hardening*

The most common use of CAC concrete is when very rapid strength development is needed such as industrial applications where the rapid repair is important, when used as shotcrete for tunnel linings, rapid repair of bridges and roadways, and cold weather placement. When used in civil engineering applications with proper accelerator dosage CAC concrete generally falls into the category of very-ultra high performance according to ASTM C 1600 (2011). The typical requirements for strength are 20.7 MPa (3000 psi) at 3 hours for civil engineering applications and rapid repair of roadways (Barborak R. , 2010).

A key contribution of this rapid hardening ability of calcium aluminate cement is to allow placement at low temperatures, which is done by maintaining a low w/c and high cement content. It has been found if the concrete mixture temperature remains above freezing for 3 hours after cement comes into contact with water then the heat of hydration will be enough to harden the cement and allow for normal strength development. This

property is used in Canada to build foundations in frozen ground and for repair of industrial cold storage rooms (Campas, 1998).

CAC concrete is also used for the rapid repair of airfield pavements to prevent closure of runways. A recent case occurred in Northern Norway, when the runway joints were replaced over night at temperatures near 5°C. A CAC mortar was used with 12% silica fume and lithium carbonate accelerator to obtain the rapid strength development needed to allow for the overnight repair of the runway and have it develop adequate strength prior to the next morning (Justines, 2008).

#### *2.7.1.2 Abrasion and Impact Resistance*

CAC concretes have been known to perform well in highly abrasive environments including in the spillway of dams, sections of roadway subjected to heavy wear, and industrial floors. CAC concretes have shown superior resistance to abrasion compared to portland cement concretes. The improvement in CAC over portland cement is attributed to the better particle packing in the interfacial transition zone between aggregates and cement hydrates. The CAC particles infill the space better and create a better bond with the aggregate (Scrivener, 2003)

#### *2.7.1.3 Pipes*

Calcium aluminate cements have excellent resistance to acids, especially acids produced from bacteria in sewers. Hydrogen sulfide gas is produced by the bacteria which can lead to degradation at the top or along the water-line of pipes. CAC has been shown to perform excellently due to the insolubility of alumina hydrates and the inability of bacteria to penetrate on the surface (Scrivener, 2003).

#### *2.7.1.4 Refractory Resistance*

CAC concrete is known to be very resistant to heating and thermal shock. Portland cements have a high lime and silica content which have lower melting points than CAC and make them unsuitable for use in the refractory market. The ability of CAC to resist heat is related to the alumina/lime ratio, thus with the higher alumina content the "whiter" the cement color (Campas, 1998).

However, the standard gray CAC (~40% $Al_2O_3$) used in civil engineering applications is considered to be a heat-resistant concrete. These concretes can resist temperatures up to 900-1000°C with the proper aggregates. This type of concrete is hard and abrasion resistant making it popular for use on industrial floors in industries such as steel and aluminum foundries. This concrete can also be used in fire training areas that might be set on fire multiple times throughout the day (Campas, 1998).

### 2.7.2 Assessment of Existing CAC Concrete

This section reviews existing publications on the long-term performance of CAC concrete. It is designed to give a review of the history of the cement, but transition to clarify the background of its use and important events. The cases are presented in a chronological order from the time of construction or the failure occurrence.

From the time of its first patent in 1909, calcium aluminate cement had difficulties. The early challenges were caused by inconsistency in the quality control of the manufactured product which resulted in batches of cement that had excellent chemical composition while others were deemed useless. A process was later improved by the Lafarge Company by 1913 when the material began being sold to the French government for use in gun emplacements. Later, as mentioned earlier, the cement was used for the construction of the P.L.M. railway tunnel in 1916 (Midgley, 1990).

In the 1920s, CAC was introduced to the United Kingdom and was used to build a bridge in Fingringhoe in Essex that is still standing today. From this time until the 1950s there were key findings about the unique microstructural development and strength loss. Thomas and Davey noted a loss of strength in warm wet conditions and named the process "inversion" (1929). Later, Lea and Desch proved that the loss of strength was due to the densification of calcium aluminate hydrate polymorphs and this process then became known as "conversion" (Midgley, 1990).

Research continued from the late 1920s until through the 1950s on the characterization of this strength loss. In 1940, guidelines for use of high alumina cement were published by the British Standard Code of Practice that covers the structural use of reinforced concrete in the U.K. Recommendations for curing and wetting the formwork for freshly placed CAC concrete were given as well as warning against placing CAC concrete at high ambient temperatures or in large masses were published (Midgley, 1990).

Known for the high early-age strength properties CAC started being used in the prestressed industry in the 1950s, which allowed for daily production cycles and stressing of concrete at 18 hours. Over the next few years from the practical use of the material, the prestressed industry determined that if the w/c was kept low and the curing temperatures were kept below 30°C that the concrete would not lose strength (Newman, 1960) and (Concrete Society, 1997).

In 1964, British Standards Code of Practice for precast concrete published new guidelines for use of calcium aluminate cement which included (Midgley, 1990):

1. A w/c of not greater than 0.50 for reinforced concrete and 0.40 for prestressed concrete should be used.
2. The concrete should be kept cool and moist during the first 24 hours.

3. The concrete should be kept reasonably dry and cool after its initial curing.

From the 1960s the use of CAC was widely used in prestressed beams with no signs of problems. However in 1973 and 1974 there were three cases of CAC beams had collapsed which included the University of Leicester, the Camden School for Girls, and the Sir John Cass School (Midgley, 1990).

At the University of Leicester the Bennett Building was constructed of precast prestressed CAC concrete where the roof was supported by a ring beam which rested on CAC concrete columns. The failure occurred between the ring beam and column connections due to inadequate bearing surface and inadequate concrete mixture design. It was later determined that the concrete was made with the incorrect specification with too high a w/cm, approximately 0.5 w/c, and too little cement. There were no accounts of the possibility of the loss of strength due to conversion and the strength loss was not thought to be relevant. The engineers concluded the failure was due to insufficient bearing surface for the ring beams and the loss in strength merely aggravated the failure. The CAC precast beams which had fallen to the ground were later re-used in the reconstruction (Midgley, 1990).

The second failure was at the Camden School for Girls where there was a collapse of the roof of the main assembly hall. The failure was attributed to the insufficient bearing of the prestressed concrete roof beams and inadequate details on the development length of the reinforcement in these connections. The investigation concluded that there was a reduction in strength due to conversion, but the strength reduction did not cause the strength to drop below the specified requirements. It was concluded if the joint detail was done satisfactorily the reduction in strength of the concrete might not have caused failure.

The third failure occurred at the Sir John Cass's Foundation and Red Coat School on the roof of the swimming pool. The prestressed concrete beams that spanned over the pool were covered with a plaster (gypsum, calcium sulfate hydrate) coating and were exposed to a wet warm environment. The concrete was found to be highly converted and had a high porosity which made it vulnerable to sulfate attack. The concrete in the beams was found to have w/c that ranged from 0.45 to 0.64 and contained ettringite which was a result of sulfate attack. The failures were later attributed to sulfate attack which was a consequence of high w/c.

After the series of events in 1973/1974, the Department of the Environment in the United Kingdom issued a document titled, "High Alumina Cement Concrete in Buildings," which warned people that all buildings made of CAC were suspect. The document required that action be taken on those buildings with the greatest risk and that CAC should not be used in structural applications (Midgley, 1990). This document led to the inspection of 1022 buildings and led to the repair and replacement 38 of those structures that were deemed hazardous, however only one of these structures was due to the loss of strength. There were believed to be around 30,000-50,000 structures containing CAC concrete at the time of the investigation (Scrivener, 2003).

Pre-cast, prestressed CAC concrete beams manufactured during the same era also experience problems in Spain in the 1990s. The worst instance happened at the "Tora de la Peira" apartment complex which experienced a major collapse. The failure was caused by poor quality concrete with high w/c and poor-quality aggregates which led to alkali hydrolysis of the highly porous concrete (Scrivener, 2003).

Today, thousands of CAC concrete structures still remain in service and the design approach for the future is aimed at expecting full conversion and designing for the

worst case scenario of the minimum strength would have prevented the collapses that did occur (Concrete Society, 1997).

### 2.7.3 Current Specifications for Use of CAC

On the market today, there are a wide selection of alternative and rapid hardening cementitious materials which generally are not incorporated in most building codes and specifications. Through the work of the CAC scientific network, it is planned to develop a test specification to capture and quantify conversion of calcium aluminate cement. The goal of the specification will be to provide a testing technique that encourages conversion to occur in the first few days after casting and allow for the determination of the ultimate lowest strength.

There are quite a few documents that are available that reference calcium aluminate cements very briefly and merely mention it as a rapid hardening cementitious material. A few documents and organizations warned against its use due to the strength loss including the American Concrete Pavement Association (1998) which is then referenced by the California Department of Transportation (CalTrans) in their guidelines for partial depth repair (Transportation, 2008).

Currently, the only specification and guidelines developed specifically for calcium aluminate cement were developed by the Texas Department of Transportation (TxDOT), TxDOT SS-4491 (Class CAC Concrete), by Barborak. Minimal strength requirements are specified for trial batching of concrete to reach 3000 psi compressive strength in 3 hours for ambient cured cylinders and an ultimate compressive strength of 4000 psi at 24 hours for cylinders cured in a semi-adiabatic curing box. This specification gives recommendations for construction to avoid cold joints, segregation, and proper curing. Testing of concrete poured for a job has the same strength

requirements as the trial batching, however this procedure aims to identify the minimal strength that will be experienced due to conversion. This is done by placing a temperature requirements on cylinders cured in the adiabatic box. If the cylinder temperature does not exceed 140°F then, the 7-Day strength, termed ultimate strength, will be required to be twice the design strength (Barborak R. , 2010). It is important to note TxDOT published a complementary document in August 2010 which provides more technical background and recommendations for use. The document provides additional clarification and mixture design recommendations for engineers (Barborak R. a., 2010).

A specification published by the American Society for Testing and Materials (ASTM), ASTM C 1600, is a specification that covers all rapid hardening hydraulic cements. The specification classifies cements based on the very early-age strength development and does not look at specific cement compositions. The document separates the cements into four different categories, Ultra, Very, Medium, and General Rapid Hardening Cements, and differentiates the cements by compressive strengths at different time intervals, 1.5 h, 3 h, 6 h, 1 day, 7 days, and 28 days. This specification also places limitations on cracking and durability behaviors in standardized test including, drying shrinkage, sulfate resistance, alkali-silica reaction resistance, and heat of hydration (ASTM C 1600, 2011). Calcium aluminate cements meet the requirements of this practice, however, the specific testing involved (ASTM C 105 mortar cubes) requires a w/cm of 0.50 which is not appropriate for use with CACs (as outlined in numerous places in this review). Therefore, it is recommended that a separate test specification be developed specifically for CAC concrete owing to its unique properties.

## 2.8 SUMMARY

A wide scope literature review was presented in this section. This array of topics was chosen to provide the reader with an overview of CAC from the microstructural level to durability to the known field performance. This literature was written to set the tone for the dissertation and the array of topics covered within it.

# Chapter 3: Experimental Materials and Procedures

This chapter describes the materials and testing procedures used to evaluate calcium aluminate cement based-systems in this dissertation.

## 3.1 MATERIALS

A variety of SCMs and chemical admixtures were investigated throughout this dissertation to characterize their effects on the hydration and early-age volume deformation. This section provides insight into the raw chemical compositions of the materials.

### 3.1.1 Cementitious Materials

Four CAC based-systems were investigated in this dissertation. These systems include plain CAC, ternary blended CAC with slag and silica fume, and binary blends of CAC with limestone and high-calcium fly ash substituted separately. Certificates of their analysis are shown in Appendix A.

The plain CAC, referred to as "CAC" throughout the dissertation investigated was sold on the market under the trademarked name, "Ciment Fondu." This was typical high-Fe calcium aluminate cement typically used for construction practices. Typical Fe concentrations for this grade of CAC range from 12-20% (Scrivener, 2003). Shipments of this plain Fondu were received in the spring 2009, Fall 2010, Spring 2011. The cement was regularly replaced to minimizing aging. All cement was stored double wrapped in plastic bags closed in 200 L (55 gal.) plastic drums in a closed outside storage unit. The XRF analysis of the cementitious system is shown in Table 7.

The ternary blended CAC with ground granulated blast furnace slag (GGBS) and silica fume (SF), referred to as "TCAC" throughout the dissertation, was sold on the market under the trademarked name, "LBC." This pre-blended mixture of cementitious

materials consisted of a 75% high-Fe CAC, made from a different bauxite source than the plain CAC, 21.5% GGBS, and 3.5% SF. Since, the materials were pre-blended it was not possible to get the separate components of the materials for XRF analysis. One shipment of this material was received in the Spring 2009, all testing was completed within the first year of receiving the material. The XRF analysis of TCAC is shown in Table 7.

Binary blends of plain CAC with pure calcium carbonate or limestone and high-Ca fly ash were investigated with 20% and 30% replacement, respectively. The blend of CAC and limestone was given the nomenclature "CAC-LF," and the blend of CAC with high-Ca fly ash was given the nomenclature "CAC-FA." The XRF analysis of these two SCMs is given in Table 7.

Table 7: XRF oxide analysis

| Oxides %wt | $SiO_2$ | $Al_2O_3$ | $Fe_2O_3$ | CaO | MgO | $Na_2O$ | $K_2O$ | $TiO_2$ | $Mn_2O_3$ | $P_2O_5$ | SrO | BaO | $SO_3$ | LOI |
|---|---|---|---|---|---|---|---|---|---|---|---|---|---|---|
| CAC | 5.93 | 39.15 | 14.23 | 35.34 | 0.70 | 0.08 | 0.19 | 1.75 | 0.48 | 0.17 | 0.03 | 0.01 | 0.16 | 1.81 |
| TCAC | 14.44 | 34.29 | 11.18 | 35.06 | 2.07 | 0.07 | 0.18 | 1.55 | 0.20 | 0.06 | 0.03 | 0.03 | 0.62 | 0.22 |
| FA | 30.78 | 17.44 | 5.89 | 29.00 | 6.47 | 2.19 | 0.34 | 1.37 | 0.05 | 0.86 | 0.47 | 0.71 | 3.83 | 0.60 |
| LF | 0.16 | 0.10 | 0.12 | 55.93 | 0.31 | 0.00 | 0.01 | 0.00 | 0.01 | 0.01 | 0.01 | 0.00 | 0.03 | 43.32 |
| CSA | 14.22 | 15.58 | 0.98 | 49.84 | 1.46 | 0.16 | 0.47 | 0.57 | 0.07 | 0.11 | 0.16 | 0.02 | 14.73 | 1.64 |

### 3.1.2 Chemical Admixture Characteristics

Results of the influence of four different chemical admixtures are presented throughout this dissertation. The admixtures investigated included an accelerator, a high range water reducer, a retarder, and a latex modifier.

The main accelerator investigated throughout this dissertation was lithium sulfate ($Li_2SO_4$), referred to as "LSA" throughout the dissertation. This chemical admixture was investigated at dosage rates of 0.5%, 1.0% and 1.75% of the weight of CAC. The higher application rates are unique to this dissertation, and are based off dosage rates used in actual field repairs where high early-age strength was required, usually 20 MPa (3000

psi) in three hours. These dosage rates had been proven to achieve these strict strength requirements based-off conversations of observations by contractors and field engineers.

A high range water reducer/retarder was investigated for controlling setting time and providing workability. This HRWR was sold on the market under the trademark name, "Optima 203." This admixture conforms to ASTM C 494, Standard Specification for Chemical Admixtures for Concrete, Type A – water reducing, Type F – water reducing, high range, and Type G, water reducing, high range and retarding (ASTM C 494, 2011). This is a polycarboxylate based water reducer that was applied at dosage rates of 0.5% and 1.0% of the CAC weight.

Citric acid was investigated as a retarding agent to use in combination with LSA accelerator. This admixture provided the working time required to cast the large-scale field specimens presented in the Chapter 7. This anhydrous fine granular citric acid was investigated at dosage rates of 0.25% and 0.5% of weight of cement. It is important to note that the citric acid was dissolved and stirred prior to mixing in all experiment in the mixing water to allow for even distribution.

A latex modifier chemical admixture was investigated for use for thin-bonded concrete overlays. The admixture investigated was sold on the market under the trademark name, "Dow Modifier A," which was a styrene butadiene polymeric emulsion with an anti- foaming, de-airing, agent. The admixture had 47.2% solids and 52.8% water by mass. When used, 15% latex (weight of solids to weight of cement) was used and water addition from the latex was removed from the mixing water to maintain consistent w/c.

## 3.2 MIXTURE PROPORTIONS AND PROCEDURES

Mixture proportions varied for each experimental investigation. The details of typical mixture designs and procedures are presented in the following section with the corresponding experiments.

## 3.3 PROCEDURES

This section introduces and provides some historical background and references for different testing procedures. These sections were not written to be a full depth discussion of the techniques and mechanisms behind the research; references to more detailed explanation documents summary documents are provided. This section was written to provide a "hands-on knowledge" of each experiment, and to provide clarity of the techniques to allow for future recreation of the testing if sought by the readers.

### 3.3.1 Isothermal Calorimetry

Generally, isothermal calorimeters are temperature controlled chambers with a thermostat and heating and cooling fan which is used to maintain the isothermal testing conditions. Inside of the chamber are generally multiple smaller cells in a large mass of aluminum. These cells act as thermal heat sinks, where the cementitious samples are inserted in closed vials. These heat sinks direct the heat flow outward through the bottom of the chamber through the use of Peltier solid-state active heat pump where the heat flow is recorded by a heat flow sensor and the difference is compared to another heat flow sensor attached to an inert material (Anatychuk, 1979) and (Microsystems, 2011). Since the heat is directed away from the sample little heat generation occurs inside of the specimen and isothermal conditions are achieved (ASTM C 1679, 2009).

Two isothermal calorimeters were used in research described in this dissertation; one was the Grace AdiaCal TC, which is an isothermal calorimeter capable of testing

paste, mortar, and concrete specimens. The other calorimeter described in the Chapter 4 was built specifically for CAC based-systems. Paste and mortar mixtures were mixed following ASTM C 305 and the materials were pre-heated or cooled to the isothermal testing temperature to minimize the amount of time to reach thermal equilibrium in the experiments (2006). A 0.40 w/cm ratio was used for the characterization of CAC based-systems in Chapters 4 and 5.

### 3.3.2 Qualitative X-Ray Diffraction

Qualitative X-Ray Diffraction (XRD) was performed on hydrated CAC based-systems to characterize the microstructural development of various CAC and CAC based-systems. The hydrated cement samples were cured at 20°C and 38°C isothermal curing in the isothermal calorimeter. Hydration was stopped on the samples at 1 hour, 4 hours, 8 hours, 1 day and 3 days to allow for characterization of the microstructural development at early-ages. The solvent exchange method was used to stop the hydration of the samples after they were removed from the calorimeter at the specified time slots. The samples were immediately crushed and submersed in acetone and soaked for 48 hours. The samples were then removed, ground, and passed through a No. 325 sieve and placed in under a vacuum desiccator for at least 24 hours or until testing in XRD.

A Siemens D500 diffractometer with a DacoMP controller was used for the XRD. The samples were scanned from 5 - 70° 2θ with a 0.02° 2θ step size and a 4 s dwell; the total scan time for all samples was 3.6 hours.

### 3.3.3 Chemical Shrinkage

Chemical shrinkage was used to track the rate of hydrate reactions of various CAC and CAC based-systems. Chemical shrinkage is the absolute volume reduction associated with the hydration reactions of cementitious materials (Jensen O. a., 2001).

The two main techniques used for measuring the chemical shrinkage of hydrating cement paste are the buoyancy method and the dilatometry method. The buoyancy method monitors the change in buoyancy of hydrating cement sample suspended in paraffin oil. Cement paste is placed in a glass dish and is covered with a uniform layer of water. The water is then covered with a uniform layer of paraffin oil and is then gently placed in a temperature controlled beaker of paraffin oil. The specimen is hung from a scale, and the change in buoyancy is recorded as the water is sorbed into the sample (Sant L. a., 2006) and (231R-10, 2010). An illustration of the buoyancy method is shown in Figure 13.

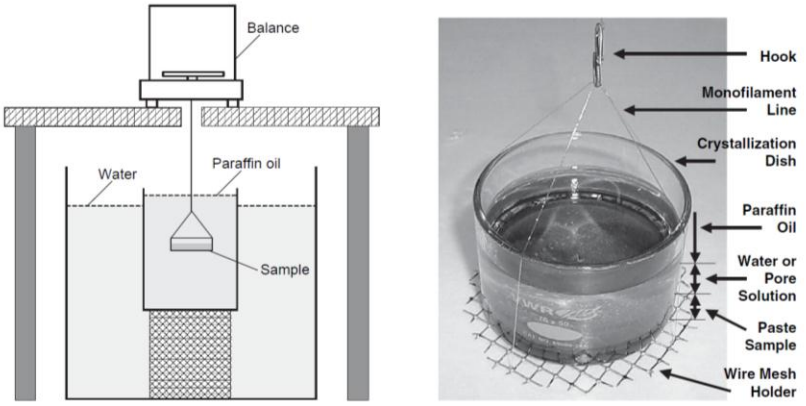


Figure 13: Illustration of the buoyancy method for measuring chemical shrinkage (Sant L. a., 2006)

The dilatometry method measures the direct water absorption into a cement paste sample. This technique was developed into a standard, ASTM C 1608. This method was used throughout the research reported in this dissertation to characterize the hydration reactions of CAC based-systems. A small cement paste sample, approximately 5 mm to 10 mm tall, is placed in a small glass vial. De-aired water is then placed over the top. Then a rubber stopper with a graduated pipette into is inserted into the vial. The water in the vial moves into the pipette and a small drop of oil is placed on top to prevent

evaporation. In the standard method, visual measurements are taken every 30 minutes or 1 hour for the first 8 hours and then periodically thereafter for 24 hours (231R-10, 2010). An illustration of the dilatometry method is shown in Figure 14.

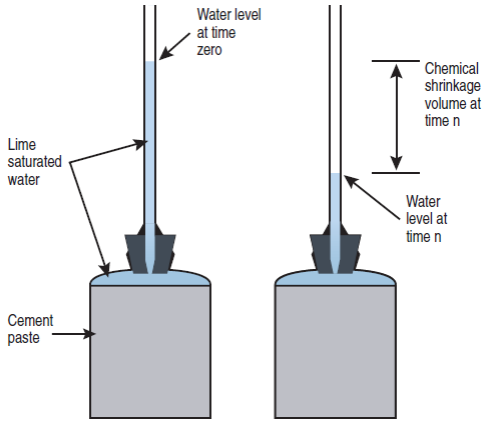


Figure 14: Illustration of the dilatometry method for measuring chemical shrinkage (Kosmatka, 2008)

The dilatometry method was automated in this study through the use of image analysis software. This improvement was used for measuring the chemical shrinkage for 14 days. A red indicator die, transmission oil, is placed on top of the water in the graduated pipette and a computer controlled web camera is used to monitor the height of the die. The webcam records pictures every 5 minutes for the typical 14 days of testing. Then, the images are analyzed by image analysis software that was developed by Bishnoi in the Laboratory of Construction Materials (LMC) at Ecole Polytechnic University in Lausanne, Switzerland (2009). Later, this technique was implemented by Ideker to characterize the hydration of CAC systems where he found that the specified glass vial would crack due to expansion of CAC at elevated temperatures, so he implemented an

improved method of using plastic vials (2008). Later, this work was continued by Fu (2011), where he used the technique to identify conversion of CAC at 38°C by the increase in the uptake of water due to the increase in porosity of the (Fu, 2011).

This automated version of ASTM C 1608 was implemented throughout the research reported in this dissertation to evaluate the hydration reaction of CAC based-systems (2007). CAC samples were mixed according to ASTM C 305 and had a w/cm of 0.40 for all test (2006). A 12 g sample weight was used for all mixtures. Tests were run for 14 days and pictures were taken every 5 min. A picture of the experimental setup is shown in Figure 15.

Figure 15: Experimental setup for chemical shrinkage at UT Austin

The chemical shrinkage experimental setup at UT Austin is capable of testing 12 specimens at once. There are two webcams setup on either side of the sample holders, which hold six samples on each side. The webcams are connected to two separate computers to record the images. Foam insulation boards are placed over the water bath to

mitigate evaporation of the water and temperature changes of the room. An example of the test photographs is shown in Figure 16.

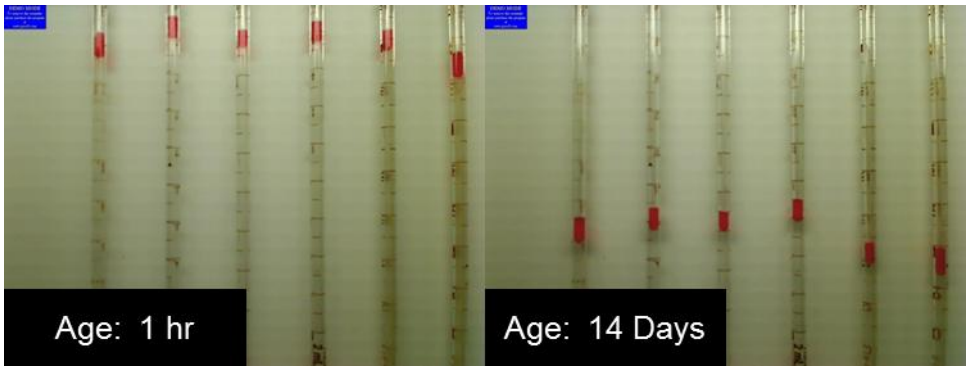


Figure 16: Example chemical shrinkage at 1 hour and 14 days

The chemical shrinkage at 1 hour and 14 days after testing is shown in Figure 16. The water uptake is noted by the movement of the red indicator dye downward over the duration of the test. To achieve acceptable repeatable between mixtures, over a year of experiments were performed. After validating the repeatability of the experiment, over 200 chemical shrinkage mixture tests of CAC based-systems were performed and are presented in Chapters 5 and 6.

### 3.3.4 Autogenous Deformation

Autogenous deformation was used to characterize the early-age volume change of various CAC and CAC based-systems to provide an understanding of the potential for early-age cracking. Autogenous deformation is the apparent volume change of a cementitious system due to the lowering of the internal relative humidity (Jensen O. a., 2001). It has been shown that autogenous shrinkage is equal to chemical shrinkage until the time of set (Sant G. D., 2009). Self-desiccation shrinkage occurs after the setting time. The amount of self-desiccation shrinkage increases with the lower w/c. When the

water evacuates the pores and participates in the hydration reaction, capillary stresses build due to the vacant pores and result in shrinkage strain (Sant G. L., 2006) and (231R-10, 2010).

There are two main techniques used for evaluating the autogenous shrinkage: the linear method and the volumetric method. The linear, dilatometer, method is performed by placing cement paste in a corrugated polyethylene tube and measuring the linear deformation using displacement transducers (Lura P. a., 2007). The method allows for direct correlation to linear strain. This method does not start until the paste has set. This method has been standardized and is now specified as ASTM C 1698 – Standard Test Method for Autogenous Strain of Cement Paste and Mortars (2009). Despite being the standardized test for monitoring autogenous strain, this method was not chosen for use in this dissertation for a few reasons. First, it would be difficult to maintain isothermal conditions of the large sample size, 29 x 420 mm (1.14 x 16.5 in.) if CAC were used in this experimental setup. Since, the measurements do not begin until after setting the early-age behavior is not captured (Jensen O. a., 1995), (Jensen O. a., 2001), (Lura P. a., 2007), and (ASTM C 1698, 2009). Thus, the volumetric method was implemented throughout the dissertation.

Generally, the volumetric method for measuring autogenous strain monitors a change in mass of a sealed paste sample in an elastic membrane, typically a polyurethane or latex condom, suspended in paraffin oil (Lura P. a., 2007). This method allows for the initiation of measurements immediately after mixing the sample; compared to the linear method where measurements are not started until set (Jensen O. a., 2001). This method requires a smaller sample size, from literature the recommended sample size is 100-150 g for PC, but a smaller size was used for the results presented in this dissertation. The lack of rigid contact between the elastic membrane is a disadvantaged to this experiment.

Large inter-user errors exist for this testing technique caused by minor flaws when preparing the sample including: entrapping air bubbles, bleeding, and the tightness of membrane (Jensen O. a., 2001), (Sant L. a., 2006), and (Lura P. a., 2007).

The experimental setup used for research reported in this dissertation at The University of Texas at Austin is shown in Figure 17.

Figure 17: Autogenous deformation experimental setup

The experimental setup of two side-by-side autogenous deformation experiments is shown in Figure 17; it should be noted that the scales are covered with a box to prevent "wind" from vibrating the scale. Two Ohaus Adventurer Pro AV812 scales, with a sensitivity of 0.01 g and capacity of 810 g, are used to record the mass directly by RS-232 connection to two computers. It should be noted that other researchers have begun using more precise scales typically with a measure sensitivity of 0.001 g (Lura P. a., 2007). The scales are placed on a solid wooden table with a concrete countertop with holes to allow for the samples to hang from the scales. A VWR 1156D

heated/refrigerated water bath is used to maintain the isothermal temperatures of two 1 L beakers, which are filled with paraffin oil.

Samples are mixed according to ASTM C 305 and placed in Trojan Supra polyurethane condoms. Mixtures investigated in this dissertation had a 0.35 w/cm. The condoms are wiped off any lubricant with paper cloths prior to filling with paste. The condom is placed on the scale in 50 mL beaker, and both were torn out. After mixing, a spatula is used to wipe the paste to one side of the mixing bowl and the paste is poured directly into the condom using a small funnel. For CAC, the average sample size used for this experiment is between 75-90 g. Examples of finished specimens are shown in the Figure 18.

Figure 18: Example samples for autogenous deformation testing

Examples of test samples that had acceptable repeatability are shown in Figure 18. These specimens were prepared by pouring the approximate weight of paste into the sample, then vibrating the sample by hand or with an ultrasonic vibrator for approximately 30s to remove any air bubbles. A small plastic zip-tie with mono-filament

fishing line pre-tied to it was slipped over the tail end of the condom. The top portion of the condom was pinched, so that a little paste was between the fingers inside the condom. Then, the sample was spun 5-10 times to tighten the membrane. Once the membrane was taut and the sample had a near spherical shape, the zip-tie, already on the sample, was tightened. The tail-end of the zip-tie was cut and the tail end of the condom was cut just above the zip-tie. The cut condom tail was weighed and the weight of the paste in the tail was subtracted from the weight of the sample. The sample was then hung from the hook below the scale and the measurements were initiated. Measurements were taken at 60 s intervals for 72 hours. At the end of the experiment, the samples were removed from the setup and weighed. This was done to ensure that no mass change of the sample occurred due to the uptake of oil. If the sample mass changed by 0.02 g than the data were discarded.

Analysis of the results from this experiment has been plagued by the problem of when to accurately identify the zero point or the starting point of the strain measurements, which is the time of set. Sant and Weiss (2006) investigated a few techniques including the identification of the deviation of chemical shrinkage and autogenous shrinkage, identifying time of setting from Vicat, electrical conductivity, and acoustic emission, and the use of Chebyshev polynomials to smooth the data to allow for the instantaneous time derivative to be calculated a specific point in time (Sant G. L., 2006). For the research reported in this dissertation, the technique of identifying the point of deviation of chemical shrinkage from autogenous shrinkage was used. An example curve is shown in Figure 19.

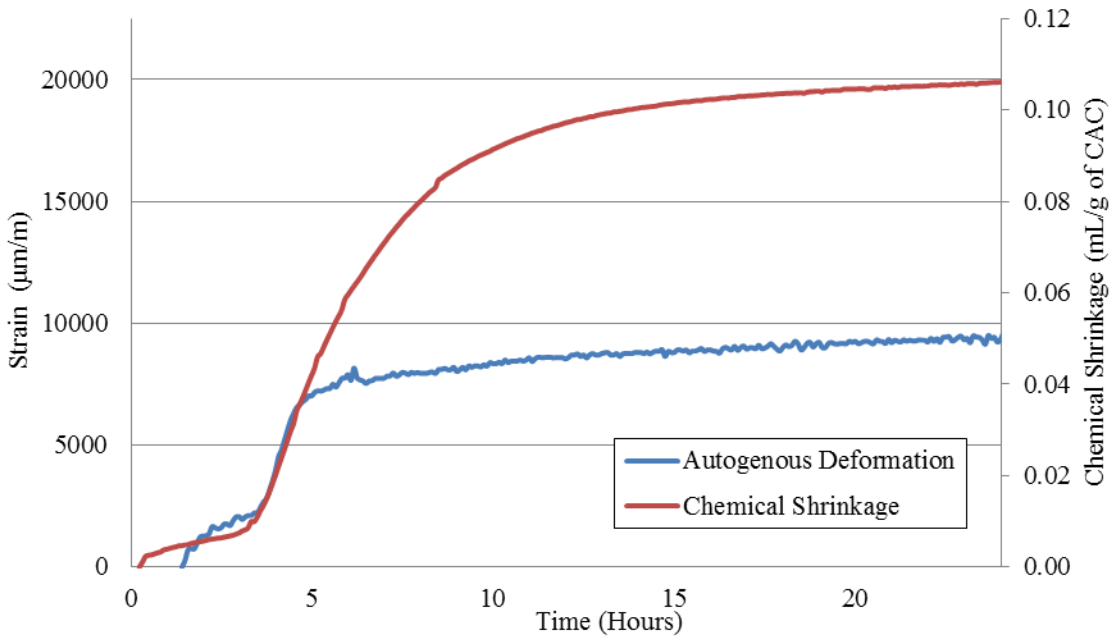


Figure 19: Example deviation of chemical shrinkage and autogenous deformation

In Figure 19, a clear deviation appears when the chemical shrinkage continues and the autogenous shrinkage slows, which is taken to be the time of set. This point was chosen as the zero point for autogenous strain measurements.

Many iterations of this experiment took place over the first-year of this project, approximately 150-200 samples were cast before repeatable results were achieved. Inter-laboratory testing was completed with Oregon State University to validate the procedures. After 2 years of testing, the experimental investigations of the impact of various SCMs and chemical admixtures were investigated. These results are presented in Chapters 5 and 6.

### 3.4 NOMENCLATURE

The research discussed in this dissertation investigated the influence of various mineral admixtures; however the replacement ratio (by mass of cement) of each mineral

admixture remained the same throughout the research. Table 8 summarizes the nomenclature and replacement percentage of each CAC based-system.

Table 8: Cement and supplementary cementitious materials nomenclature and replacement ratios by mass of cement

| Nomenclature | Cementitious System |
|---|---|
| CAC | Plain Calcium Aluminate Cement |
| TCAC | Ternary Blended Calcium Aluminate Cement - CAC + 21.5% Slag + 3.5% Silica Fume |
| CAC-LF | Calcium Aluminate Cement + 20% Inert Limestone Filler |
| CAC-FA | Calcium Aluminate Cement + 30% Class C Fly Ash |

In addition to various cementitious material combinations, various chemical admixtures were studied. The dissertation identifies the addition percentage by mass of cement throughout, however the nomenclature and basic composition of the chemical admixture types are listed in Table 9.

Table 9: Chemical admixture nomenclature and basic composition

| Nomenclature | Chemical Admixture |
|---|---|
| LSA | Lithium Suflate Accelerator - $Li_2SO_4$ |
| HRWR | Polycarboxylate Based Water-reducer |
| Citric | Citric Acid Set Retarder |
| Latex | Carboxylated Styrene Butadiene Copolymer Latex Admixture |

# Chapter 4: Characterization and Development of a Paste and Mortar Isothermal Calorimeter for Calcium Aluminate Cements

This chapter describes a comprehensive study of a new class of isothermal calorimeters that were built specifically for PC paste, mortar, and concrete based-systems. Investigations of the precision and repeatability of the equipment were initiated with PC. Then, initial testing on CAC based-systems was completed. This screening revealed that the equipment was not capable of handling the excessive heat release of CAC. A new calorimeter was then designed and constructed specifically for CAC-based system, and this technique was then evaluated for repeatability and subsequently used to evaluate a wide range of binders, chemical admixtures, and inert fillers, as described in later chapters in this dissertation.

## 4.1 INTRODUCTION

Isothermal calorimetry was chosen as the method for investigating the hydration of various material combinations of CAC based-systems for this dissertation. Isothermal calorimetry measures the heat flow from cement hydration reactions by differential heat flow sensors that allow for comparison of different mixtures and provide time-lapsed understanding of the hydration mechanisms. The timing and shape of heat flow curves can provide an understanding of the performance of different cementitious systems, especially for the addition of chemical admixtures, such as retarders and accelerators. In isothermal calorimeters, the temperature of a chamber is maintained and allows for hydration under a uniform temperature. Investigating material combinations at different isothermal temperatures allows one to calculate an apparent activation energy for portland cement-based systems, and this can be combined with data/information from semi-adiabatic calorimetry to predict thermal distributions in mass concrete applications

(Poole J. , 2007) and (Riding, 2007). A similar approach using activation energy is likely not possible for CAC-based systems as different hydration products form under different time-temperature histories; however, significant information can be gleaned from isothermal calorimetry for CAC-based systems. As described later in this dissertation, isothermal calorimetry, when optimized specifically for CAC-based systems, can be a useful screening tool for evaluating compatibility issues or and quantifying the effects of chemical admixtures, which are always used in CAC concrete in field applications.

Before describing the development of the calorimeter used in the bulk of this research, some typical examples of portland cement behavior under isothermal calorimetry testing is shown, followed by typical examples for CAC. Figure 20 shows the isothermal calorimetry curves at 23°C and 38°C for PC paste and mortar. The sand accelerates the reaction, identified by the shifting of the curve to the left. Also, the addition of sand to the mixture increases the peak heat release, indicated by the increased peak height (Gosselin C. , 2009). However, the overall shape and area under the curves are approximately the same, thus the effect of aggregate has minimal effects especially compared to the effects the sand has on the hydration of CAC, as discussed next.

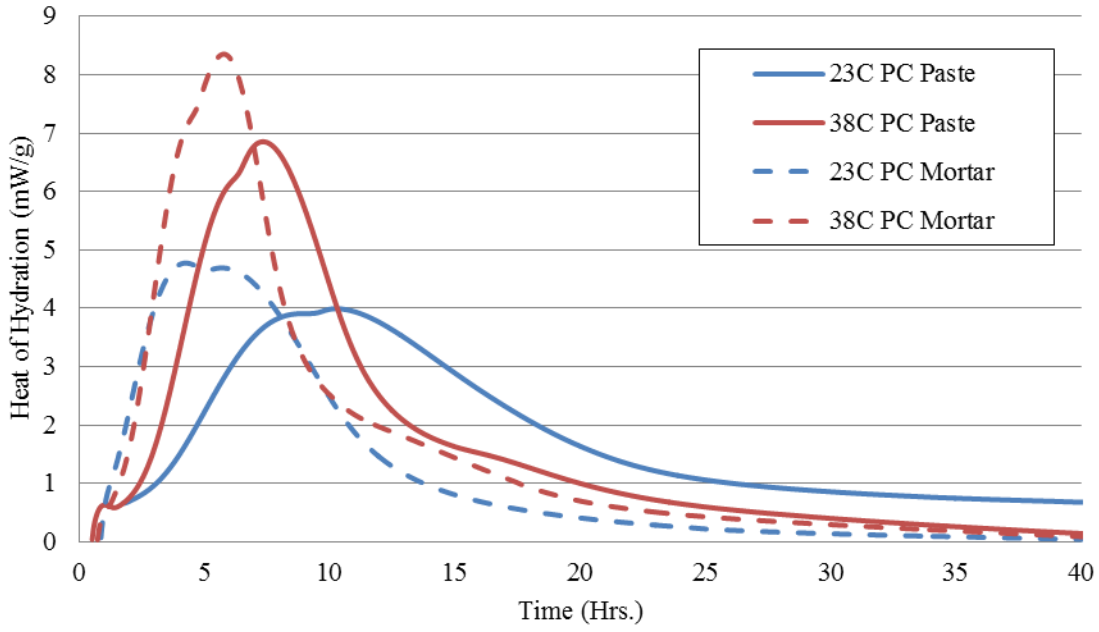


Figure 20: Example PC paste and mortar isothermal calorimetry heat flow at 23°C and 38°C

Figure 21 shows a similar comparison for CAC, with isothermal testing performed at 23°C and 38°C for both paste and mortar. It should be noted that these curves were generated using the new isothermal calorimeter built specifically for CAC, as described later in this chapter. At 23°C, the paste samples have an extended induction phase that can take 10-14 hours. When fine aggregate is added to the system at 23°C, the reaction is accelerated so the peak heat of hydration occurs in nearly half the amount of time as the paste. At 38°C, CAC paste has a heat flow curve with two distinct peaks. However, when aggregate is added to the system, the first peak is drastically reduced and two nearly equal peaks are generated. Fine aggregate particles have a significant effect in acting as nucleation sites for CAC hydration, in a fashion that is much more pronounced that for PC hydration (Gosselin C. , 2009).

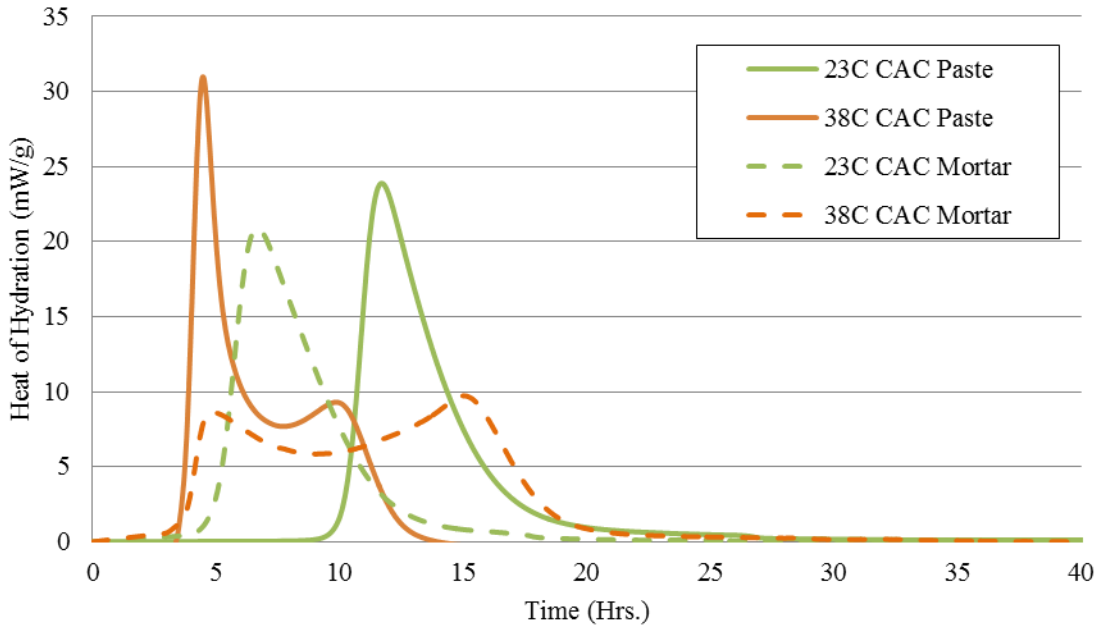


Figure 21: Example PC paste and mortar isothermal calorimetry heat flow at 23°C and 38°C

### 4.2 GRACE ADIACAL ISOTHERMAL CALORIMETER

The Grace Adiacal TC Isothermal Calorimeter was chosen to investigate paste and mortar cementitious mixtures. The characteristics unique to this equipment are presented in this section to give the reader a thorough understanding of the equipment and explanation of changes made from existing technology.

The Grace AdiaCal TC Isothermal Calorimeter was designed for testing PC paste, mortars, and concretes. The equipment was received at UT Austin in the summer of 2009. Figure 22 A-B, illustrate the external and internal views of the calorimeter, respectively.

Figure 22: A) External View of the Grace AdiaCal Isothermal Calorimeter B) Internal View of Sample Placement.

The calorimeter was constructed in an insulated 0.5m L X 0.5m W X 0.43m H (20in. L x 20in. W x 17in. H) box capable of isolating the internal chamber from changes in the external temperature. The Grace AdiaCal TC can test eight separate specimens under isothermal temperatures ranges from 5°C to 60°C. The manufacture recommends samples sizes for PC paste of 50g, for mortar of 100g, and to the fill cup completely for PC concretes (approximately 400 g). Figure 23 shows the 125 mL polymer sample holder.

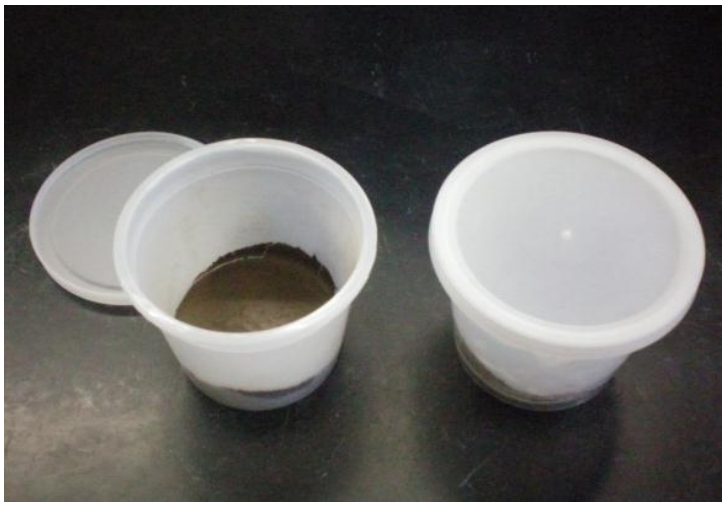

Figure 23: Grace AdiaCal TC Sample Holder.

ASTM C 305 is recommended when using this calorimeter for preparation of paste and mortar samples (ASTM C 305, 2006). The mixture design and proportions are entered into the Grace AdiaCal General User Interface (GUI). Figure 24 is a screen capture of the software user interface that allows for the input of mixture designs and live hydration feedback.

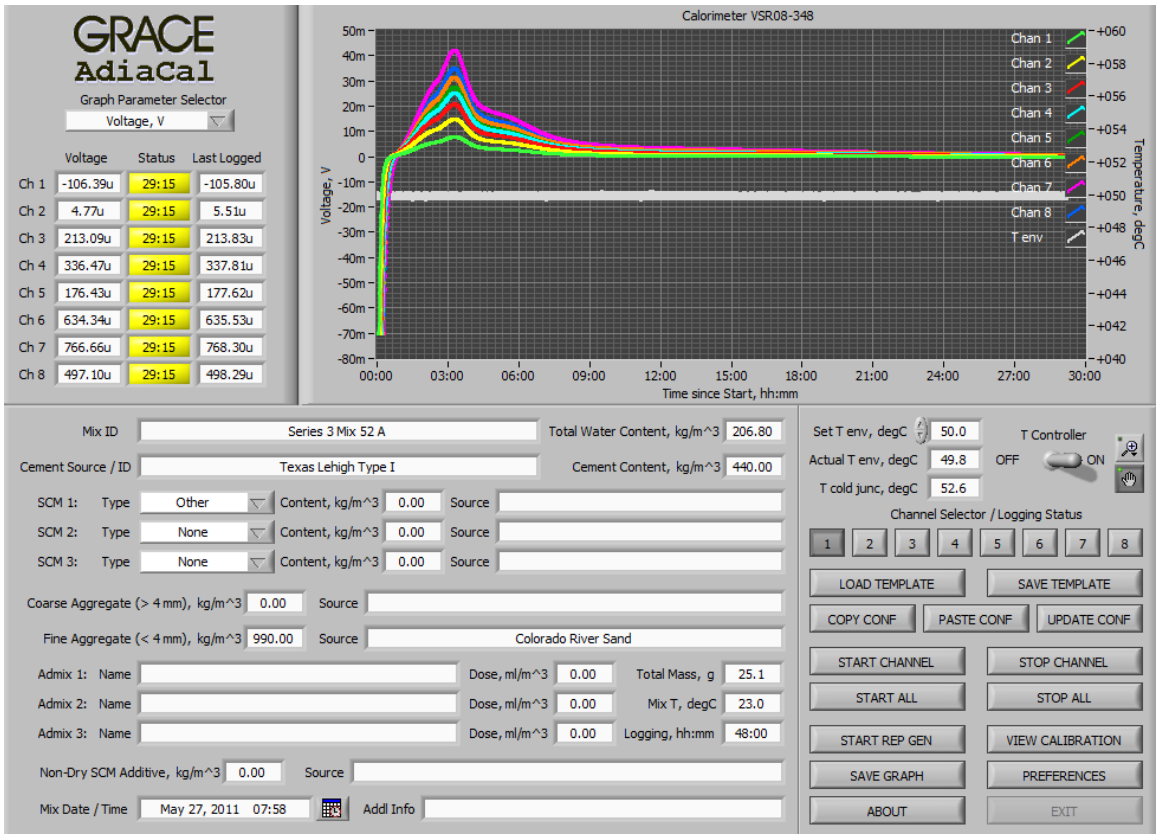


Figure 24: Grace AdiaCal TC GUI.

When mixtures are placed in the calorimeter, each individual channel can be activated separately. This represents a significant change from other calorimeters on the market where all channels are initiated at the same time. Each channel provides a live display on an x-y plot where the power of each mixture is normalized to the mass of cementitious material as a function of the hydration time. The individual components of the mixture design can be entered and include cement, SCMs, water, chemical admixtures, and aggregates contents. The user identifies the duration of each test, and at the termination of the test a text document containing all mixture design user inputs, raw data outputs and data normalized for the mixture design is created.

There was interest in using the new isothermal calorimeter for investigating material combinations of CAC based-systems for this project due to its ability to be used on larger samples and mortar. Before any testing could be completed with CAC, a thorough study was done to validate its precision for use with PC paste and mortars.

### 4.3 Repeatability of PC Mortar and Paste

Before the AdiaCal could be used to evaluate material combinations for CAC based-systems, it was important to validate the equipment repeatability with PC. The calorimeter was evaluated at four different isothermal temperatures: 5, 23, 38, and 60°C. One sample each was cast from eight different mixtures at each of the various temperatures. ASTM C 1679, Standard Practice for Measuring Hydration Kinetics of Hydraulic Cementitious Mixtures Using Isothermal Calorimetry, recommends six specimens should be cast from six different batches and standard deviation of the time to reach the maximum of the main hydration peak to validate new isothermal calorimeters should be reported (ASTM C 1679, 2009).

PC paste and mortars were both evaluated. A local ASTM C 150 Type I portland cement was used for all repeatability studies. A 0.40 w/c was used for both paste and mortar mixtures. The mortar mixtures had a 2.25 aggregate/binder ratio. ASTM C 305 was used to prepare the paste and mortar samples for the repeatability study (ASTM C 305, 2006). The testing matrix for PC mortar repeatability is summarized in Table 10.

Table 10: PC Testing Matrix

| | Testing Temperature (°C) | No. Mixtures Completed | No. Samples Per Mixture | Sample Size (g) |
|---|---|---|---|---|
| PC Mortar - Repeatability | 5 | 8 | 1 | 100 |
| | 23 | 8 | 1 | 100 |
| | 38 | 8 | 1 | 100 |
| | 60 | 8 | 1 | 100 |
| PC Paste - Repeatability | 5 | 8 | 1 | 50 |
| | 23 | 8 | 1 | 50 |
| | 38 | 8 | 1 | 50 |
| | 60 | 8 | 1 | 50 |

To reduce the amount of time to reach thermal equilibrium, the separate materials were pre-heated/cooled to their respective testing temperatures 24 hrs prior to testing. The manufacturer's recommended sample size (50 g for PC paste and 100 g for PC mortar) was used. Figure 25 illustrates the average and one standard deviation of eight different mortar mixtures at 23°C.

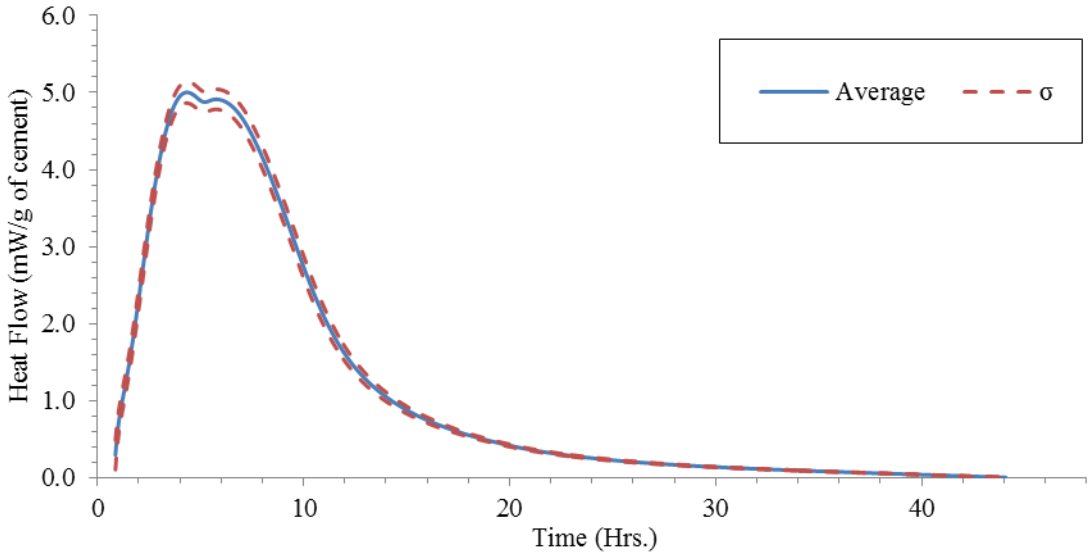


Figure 25: Heat flow of portland cement mortar at 23°C isothermal

At 23°C, the variability of the time and amount of heat released throughout the 48 hour duration was minimal. The standard deviation of the peak heat at a time of 4.339 hours was 0.138 mW/g of cement and the standard deviation of the time was 0.042 hrs. In Appendix B.1 the plots of the heat of hydration of PC mortar at 5°C, 38°C, and 60°C are presented. Table 11 summarizes the average heat of hydration and time of the peak heat of hydration.

Table 11: Portland cement mortar repeatability at various temperatures

| Temp. (°C) | Avg. Peak Heat Flow (mW/g cement) | Peak Heat Flow Repeatibility (σ) | Avg. Time until Peak Heat Flow (h) | Time until Peak Heat Flow Repeatibility (σ) |
|---|---|---|---|---|
| 5 | 0.576 | 0.017 | 17.411 | 0.111 |
| 23 | 5.004 | 0.138 | 4.339 | 0.042 |
| 38 | 8.718 | 0.153 | 5.736 | 0.022 |
| 60 | 18.338 | 0.623 | 3.758 | 0.066 |

At 5°C, the greatest standard deviation, 0.111 hours, of the time of the peak heat of hydration was observed. This was due broader heat of hydration curve compared to the most precise at 38°C, which had a standard deviation of 0.022 hours. At 60°C the largest standard deviation, 0.623 mW/g of cement for the peak heat of hydration was observed. Figure 26 illustrates the average and standard deviation of eight different paste mixtures at 23°C.

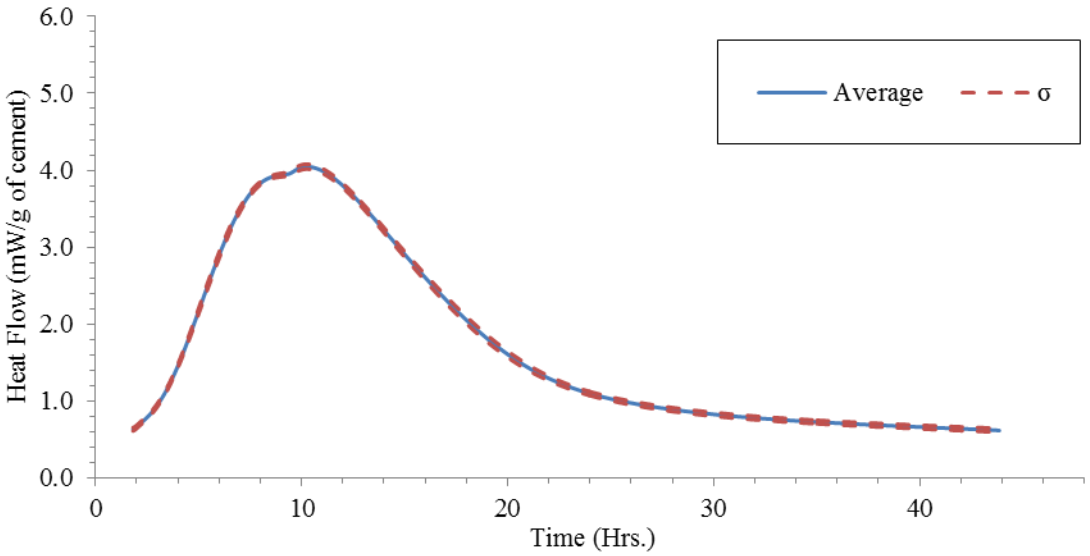


Figure 26: Heat flow of portland cement paste at 23°C isothermal

At 23°C, the standard deviation lines are difficult to distinguish from the average line which illustrates the improved precision of the paste samples versus the mortar samples. The homogeneity of the paste compared to mortar minimizes the error caused from sampling the material from a mixing bowl. Table 12 summarizes the average and standard deviation of the peak heat of hydration and times of the peak heat of hydration.

Table 12: Portland cement paste repeatability at various temperatures

| Temp. (°C) | Avg. Peak Heat Flow (mW/g cement) | Peak Heat Flow Repeatibility (σ) | Avg. Time until Peak Heat Flow (h) | Time until Peak Heat Flow Repeatibility (σ) |
|---|---|---|---|---|
| 5 | 1.410 | 0.012 | 21.787 | 1.419 |
| 23 | 4.047 | 0.032 | 10.258 | 0.053 |
| 38 | 7.320 | 0.138 | 7.300 | 0.062 |
| 60 | 30.403 | 0.927 | 2.590 | 0.028 |

Similar to the repeatability of the mortar mixtures, the paste mixtures at 5°C had the largest standard deviation, 1.419 hours, of the time of the peak heat of hydration and the 60°C had the largest standard deviation, 0.927 mW/g of cement, of the peak heat

flow. The results of the repeatability studies for the PC paste mixtures at 5°C, 38°C, and 60°C are located in Appendix B.2.

The 64 mixtures tested and described in this section showed an increase in standard deviation at the outer temperature ranges, 5°C and 60°C; however, these values were not higher than recommended in ASTM C 1679. The highest precision measurements were observed at 23°C. The Grace AdiaCal calorimeter was shown to be repeatable for use with PC paste and mortar mixtures. The next step was to evaluate the influence of variability of sample sizes.

### 4.4 Influence of Sample Size Variability of PC Paste and Mortar

After confirming the repeatability of the isothermal calorimeter, the next phase of testing was to evaluate the influence of sample size variability of mortar and paste mixtures at the four different temperatures. This testing was important to validate that smaller samples sizes could be used and maintain the repeatability. The smaller sample sizes are important because when testing CAC, a smaller sample size is needed because of the excessive heat that CAC generates during hydration.

Eight specimens were cast from one mixture at each of the four isothermal testing temperatures: 5, 23, 38, and 60°C. The specimens weighed 10, 20, 30, 40, 60, 80, 100, and 120 g for each mortar mixture. The manufactures recommended sample size for PC mortar was 100 g. A 0.47 w/c and a 2.25 binder/aggregate were used for these mixtures. The materials were pre-heated/cooled for 24 hours prior to mixing, and ASTM C 305 was used to prepare the mortar for each experiment (ASTM C 305, 2006). The testing matrix for PC mortar repeatability of variable sample sizes is summarized in Table 13.

Table 13: Mixture matrix for the repeatability of PC mortars with variable samples sizes

| | Testing Temperature (°C) | No. Mixtures Completed | No. Samples Per Mixture | Sample Size (g) |
|---|---|---|---|---|
| PC Mortar - Sample Size Variability | 5 | 1 | 8 | 10, 20, 30, 40, 60, 80, 100, and 120 |
| | 23 | 1 | 8 | 10, 20, 30, 40, 60, 80, 100, and 120 |
| | 38 | 1 | 8 | 10, 20, 30, 40, 60, 80, 100, and 120 |
| | 60 | 1 | 8 | 10, 20, 30, 40, 60, 80, 100, and 120 |

Figure 27 illustrates the repeatability of the mixture with the variable sample sizes at 23°C isothermal testing.

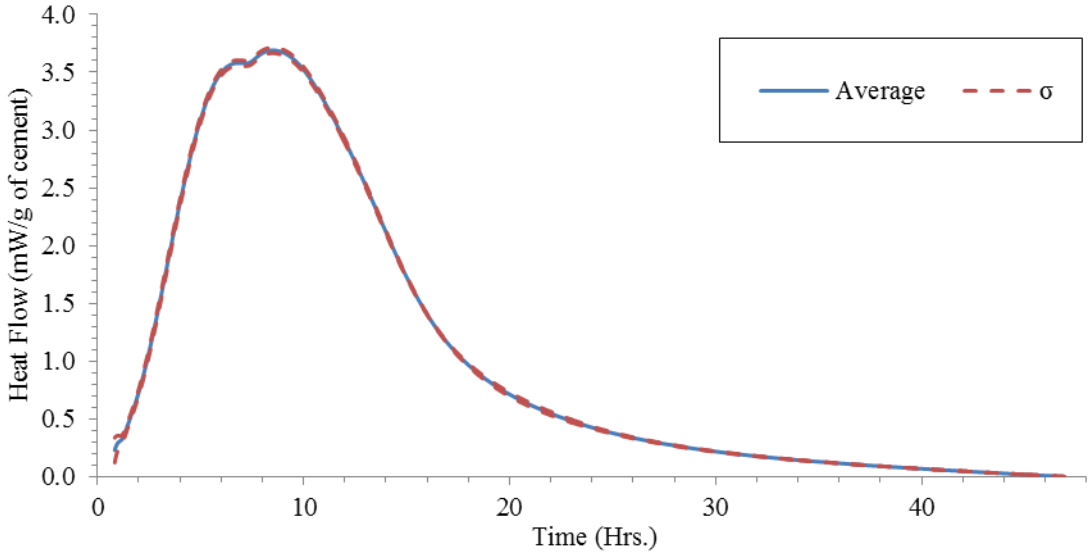


Figure 27: Heat flow of various PC mortar sample size at 23°C isothermal

The variability in sample size had little influence on the standard deviation at 23°C; the standard deviation of the peak heat flow was 0.025 mW/g. These results were expected because the specimens all came from the same mixture; however it was unknown whether the equipment would maintain the repeatability with the sample sizes smaller than the manufacturers recommended size. Appendix B.3 contains all the heat

flow graphs for the variability of sample sizes for PC mortars at 5°C, 38°C, and 60°C. Table 14 summarizes the variability of the peak heat of hydration and the time of the peak heat of hydration for these mixtures.

Table 14: Portland cement mortar repeatability at various temperatures and various sample sizes

| Temp. (°C) | Avg. Peak Heat Flow (mW/g cement) | Peak Heat Flow Repeatability (σ) | Avg. Time until Peak Heat Flow (h) | Time until Peak Heat Flow Repeatability (σ) |
|---|---|---|---|---|
| 5 | 1.450 | 0.020 | 17.22 | 0.192 |
| 23 | 3.690 | 0.025 | 8.467 | 0.037 |
| 38 | 9.349 | 0.184 | 4.925 | 0.032 |
| 60 | 18.879 | 0.321 | 3.281 | 0.006 |

From the results in Table 14, the largest standard deviation of the time of peak heat of hydration occurred at 5°C, 0.192 hours, and the largest standard deviation of the peak heat of hydration occurred at 60°C, 0.321 mW/g. These results are similar to those displayed in Table 11, but instead of being cast from eight different mixtures these were all cast from one mixture at each of the isothermal temperatures.

In addition, the repeatability of the various sample sizes were investigated for PC paste. The manufacturers recommended sample size was 50g, thus smaller sample sizes (5, 10, 15, 20, 25, 30, 40, and 50g) were investigated. A 0.47 w/c was used to prepare each mixture and ASTM C 305 procedures for preparing paste were followed (ASTM C 305, 2006). The testing matrix for the repeatability of variable sample sizes of PC Paste is summarized in Table 15.

Table 15: Mixture matrix for the repeatability of PC pastes with variable samples sizes

| | Testing Temperature (°C) | No. Mixtures Completed | No. Samples Per Mixture | Sample Size (g) |
|---|---|---|---|---|
| PC Mortar - Sample Size Variability | 5 | 1 | 8 | 10, 20, 30, 40, 60, 80, 100, and 120 |
| | 23 | 1 | 8 | 10, 20, 30, 40, 60, 80, 100, and 120 |
| | 38 | 1 | 8 | 10, 20, 30, 40, 60, 80, 100, and 120 |
| | 60 | 1 | 8 | 10, 20, 30, 40, 60, 80, 100, and 120 |

Figure 28 illustrates the repeatability of various PC paste sample sizes at 23°C.

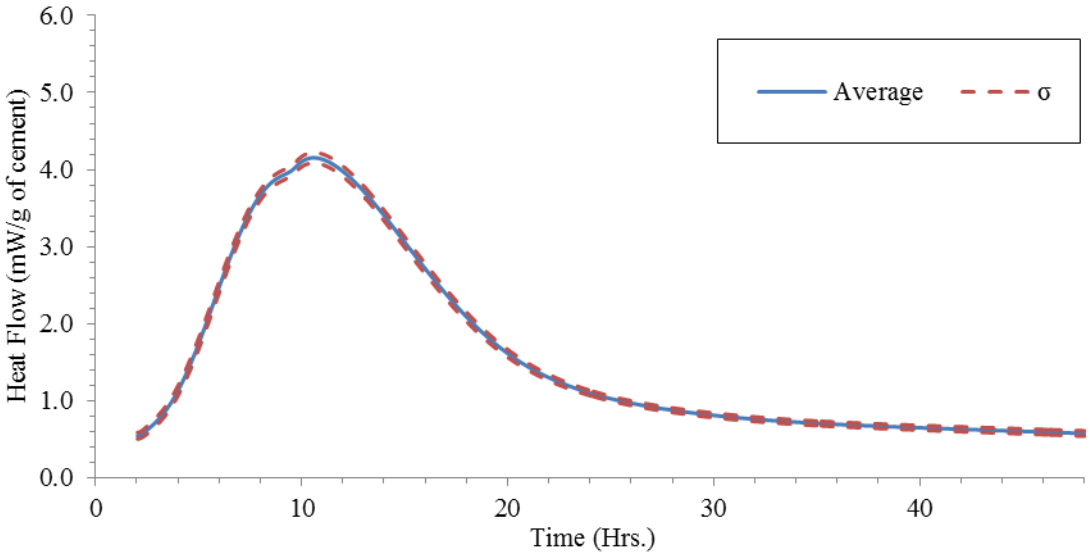


Figure 28: Heat flow of various PC paste sample size at 23°C isothermal

At 23°C, good repeatability of the paste mixtures was observed with the variability in sample sizes; a standard deviation of 0.068 mW/g and 0.018 hours of the peak heat flow and time of peak heat flow, respectively were observed. Figure 28 shows the standard deviation as a function of time throughout the 48 hour testing. A slight increase in variability is seen at the second peak of the hydration curve; however, these errors were minimal. The results of the repeatability of the variable sample sizes for the PC paste mixtures at 5°C, 38°C, and 60°C are located in Appendix B.4. Table 16

summarizes the average and standard deviations of the peak heat of hydration and time of peak heat of hydration at each of the four isothermal testing temperatures.

Table 16: Portland cement paste repeatability at various temperatures and various sample sizes

| Temp. (°C) | Avg. Peak Heat Flow (mW/g cement) | Peak Heat Flow Repeatability (σ) | Avg. Time until Peak Heat Flow (h) | Time until Peak Heat Flow Repeatability (σ) |
|---|---|---|---|---|
| 5 | 1.636 | 0.009 | 24.214 | 0.204 |
| 23 | 4.153 | 0.068 | 10.531 | 0.018 |
| 38 | 9.760 | 0.139 | 5.286 | 0.022 |
| 60 | 20.084 | 0.192 | 2.443 | 0.009 |

Overall, a reduction in the standard deviations was observed for the variability in sample size testing compared to the variability between mixtures. These results were expected since all the specimens came from one mixture rather than eight separate mixtures.

The work completed in Section 4.3 and 4.4 verified that the Grace AdiaCal TC isothermal calorimeter was repeatable for use with PC mortar and paste mixtures at four different isothermal temperatures (5°C, 23°C, 38°C, and 60°C) and with various sample sizes.

### 4.5 Initial Evaluation of CAC Paste and Mortar

After validating the repeatability of the Grace AdiaCal calorimeter the next stage of testing was to investigate material combinations of CAC based-systems. This was done initially under the assumption that if the calorimeter were repeatable for PC systems, then it would be acceptable for CAC based-systems. A few results from the preliminary testing are provided in this section. First, Figure 29 illustrates initial screening of a ternary blended CAC (TCAC) based-system with slag and silica fume mixture with varying dosage of lithium sulfate accelerator (LSA) at 23°C.

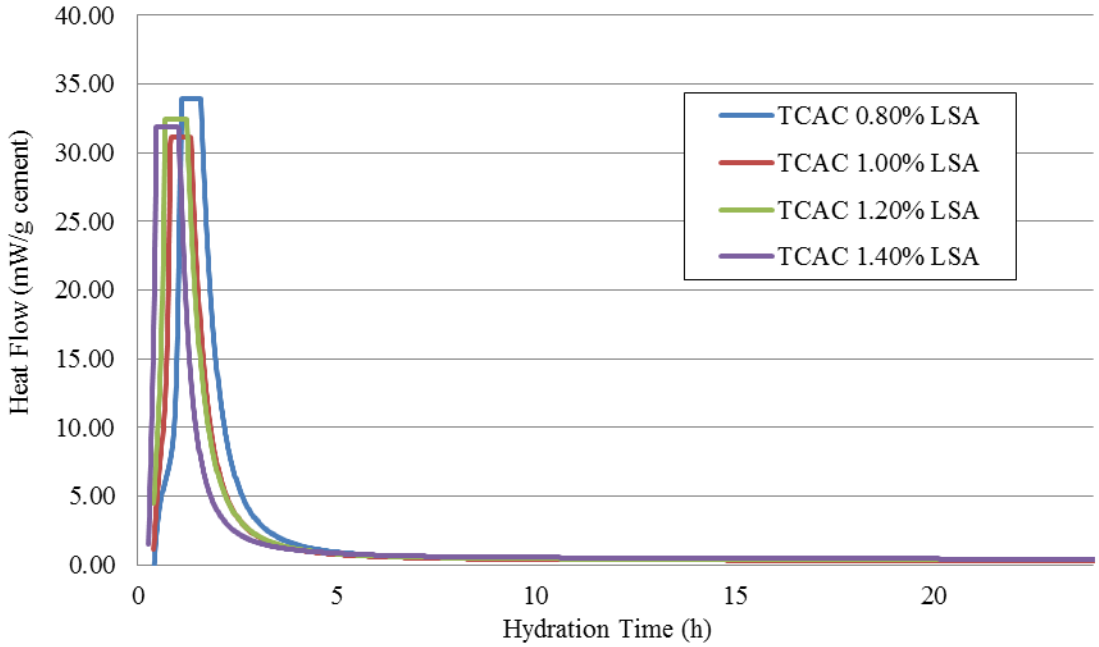


Figure 29: Measurement failure due to excessive heat generation of TCAC system at 38°C

These four mixtures investigated the effect of varying LSA dosages on TCAC hydration at 38°C isothermal testing. From the heat flow curve, it was evident that the amount of heat generated by the CAC samples was greater than the capacity of the heat flux sensors. This resulted in the "topping out" or flat line seen at the top of each of the peak heats of hydration. The next graph, Figure 30, illustrates heat flow curves of variable CAC sample sizes at 60°C.

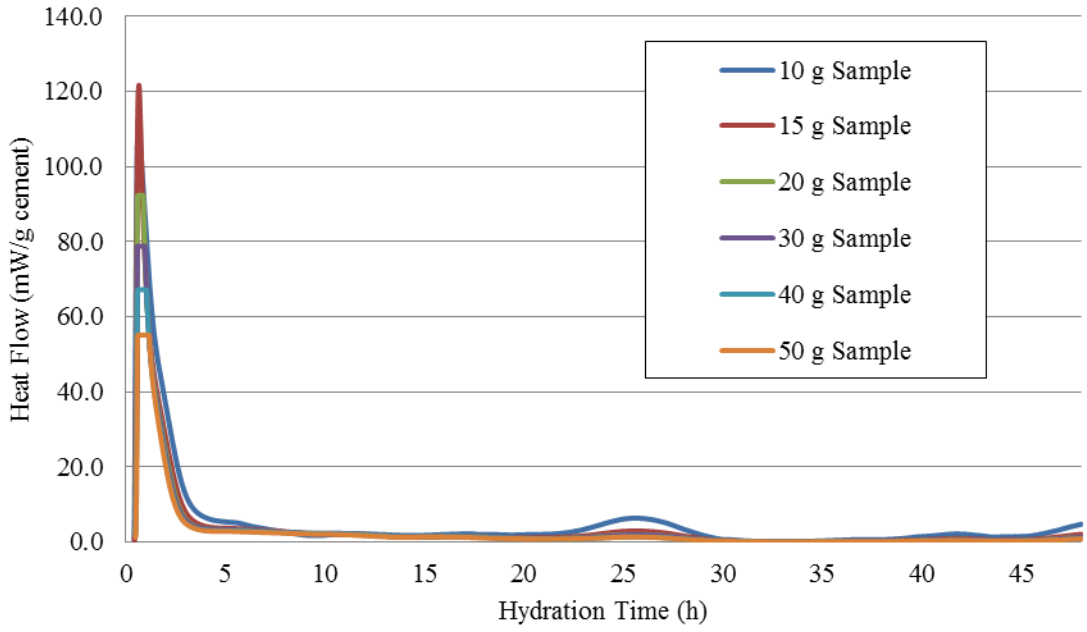


Figure 30: Measurement failure due to excessive heat release and ambient temperature variation at 60°C

This graph shows the repeatability of six samples from one mortar mixture with varying sample sizes from 10-50g. The two smallest sample sizes were able to be recorded without exceeding the capacity of the heat flux sensors. From these heat curves and those on the previous graph it was evident that the manufacturers recommended sample sizes were not appropriate for CAC based-systems. Additionally, in Figure 30 a spike in the heat flow curve is observed between 20 and 30 hours of testing and again near the end of the test. These spikes were caused by fluctuations in the ambient temperature outside of the insulated box. Figure 31 illustrates the repeatability of variable sample sizes of CAC paste at 60°C.

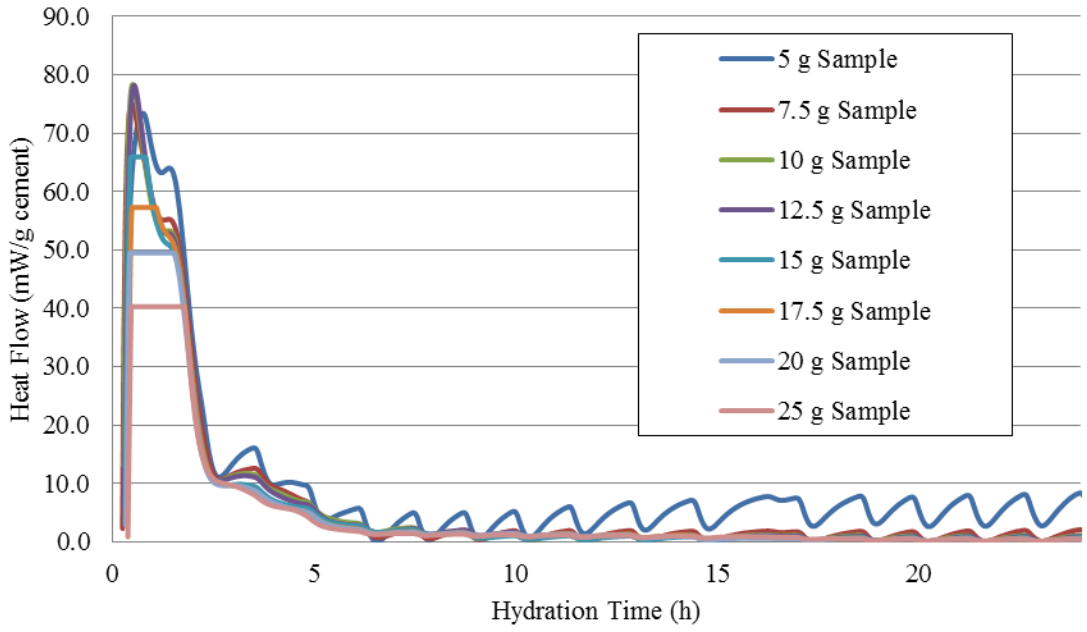


Figure 31: Excessive heat release and sluggish temperature control

From the heat flow curve it was evident that there were a few problems with testing the CAC paste at this higher isothermal temperature. The sample sizes varied from 5-25g and exceeded the heat capacity of the heat flux sensors for most of the specimens. In addition, after the initial heat of hydration curve, random temperature fluctuations are seen throughout the later part of the test. The smallest sample, 5 g, illustrated these fluctuations more than the others due to its smaller thermal mass. These fluctuations were determined to be caused by lethargic temperature control. The temperature control of calorimeter is usually maintained by a proportional, derivative algorithm or PID controller. Simply, a PID controller is a control feedback loop algorithm that is used to maintain the temperature of the calorimeter by correcting errors and forecasting the future temperature. This then allows for the most steady temperature control possible for the testing in the isothermal conditions.

From the problems identified in these tests, it was determined that modifications were needed to be able to test representative paste and mortar CAC samples without the "topping out" effect. The next section presents detailed information on the changes made to the calorimeter specifically for CAC.

## 4.6 Development of CAC Isothermal Calorimeter

In Sections 4.3, a summary of the work completed showed that the Grace AdiaCAL isothermal calorimeter was repeatable for PC paste and mortar mixtures at four different isothermal temperatures. Then, Section 4.4 highlighted that the calorimeter maintained its repeatability when the sample sizes were varied from the manufactures recommendations. Section 4.5 detailed the initial screening test with CAC based-systems and highlighted areas of weakness. This section addresses each of these areas of weakness and describes the construction of a calorimeter built specifically for CAC that improves upon the AdiaCal calorimeter.

### 4.6.1 Physical Modifications

The most noticeable and simplest changes made to the new calorimeter were the improved insulated box and of the individual chambers. The insulated chamber is shown in Figure 32 and machined lids shown in Figure 33.

Figure 32: Stainless steel calorimeter chamber

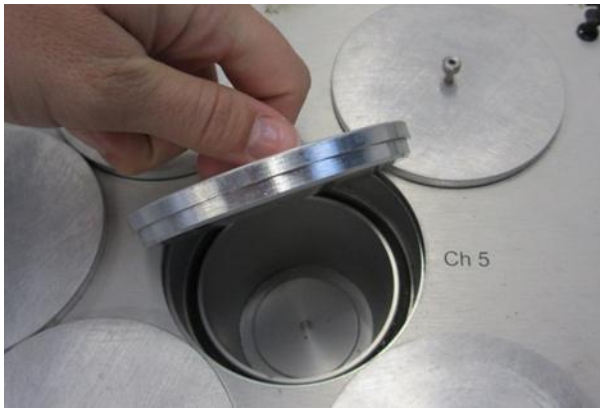


Figure 33: Machined aluminum lids

The new stainless steel chamber provided better insulation from external temperatures. This chamber is a 54 qt. commercially available food type cooler with 0.44m L X 0.65m W X 0.45m H (17.25in. L x 25.5in. W x 17.75in. H). The chamber mitigated the influence of ambient temperature changes on the isothermal conditions inside the cooler. The machined lids were made of aluminum caps that were built to a tighter tolerance of the width of the individual sample chambers. These lids minimize the amount of heat loss through the top of the specimens and forced more heat to escape through the bottom of the heat sink, as designed.

### 4.6.2 Improved Temperature Control System

The Laird Technologies PR-59 temperature controller was used to manage the internal temperature of the isothermal chamber. This thermostat was controlled via computer versus common thermostats that are manually set. The temperature controller provides constant temperature control with ±0.05°C via real-time feedback loop. All specifications for PR-59 are included in Appendix B.5. The thermostat was used to power the Laird Technologies air-to-air thermoelectric heater/cooler. The specifications on the air-to-air heater/cooler are located in Appendix B.6.

### 4.6.3 Altered PID Algorithm

As briefly mentioned in Section 4.5, a problem with existing calorimeters is the slow temperature control program used to regulate the temperature of the calorimeter when used for CAC, which has rapid heat release. The temperature controllers for isothermal calorimeters are often controlled by proportion-integral-derivate controllers (PID controller). These control systems are often used to control industrial control systems with real-time feedback loops.

The algorithm calculates the error of a measured point from the difference of the desired set point. The algorithm has three separate parameters: the proportional (P) which looks at the present error, the integral (I) that looks at the accumulation of past errors, and the derivative (D) that attempts to predict the future errors. The weighted sum of the three errors is used to adjust the temperature of the calorimeter. Equation 6 below defines the equation for a PID controller/algorithm where u(t) is the output to the actual controller, in this case the thermostat (Bennett, 1993).

$$u(t) = MV(t) = K_p e(t) + K_i \int_0^t e(T)dT + K_d \frac{d}{dt} e(t) \quad (6)$$

In Equation 6, *MV* is the manipulated variable that is relayed to thermostat of the temperature controller, $K_p$ is the proportional gain which is used to weight the present error, $K_i$ is the integral gain used to weight the past errors, $K_d$ is used to weight the future errors, and *e* is the error for that time step *(t)* (Bennett, 1993). In order to manipulate the equation for tighter precision when testing CAC samples, the algorithm went through multiple iterations to minimize the weighted average of past error and focus on the present error. The influence of the future error was changed to zero to prevent the thermostat from over-correcting for predicted errors and creating the same problem shown in Section 4.5. From this exercise, the equation that worked the best for the calorimeter had the weight proportional gains for $K_{p,}$ $K_{i,}$ and $K_d$ set at 7, 0.0001, and 0, respectively. These values gave the best results when testing CAC paste and mortars.

### 4.6.4 Calibration System

One of the more unique aspects that went into the development of this CAC-optimized calorimeter was the development of a temperature and cement-specific calibration system. As stated in Section 4.1, CAC hydration produces significantly higher amounts of heat than ordinary PC based-systems over a shorter time period and the amount of heat it generates is different at various temperatures. Thus, typical calorimeters and calibration systems for calorimeters used for PC may not be the most accurate or precise for CAC. This section describes how a calibration curve works for existing calorimeters and the changes made to it for this calorimeter.

First, all isothermal calorimeters require a calibration factor. This factor merely converts a voltage reading recorded from the differential heat flow sensors due to cement hydration to a power reading, typically in units of mW. This calibration factor is typically determined from a calibration curve, similar to the one shown in Figure 34.

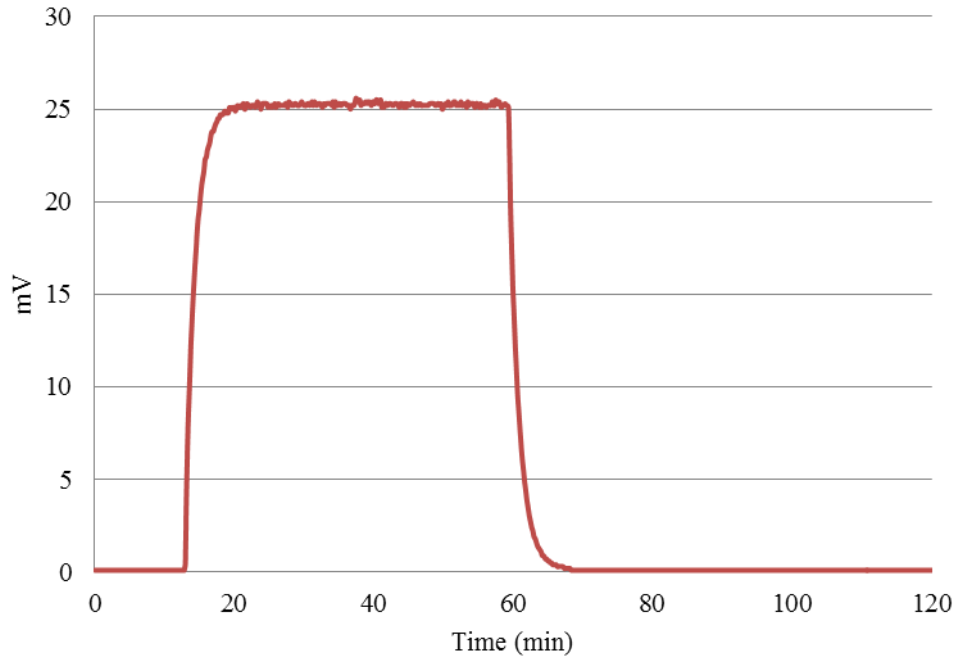


Figure 34: Typical calibration curve for a TAM Air Calorimeter.

In a typical calorimeter (TAM air type for reference only) the calibration curve is created by supplying power, typically 2.107 V, to a series of eight 100.0 Ω resistors built into the calorimeter below each of the sample chambers. From the known resistance and voltage in the series circuit the actual power supplied to each channel can be determined by using Equation 7.

$$P = \frac{V^2}{R} \quad (7)$$

With known power supplied to the calibration system, the reading is divided by eight to determine the power supplied to each channel. From the peak reading recorded in Figure 34, a conversion factor (W/mV) can be determine that converts the mV reading to a power reading in terms of mW and provides the typical power reading seen with calorimetry heat flow curves, represented by Equation 8.

$$\mathcal{E} = \frac{\frac{P}{8}}{V} \quad (8)$$

This calibration procedure and calculation is widely accepted and used across research institutes and industries; however, where this procedure is lacking is its ability to be manipulated for the variations in power output due to the hydration of different cementitious systems at different temperatures. This procedure only provides one constant voltage for all calibration files at all isothermal temperatures.

The calibration system developed for this calorimeter connects eight resistors that are placed in the actual sample holder rather than below the sample holders. Figure 35 and Figure 36 show the resistors and the wiring schematic, respectively.

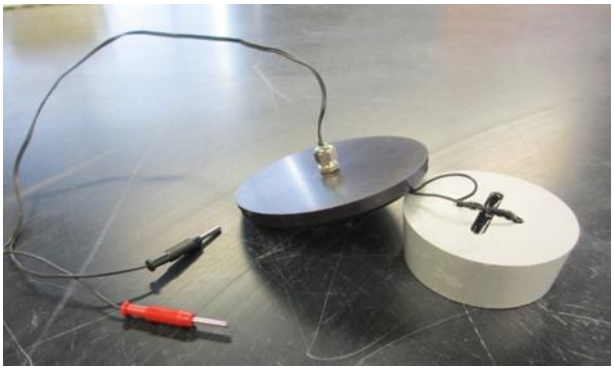

Figure 35: Resistors

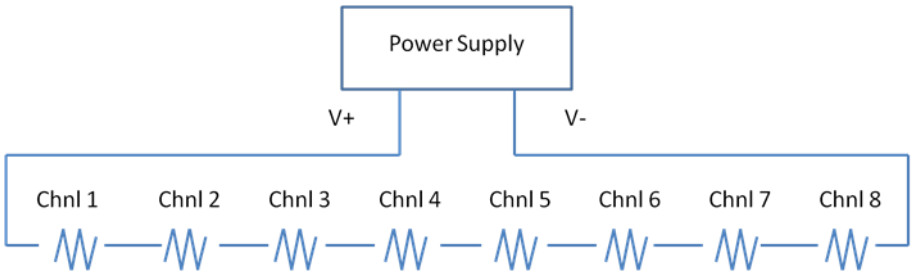


Figure 36: Wiring schematic for series circuit for calibration diagram

Figure 35 shows the resistor built for the calibrations system. The actual 1500 Ω resistor is imbedded in an aluminum cast that rests where the sample is placed during the calibration process. The black lid is made of aluminum and is designed to close the sample chamber to prevent heat loss through the top. The eight resistors are connected in a series circuit just as the one shown in Figure 36. These resistors are then connected to an external power supply. A 250 V direct current power supply was used to provide power to the resistors.

This system is able to adjust the amount of power applied to each sample to mimic the amount of heat expected for the hydration process. The power is calculated by estimating the amount of heat that would be generated from a cement source at a given temperature for a given sample size. From these assumptions, the total power can be estimated for all eight channels. With the total power known and the total resistance of the series circuit known, the amount of voltage can be determined. Figure 37 shows example calibration curves for three different temperatures.

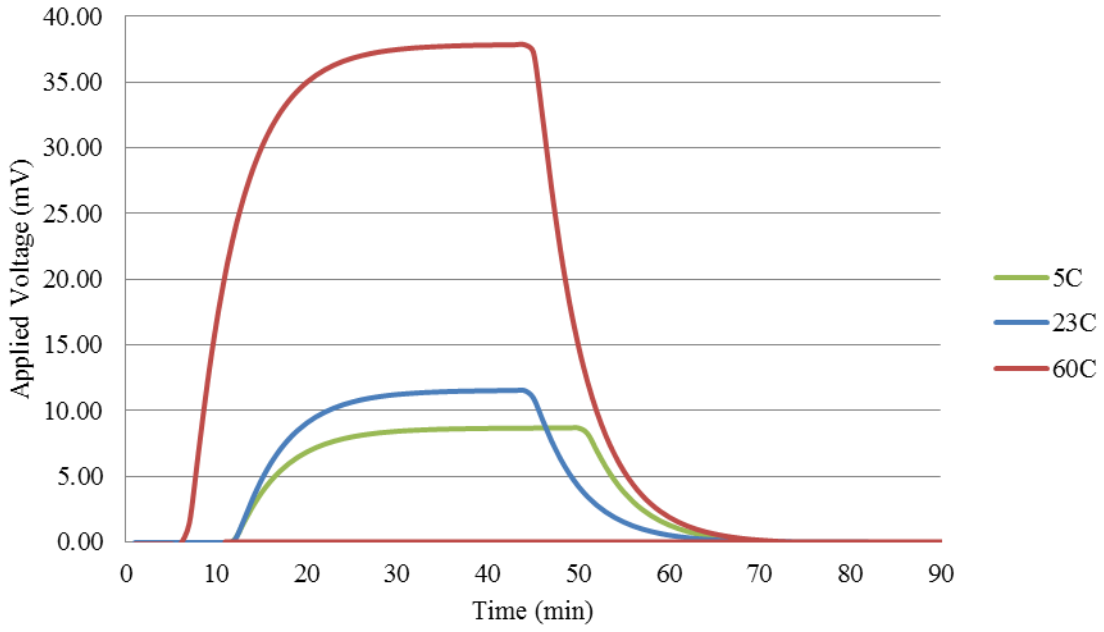


Figure 37: Calibration curves for CAC at 5°C, 23°C, and 60°C

From the graph, it is evident that the calibration system created three specific calibration curves for three different isothermal testing temperatures. Compared to the old systems where one calibration "fits all" this allows for improved precision in the determination of the calibration factor for each isothermal temperature. The calibration factors are able to be entered into one text file and the calibration factors are linearly interpolated when testing occurs at temperatures where specific calibration factors were not determined. However, it is always possible to perform the calibration for the exact temperature being investigated.

### 4.6.5 Summary

This section summarized the development of an isothermal calorimeter specifically built and calibrated for CAC based-systems. The new calorimeter specifically contains:

- Improved insulated chamber to minimize ambient temperature influence
- Machined lids to prevent heat loss from sample chambers
- Computer controlled temperature management system
- Improved air-to-air heater exchanger
- Altered PID algorithm
- Temperature and cement specific calibration system

The following sections summarize the work completed to verify the new calorimeter is capable of testing CAC and verify the precision of the device.

### 4.7 Sample Size Variability CAC Paste and Mortar

After construction of the new version of the isothermal calorimeter and testing of preliminary mixtures to validate that the equipment was capable of maintaining isothermal conditions at all temperatures for paste and mortar, it was possible to begin testing CAC. The first series of tests was aimed at identifying the largest sample sizes that could be used at four different isothermal temperatures. Selecting the largest sample size was important to distinguish this calorimeter from others available on the market and to know the upper bound limitations for the calorimeter.

To determine the largest sample sizes, a repeatability study was completed with CAC mortars with variable sample sizes at the four isothermal temperatures. The mortar mixtures had a 0.40 w/c and 2.25 binder to aggregate ratio. The mortar mixtures were prepared using ASTM C 305 (ASTM C 305, 2006). The sample sizes varied from 5-50g and eight specimens were cast from each mixture. The mixture matrix for evaluating the influence of variability of sample sizes for CAC mortar is shown in Table 17.

Table 17: CAC mortar mixture matrix variability in sample size

| | Testing Temperature (°C) | No. Mixtures Completed | No. Samples Per Mixture | Sample Size (g) |
|---|---|---|---|---|
| CAC Mortar - Sample Size Variability | 5 | 1 | 8 | 5, 10, 20, 25, 30, 35, 40, and 50 |
| | 23 | 1 | 8 | 5, 10, 20, 25, 30, 35, 40, and 50 |
| | 38 | 1 | 8 | 5, 10, 20, 25, 30, 35, 40, and 50 |
| | 60 | 1 | 8 | 5, 10, 20, 25, 30, 35, 40, and 50 |

Figure 38 illustrates the typical repeatability curve for the various CAC sample sizes at 23°C.

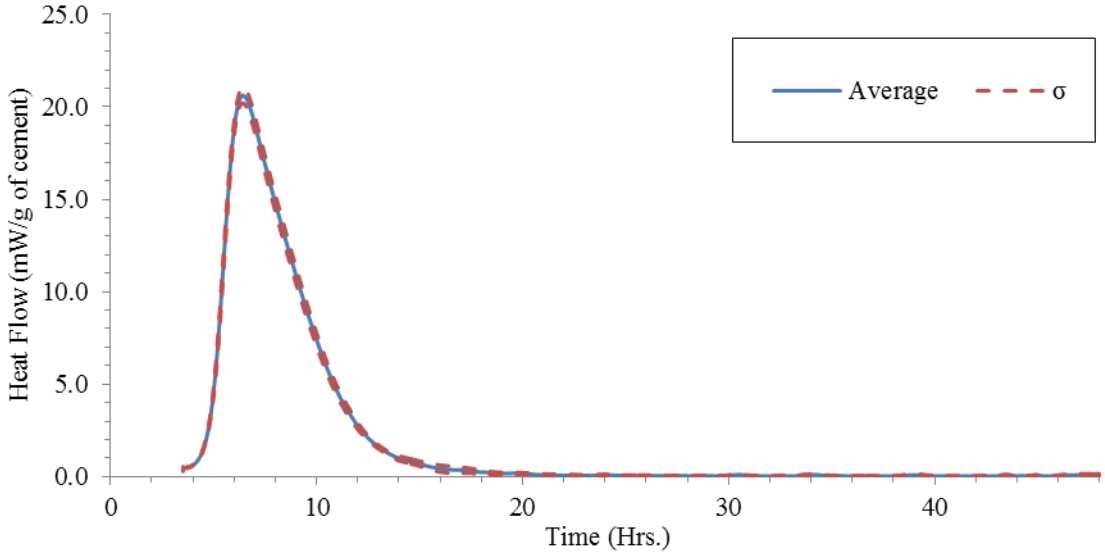


Figure 38: Repeatability of various CAC mortar sample sizes at 23°C

At 23°C all sample sizes were able to be read without exceeding the capacity of the heat flow sensors of the channel. The repeatability of this mixture was acceptable and validated that CAC mortars could be tested at 23°C. The plots of the heat flow of various sample sizes at 5°C, 38°C, and 60°C are presented in Appendix B.5, and Table 18

summarizes the standard deviations of the peak heat of hydration and the time of the peak of hydration.

Table 18: CAC mortar repeatability at various temperatures and various sample sizes

| Temp. (°C) | Avg. Peak Heat Flow (mW/g cement) | Peak Heat Flow Repeatibility (σ) | Avg. Time until Peak Heat Flow (h) | Time until Peak Heat Flow Repeatibility (σ) |
|---|---|---|---|---|
| 5 | 11.819 | 0.302 | 3.694 | 0.109 |
| 23 | 20.626 | 0.414 | 6.414 | 0.035 |
| 38 | 9.384 | 0.183 | 4.228 | 0.044 |
| 60 | 124.166 | 6.630 | 0.336 | 0.022 |

From the results of the CAC variability of sample size testing acceptable repeatability of the time of the peak heat flow was observed. The largest standard deviation occurred at the 5°C isothermal testing (similar to that for the Grace AdiaCal system). However, although the standard deviations of the peak heat of hydration were larger, they were still small relative to the amount of heat released. These results are further compared to the PC mixtures later in the chapter.

Next the repeatability of various sample sizes of CAC paste was investigated. These sample sizes varied from 5-25g and were prepared in a bowl mixture according to ASTM C 305 (ASTM C 305, 2006). A 0.40 w/c was used for the CAC paste mixtures. The mixture matrix for evaluating the influence of variability of sample sizes for CAC paste is shown in Table 19.

Table 19: CAC paste mixture matrix variability in sample size

| | Testing Temperature (°C) | No. Mixtures Completed | No. Samples Per Mixture | Sample Size (g) |
|---|---|---|---|---|
| CAC Paste - Sample Size Variability | 5 | 1 | 8 | 5, 8, 10, 12, 15, 17, 20, and 25 |
| | 23 | 1 | 8 | 5, 8, 10, 12, 15, 17, 20, and 25 |
| | 38 | 1 | 8 | 5, 8, 10, 12, 15, 17, 20, and 25 |
| | 60 | 1 | 8 | 5, 8, 10, 12, 15, 17, 20, and 25 |

Figure 39 illustrates the repeatability of the CAC paste mixtures at 23°C.

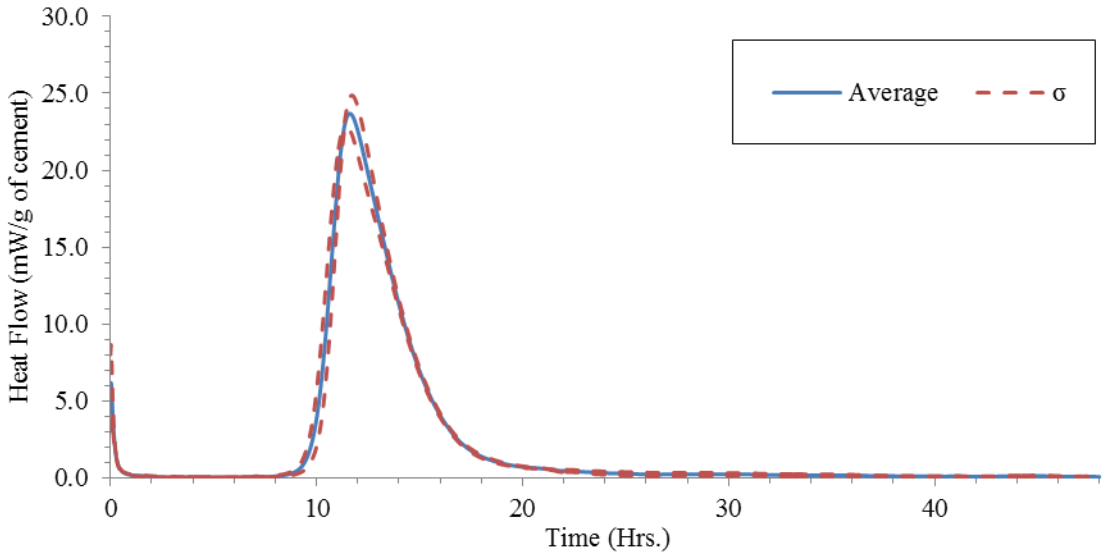


Figure 39: Repeatability of various CAC paste sample sizes at 23°C

At 23°C, the acceptable repeatability of the paste mixtures was measured. Figure 39 displayed the standard deviation as a function of time throughout the 48 hour duration of testing. The results of the repeatability of the variable sample sizes for the CAC paste mixtures at 5°C, 38°C, and 60°C are located in Appendix B.6. Table 20 summarizes the average and standard deviations of the peak heat of hydration and time of peak heat of hydration at each of the four isothermal testing temperatures.

Table 20: CAC paste repeatability at various temperatures and various sample sizes

| Temp. (°C) | Avg. Peak Heat Flow (mW/g cement) | Peak Heat Flow Repeatibility (σ) | Avg. Time until Peak Heat Flow (h) | Time until Peak Heat Flow Repeatibility (σ) |
|---|---|---|---|---|
| 5 | 13.514 | 0.176 | 4.128 | 0.141 |
| 23 | 23.911 | 0.938 | 11.558 | 0.158 |
| 38 | 19.820 | 1.244 | 4.519 | 0.033 |
| 60 | 57.296 | 11.113 | 1.410 | 0.059 |

CAC paste had a very high standard deviation for the peak heat of hydration at higher temperatures. The 11.113 mW/g of cement standard deviation of the peak heat of hydration at 60°C demonstrates the difficultly in characterizing the peak heat flow with such a reactive material. However, the repeatability of the time of peak heat of hydration was good, and illustrates that the calorimeter could still be used to identify when the peak heat of hydration occurred.

From the characterization of the repeatability of various sample sizes, different factors were attributed to the repeatability of the equipment. At the lower temperatures a wider range of sample sizes were shown to be repeatable and measurable below the threshold values of the calorimeter. At the higher temperatures, a much higher standard deviation was observed for the peak heat of hydration.

### 4.8 Repeatability of CAC Paste and Mortar

A summary of the investigation of the repeatability of the CAC paste and mortar mixtures is presented in this section. These studies are aimed to characterize the variability between different mixtures and procedures for sampling from the mixtures. The standard deviation of the peak heat of hydration and time of peak heat of hydration are presented in tabular format as well as time the standard deviations as a function of time.

After evaluating the mixtures to identify the largest paste and mortar CAC samples sizes that could be used at each temperature, the next study was to investigate the repeatability of different mixtures. Similar to the repeatability studies discussed in Section 4.3, one sample from eight different mixtures was tested at four different isothermal temperatures (5°C, 23°C, 38°C, and 60°C) for both paste and mortars. All materials were preheated/cooled to their respective isothermal temperatures 24 hours

prior to testing to minimize the amount of time to reach thermal equilibrium during testing. The CAC mortar mixtures had a 0.40 w/c and 2.25 aggregate/binder ratio. The mixtures were prepared according to ASTM C 305 and samples were immediately placed in the calorimeter after mixing. From the variability in sample size studies, these were the recommended sample sizes for CAC at the corresponding temperatures: 30g at 5°C, 25g at 23°C, 15g at 38°C, and 8g at 60°C. These actual masses varied ±1.0g and the data were normalized according to the actual mass of the sample. The mixture matrix for the repeatability of CAC mortar is shown in Table 21.

Table 21: CAC mixture matrix for CAC mortar repeatability

| | Testing Temperature (°C) | No. Mixtures Completed | No. Samples Per Mixture | Sample Size (g) |
|---|---|---|---|---|
| CAC Mortar - Repeatability | 5 | 8 | 1 | 30 |
| | 23 | 8 | 1 | 25 |
| | 38 | 8 | 1 | 15 |
| | 60 | 8 | 1 | 8 |

Figure 40 illustrates the heat of hydration curve for the eight 23°C mortar mixtures.

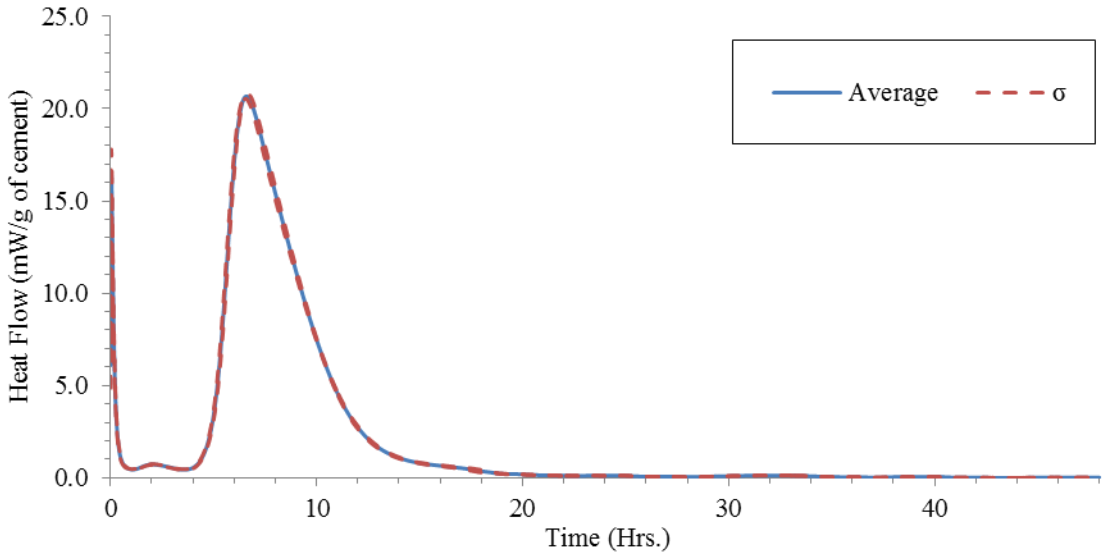


Figure 40: Heat flow of CAC mortar at 23°C isothermal

At 23°C, the repeatability of the eight different mortar mixtures at the recommended sample size showed an improved repeatability at the peak heat of hydration. The standard deviation lines are difficult to differentiate from the line of the average heat of hydration. Appendix B.7 contains the individual plots at three other isothermal temperatures. Table 22 summarizes the repeatability of the other CAC mortar mixtures at the three other isothermal temperatures.

Table 22: CAC mortar repeatability at various temperatures

| Temp. (°C) | Avg. Peak Heat Flow (mW/g cement) | Peak Heat Flow Repeatibility (σ) | Avg. Time until Peak Heat Flow (h) | Time until Peak Heat Flow Repeatibility (σ) |
|---|---|---|---|---|
| 5 | 11.800 | 0.238 | 3.958 | 0.074 |
| 23 | 20.695 | 0.153 | 6.572 | 0.051 |
| 38 | 8.990 | 0.233 | 4.800 | 0.037 |
| 60 | 122.107 | 5.799 | 0.337 | 0.009 |

Table 22 summarized the acceptable repeatability of the time of the peak heat of hydration of the eight different mortar mixtures at four different temperatures. This again validates that the equipment can be used to compare the times of peak heat of hydration

of different mixtures. The largest standard deviation was observed at 60°C; however, this was reduced by about half once the ideal sample size was identified.

Similar to the repeatability study completed with the mortar samples, CAC paste mixtures were evaluated at four different isothermal temperatures. Eight different mixtures were cast for four different isothermal temperatures (5°C, 23°C, 38°C, and 60°C). The CAC paste mixtures had a 0.40 w/c. The mixtures were prepared according to ASTM C 305 and were immediately sample and placed in the calorimeter after mixing. The theoretical samples sizes for CAC paste were: 25 g at 5°C, 15 g at 23°C, 15 g at 38°C, and 5 g at 60°C. The actual masses varied by ±0.5 g and the data were normalized according to the actual weight of the sample. The mixture matrix for the repeatability of CAC paste is shown in Table 25.

Table 23: CAC mixture matrix for CAC paste repeatability

| | Testing Temperature (°C) | No. Mixtures Completed | No. Samples Per Mixture | Sample Size (g) |
|---|---|---|---|---|
| CAC Paste - Repeatability | 5 | 8 | 1 | 25 |
| | 23 | 8 | 1 | 15 |
| | 38 | 8 | 1 | 15 |
| | 60 | 8 | 1 | 5 |

Figure 41 illustrates the heat of hydration curve for the eight 23°C paste mixtures.

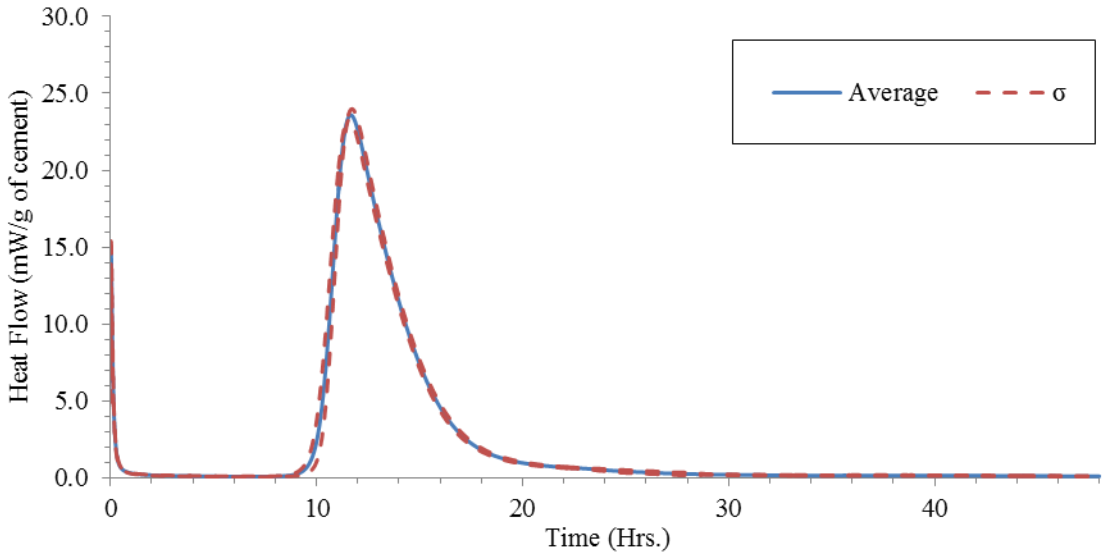


Figure 41: Heat flow of CAC paste at 23°C

In Figure 41, it is evident that the standard deviation of the heat of hydration is small relative to the amount of heat released from each sample. Using the recommended sample size decreased the standard deviation. Table 24 summarizes the repeatability of eight mixtures at four isothermal temperatures.

Table 24: CAC paste repeatability at various temperatures and various sample sizes

| Temp. (°C) | Avg. Peak Heat Flow (mW/g cement) | Peak Heat Flow Repeatibility (σ) | Avg. Time until Peak Heat Flow (h) | Time until Peak Heat Flow Repeatibility (σ) |
|---|---|---|---|---|
| 5 | 13.795 | 0.182 | 4.431 | 0.089 |
| 23 | 23.659 | 0.310 | 11.636 | 0.086 |
| 38 | 12.830 | 0.961 | 4.910 | 0.015 |
| 60 | 90.132 | 2.838 | 0.875 | 0.021 |

From Table 24, the repeatability was improved for the peak heat of hydration for the paste samples compared to the mortar samples. These results are assumed to be due to the homogeneity of the paste mixtures compared to the mortar mixtures. When sampling the mixtures, it was possible that the sampling caused the errors seen in the

mortars compared to the paste. The repeatability of the time of the peak heat of hydration for the CAC paste samples was acceptable for all testing temperatures.

From the work completed in this section, it was shown that the newly developed isothermal calorimeter was repeatable at the recommended sample sizes. The standard deviations of the time of the peak heat of hydrations were minimal. The equipment was repeatable in testing CAC paste and mortar samples at all temperatures; however, there was an increase in error at the highest isothermal temperature (60°C).

## 4.9 Calorimetry Analysis Techniques

To complete this chapter this section discusses techniques for analysis of isothermal calorimetry data. Some of the techniques are more intuitive but for clarity and completeness they are briefly discussed and provide comparison of CAC and PC behavior. The methods that are discussed include the comparison of the heat flow and cumulative heat release.

### 4.9.1 Heat Flow (mW/g)

The most common method for comparing material combinations when using isothermal calorimetry is to compare the heat flow of different mixtures. The heat flow was recorded by differential heat flow sensors that are located underneath each sample. The sensors record a voltage of the difference of heat across a known thickness of aluminum with one sensor directly below the sample and one sensor in ambient conditions. Then from calibration factors computed prior to testing, the voltage is converted to a power, typically in milliwatts (mW). This power reading was normalized per gram of cement or cementitious material in each individual sample. The normalized data allow for an equal comparison of the various mixtures.

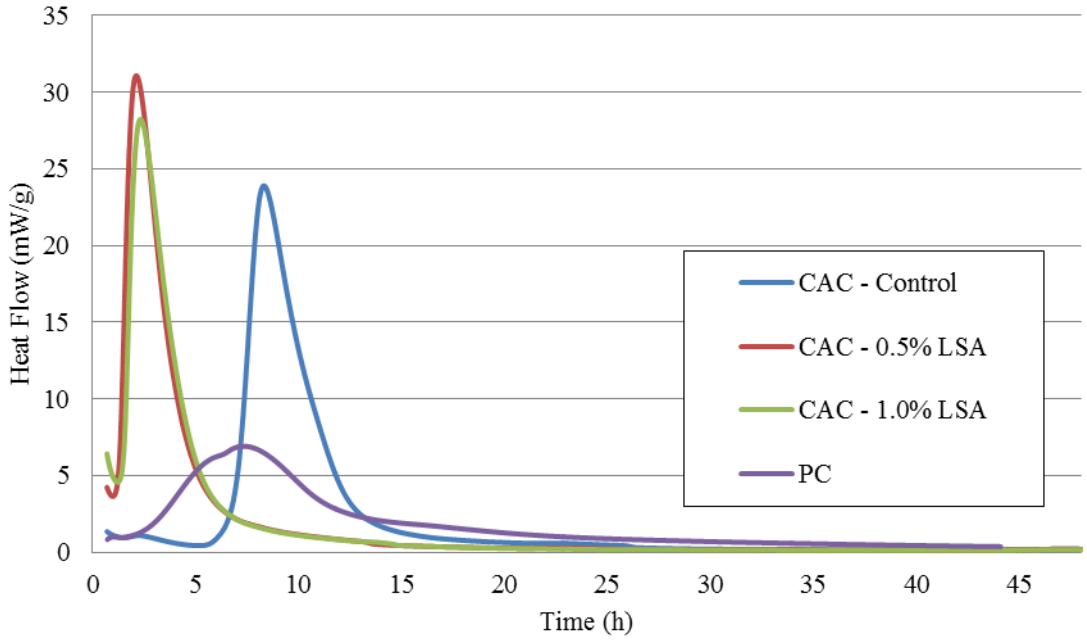


Figure 42: Example heat of hydration of CAC and OPC paste with varying LSA dosages at 23°C

Figure 42 compares the effects of different percentages of LSA on CAC paste at 23°C and a comparison to a typical PC. The graph illustrates the long induction period of CAC control paste mixtures and highlights the acceleration of this process when an LSA is used. The graph also illustrates the amount of heat generated by CAC mixtures compared to the reference PC. The sharp deceleration of CAC mixtures illustrates the rapid slowing of hydration due to the lack of space for continued formation of hydration products (Gosselin C. , 2009). From these data, the user is able to compare the induction periods before precipitation and strength gain, the time of peak heat of hydration and generally compare the rate of reaction of different mixtures. These graphs are not always an indication of strength development and ultimate strength magnitudes. Maturity of mixtures can be estimated or calculated from these curves by determining the area under the curve or the cumulative heat release, which is discussed in the next section.

### 4.9.2 Cumulative Heat Release (J/g)

Another technique for analyzing material combinations in isothermal calorimetry was to compare the area under the heat flow curve or the cumulative heat release. This was measured in the units of Joules/gram of cement, a unit of energy that is normalized per gram of cement or cementitious material for each sample. A graph of the cumulative heat of the mixtures presented in Figure 42 is shown in Figure 43.

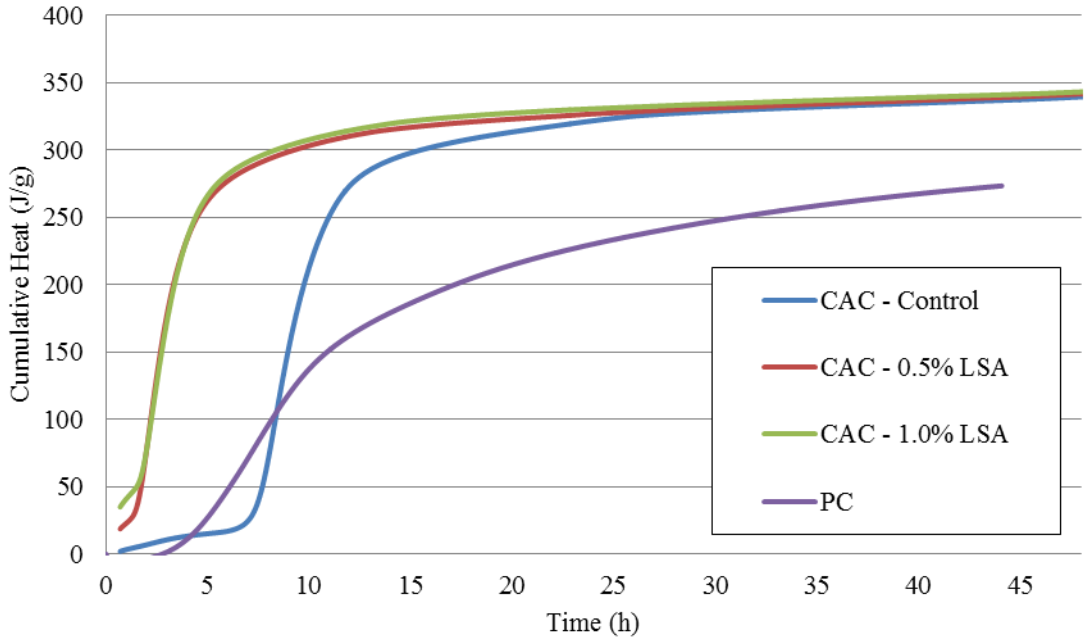


Figure 43: Example cumulative heat release of CAC paste with varying LSA dosages at 23°C

The cumulative heat release was calculated by using Simpson's rule for numerical integration, which determines the area under the heat flow curve from the previous section. From Figure 44, the speed or acceleration of the hydration reaction can easily be compared by looking at the angle of the slopes as well as when the slopes occur for the different mixtures. These curves are often used to give a better comparison of strength

development and comparison of total hydration. From Figure 43, it was evident that the reaction was delayed for the control CAC mixture compared to those with accelerator. However, the total heat release of the three mixtures is nearly identical. The PC total heat release curve had a more gradual slope with less heat release that is reflected in the heat flow curve shown in Figure 42. When combined, the two graphs can provide a large amount of information on the hydration of cementitious systems. These techniques employed throughout the research reported in this dissertation.

## 4.10 DISCUSSION

Over 500 paste and mortar mixtures were analyzed in this chapter for the characterization and development of the new isothermal calorimeter built specifically for CAC. This study was the most comprehensive study investigating the repeatability of an isothermal calorimeter for PC and especially CAC cement. Figure 44 and Figure 45 summarize the standard deviation of the time of the peak heat of hydration for PC and CAC paste and mortar mixtures, respectively.

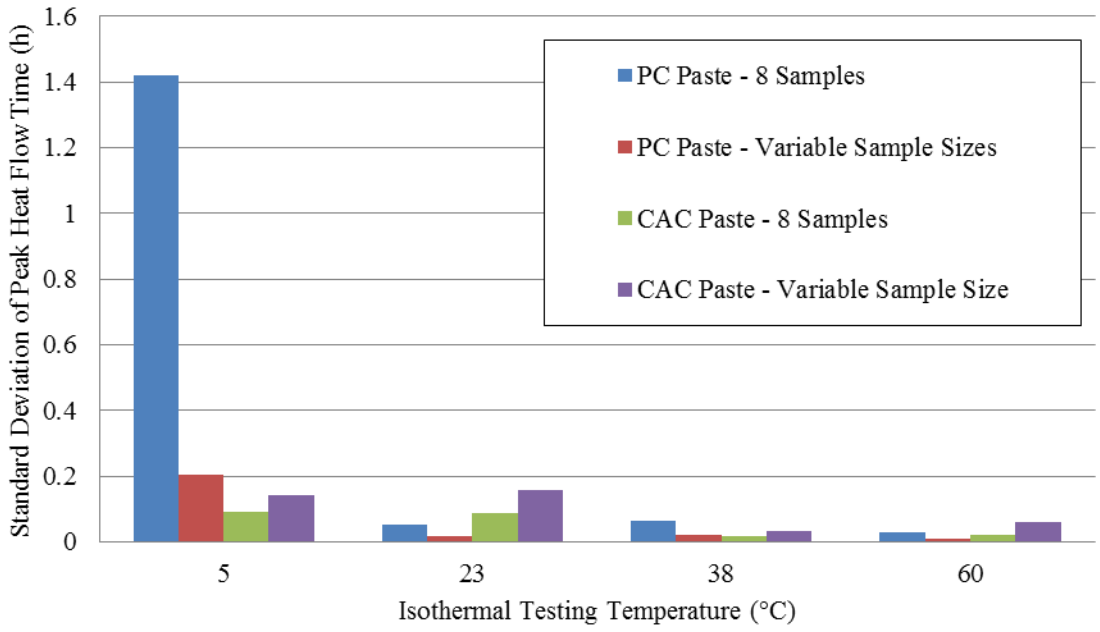


Figure 44: Standard deviation of the time of peak heat of hydration for PC and CAC paste

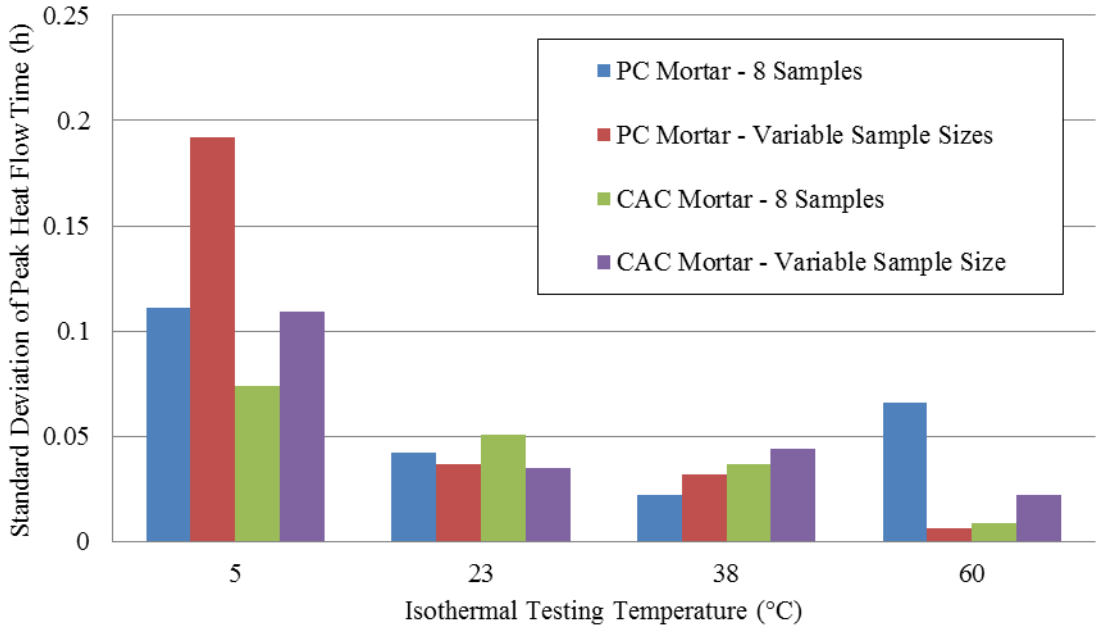


Figure 45: Standard deviation of the time of peak heat of hydration for PC and CAC mortar

The PC repeatability studies were completed with the Grace AdiaCal calorimeter and the results presented with the CAC were completed with the new isothermal calorimeter. The repeatability of the time for the peak heat of hydration detected for both the paste and mortars were acceptable. The repeatability between calorimeters, eight different mixtures, variable sample sizes, and cements were comparable and illustrate that improved repeatability of the new calorimeter to match that of the Grace AdiaCal system. The only flaw that stands out is the larger variability with PC paste at 5°C. At this temperature a broad heat flow curve was generated making it difficult to pinpoint the exact time of the peak heat of hydration, resulting in the larger standard deviation. Figure 46 and Figure 47 summarize the standard deviations of the peak heat of hydration for PC and CAC paste and mortar mixtures, respectively.

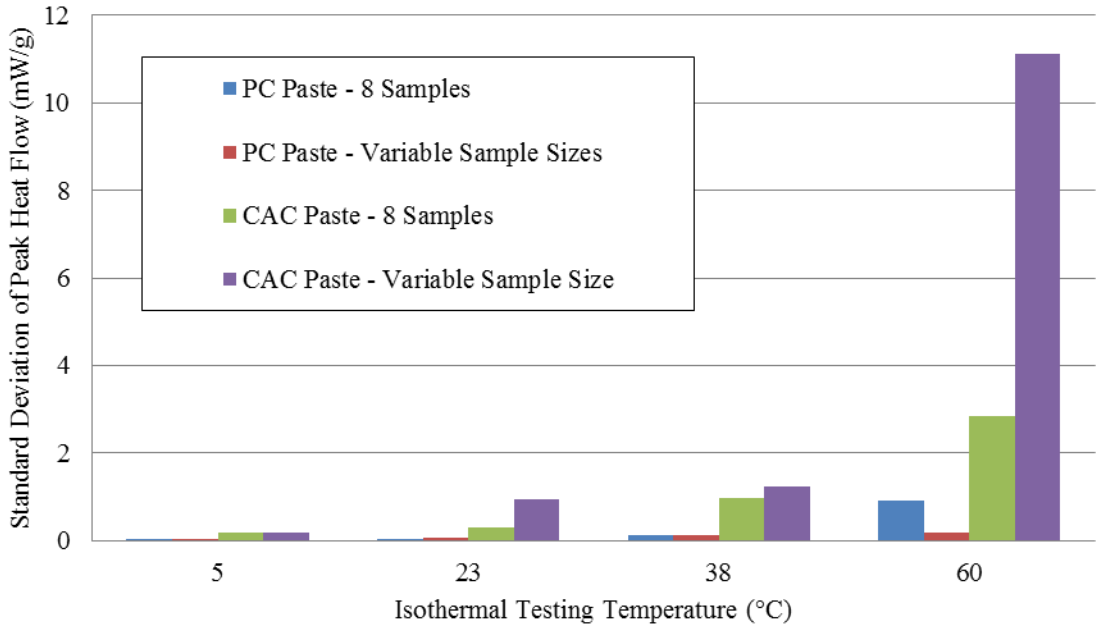


Figure 46: Standard deviation of peak heat of hydration for PC and CAC paste

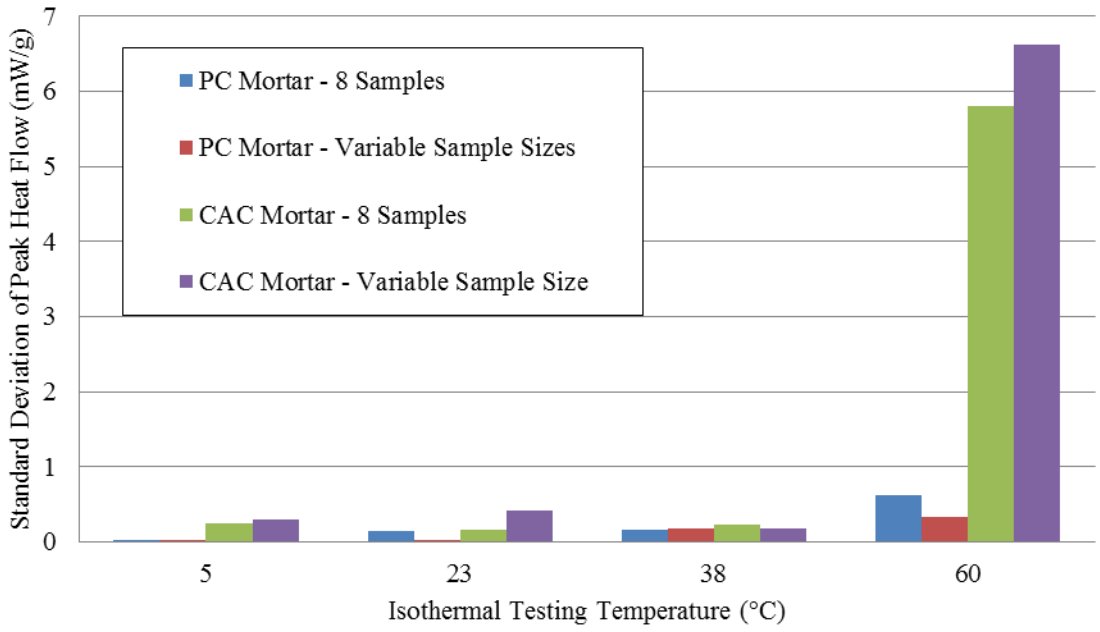


Figure 47: Standard deviation of peak heat of hydration for PC and CAC mortar

The standard deviations of PC and CAC paste and mortar are comparable at 5°C, 23°C, and 38°C. However, a 2.84 mW/g and 5.80 mW/g error was measured with the CAC paste and mortar mixtures at 60°C, respectively. The reaction of CAC at this higher temperature generates 5 times the amount of heat, causing the lack of repeatability at the higher temperature. From the testing completed with these studies and others not presented, it is recommended that isothermal testing of CAC based-systems in this calorimeter should not be tested over 45°C, if the key interest of future studies to identify the amount of heat flow. Besides that one fault, the new calorimeter built specifically for CAC appears to be repeatable for use for the study of CAC paste and mortars.

### 4.11 Conclusions

This chapter discussed the characterization of the Grace AdiaCal isothermal calorimeter for use with PC and CAC. It was shown that the original design was

repeatable for testing PC paste and mortar samples between mixes and with variable sample sizes. The calorimeter was not capable of maintaining isothermal conditions due to the excessive heat release associated with CAC hydration. Thus, a demand for a new calorimeter existed. The chapter contained a summary of the development and specific changes made to build a calorimeter built specifically for CAC. Later, the new calorimeter was shown to be repeatable for CAC paste and mortars; however, a challenge remains with testing CAC at the highest testing temperature (60°C). The calorimeter was used to evaluate the hydration kinetics of various material combinations, and the results are presented in the remainder of the dissertation.

# Chapter 5: Hydration and Early-age Volume Deformation of Plain CAC

The experimental results of studies on the hydration and early-age volume deformation of plain CAC with LSA and HRWR are presented in this chapter. Investigations were completed at 20°C and 38°C isothermal conditions for all experiments, unless otherwise noted. Techniques introduced and described in Chapter 3 were implemented to characterize the hydration and early-age volume deformation of these systems. It should be noted, that the CAC specific calorimeter described in Chapter 4 was used throughout the remainder of the dissertation to evaluate the material combinations of CAC based-systems on the hydration kinetics. Over 250 specimens were evaluated in calorimetry, qualitative XRD, chemical shrinkage, and autogenous shrinkage, with the objective of understanding the influence of these two admixtures on plain CAC.

Previous work by Ideker and Gosselin investigated the influence of these admixtures on the early-age volume deformation and micro-structural development on a similar high-Fe CAC (Ideker, 2008) and (Gosselin C. , 2009). The studies described in this chapter aimed to characterize the influence of these admixtures at higher addition amounts to achieve the high early-age strength and workability required for rapid repairs in field applications. A summary of the individual influences of these materials as well as the combined effects is presented in this chapter. Experimental techniques developed and tailored specifically for CAC were implemented to provide a database of testing that could be used to screen other material combinations presented later in this dissertation.

## 5.1 HYDRATION OF CAC AT 20°C

This section first presents the investigations of the influence of LSA and HRWR separately at 20°C. Then, investigations of the combined effects of the chemical admixtures are presented.

### 5.1.1 Influence of LSA at 20°C

As discussed in Chapter 2, lithium-based accelerators are the most commonly used accelerators in CAC-based systems. The addition of this chemical admixtures leads to the formation of lithium alumina hydrates that act as nucleation sites that minimize the time of the induction period (Gosselin C. , 2009). The effects of varying LSA dosages on the heat flow and cumulative heat release of CAC are shown in Figure 48 and Figure 49, respectively.

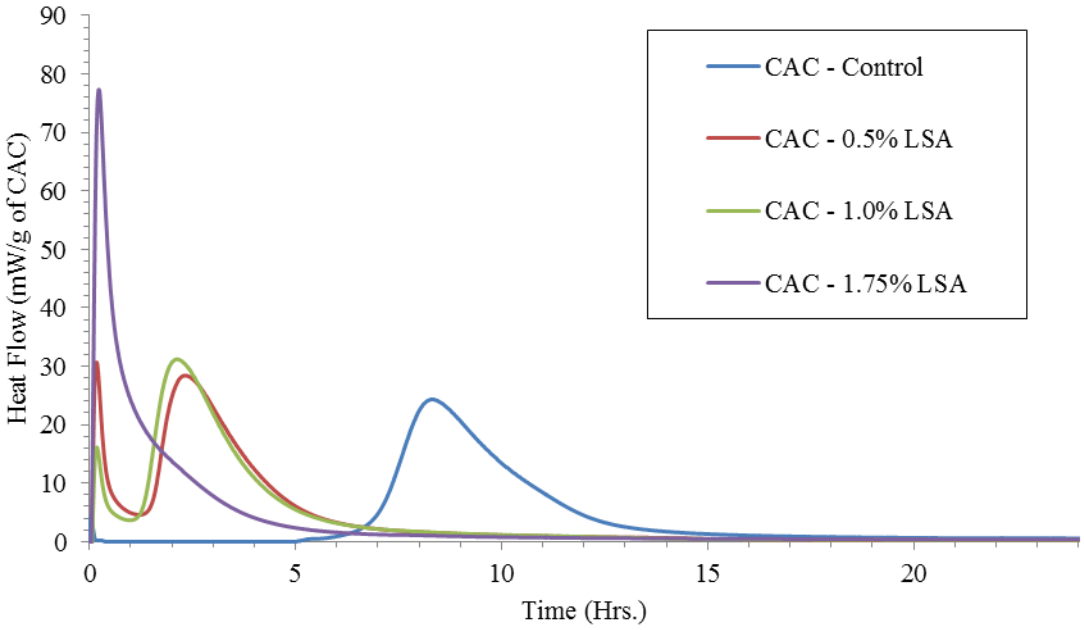


Figure 48: Heat flow of CAC hydrated at 20°C for varying LSA dosages

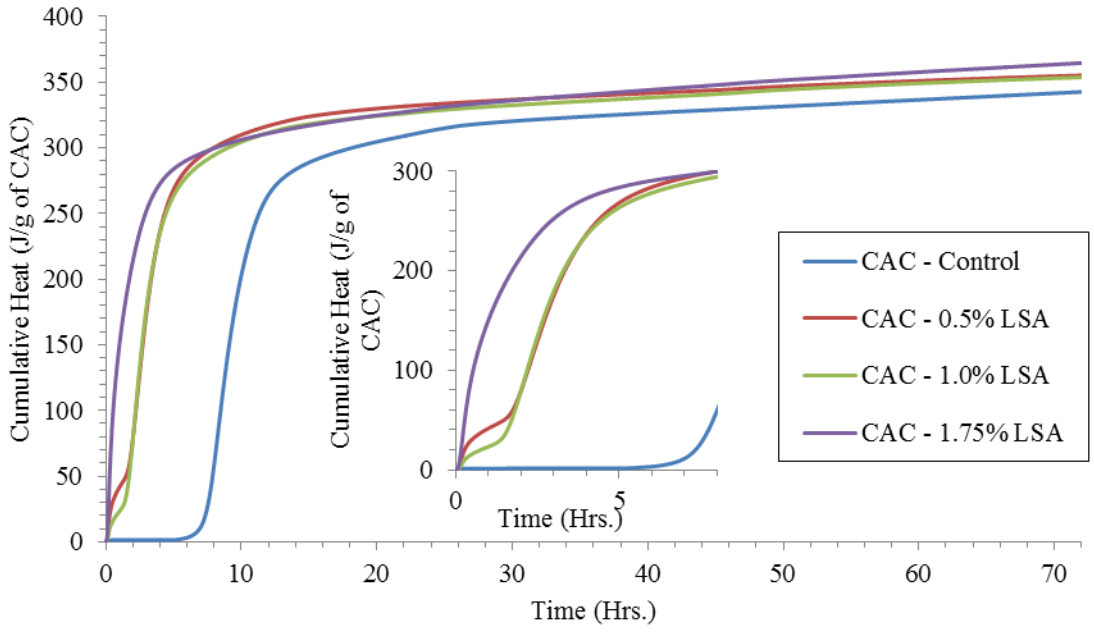


Figure 49: Cumulative heat release of CAC hydrated at 20°C for varying LSA dosages

From Figure 48, general observations can be made about the exothermic heat release of the hydrating cement paste. The CAC control mixture experienced a long induction period of approximately seven hours. This induction period was drastically reduced by the addition of LSA admixtures. Minimal difference in the time of the induction period was observed between mixtures containing 0.5% and 1.0% LSA.

Typically, CAC with 1.75% LSA would not be used in field applications because this dosage would cause immediate flash setting. However, this dosage was used with plain CAC because work presented in Chapter 7 used this high dosage in conjunction amount with different retarders. The potency of the high dosage of LSA is quite evident. Over 3 times the amount of heat was released compared to the control mixture, and the peak heat flow occurred at 0.20 hours compared to the control at 8 hours.

From Figure 49, similar quantities of cumulative heat released were observed for the four mixtures at the termination of the experiment at 72 hours. These observations were different than expected due to the drastically different shapes of the heat flow curves, shown in Figure 48. From the slope of the cumulative heat curves and the point of initiation of hydration, the acceleration due to LSA was evident. The addition of LSA did not affect the total amount of heat released.

Qualitative XRD was completed on the CAC control mixture and the CAC mixture with 1.0% LSA. The hydration of the samples was stopped using the solvent exchange method at 1 hour, 4 hours, 8 hours, 1 day, and 3 days. The time-lapsed XRD is shown in Figure 50.

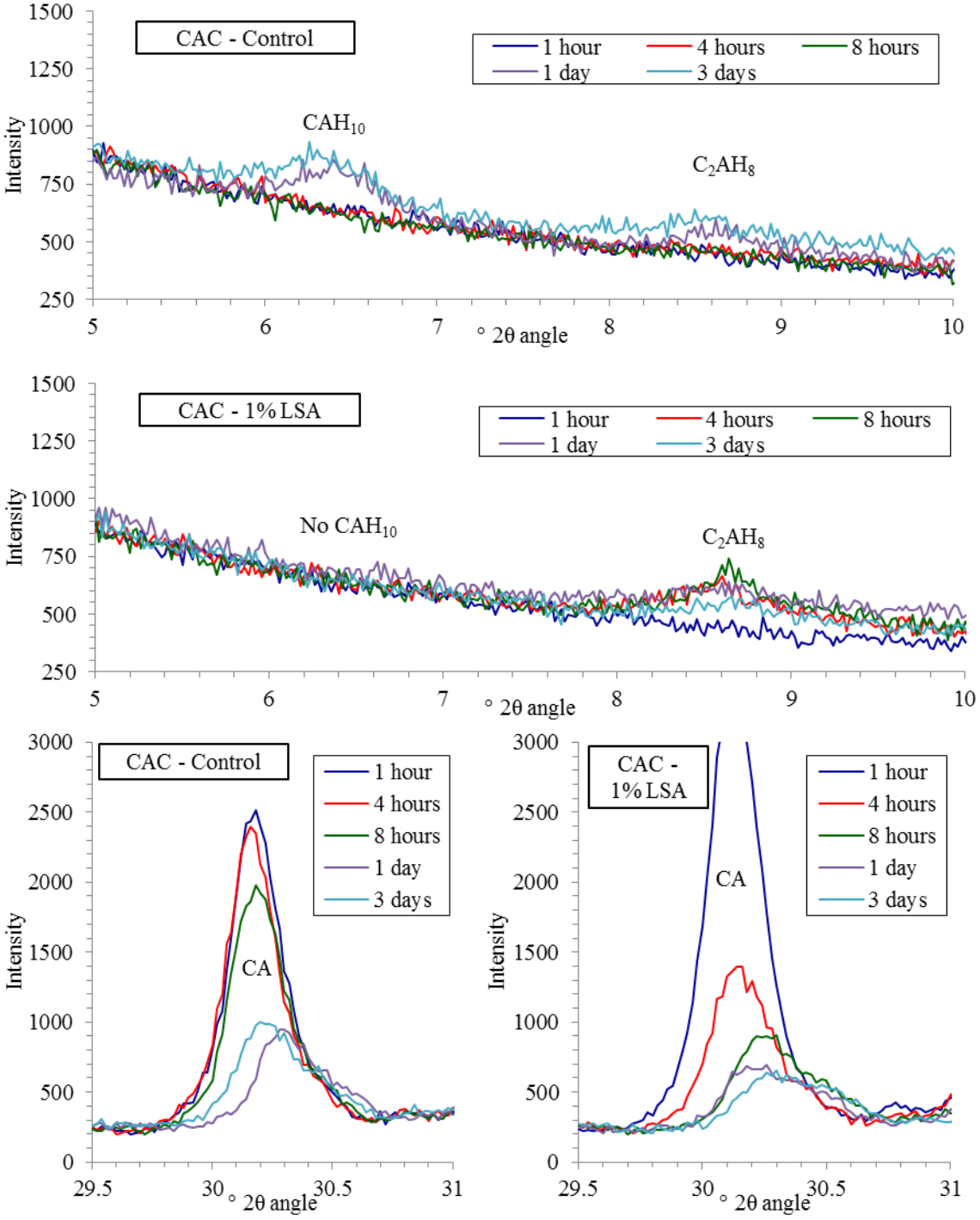


Figure 50: Qualitative XRD of CAC with and without 1% LSA hydrated at 20°C, characterizing the formation of $CAH_{10}$ and $C_2AH_8$ and the depletion of CA

The XRD patterns from 5° to 10° 2θ characterize the formation of the two metastable hydrates, $CAH_{10}$ and $C_2AH_8$. The CAC control mixture began forming both hydrates between 8 hours and 1 day. Both of these hydrates have broad peaks due to the poor crystallinity and disorganization of the microstructure. In the CAC mixture with 1.0% LSA, the direct formation of $C_2AH_8$ was observed without the precipitation $CAH_{10}$. This observation was unique and highlighted the complex influence LSA had on the hydration of CAC (Gosselin C. , 2009).

To look more specifically at the rate of hydration, the XRD pattern from 29.5° to 31° 2θ of monocalcium aluminate (CA) is isolated and shown in Figure 3. On these graphs, the rate of reaction of the two mixtures can be compared based on the dissolution of this CA phase. The control mixture has minimal dissolution of the CA phase until after 8 hours of hydration, while the mixture with 1.0% LSA had drastic reduction in CA in the first 4 hours.

The isothermal calorimetry and qualitative XRD analysis of CAC with the addition of LSA illustrated the rapid hydration with these two material combinations. To control this rapid reaction, LSA is often combined with a HRWR or other retarder to control the setting time but still provide a high early-age strength mixture.

### 5.1.2 Influence of HRWR at 20°C

This section discusses the characterization of the influence of the HRWR on the hydration kinetics and microstructural development. The results of 20°C isothermal calorimetry of CAC with varying HRWR dosages are presented in Figure 51 and Figure 52.

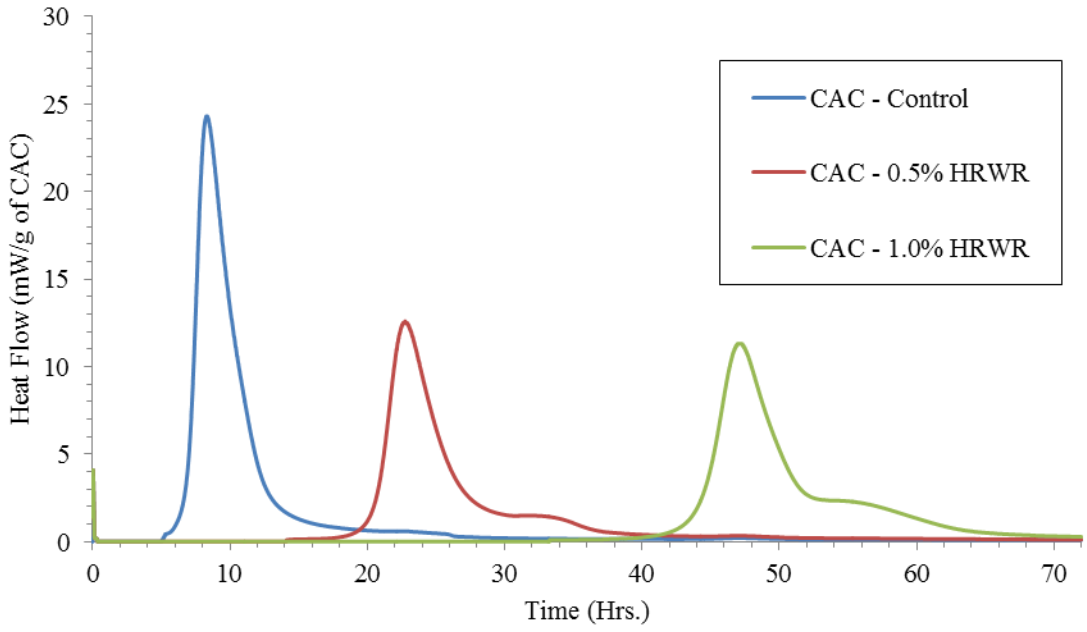


Figure 51: Heat flow of CAC hydrated at 20°C for varying HRWR dosages

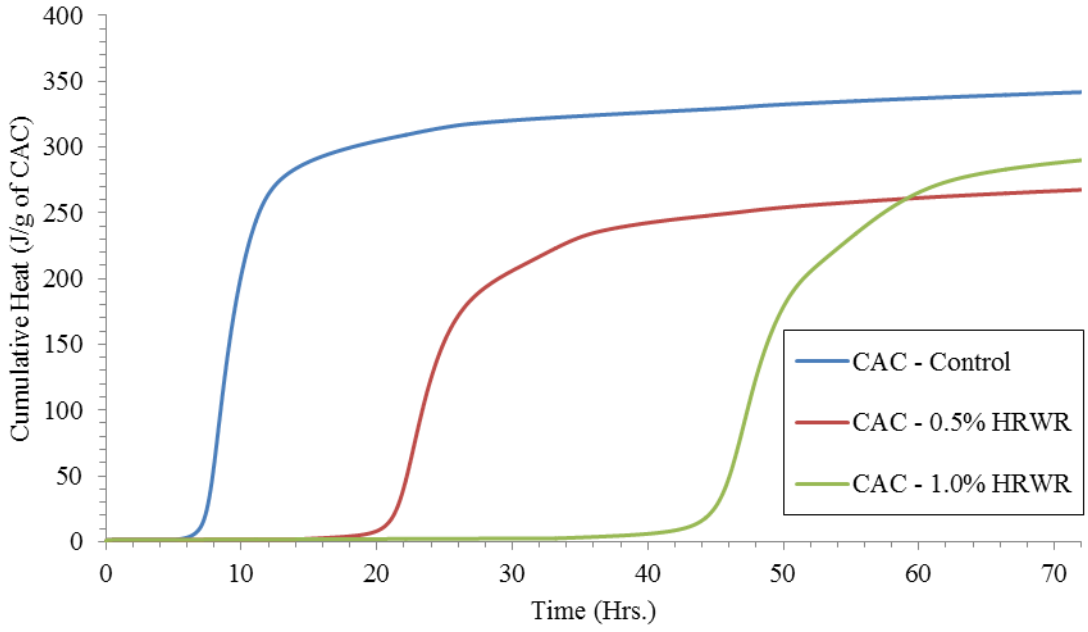


Figure 52: Cumulative heat release of CAC hydrated at 20°C for varying HRWR dosages

The use of 0.5% and 1.0% HRWR represents a higher than typical dosage for many field applications. However, these high dosage rates were chosen based on the need to control the hydration reaction when high dosages of LSA admixtures were added to the mixtures. From the Figure 51 and Figure 52, the strong influence that this admixture had on the rate of hydration was evident in both the heat flow curve and cumulative heat release. The mixture containing 1.0% HRWR had an induction period that lasted nearly 42 hours, and the mixture containing 0.5% HRWR had an induction period that lasted 20 hours.

The HRWR had a large impact on the total amount of heat released as shown in Figure 52. The CAC control mixture had a total cumulative heat release of 340 J/g and the mixtures containing 0.5% and 1.0% HRWR had 260 J/g and 280 J/g, respectively. To compare, the cumulative heat of the mixtures containing LSA were plotted with the mixtures containing HRWR in Figure 53, where it can be seen that these two chemical admixtures had drastically different effects on the hydration of CAC. The LSA reduced the induction period and caused the rapid hydration of CAC. The HRWR extended this period and prevented the precipitation of hydration products for over 20 hours and nearly 42 hours for 0.5% and 1.0%, respectively. It also lowered the total cumulative heat released. Thus, these materials would typically not be used separately in applications where high early-age strength and workability are required: however, it was deemed necessary to characterize the independent influence each has on the CAC.

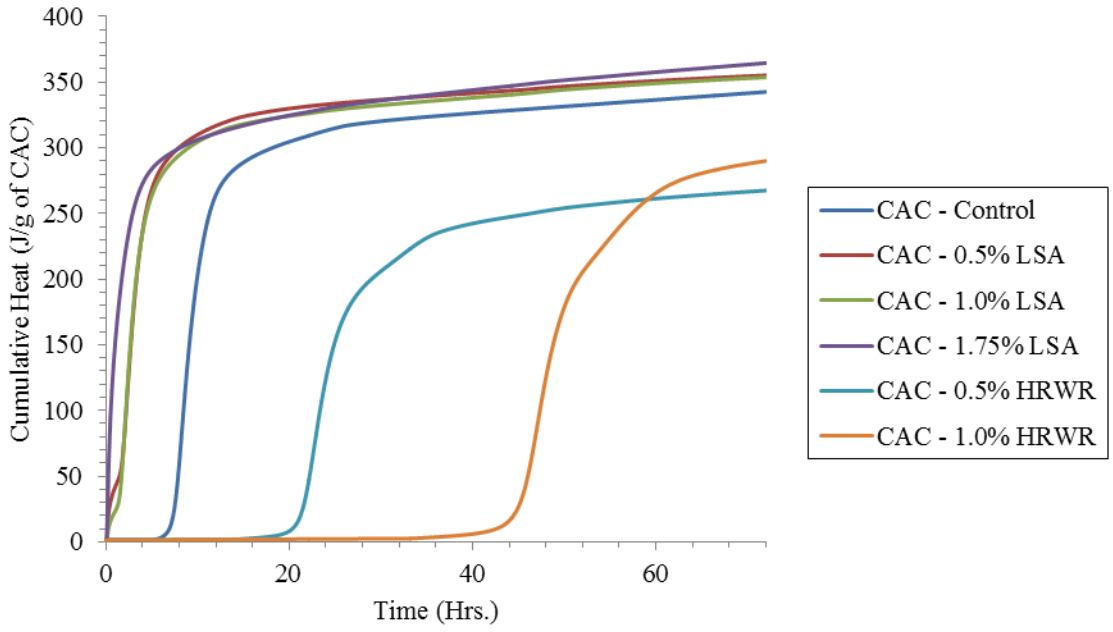


Figure 53: Cumulative heat release of CAC hydrated at 20°C with varying LSA and HRWR dosages added separately

Qualitative XRD analyses were carried out on CAC with and without 1% HRWR, and the patterns are presented in Figure 54. Hydration was stopped at 1 hour, 4 hours, 8 hours, 1 day, and 3 days using the solvent exchange method.

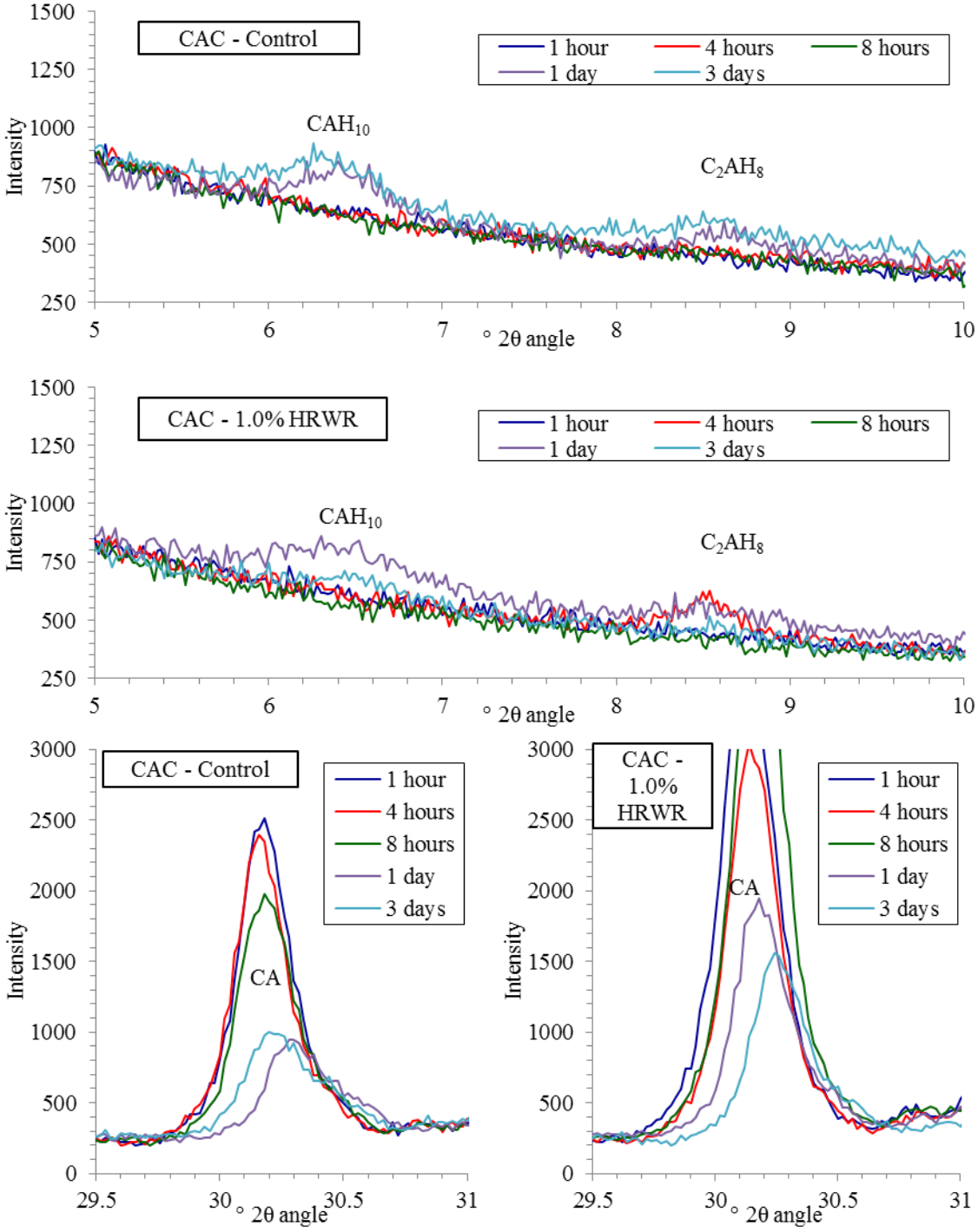


Figure 54: Qualitative XRD of CAC with and without 1% HRWR hydrated at 20°C, characterizing the minimal formation of $CAH_{10}$ and $C_2AH_8$ and the depletion of CA

The CAC control mixture was compared to the mixture containing 1% HRWR in Figure 54. The top graphs illustrate the formation of the metastable hydration products, $CAH_{10}$ and $C_2AH_8$. The control mixture had minimal formation of these products, while the mixture with 1% HRWR had negligible amounts that could barely be distinguished from the noise of the experiment. The bottom graphs illustrate the consumption of CA. These graphs show that the HRWR severely retarded the consumption of CA, therefore slowing the hydration reaction.

From the isothermal calorimetry and the qualitative time-lapsed XRD, it was evident that the HRWR admixture was a powerful retarder that slowed the consumption of the CA. Also, the HRWR minimized the formation of the calcium aluminate hydrates, $CAH_{10}$ and $C_2AH_8$. Due to the powerful retardation of this admixture, it would not typically be used independently in the field with CAC. The next section investigated the combination of LSA and HRWR to achieve the rapid strength gain and workability needed in field applications.

### 5.1.3 Influence of Combined LSA and HRWR at 20°C

This section presents the results of experimental testing of plain CAC with varying dosages of LSA and HRWR less than 20°C isothermal testing.

#### *5.1.3.1 Isothermal Calorimetry at 20°C*

The effect of the combination of LSA and HRWR on the heat flow and cumulative heat release of plain CAC is shown in Figure 55 and Figure 56, respectively.

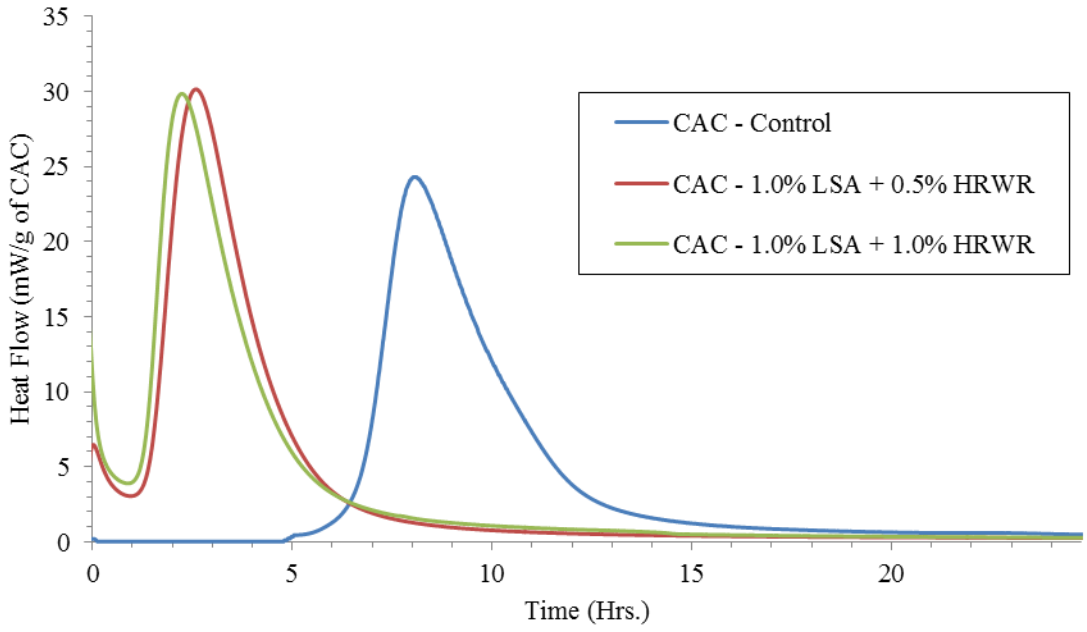


Figure 55: Heat flow of CAC hydrated at 20°C for varying LSA and HRWR dosages

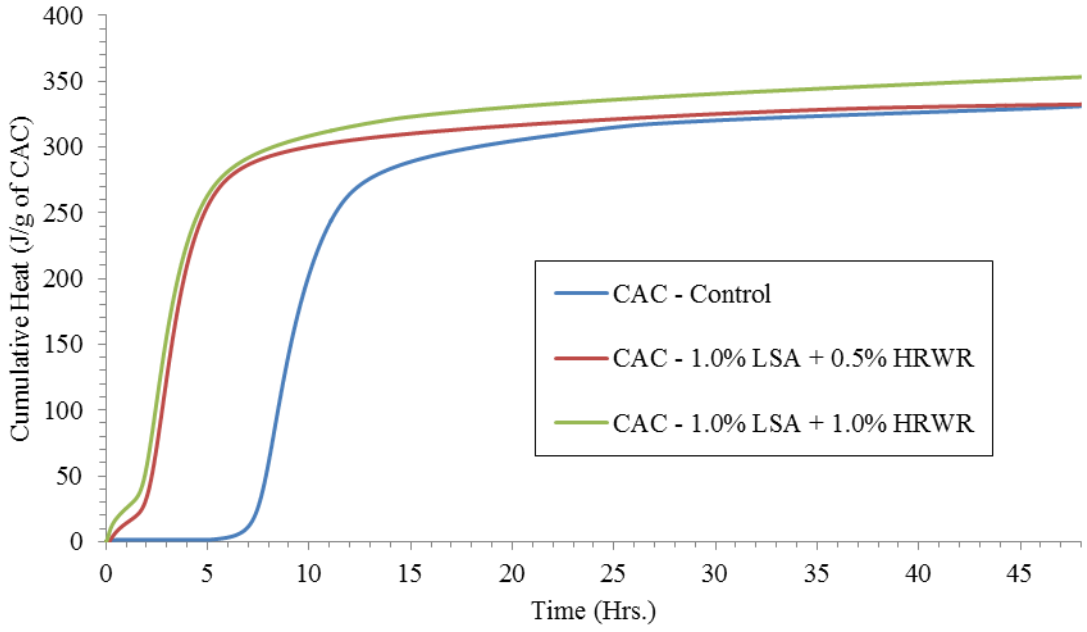


Figure 56: Cumulative heat release of CAC with varying dosages of LSA and HRWR at 20°C

The addition of the 1.0% LSA was selected based on previous work completed in the field to achieve 20 MPa (3000 psi) in three hours. The addition of 0.5% and 1.0% HRWR was selected based on trial concrete mixtures to achieve approximately 10-20 minutes of working time. This dosage of HRWR was excessive and did have the tendency to cause segregation in the samples; however, it was the application rate required to achieve the workability requirements.

From Figure 55 and Figure 56, the influence of 0.5% and 1.0% HRWR appears to slightly delay the precipitation of hydrates and the peak heat flow for the mixture containing more HRWR. However, both of these mixtures are accelerated compared to the control mixture. The amount of total heat release by the different mixtures was comparable.

#### *5.1.3.2 Qualitative XRD at 20°C*

To characterize the influence of LSA and HRWR on the microstructural development at 20°C isothermal conditions, qualitative XRD was completed. The XRD patterns for 1 hour, 4 hours, 8 hours, 1 day, and 3 days are shown in Figure 57.

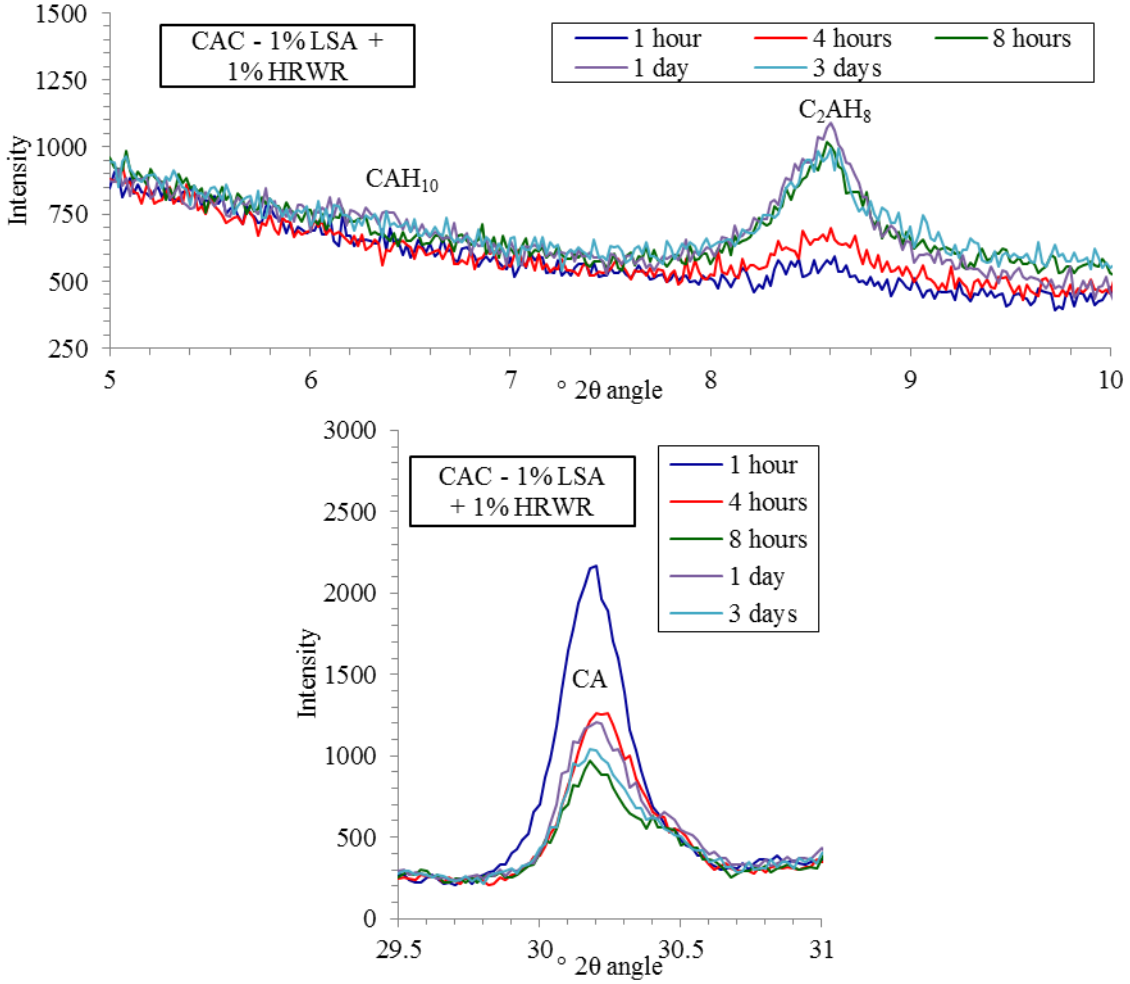


Figure 57: Qualitative XRD of CAC with 1.0% LSA and 1.0% HRWR hydrated at 20°C, illustrating the formation $C_2AH_8$ and the depletion of CA

The addition of 1% LSA and 1.0% HRWR led to the formation of $C_2AH_8$ after 4 hours of hydration at 20°C. Uniquely, there was no indication of the formation of $CAH_{10}$ at the primary peak, 12.4° 2θ, and at the secondary peak, 6.2° 2θ. The most distinguished $C_2AH_8$ peak was observed when these two admixtures were combined compared to their separate additions, mentioned previously. When the 1% LSA was used alone, a broad unorganized peak was observed, and when 1% HRWR was used no $C_2AH_8$ was observed. This precipitation of $C_2AH_8$ was unexpected at these isothermal temperatures.

From literature, the precipitation of solely $C_2AH_8$ has been noted to occur at temperatures higher than 27°C (Campas, 1998). Thus, there was concerned that samples were not maintaining isothermal conditions at the 20°C testing temperature. To reconcile that concern, two Thermochron iButtons were cast in the paste specimens to monitor the in-situ heat of two samples. The time-temperature history of the isothermal specimens is presented in Figure 58.

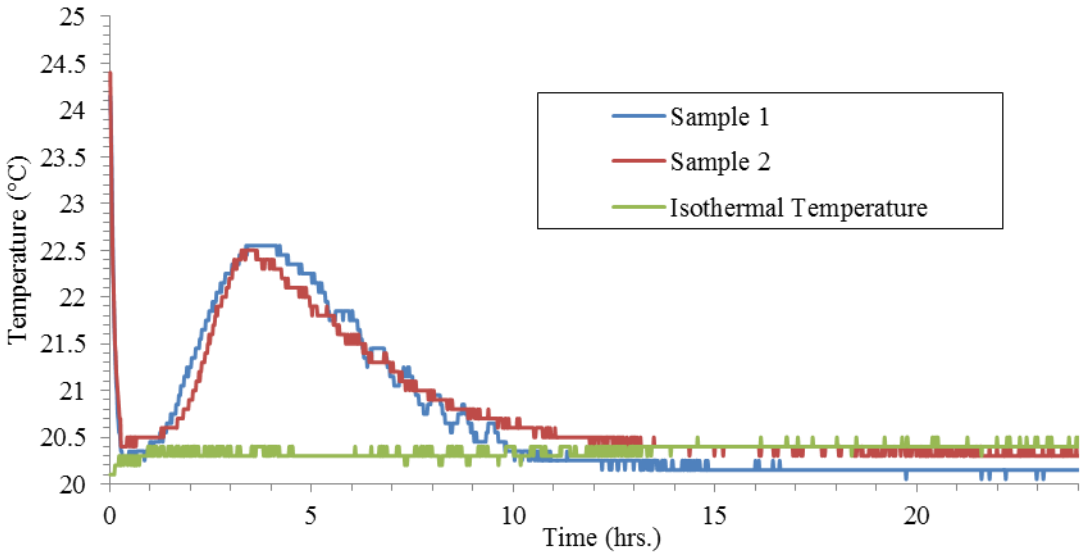


Figure 58: In-situ temperature of CAC – 1.0% LSA + 1.0% HRWR in isothermal calorimeter at 20°C

Thermochron iButtons are small temperature sensors, 16.3 x 6.35 mm (0.642 x 0.250 in.), capable of logging temperature, date, and time. The buttons are only accurate to ±1.0°C, thus the true values are not weighted heavily. The iButtons were embedded in the fresh paste samples immediately after mixing and then placed in the calorimeter. The baseline reading of the sample seems to be shifted by 0.25°C upward. The samples varied by approximately 2.0°C from the isothermal testing temperature. This temperature generation was slightly higher than experienced in other testing completed in the

development of the calorimeter and was probably due to the addition of the LSA admixture. However, with only a 2.0°C shift in the testing temperature this was not enough to prevent the formation of the $CAH_{10}$ hydration product. One would expect the co-formation of both metastable hydrates at this temperature range.

From the qualitative XRD patterns at 1 hour, 3 hours, 5 hours, 1 day, and 3 days, it was shown that the addition of 1.0% LSA and 1.0% HRWR accelerated the reaction of CAC. The admixtures led to the formation of $C_2AH_8$ and prevented the formation of $CAH_{10}$ at near isothermal conditions at 20°C. The heat generated by the sample was due to the addition of the LSA admixture, which was shown to generate more heat than samples without it.

#### *5.1.3.3 Chemical Shrinkage at 20°C*

To further investigate the hydration reaction of the plain CAC with varying dosages of LSA and HRWR, chemical shrinkage testing was performed. The experiment was run for two weeks and measurements were taken using an automated image analysis program that measured readings every five minutes. Each different mixture plot is the average of two samples from three different mixtures. The chemical shrinkage of CAC with LSA and HRWR at 20°C is shown in Figure 59 and Figure 60.

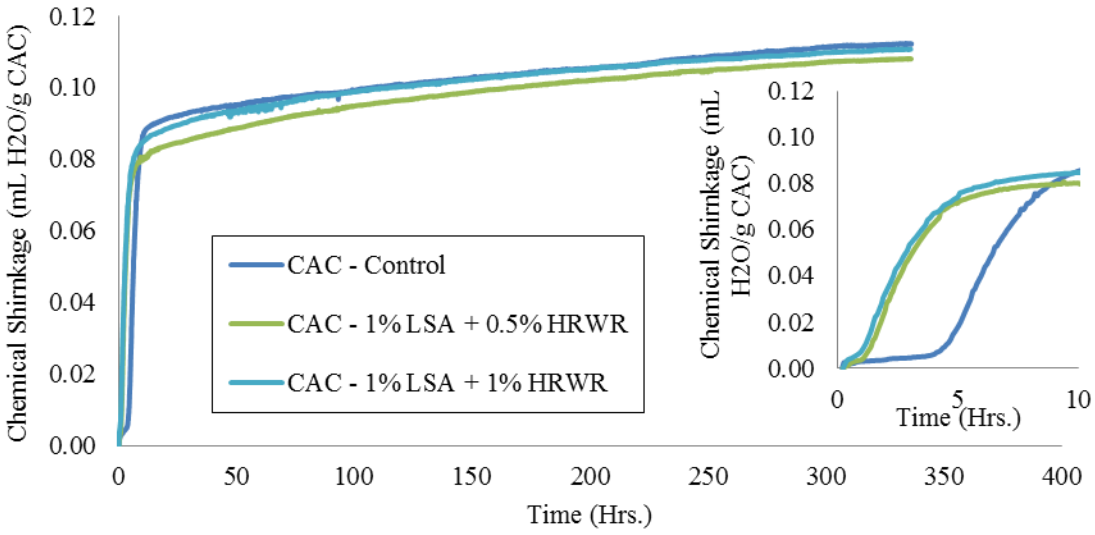


Figure 59: Chemical shrinkage of CAC with varying dosages of LSA and HRWR at 20°C

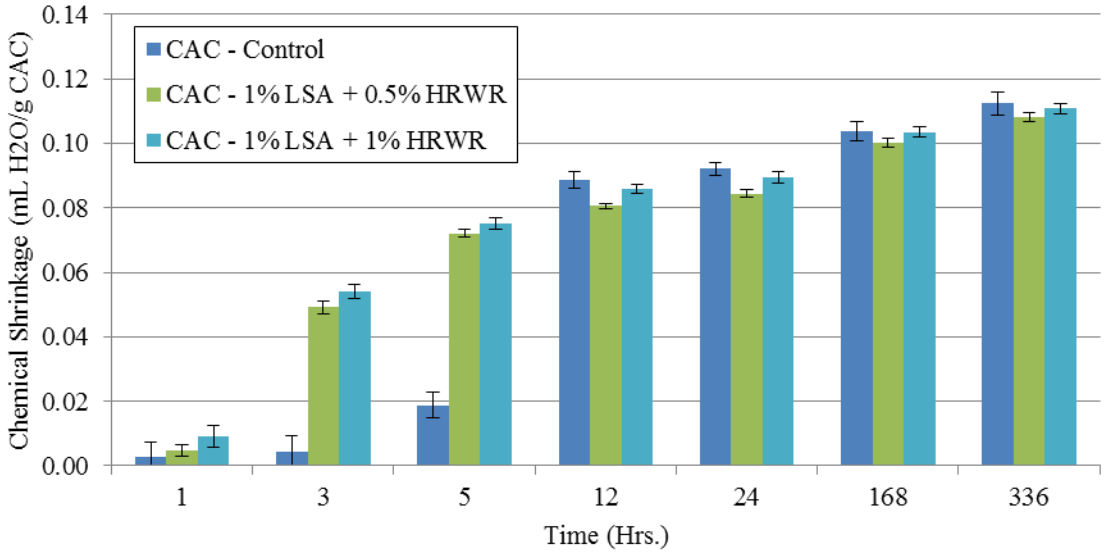


Figure 60: Chemical shrinkage with standard deviation for CAC with varying dosages of LSA and HRWR at 20°C

Figure 59 illustrates the average chemical shrinkage of two samples from three different mixtures for each material combination at 20°C for 14 days or 336 hours. Slower hydration of the CAC control mixture was observed compared to those containing

LSA. The majority of chemical shrinkage occurred between 4 and 9 hours, similar to when most of the heat flow was observed in the isothermal calorimeter. For the mixtures containing LSA, the majority of the chemical shrinkage occurred between 1 and 5 hours. Similar amounts of chemical shrinkage were experienced from a period of 10 hours until the termination of the experiment for all mixtures. It is important to note that this amount of chemical shrinkage after the initial ascent in the chemical shrinkage is minimal. However, the amount thereafter was minimal, therefore so was the amount of hydration.

Figure 60 shows the chemical shrinkage at distinct time increments to allow for the identification of the standard deviation. The bar graph shows good repeatability of the mixtures with little error that does not appear to affect the comprehension of the results. A comparison of the cumulative heat release and the chemical shrinkage of the first 48 hours are shown in Figure 61.

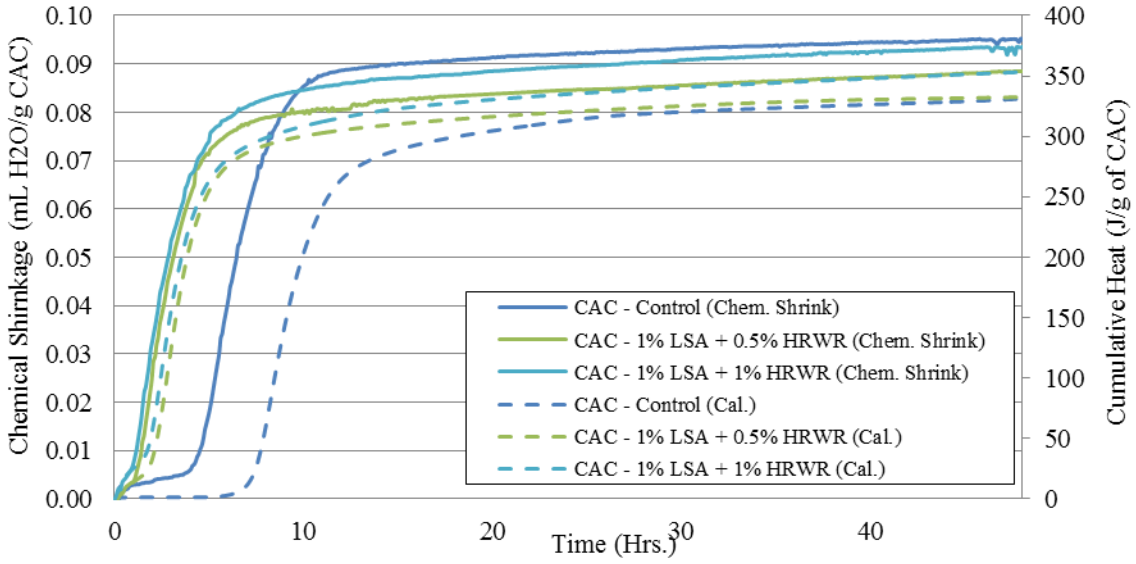


Figure 61: Comparison of chemical shrinkage with isothermal calorimetry cumulative heat release

From Figure 61, there was good agreement between the chemical shrinkage and cumulative heat release from isothermal calorimetry for the plain CAC with varying LSA and HRWR dosages. The slight delay in the hydration reaction was observed with the samples in the isothermal calorimetry compared to the samples in chemical shrinkage. The delay in reaction could be due to the different sample preparation procedures and variability in time that it took to prepare each. As an additional comparison of these techniques, the chemical shrinkage was plotted as a function of the cumulative heat release as shown in Figure 62.

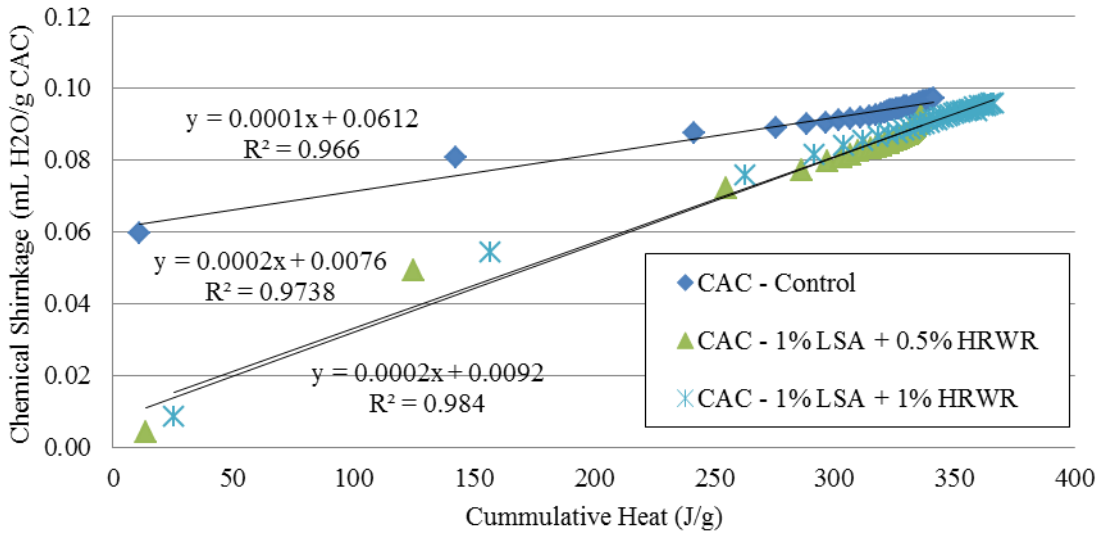


Figure 62: Chemical shrinkage as a function of cumulative heat of CAC with varying LSA dosages

Figure 62 combines the chemical shrinkage and cumulative heat release from isothermal calorimetry for the initial 72 hours of hydration for CAC hydrated at 20°C with varying dosages of LSA and HRWR. A linear line of best-fit shows a strong correlation coefficient with values greater than 96.6%. From these best-fit linear regressions, the slopes of the lines can be used as a quantitative comparison of the rate of

the reaction. The graph highlights the influence of LSA admixture, by the steeper slopes of those lines compared to the control mixture. The different dosage rates of HRWR did not appear to have that large effect on the rate of the reaction, illustrated by similar y-intercept values and correlation to the isothermal calorimetry results. These graphs are used throughout the dissertation to characterize the hydration reaction and may serve to help characterize the influence of other chemical and mineral admixture additions.

#### *5.1.3.4 Autogenous Deformation at 20°C*

In addition to monitoring the hydration of these systems, the autogenous deformation was evaluated to characterize the early-age volume deformation. The autogenous shrinkage of three different mixture combinations at 20°C is shown in Figure 63.

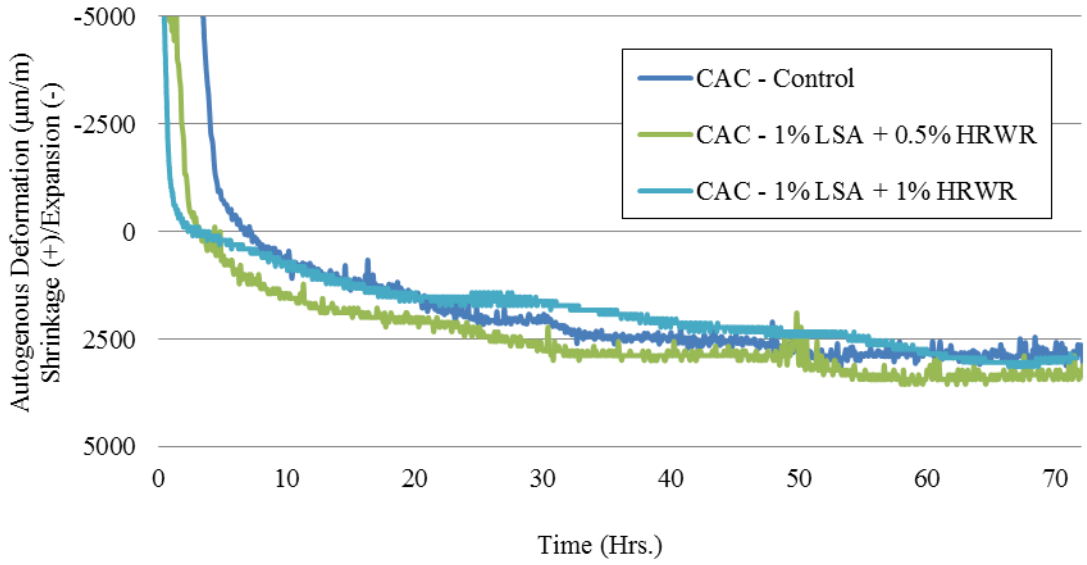


Figure 63: Autogenous deformation of CAC with varying dosages of LSA and HRWR at 20°C

The plots of the lines are averages of three different samples for each mixture. All specimens displayed a similar shrinkage behavior and similar ultimate shrinkage at

the termination of the test. The specimens experience about 3000 μm/m strain at 72 hours. These values are similar to those results found by Fu (2011).

## 5.2 HYDRATION OF CAC AT 38°C

Plain CAC was investigated at 38°C isothermal testing with the addition of LSA and HRWR, added separately, as well as combined.

### 5.2.1 Influence of LSA at 38°C

The isothermal calorimeter results of CAC mixtures with LSA admixture at 38°C are shown in Figure 64 and Figure 65.

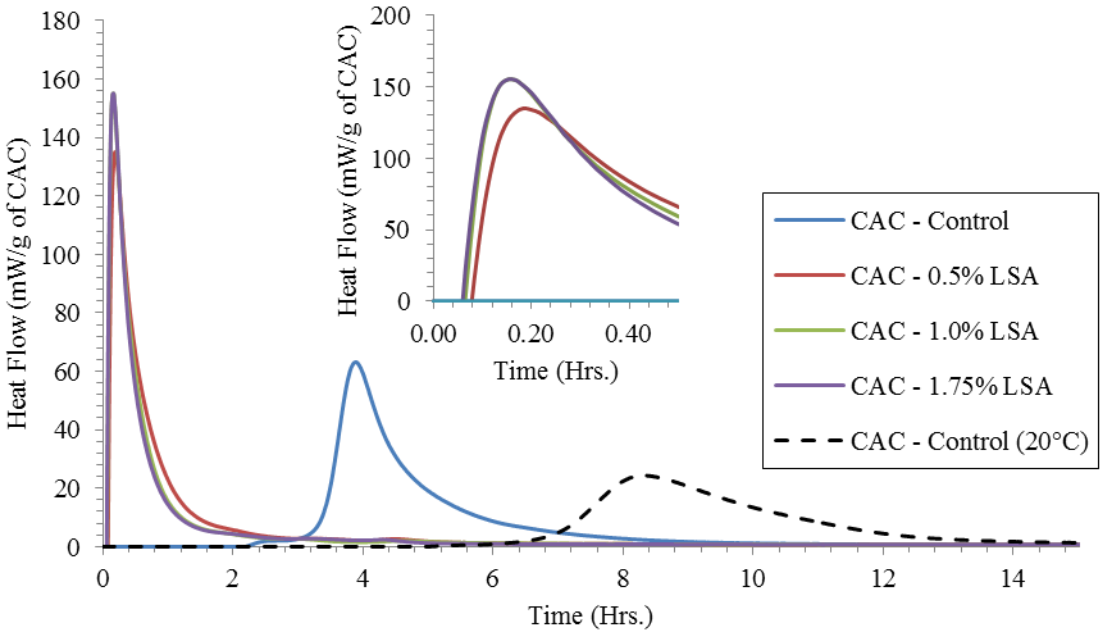


Figure 64: Heat flow of CAC hydrated at 38°C for varying LSA dosages

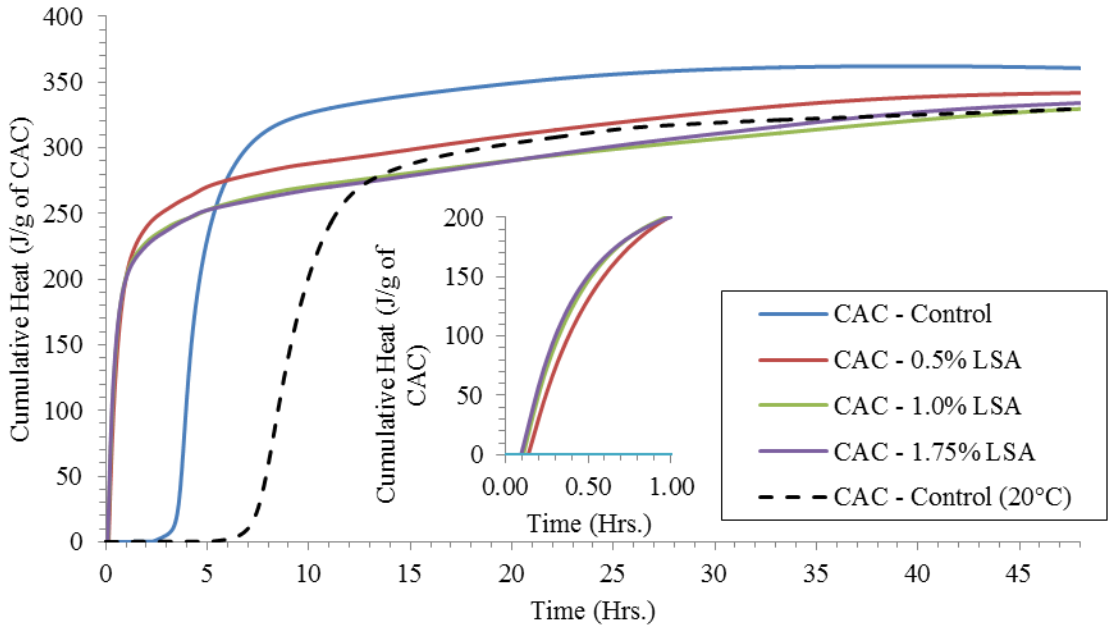


Figure 65: Cumulative heat release of CAC hydrated at 38°C for varying LSA dosages

From Figure 64 and Figure 65, general observations can be made on the induction period, the heat flow pattern, and the influence of LSA. At 38°C, the induction period for the control mixture was reduced to about half the amount of time of the control mixture at 20°C. A distinct difference in the heat flow patterns of the two mixtures was also observed. When LSA was added to the mixtures, a very sharp heat generation curve was observed. The three mixtures containing LSA had similar heat flow patterns that rapidly released heat in the first 30 minutes then nearly stopped generating heat after 2 to 3 hours. These results are similar to those found by Gosselin when he investigated the addition of 0.3% LSA at higher temperatures (2009). These rapid reactions highlight the demand for retarders in combination with LSA at higher temperatures. The next section investigated the individual influence of the HRWR at 38°C.

### 5.2.2 Influence of HRWR at 38°C

The results of isothermal calorimetry at 38°C of CAC with HRWR are shown in Figure 66 and Figure 67.

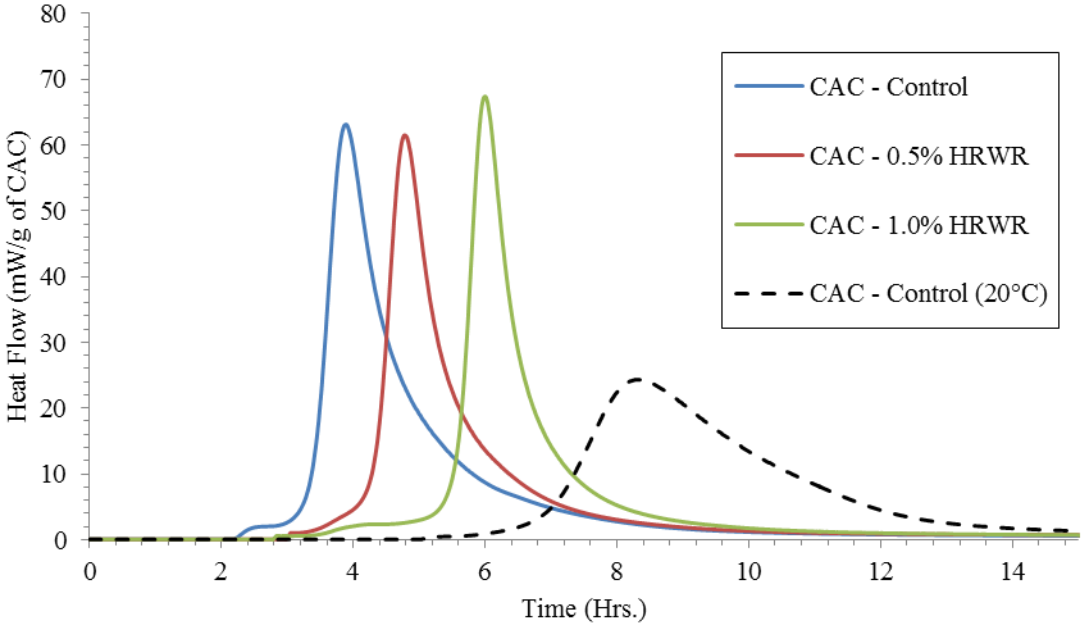


Figure 66: Heat flow of CAC hydrated at 38°C for varying HRWR dosages

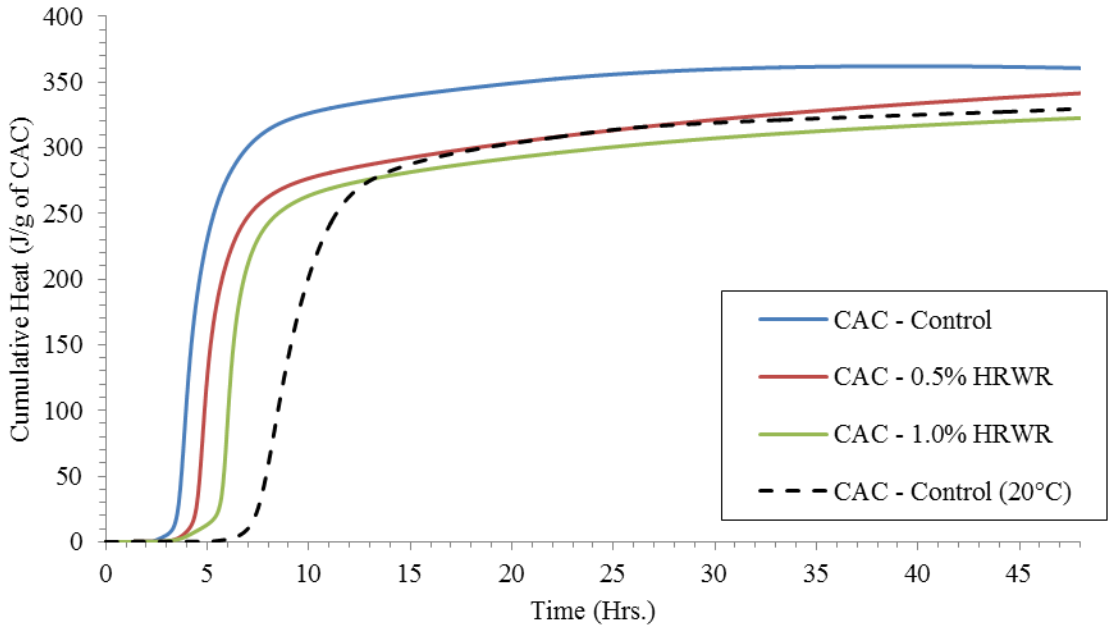


Figure 67: Cumulative heat release of CAC hydrated at 38°C for varying HRWR dosages

The addition of HRWR was able to slow the hydration reaction of the cement beyond the rate of the control mixture at 38°C. The heat flow patterns of the various mixtures were similar with increases in time of the reaction with increased dosages of the HRWR. From the cumulative heat release data, similar amounts of total heat released were measured from the each mixture and with the control mixture at 20°C. From the isothermal calorimetry data of CAC at 38°C with varying dosages of HRWR, the admixture appeared to have little effect on the final degree of hydration of the samples.

### 5.2.3 Influence of Combined LSA and HRWR at 38°C

The results of investigations of plain CAC at 38°C with varying dosages of LSA and HRWR are presented in this section.

### *5.2.3.1 Isothermal Calorimetry*

The isothermal hydration of CAC with both LSA and HRWR is shown in Figure 68 and Figure 69.

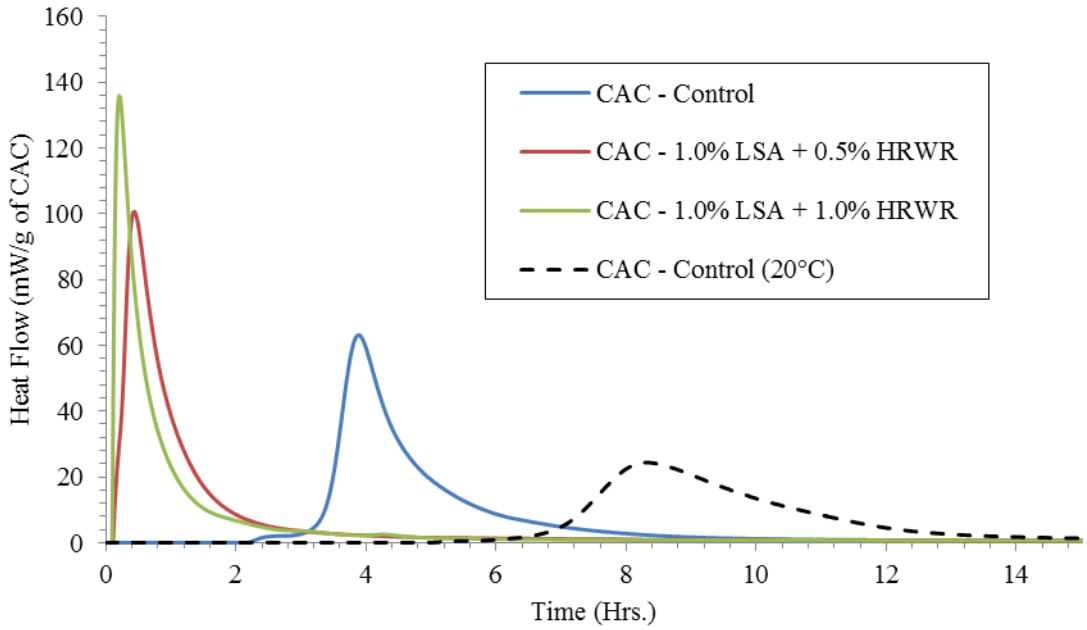


Figure 68: Heat flow of CAC hydrated at 38°C with varying dosages of LSA and HRWR

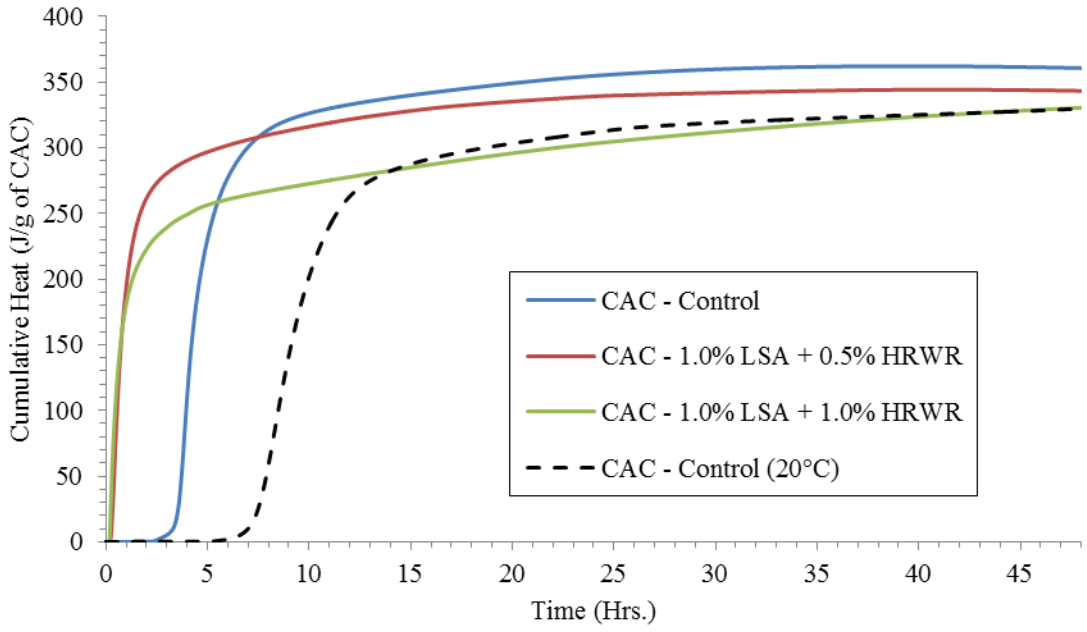


Figure 69: Cumulative heat release of CAC hydrated at 38°C with varying dosages of LSA and HRWR

As discussed earlier and shown in Figure 68 and Figure 69, the LSA dominated the rate of hydration even with the addition of HRWR. However, there was clearly a retarding effect that was still present even at the higher temperature. A unique effect was observed with the mixture containing 1.0% LSA and 1.0% HRWR, this mixture actually hydrated at a faster rate than the mixture containing 1.0% LSA and 0.5% HRWR. This was opposite of what was expected with the additional amount of HRWR. From the cumulative heat curves, slightly less heat was released from the specimens containing chemical admixtures, as seen by the addition of the admixtures individually.

#### *5.2.3.2 Qualitative XRD at 38°C*

The combination of LSA and HRWR was investigated using XRD to characterize the microstructural development with these different material additions at 38°C. The

samples were cast and placed in the calorimeter immediately after mixing and remained in the calorimeter until their designated time to stop hydration was reached. Hydration was stopped using the solvent exchange method at 1 hour, 4 hours, 8 hours, 1 day, and 3 days. Qualitative XRD comparisons of the microstructural development of $C_2AH_8$ are shown in Figure 70.

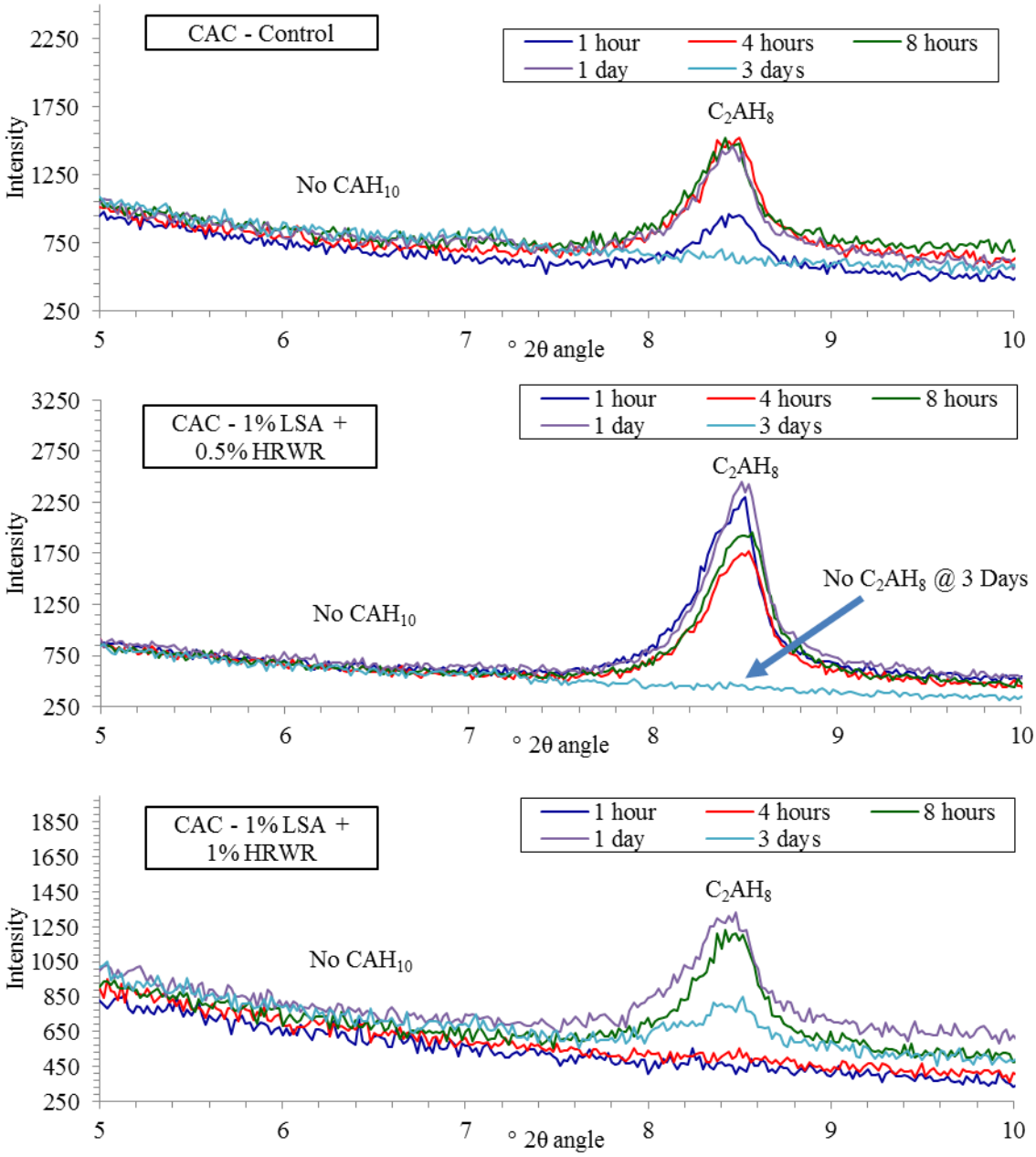


Figure 70: (Part A) Qualitative XRD of CAC with LSA and HRWR hydrated at 38°C, illustrating the formation $C_2AH_8$

The time-lapsed XRD pattern for three mixtures hydrated at 38°C isothermal testing, as shown in Figure 70, indicated that there was no precipitation of $CAH_{10}$ during

the first three days of hydration. However, significant amounts of $C_2AH_8$ precipitated in all specimens. The control mixture developed it between 4 and 8 hours of hydration. Complementary to the isothermal calorimetry graph, Figure 68, the mixture containing 0.5% HRWR appeared to form this hydrate phase slower than the mixture containing 1.0% of the HRWR. Figure 71 shows the qualitative XRD of the CA peak for the three mixtures at 38°C.

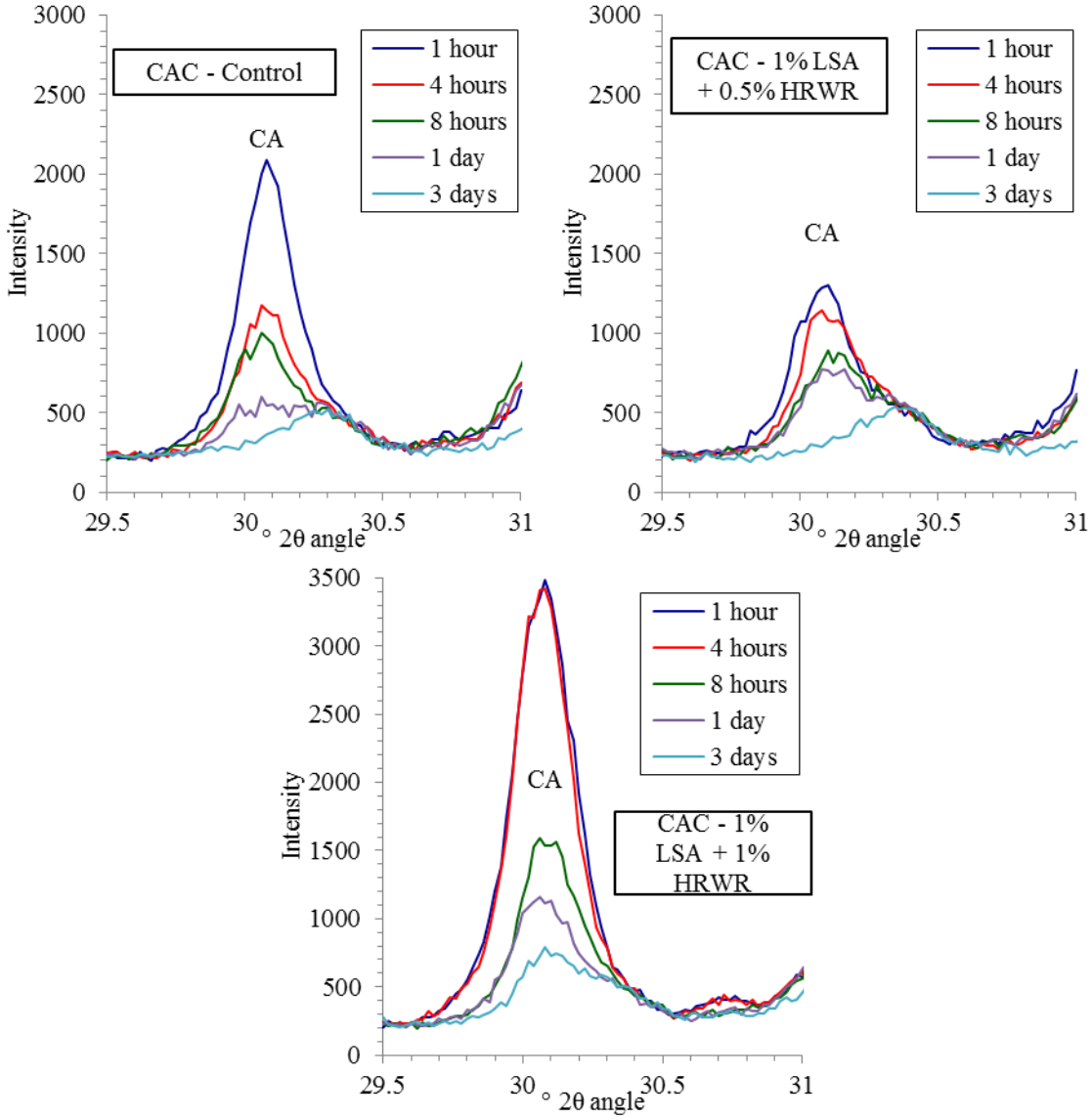


Figure 71: (Part B) Qualitative XRD of CAC with LSA and HRWR hydrated at 38°C, illustrating the reduction of CA

Figure 25 shows the reduction in the amount of CA over the first three days of hydration at 38°C. The mixture containing 1.0% LSA and 0.5% HRWR had the lowest intensity of CA at 1 and 4 hours compared to the other mixtures. A unique observation from these graphs was that the mixture containing 1% LSA and 1% HRWR had the

highest intensity of CA in the first four hours. This was unexpected because of the rapid speed of this reaction compared to the control. In addition, these phases converted and formed the stable hydrate $C_3AH_6$ as shown in Figure 72.

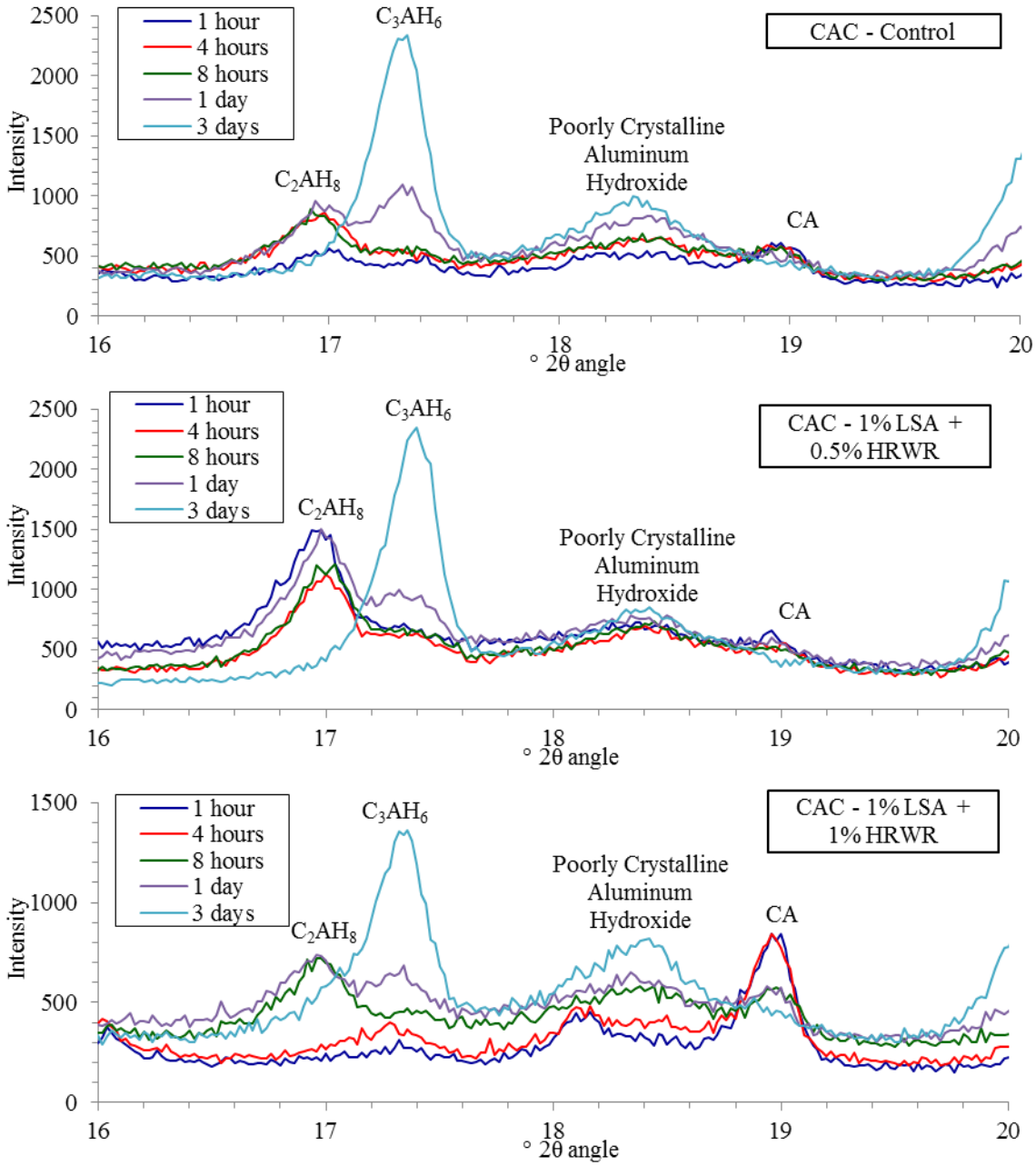


Figure 72: (Part C) Qualitative XRD of CAC with LSA and HRWR hydrated at 38°C, illustrating conversion

From Figure 72, the XRD patterns characterize the occurrence of conversion at 38°C from 8 hours to 3 days. First, the metastable phase, $C_2AH_8$, rapidly precipitated

within the first hour, and then between 8 hours and 3 days a conversion of hydration products was evident. The CAC mixture with 1% LSA and 0.5% HRWR, again, appeared to be the slowest reacting mixture with noticeable amounts of CA up to four hours after mixing. Also, this mixture appeared to form the most aluminum hydroxide phase.

From the qualitative XRD patterns at 38°C isothermal curing these observations were made:

- Conversion began occurring from 8 hours after mixing for all mixtures, with and without LSA and HRWR.
- There was no evidence of $C_2AH8$ remaining at the main peak, 8.7° 2θ, after three days of hydrating at 38°C for the mixture containing 1% LSA and 1% HRWR.
- 1.0% LSA and 0.5% HRWR admixture combination seemed to slow the dissolution of the CA phase, therefore slowing the reaction.
- The formation of $CAH_{10}$ was not observed in any of the mixtures.

#### *5.2.3.3 Chemical Shrinkage at 38° C*

The chemical shrinkage of the mixtures containing both LSA and HRWR is shown in Figure 73.

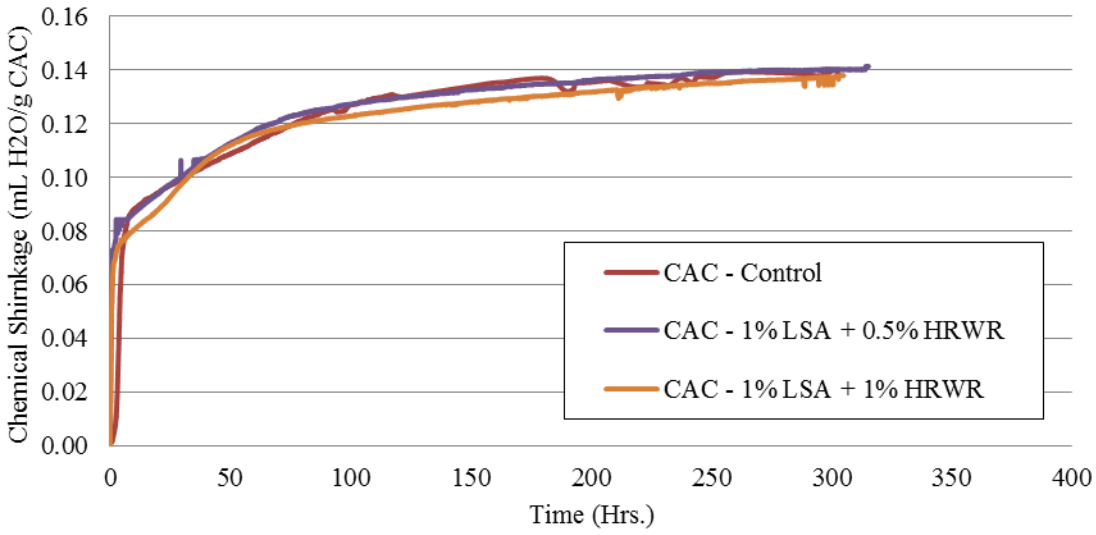


Figure 73: Chemical shrinkage of CAC with varying dosages of LSA and HRWR at 38°C

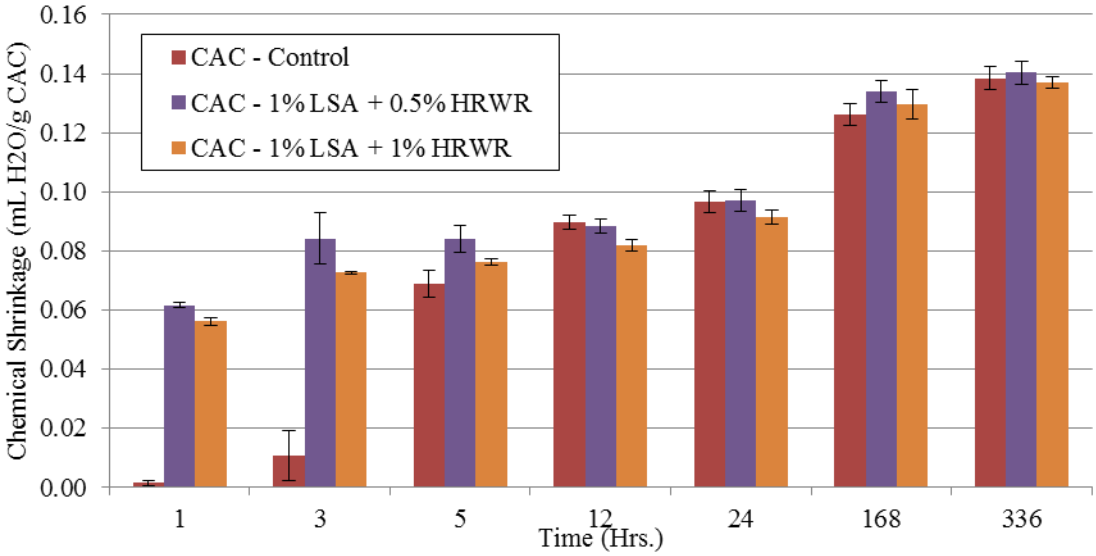


Figure 74: Chemical shrinkage with standard deviations for CAC with varying dosages of LSA and HRWR at 38°C

In Figure 73, the chemical shrinkage of the plain CAC mixtures with LSA and HRWR is presented. Slightly more error was observed with the testing of the samples at 38°C, as shown by the stray deviations in the data due to the image analysis software.

Similar amounts of ultimate chemical shrinkage were observed at the termination of the test. One key observation was the continued expansion noted after the initial shrinkage phase at approximately 10 hours. At 20°C, the shrinkage reached a plateau at this time, while the mixtures at 38°C had a secondary shrinkage phase. This was previously observed by Fu and Ideker and was believed to be caused by the densification of hydration products from the metastable to the stable phase (2008) and (2011). This secondary shrinkage phase led to an approximate 45% increase in total chemical shrinkage at the termination of the experiment. From the bar graphs shown in Figure 74, the larger error between specimens was evident compared to the mixtures tested at 20°C especially at earlier ages.

A comparison of the chemical shrinkage and the cumulative heat release at 38°C is presented in Figure 75.

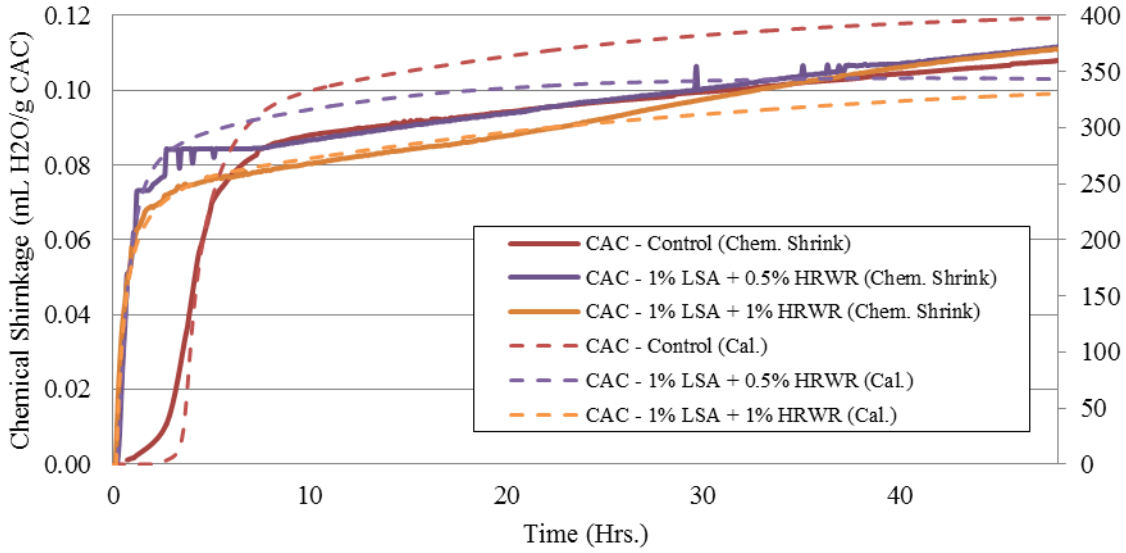


Figure 75: Comparison of chemical shrinkage with isothermal calorimetry cumulative heat release

From Figure 75, similar trends in the early-age hydration behavior were observed with the two different techniques. However, it appears that there seem to be a point of deviation where the chemical shrinkage continues to increase, noticed by an ascending slope, and the cumulative heat tends to flat line. To further highlight this behavior, the chemical shrinkage was plotted as a function of the cumulative heat, shown if Figure 76.

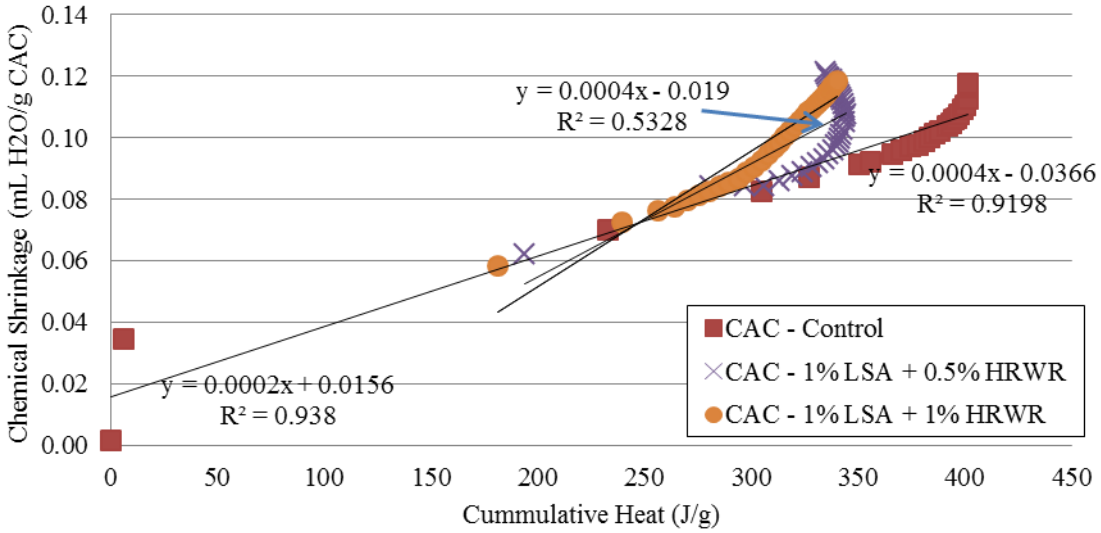


Figure 76: Chemical shrinkage as a function of cumulative heat of CAC with varying LSA dosages.

From Figure 76, there were a few observations made:

- The control mixture had the lowest slope of the three mixtures presented confirming the slower reaction.
- Compared to the same figure created at 20°C the best-fit lines have a lower $R^2$ value.
- The mixtures containing LSA had steeper lines due to the acceleration of the reaction.

- From Figure 76, the plot appears to identify the occurrence of conversion when the line points continue to move upward as part of the chemical shrinkage. This further confirms and possibly highlights the observations by Fu (2011), that conversion can be identified in chemical shrinkage. Longer-term testing is needed to further characterize this behavior.

#### *5.2.3.4 Autogenous Deformation at 38° C*

The autogenous deformation of the mixtures containing both LSA and HRWR is shown in Figure 77.

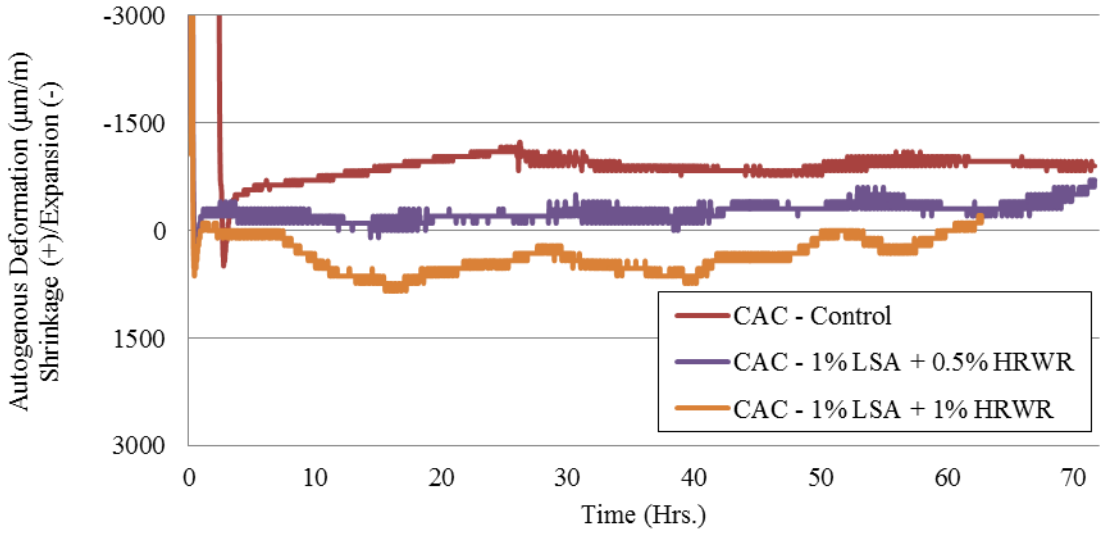


Figure 77: Autogenous deformation of CAC with varying dosages of LSA and HRWR at 38°C

From Figure 77, the unique phenomenon associated with the early-age expansion of CAC when cured at higher temperatures was observed similarly to the results found by Ideker with a free deformation frame and by Fu, who was using the identical method (Ideker, 2008) and (Fu, 2011). The mixtures underwent a uniform shrinkage during the

initial hydration that led to a drastic inflection point upon setting. After reaching this setting point, a sharp increase in the curves was observed, due to an autogenous expansion. While ultimate shrinkage/expansion measurements of these mixtures vary compared to those of Fu, the behavior was quite similar. The difference was merely due to the identification of zero strain or setting point. Ultimately, these three mixtures experienced little to no shrinkage in the first three days of testing when cured at 38°C, which was significantly less than the 3000 μm/m observed in the same mixtures at 20°C.

## 5.3 CONCLUSIONS

Many experimental techniques were completed for this chapter to characterize the hydration of plain CAC with the addition of high dosages of LSA and HRWR. The isothermal calorimeter built specifically for CAC and described in Chapter 4 was implemented to characterize the hydration kinetics and behavior of these material combinations. Time-lapsed XRD was used to provide an understanding of the microstructural development during the early-age hydration. An automated image analysis program was used to capture the water uptake for chemical shrinkage, which the results were used to compare cumulative heat released measured in isothermal calorimetry. Evaluations of the early-age volume deformation of these systems were evaluated using the buoyancy method for autogenous shrinkage. From these techniques these conclusions and findings were drawn from testing at 20°C isothermal conditions:

- The addition of 0.5% and 1% LSA had no effect on the cumulative heat release at 72 hours during the hydration of plain CAC. From the XRD patterns, the addition of this admixture led to the direct formation of $C_2AH_8$ compared to the plain CAC mixture where both metastable hydrates, $C_2AH_8$ and $CAH_{10}$, were formed.

- The HRWR acted as a strong retarder that drastically slowed the hydration of CAC.
- When both LSA and HRWR were used, the qualitative XRD confirmed the direct formation of the $C_2AH_8$, as was observed with the testing of LSA addition by itself.
- Chemical shrinkage showed negligible influence of chemical admixtures on the ultimate shrinkage of the systems.
- Similar amounts of autogenous shrinkage (3000 μm/m) were observed for all mixtures.

From the isothermal testing conditions at 38°C, these key conclusions were found:

- The addition of the LSA admixture drastically shortened the induction period of the plain CAC system, and flash setting was bound to occur.
- The effects of the HRWR on the retardation of the hydration kinetics were still evident; however, the retardation was reduced from the testing at 20°C.
- As with the testing at 20°C, similar amounts of final chemical shrinkage were observed for the three mixtures containing both LSA and HRWR. A secondary increase in chemical shrinkage was observed during the time that conversion was monitored in the qualitative XRD patterns. Thus, Fu's (2011) observations of identification of conversion through chemical shrinkage were confirmed.
- Autogenous expansion was observed for these mixtures when hydrated at 38°C.

# Chapter 6: Influence of Chemical Admixtures, SCMs, and Fillers on CAC Hydration and Early-age Volume Deformation

The results of the microstructural development, hydration, and early-age volume deformation testing of various blends of cementitious materials with CAC are presented in this chapter. The same techniques described in the previous chapter were used to allow for comparison of blended systems to plain CAC. Blends of ground granulated blast-furnace slag (GGBS), silica fume (SF), fly ash (FA), limestone filler (LF), and various chemical admixtures were investigated and are discussed in this chapter. A variety of material combinations were examined that were expected to improve the performance of CAC with respect to mitigation or reduction of conversion, improvement of early-age strength development, and increasing bonding strength for concrete overlays.

## 6.1 Influence of Ternary Blended CAC with Slag and Silica Fume

The first combination of materials investigated during this dissertation was a ternary blend (TCAC) of 75%wt high-Fe CAC (which was similar to the plain CAC discussed in the previous chapter but was manufactured from a different bauxite source), 21.5%wt GGBS, and 3.5%wt SF. Investigations were completed at 20°C and 38°C to investigate the temperature effects on microstructural development and early-age volume change.

The chemical admixture dosages were based on the total binder weight. Thus, the additions of the chemical admixtures used in the work discussed in Chapter 5 of 0.5%, 1.0%, and 1.75% were equal to 0.67%, 1.33%, and 2.33% by weight of CAC, respectively, for this study. The individual effects of LSA and HRWR at 20°C and 38°C on the hydration for isothermal calorimetry and qualitative XRD are presented in Appendix C.

### 6.1.1 Hydration of TCAC at 20°C

The results of the isothermal calorimetry and early-age volume deformation testing of TCAC at 20°C are presented in this section using LSA and HRWR combined at varying dosages. In Appendix C, the individual results of LSA and HRWR are presented.

#### *6.1.1.1 Influence of TCAC on Isothermal Calorimetry and Qualitative XRD at 20°C*

The isothermal calorimetry heat flow data and cumulative heat release for the TCAC cementitious system with combined LSA and HRWR are shown in Figure 78 and Figure 79, respectively.

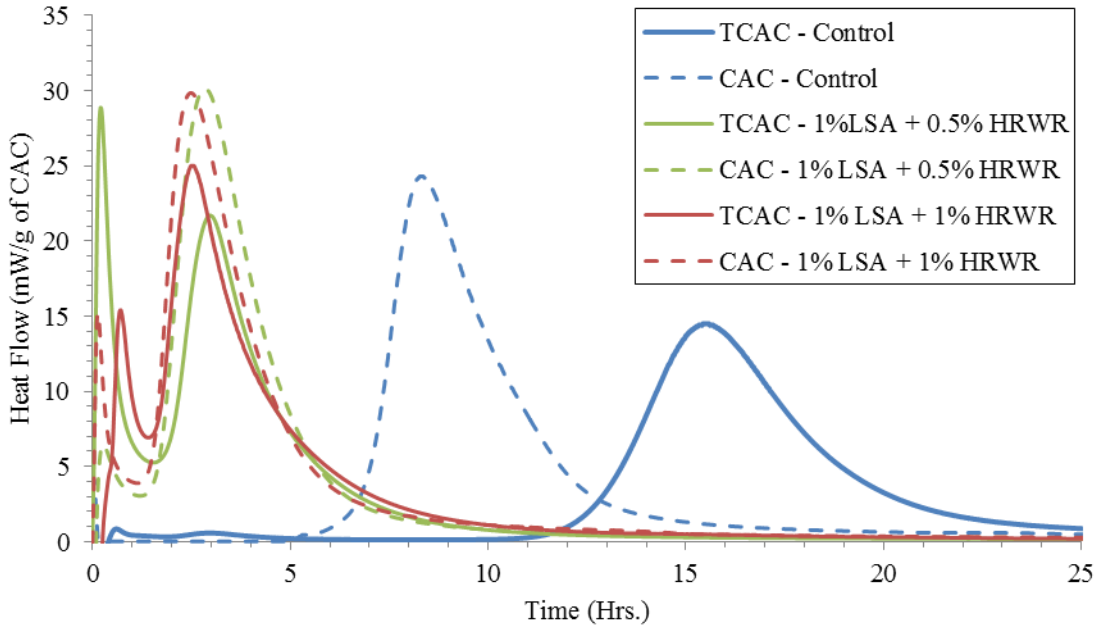


Figure 78: Heat flow of TCAC hydrated at 20°C for varying LSA and HRWR dosages

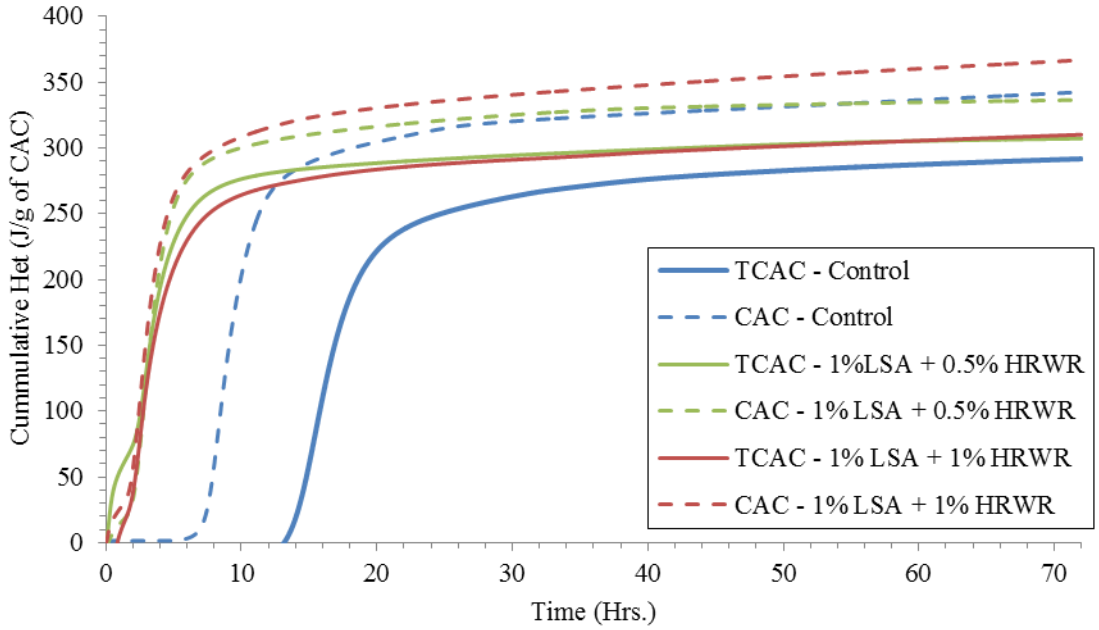


Figure 79: Cumulative heat release of TCAC hydrated at 20°C for varying LSA and HRWR dosages

From the heat flow curve in Figure 78, a few observations were evident. Overall, the addition of SCMs in the TCAC system appeared to slow the hydration reactions as evidenced by an increased induction period. The TCAC control mixture reached the peak heat flow at 15.2 hours compared to the control CAC mixture which reached the peak at 8.1 hours, nearly doubling the time to reach the peak heat flow. A reduction in the peak heat flow with and without the addition of chemical admixtures was also observed. The TCAC and plain CAC control mixtures had a peak heat flow of 14.2 and 23.5 mW/g, respectively.

The cumulative heat flow confirmed the trends seen in the heat flow curves with a reduced total heat release. The three TCAC mixtures with and without admixtures had similar amounts of cumulative heat that were proportionally lower than the plain CAC

mixtures. This trend is further magnified by the addition of only LSA admixture as shown in Figure 80.

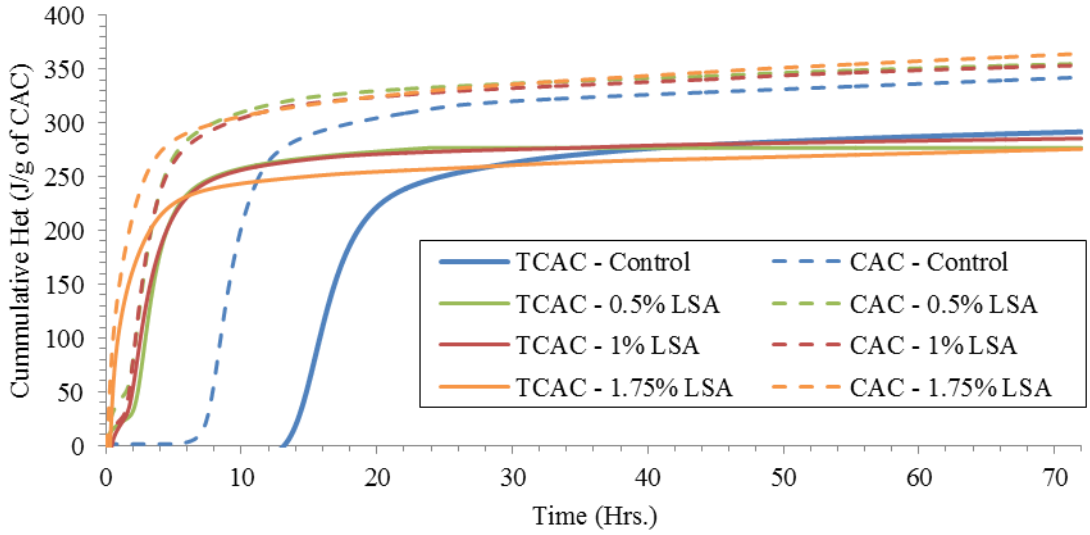


Figure 80: Cumulative heat release of TCAC hydrated at 20°C for varying LSA dosages

The addition of the LSA intensified the difference of the cumulative heat between the plain CAC and the TCAC systems. From the two cumulative heat flow curves, a similar reduction in cumulative heat was observed for the TCAC with the addition of the LSA admixture and the control mixture compared to plain CAC. To investigate the microstructural development of these systems, time-lapsed qualitative XRD was used. Figure 81 compares the microstructural development of TCAC to plain CAC under 20°C isothermal conditions.

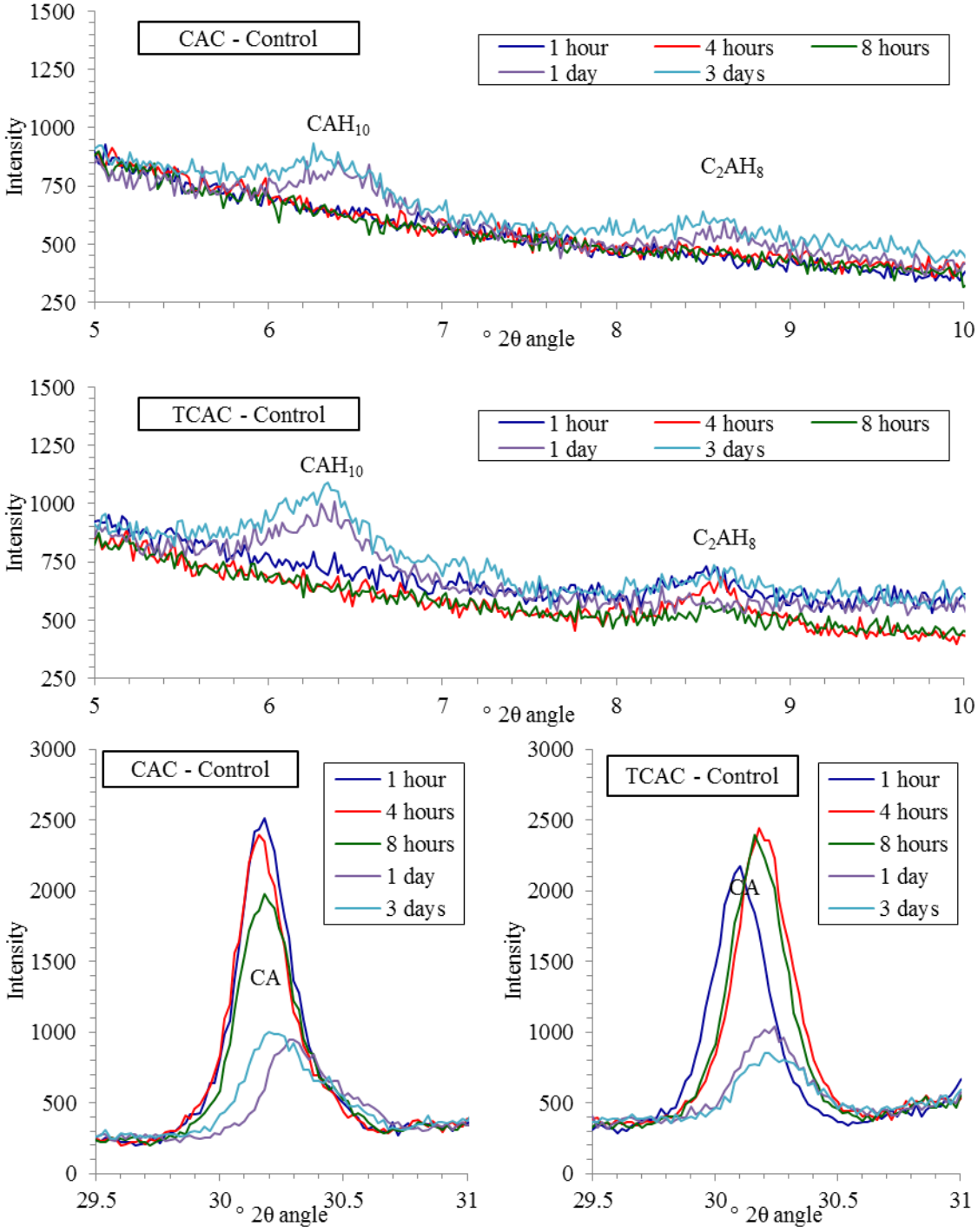


Figure 81: Qualitative XRD of plain CAC and TCAC hydrated at 20°C, illustrating the minimal formation of $CAH_{10}$ and $C_2AH_8$ and the depletion of CA

From Figure 81, the microstructural development of CAC and TCAC were presented. Similar XRD patterns are shown for each of the mixtures. First, each mixture formed similar amounts of $CAH_{10}$ and $C_2AH_8$ at 20°C. The dissolution of the CA phase appeared to occur at similar rates; however, the TCAC mixture was slightly slower. Next, the effect of 1% LSA and 1% HRWR were investigated and the results of the microstructural development are presented in Figure 82.

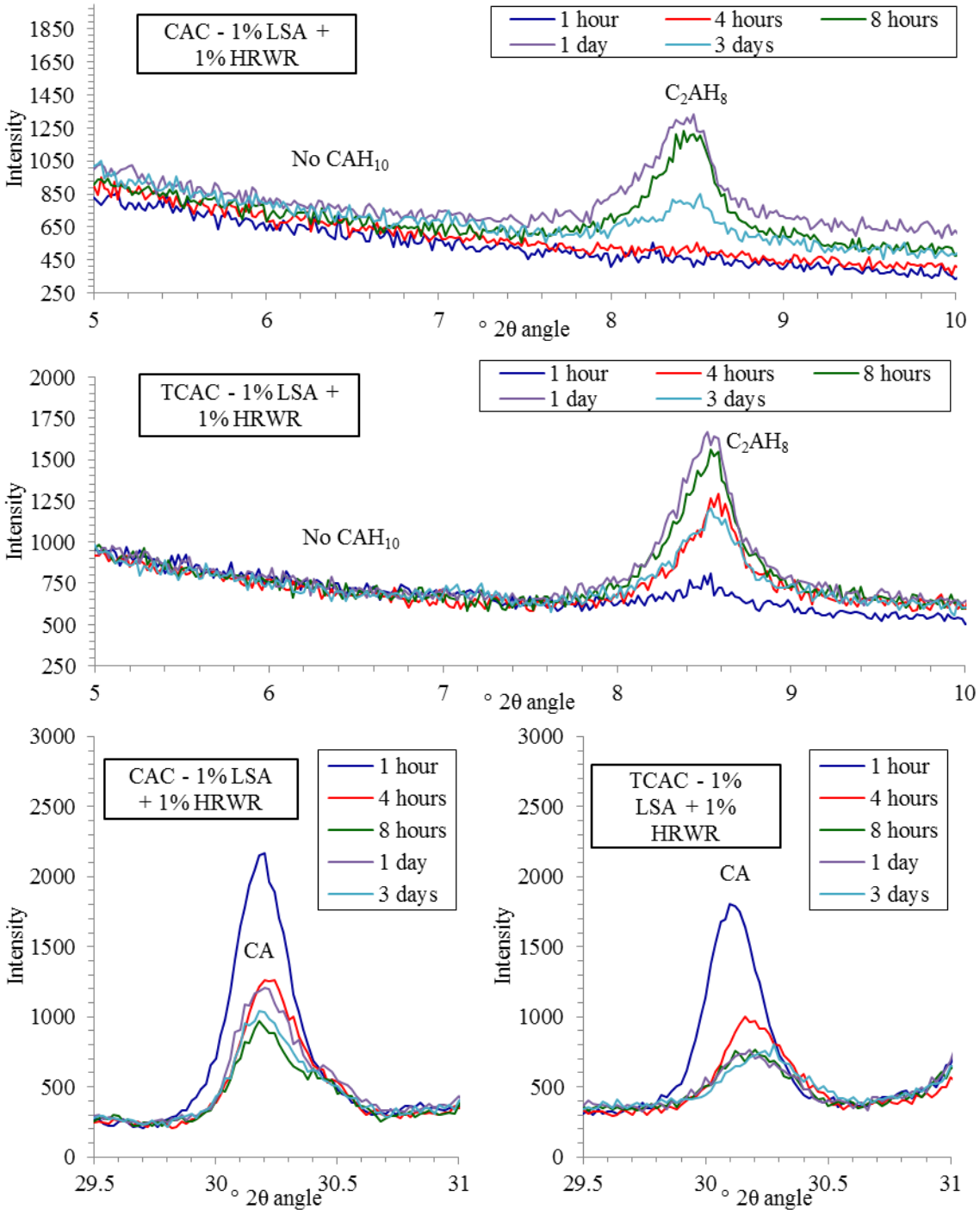


Figure 82: Qualitative XRD of plain CAC and TCAC with 1% LSA and 1% HRWR hydrated at 20°C, illustrating the minimal formation of $CAH_{10}$ and $C_2AH_8$ and the depletion of CA

From the qualitative XRD curves presented in Figure 82, the acceleration of the hydration kinetics due to the LSA admixture was visible. In the top two XRD patterns, the addition of LSA and HRWR led to the direct formation of the $C_2AH_8$ with no indication of the formation of the $CAH_{10}$. The increased rate of the reaction of the TCAC mixture with the combined admixtures can be seen in the plot of the peak CA curve at 30.1° 2θ. The initial height of the CA curve should be lower for the TCAC mixture due to the fact that 75%wt of the mixture was CA and the other 25% was SCMs. After 1 hour of hydration, a large reduction in the peak height was observed compared to the plain CAC mixture, and after 4 hours, minimal to no CA was detected in the samples.

### *6.1.1.2 Influence of TCAC on Chemical Shrinkage at 20°C*

The experimental results of the chemical shrinkage of the TCAC binder are compared to the plain CAC binder in Figure 83. The chemical shrinkage plotted with standard deviation error bars at 20°C isothermal testing is presented in Appendix C.

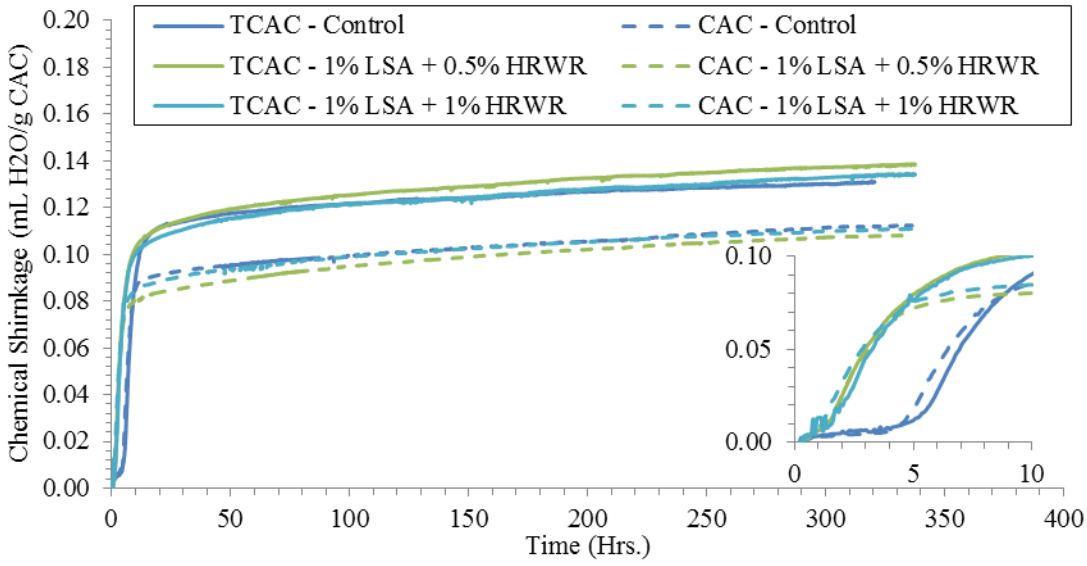


Figure 83: Chemical shrinkage of TCAC with varying dosages of LSA and HRWR at 20°C

From Figure 83, the addition of the SCMs had a large impact on the total amount of chemical shrinkage, which showed the opposite observations from the cumulative heat release. A 20% increase in ultimate chemical shrinkage was observed for TCAC mixtures compared to plain CAC when the graphs were normalized by the weight of CAC. This behavior was the opposite of what was observed from the cumulative heat release from isothermal calorimetry. These observations raise questions about the porosity and hydration kinetics of these complex systems. To further compare the results of the chemical shrinkage to the cumulative heat release, these plots were graphed with linear best-fit lines in Figure 84.

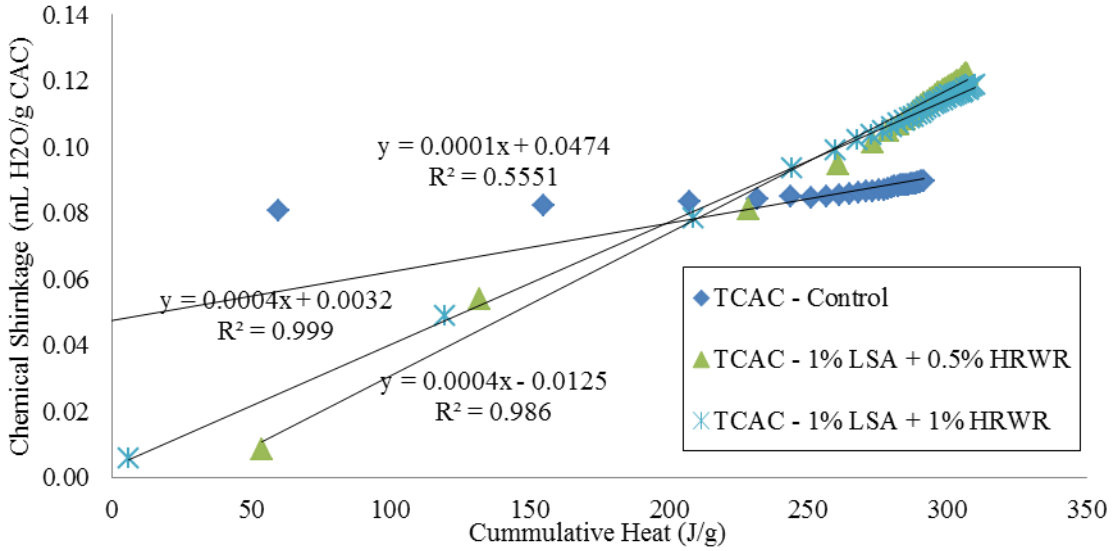


Figure 84: Chemical shrinkage as a function of cumulative heat of CAC with varying LSA dosages.

From Figure 84, a few observations can be made about the hydration kinetics of the TCAC mixtures with varying LSA and HRWR additions. First, the TCAC control mixture had a relatively low correlation coefficient of 55.51%, which would typically be considered poor or bad correlation. However, what this coefficient and stray data points

indicate was that the hydration reaction was slow at first where there was essentially no heat release or chemical shrinkage. Then, the mixture rapidly hydrated and the data points shifted upward, meaning more chemical shrinkage and more heat release, due to the rapid hydration of this mixture. A more horizontal best-fit line could be drawn to achieve a better correlation coefficient, but the key point in this figure was that the hydration reaction was initially slow in both chemical shrinkage and isothermal calorimetry; however, once the reaction began it occurred quickly.

From the other two mixtures, a much higher correlation coefficient was observed and more uniform hydration as a function of time was observed. The additional retardation or slower hydration reaction of the mixture containing 1.0% HRWR was observed with the lower sloped best-fit line.

#### *6.1.1.3 Influence of TCAC on Autogenous Deformation at 20°C*

To investigate the influence of the TCAC on the early-age volume deformation, the mixtures containing LSA and HRWR were evaluated in autogenous shrinkage.

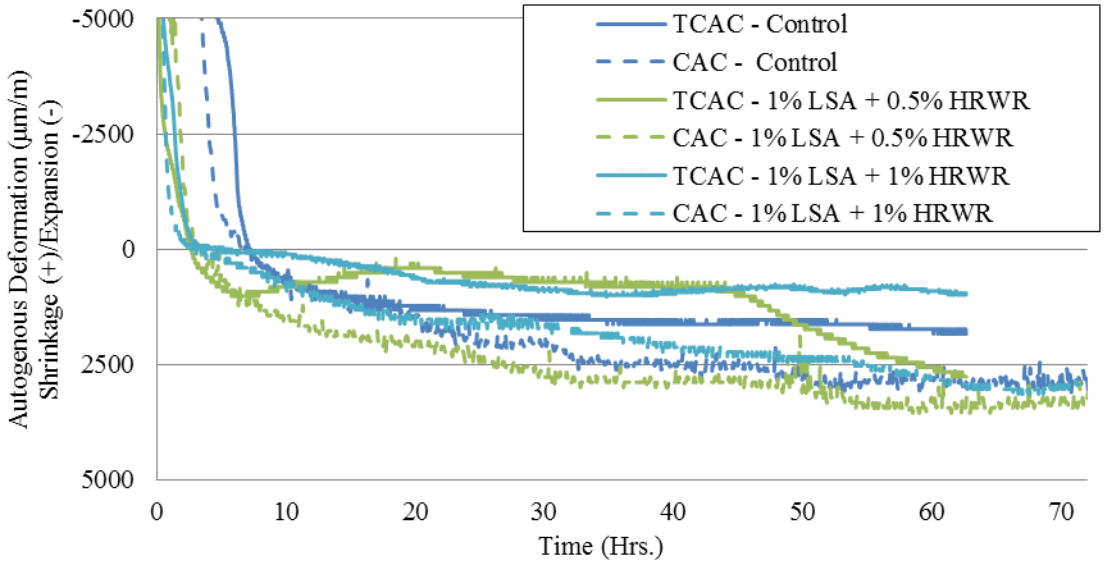


Figure 85: Autogenous Shrinkage of TCAC with varying dosages of LSA and HRWR at 20°C

From Figure 85, early-age autogenous shrinkage was measured for the TCAC mixtures under the 20°C isothermal conditions. TCAC had slightly less autogenous shrinkage than the plain CAC systems. The two mixtures containing LSA and HRWR had nearly identical amounts of ultimate autogenous shrinkage. The two mixtures had approximately 950 µm/m of shrinkage compared to the same mixtures with the plain CAC where around 3000 µm/m of shrinkage was observed. This reduction in the shrinkage was due to the reduction in the amount of CAC in the TCAC binder and the slower hydration kinetics.

### 6.1.2 Hydration of TCAC at 38°C

This section of the study investigated the hydration kinetics and early-age volume deformation of the TCAC with the combined addition of LSA and HRWR at 38°C.

### *6.1.2.1 Influence of TCAC on Isothermal Calorimetry and Qualitative XRD at 38°C*

The isothermal calorimetry results for TCAC with LSA and HRWR added separately are presented in Appendix C. Figure 86 and Figure 87 show the heat flow and the cumulative heat release of the combined effects of these admixtures.

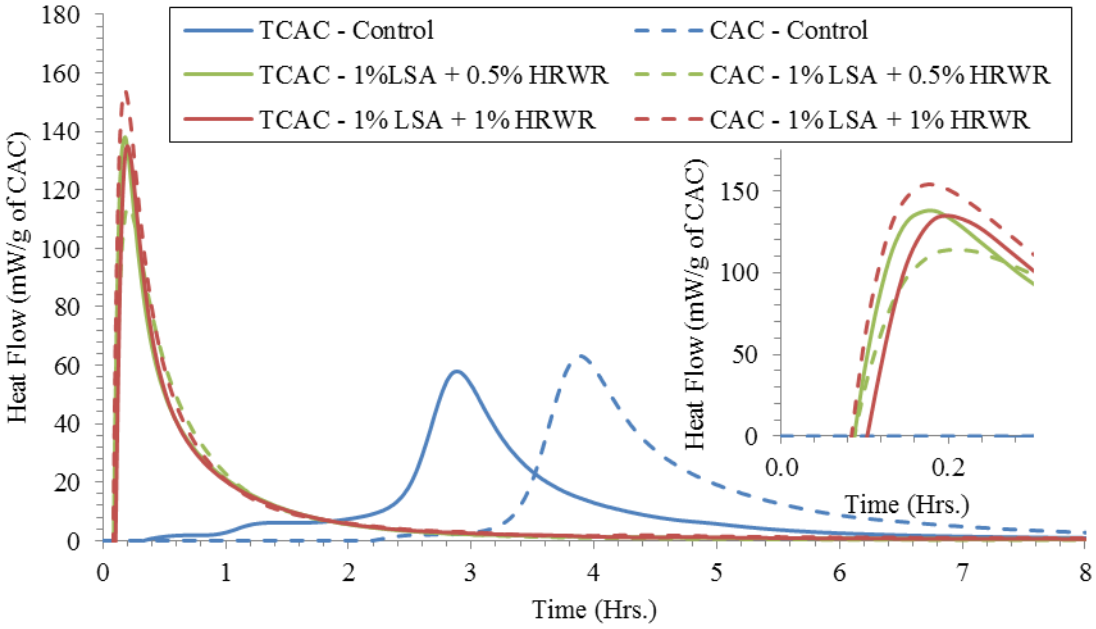


Figure 86: Heat flow of TCAC hydrated at 38°C for varying LSA and HRWR dosages

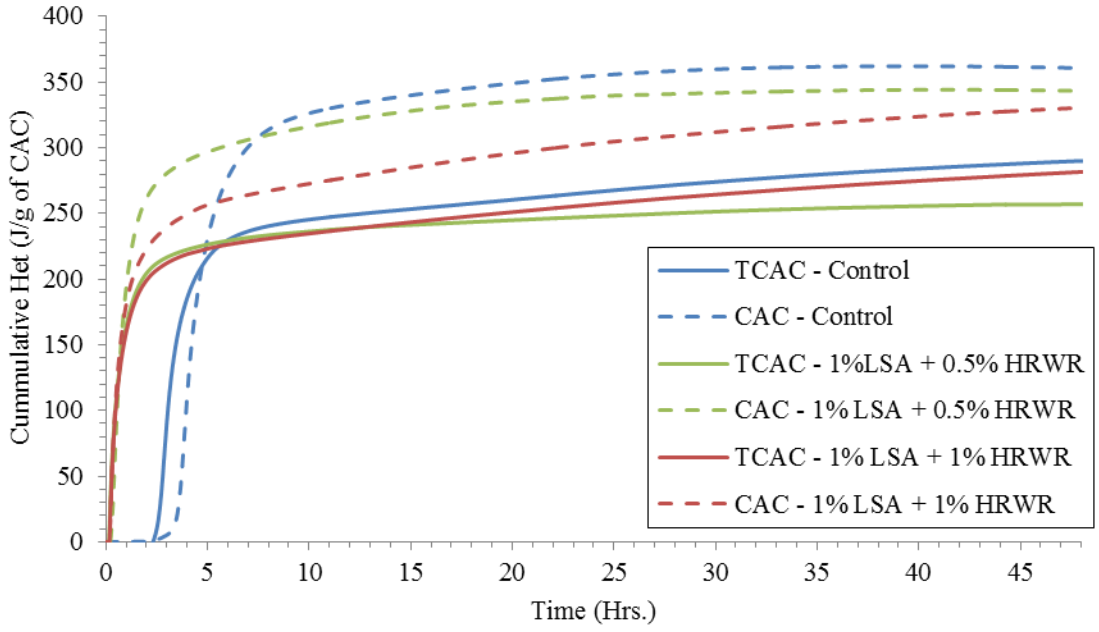


Figure 87: Cumulative heat release of TCAC hydrated at 38°C for varying LSA and HRWR dosages

From Figure 87, the TCAC and CAC mixtures containing LSA and HRWR had similar heat flow patterns in the initial hydration. Similar amounts of peak heat were observed in the insert in Figure 86. The key observation was the drastic reduction in the induction period for the TCAC control mixture at the higher temperature. At 20°C, the induction period lasted approximately 11 hours compared to the 2 hour induction period at 38°C. Also, this mixture's induction period was shorter than the plain CAC control mixture. From the cumulative heat flow curves, a dilution effect of the cumulative heat release was observed for the TCAC mixtures compared to the plain CAC mixtures due to the addition of the SCMs.

The qualitative XRD patterns for the TCAC control and 1% LSA and 1% HRWR are presented in this section. Other XRD patterns including separate HRWR addition and combinations are presented in Appendix C.

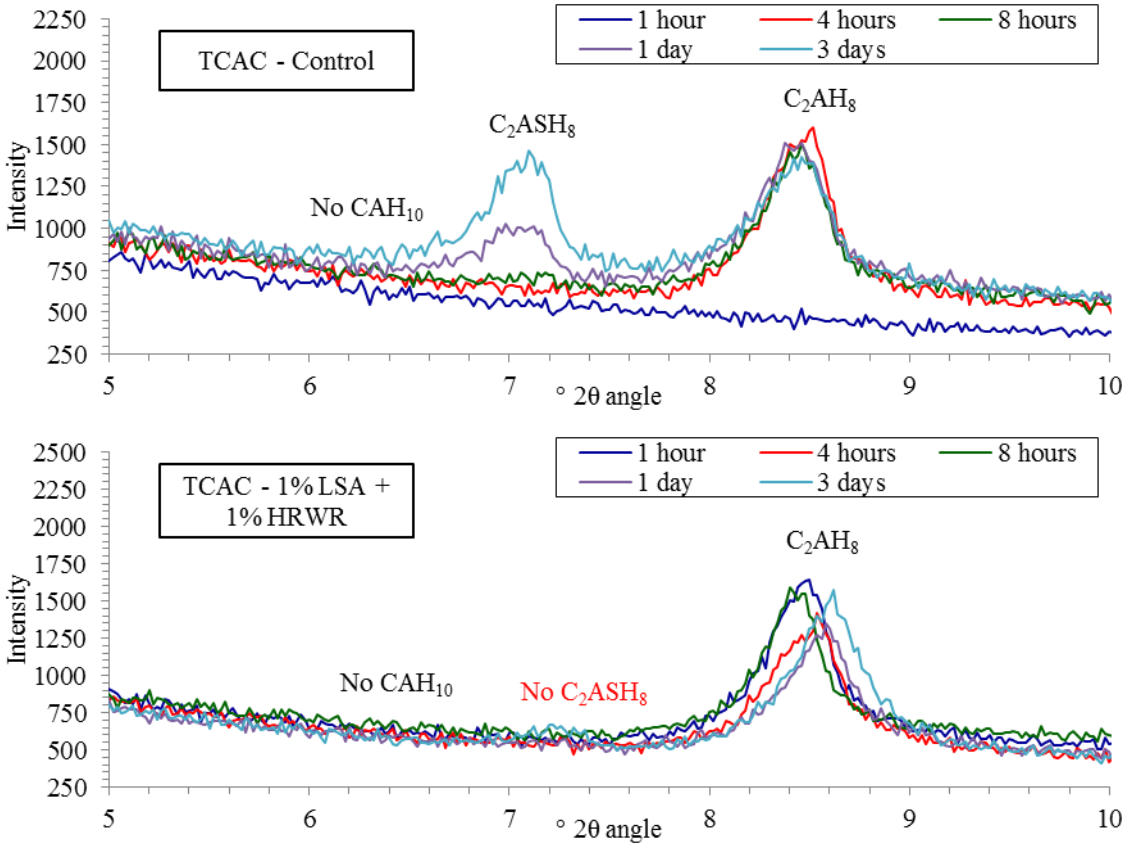


Figure 88: (Part A) Qualitative XRD of TCAC with LSA and HRWR hydrated at 38°C, illustrating the formation $C_2AH_8$ and $C_2AH_8$

In Figure 88, the microstructural development of the TCAC binder at 38°C was shown. First, there was no indication of the development of $CAH_{10}$ phase; however, significant amounts of $C_2AH_8$ were observed. The development of $C_2ASH_8$, stratlingite, was observed in the control mixture after 8 hours of hydration at 38°C. As mentioned in the literature review from work by Collepardi and Gosselin, stratlingite is a stable hydration product that has been show to prevent strength reductions associated with conversion (Collepardi, 1995) and (Gosselin C. , 2009). This work showed the development of this phase after only 8 hours of hydration at higher temperatures while

work by the others did not observe this hydration product until after 17 days of hydration. However, it was interesting to note that the formation of this stable phase was not identified when the chemical admixtures were added to the mixture. The development of another stable hydrate $C_3AH_6$ is shown in Figure 89.

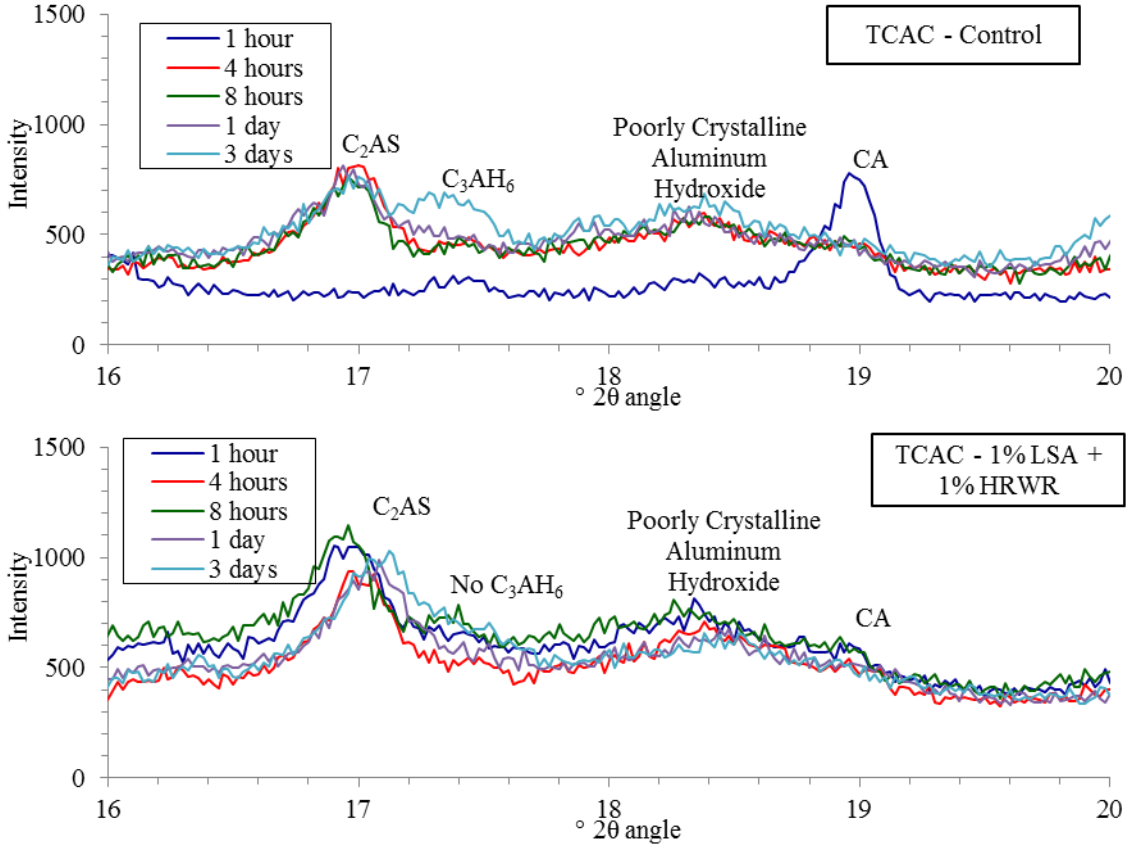


Figure 89: (Part B) Qualitative XRD of TCAC with LSA and HRWR hydrated at 38°C, illustrating formation of some $C_3AH_6$

In Figure 89, the XRD pattern shows the conversion of the TCAC control mixture. The TCAC mixture with LSA and HRWR does not show any signs of the formation of $C_3AH_6$. Typically, the formation of this stable hydrate would not be expected to form for a period of three to five days after hydration at this higher

temperature. It was interesting to see the formation in the mixture that had the slower hydration reactions.

### *6.1.2.2 Influence of TCAC on Chemical Shrinkage at 38°C*

The influence of this ternary blended system on chemical shrinkage at 38°C was investigated, and the results are presented in Figure 90. The chemical shrinkage results with the standard deviation error bars are shown in Appendix C.

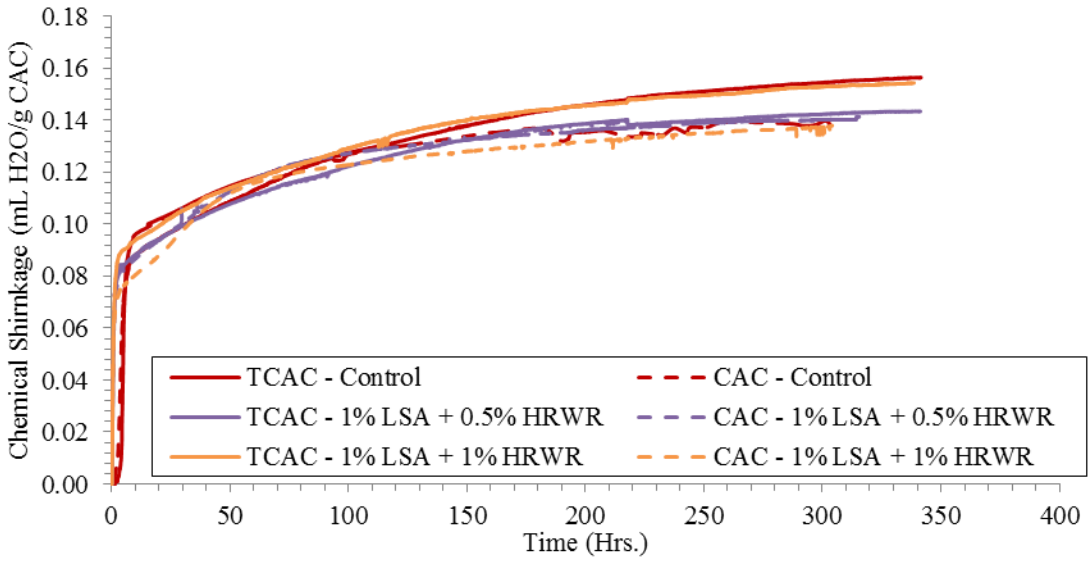


Figure 90: Chemical shrinkage of TCAC with varying dosages of LSA and HRWR at 38°C

From Figure 90, the ultimate chemical shrinkages of the TCAC systems were similar with and without the addition of LSA and HRWR. The final chemical shrinkage values of these systems were slightly lower than those of the plain CAC. To investigate the early-age shrinkage of the TCAC binder the first 10 hours was plotted in Figure 93.

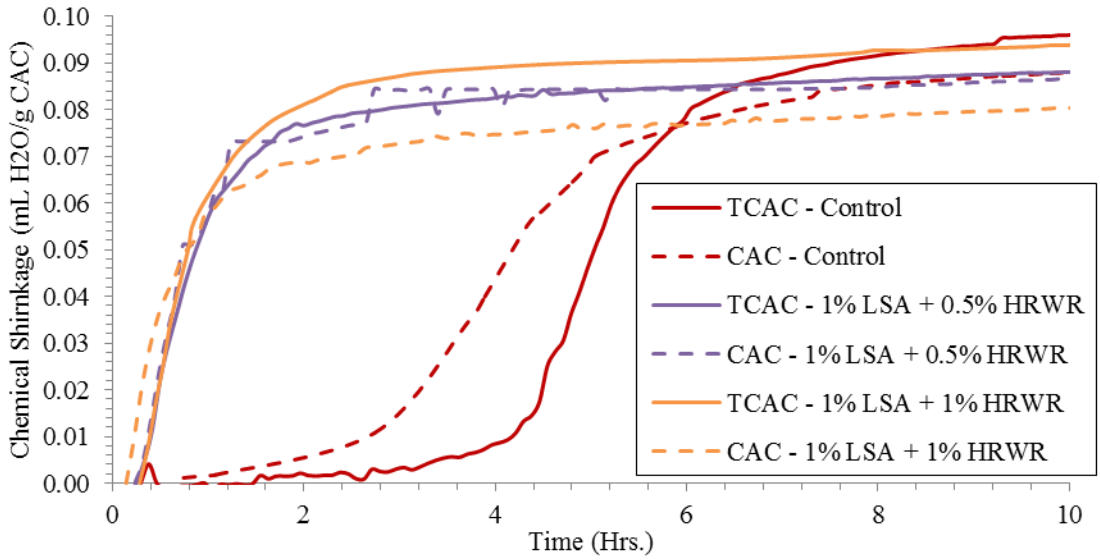


Figure 91: Early-age chemical shrinkage of TCAC with varying dosages of LSA and HRWR at 38°C

In Figure 44, because of the focus on very early age behavior, the errors of the image analysis techniques were magnified. The deviations in the image analysis are larger at the higher temperature than at the lower 20°C testing temperature. The explanation for this error is not fully known, but the error occured with all the cementitious systems investigated. Despite the errors, a unique observation was made from the rate of the reaction of the control TCAC mixture. The mixture hydrated slower than the plain CAC control mixture, which was opposite of what was shown in the isothermal calorimetry results. To further look at the rate of hydration of these systems, the chemical shrinkage was plotted as a function of the cumulative heat release in Figure 92.

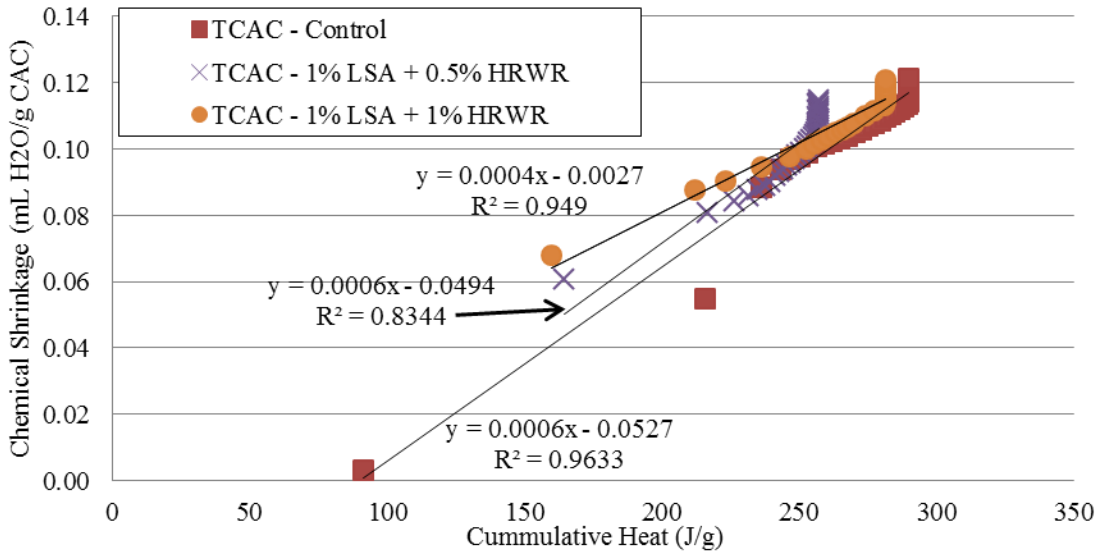


Figure 92: Chemical shrinkage as a function of cumulative heat of CAC with varying LSA dosages.

Figure 92 illustrates the rate of reaction of the TCAC mixtures with varying additions of LSA and HRWR by plotting the chemical shrinkage as a function of the cumulative heat release. From the figure, the comparisons of the rates of reaction were a bit misleading based off solely the slope of the best-fit lines. It would appear that both mixtures containing the chemical admixtures were reacting more slowly than the control mixture if the rate of reaction was based solely off the slope of the lines. However, the key observation necessary for accurate understanding of this plot was the location of the first data point of each mixture. The first data point for the two mixtures with admixtures occured at approximately 170 J/g of cumulative heat release, which illustrated that the reaction started much more rapidly compared to the control mixture where the first data point occurred at 90 J/g. Another point of interest was the sharp inflection point that occured once the cumulative heat release reached a stagnation point. This inflection point occurred when the samples underwent the conversion process. There was a large

uptake of water recorded by the chemical shrinkage testing due to the increased porosity from conversion of the hydration products from the meat-stable phase the stable phase.

### *6.1.2.3 Influence of TCAC on Autogenous Deformation at 38°C*

The influence of this ternary blended system on the early-age autogenous deformation is presented in Figure 93.

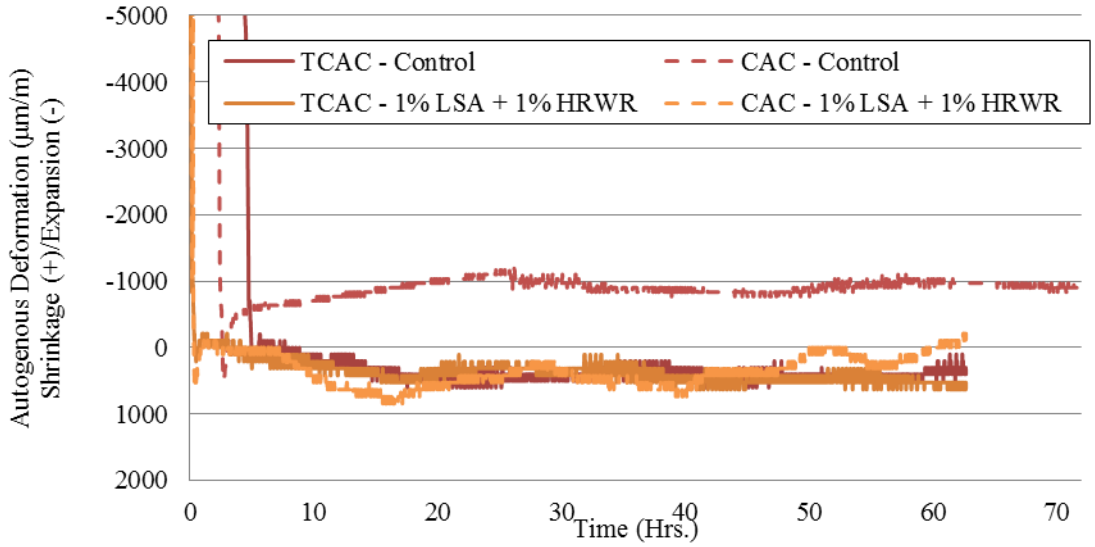


Figure 93: Autogenous deformation of TCAC with varying dosages of LSA and HRWR at 38°C

At 38°C, similar amounts of autogenous deformation were measured for the plain CAC and the TCAC mixtures. A reduction in the amount of autogenous expansion was evident in the control mixture when the SCMs were added to the system; however, the amount of shrinkage the system experienced was minimal. The addition of the LSA and HRWR had no effect on the autogenous deformation where similar performance was observed for the control mixture and the mixture with admixtures.

### 6.1.3 Summary

To summarize the influence of ternary blended calcium aluminate cement based system, the key observations and conclusions were found:

- From isothermal calorimetry, the addition of the SCMs to CAC slowed the hydration reaction, lowering the peak heat flow, and reduced the cumulative heat release at 20°C. However, at 38°C, acceleration of the hydration reaction was observed.
- From the qualitative XRD patterns of 20°C isothermal hydration, similar amounts of metastable hydration products were formed in the first three days of hydration for the plain CAC and the TCAC binder. However, when LSA and HRWR were used, the direct formation of $C_2AH_8$ was observed without the formation $CAH_{10}$.
- From the qualitative XRD patterns of 38°C isothermal hydration, the TCAC control mixture only formed the $C_2AH_8$ metastable hydration product. In addition, $C_2ASH_8$ and $C_3AH_6$ stable hydration products were found. Unexpectedly, in the mixture containing LSA and HRWR, no stable hydration products were found. Conversion was assumed to have occurred from observations of the chemical shrinkage plot as a function of cumulative heat.
- The TCAC binder system had less autogenous shrinkage and less autogenous expansion at 20°C and 38°C, respectively.
- From the work completed in this section, conversion of the metastable hydration products was still observed with the ternary blended system. The use of the LSA and HRWR were proven to be power admixtures that greatly alter the microstructural development and performance of these systems. Future work investigating the long-term microstructural development of these systems is

needed to understand the influence of the higher dosage rates of the LSA admixture.

## 6.2 Influence of Limestone

From literature, it was not clear whether the addition of high percentages of limestone powder would eliminate or reduce conversion or conversion-related effects due to CAC hydration, and it was not clear whether this limestone would react or act as an inert filler. Thus, in the literature review, the background information was presented in the filler section and the nomenclature given to this mixture combination was LF or limestone filler. This section investigates the substitution of 20% limestone by weight of CAC.

Investigations of this material combination and substitution rate were recommended by the project sponsor from preliminary work completed in their testing laboratory. The aim of this section was to investigate the influence of 20% LF on CAC hydration and early-age volume deformation. Investigations of calorimetry, chemical shrinkage and autogenous shrinkage were completed at 20°C and 38°C isothermal testing to study the chemical effects of the substitution.

### 6.2.1 Hydration of CAC-LF at 20°C

#### *6.2.1.1 Influence of CAC-LF on Isothermal Calorimetry at 20°C*

The characterization of the hydration kinetics of the CAC-LF binder system with the addition of the LSA and HRWR is presented in Figure 94 and Figure 95. Additional isothermal calorimetry results on the independent influence of the LSA and HRWR are presented in Appendix D.

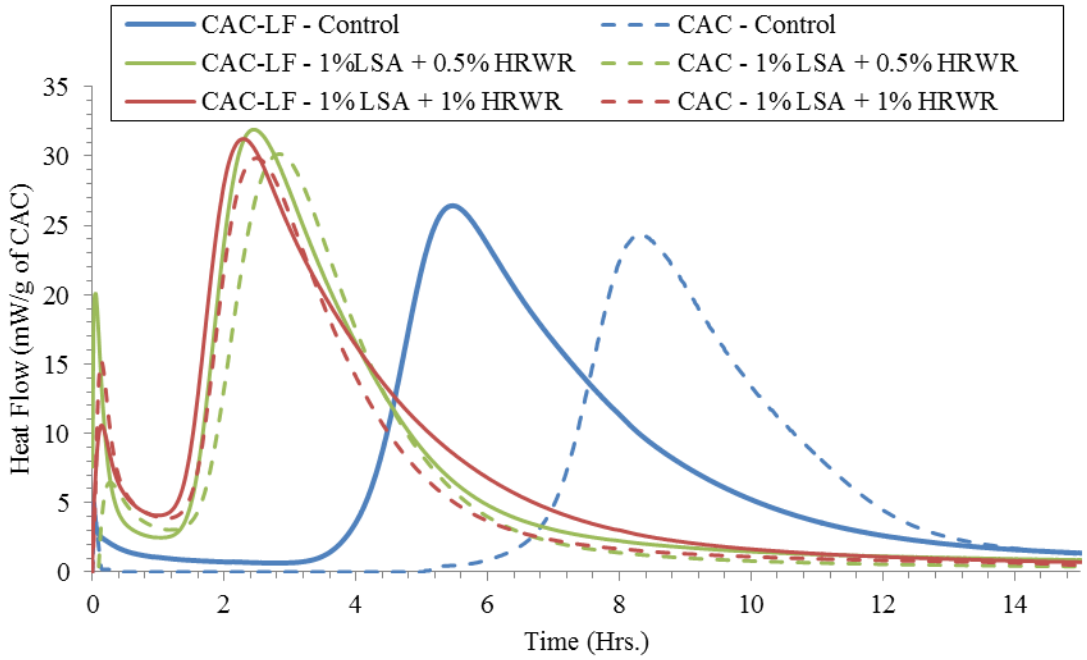


Figure 94: Heat flow of CAC-LF hydrated at 20°C for varying LSA and HRWR dosages

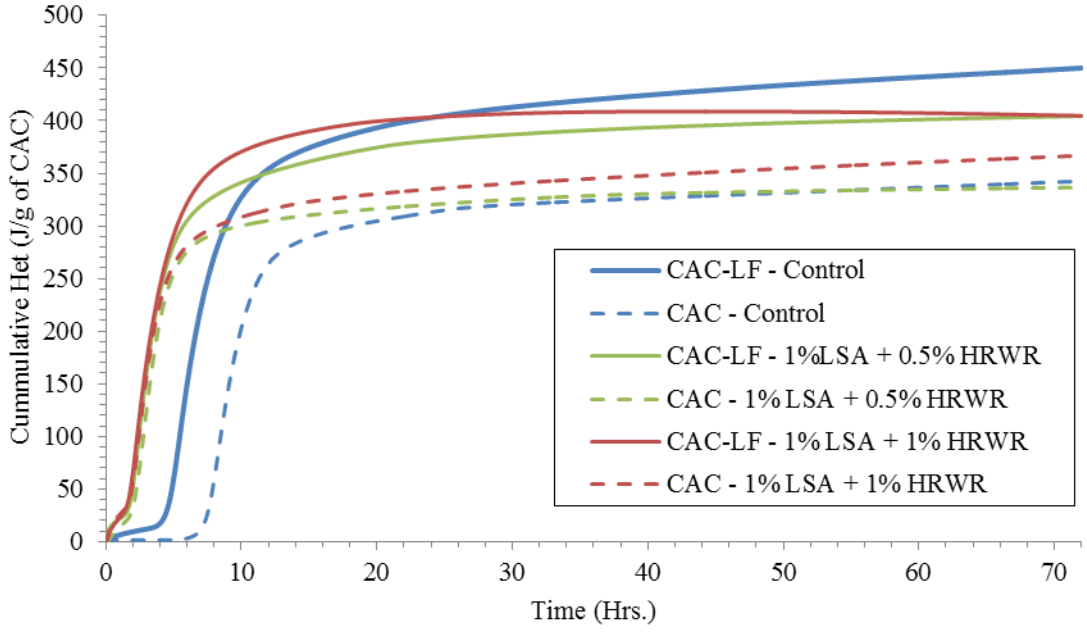


Figure 95: Cumulative heat release of CAC-LF hydrated at 20°C for varying LSA and HRWR dosages

From the heat flow patterns, the addition of the limestone filler accelerated the hydration reaction, which resulted in a reduction in the induction period for all three CAC-LF mixtures. The CAC-LF control mixture had a 3.5 hour induction period compared to the 7 hour induction period of the plain CAC system. The LF likely acted as a nucleation site and reduced the time to precipitate the CA hydration products. The addition of LF led to an increase in the peak heat flow of all mixtures with and without the addition of chemical admixtures.

From the cumulative heat curves, the same acceleration in the hydration reaction was observed in these patterns. A higher cumulative heat release was observed for all mixtures containing the LF with the data normalized by the weight of the CAC. This illustrates the LF may be chemically reacting with the CAC.

#### *6.2.1.2 Influence of CAC-LF on Chemical Shrinkage at 20°C*

To further investigate the rate of reaction, chemical shrinkage was performed; the results are shown in Figure 96. The results of chemical shrinkage at 20°C are presented in bar graph form to report the standard deviation of the measurements in Appendix D.

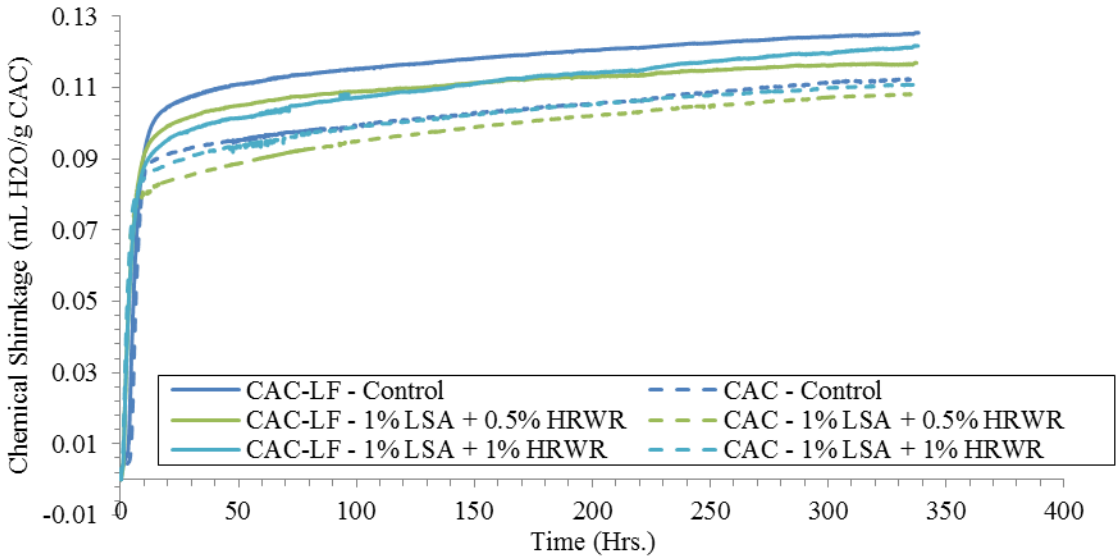


Figure 96: Chemical shrinkage of CAC-LF with varying dosages of LSA and HRWR at 20°C

The chemical shrinkage of the three limestone filler mixtures and three plain CAC mixtures is shown in Figure 96. The chemical shrinkage for each mixture was normalized per gram of CAC. The CAC-LF sample had an increase in the ultimate chemical shrinkage for each of three mixtures compared to the plain CAC mixtures. The addition of LSA and HRWR reduced the ultimate amount of chemical shrinkage compared to the CAC-LF control mixture.

As a better comparison of the early-age hydration kinetics of the CAC-LF systems at 20°C, the chemical shrinkage was plotted as a function of the cumulative heat release in Figure 97.

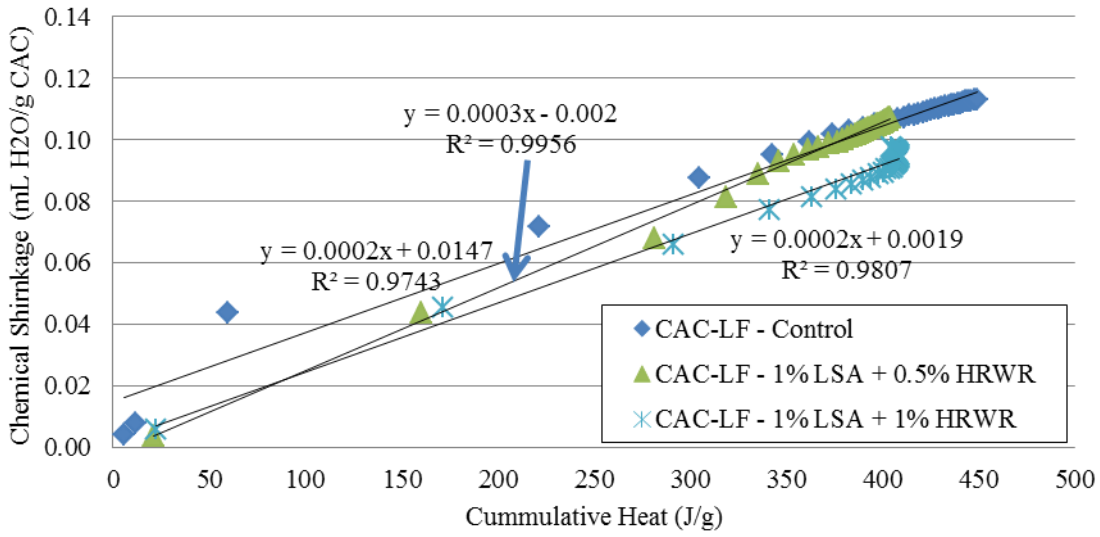


Figure 97: Chemical shrinkage as a function of cumulative heat of CAC-LF with varying LSA dosages.

In Figure 97, chemical shrinkage was plotted as a function of cumulative heat, and linear best-fit lines were drawn between these data points. These lines show the influence of the LF and LSA and HRWR on the hydration reaction of the CAC based-system. The three linear best-fit lines had similar slopes, which illustrate equivalent rates of reaction of the different mixtures. The lines also show that hydration kinetics of this system are dominated by the LF addition and not the chemical admixtures. A slight increase in the rate of reaction, meaning increase in slope of the line, for the mixture containing 1% LSA and 0.5% HRWR was noted, but overall similar hydration behaviors were observed.

#### *6.2.1.3 Influence of CAC-LF on Autogenous Deformation at 20°C*

Results of the investigations on the influence of LF on the early-age volume deformation are presented in Figure 98.

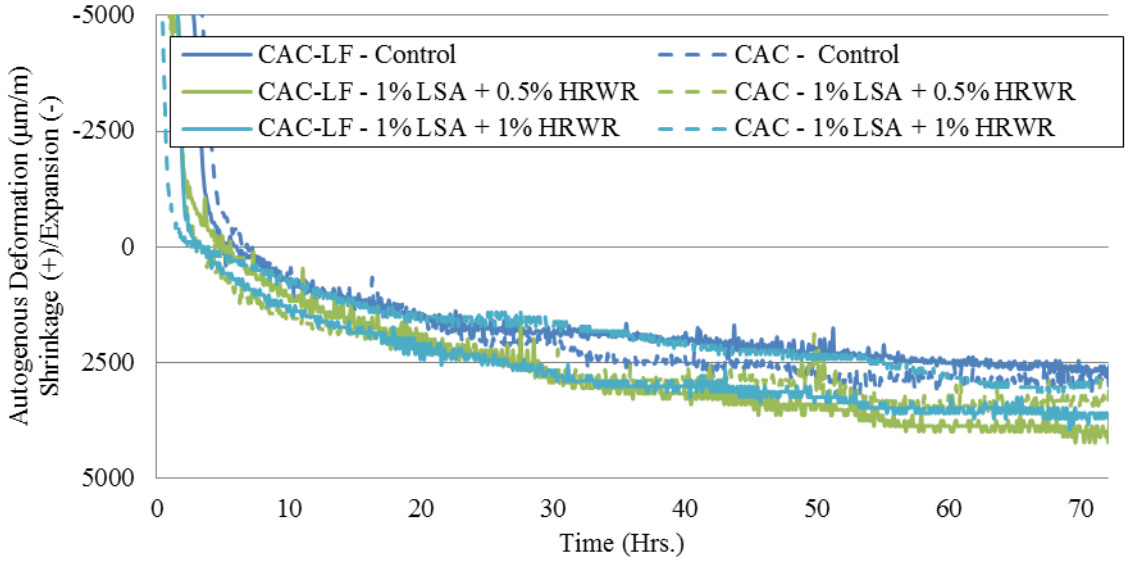


Figure 98: Autogenous deformation of CAC-LF with varying dosages of LSA and HRWR at 20°C

From Figure 98, similar amounts of early-age autogenous shrinkage were observed for all three CAC-LF mixtures. The ultimate shrinkage values were similar to those of the plain CAC mixtures. There did not appear to be any influence of the LSA and HRWR on the early-age deformation of these systems.

### 6.2.2 Hydration of CAC-LF at 38°C

#### *6.2.2.1 Influence of CAC-LF on Isothermal Calorimetry at 38°C*

The isothermal calorimetry of CAC-LF at 38°C is shown in Figure 99 and Figure 100.

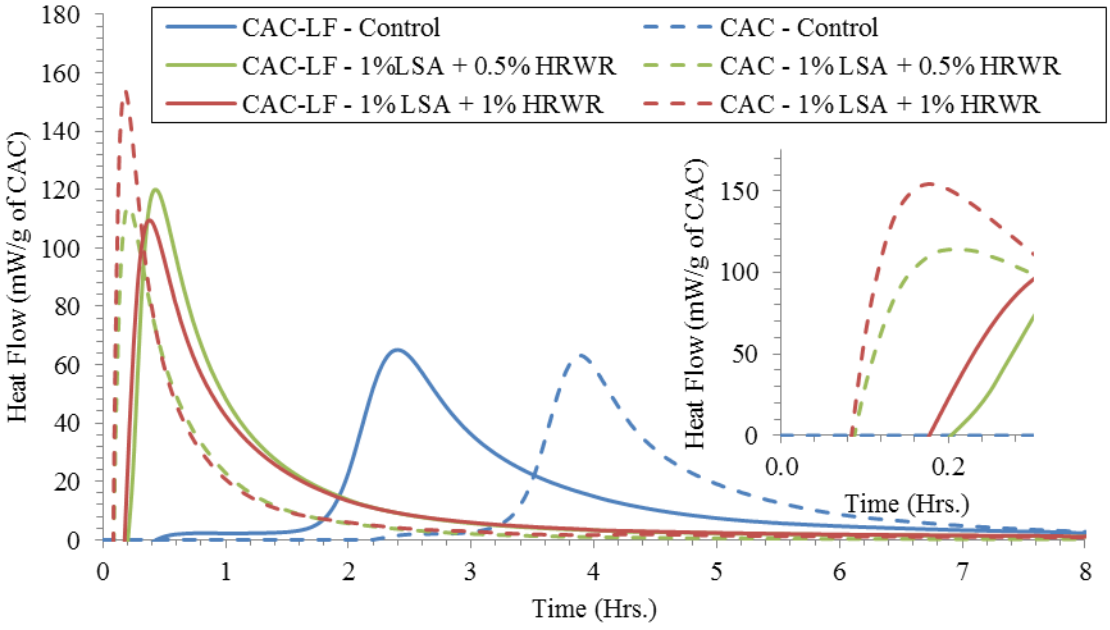


Figure 99: Heat flow of CAC-LF hydrated at 38°C for varying LSA and HRWR dosages

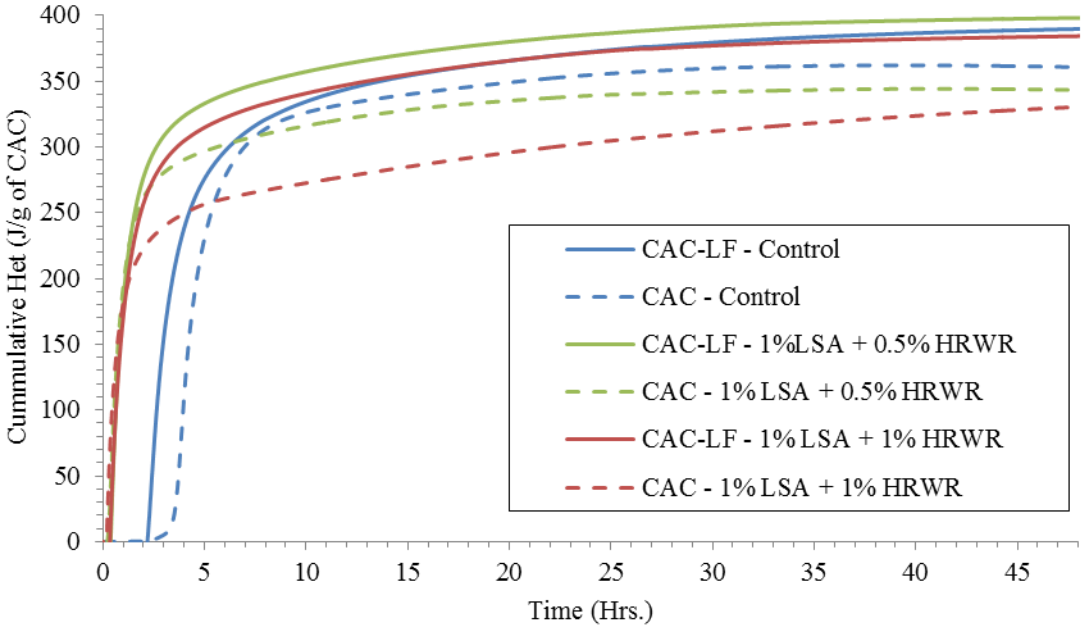


Figure 100: Cumulative heat release of CAC-LF hydrated at 38°C for varying LSA and HRWR dosages

From Figure 99, the acceleration of the control mixture was evident at 38°C as was shown at 20°C. The peak heat flow was reduced the time from 3.8 hours to 2.3 hours, and an increase in the amount of heat release was observed. Interestingly, this behavior was opposite with the addition of the LSA and HRWR at 38°C. The combination of the admixtures and LF seemed to slow the mixture and reduce the peak heat flow. The deceleration of the peak flow was more gradual for the mixtures containing LF than the control mixtures. From Figure 100, an increase in the total heat release of the CAC-LF mixtures was seen compared to the plain CAC control. The additions of the LSA and HRWR had negligible effects on the total heat release.

#### *6.2.2.2 Influence of CAC-LF on Chemical Shrinkage at 38°C*

The chemical shrinkage of the CAC-LF mixtures with and without LSA and HRWR are presented in Figure 99.

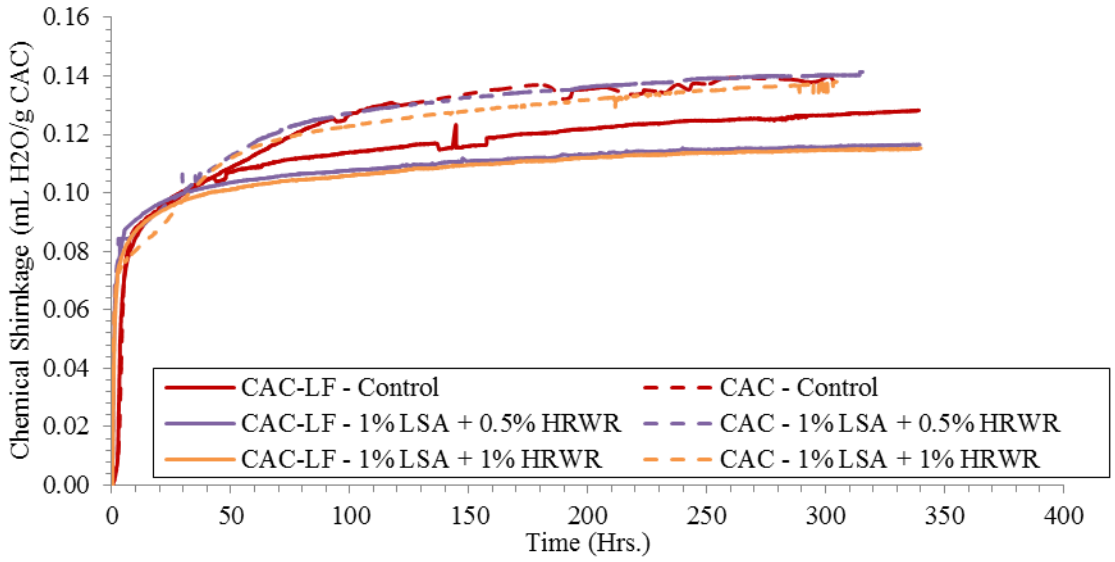


Figure 101: Chemical shrinkage of CAC-LF with varying dosages of LSA and HRWR at 20°C

From Figure 101, there was a reduced amount of chemical shrinkage due to the addition of the LF. This was opposite of the amount of total heat release seen from the cumulative heat release curves. The CAC-LF control mixture had more chemical shrinkage than the mixtures containing LSA and HRWR, 0.13 mL/g and 0.11 mL/g, respectively. A key observation was the reduction in the secondary ascent in the chemical shrinkage after 24-36 hours of testing at this higher temperature. The plain CAC mixture continues to undergo chemical shrinkage, while the CAC-LF mixture has much more gradual ascent, which may be an indication of the reduced or limited amount of conversion. The comparison of chemical shrinkage plotted as a function of cumulative heat release is plotted in Figure 102.

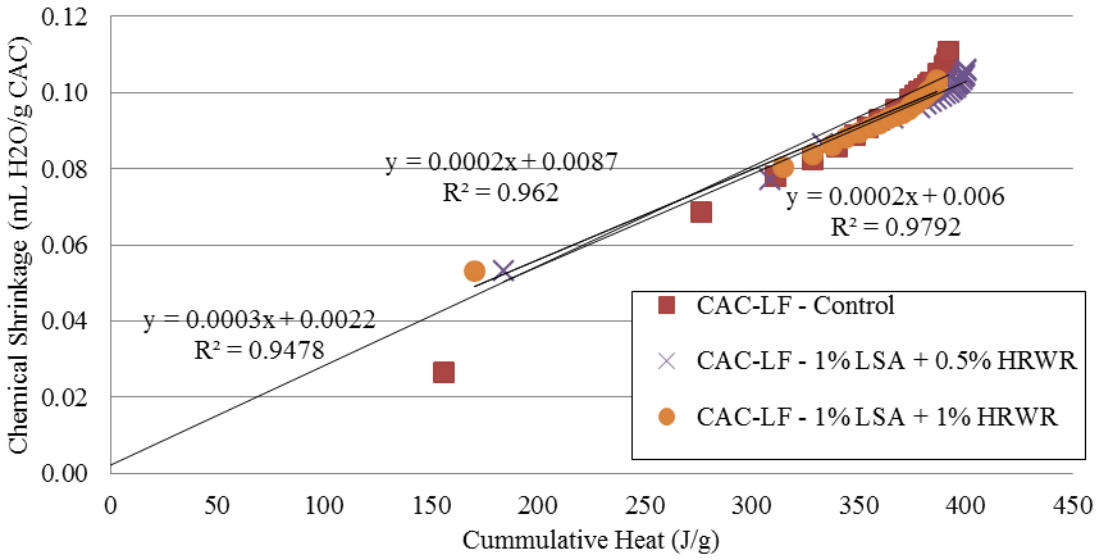


Figure 102: Chemical shrinkage as a function of cumulative heat of CAC-LF with varying LSA dosages at 38°C.

From Figure 102, it is clearly evident that the addition of the LF had little impact on the three day hydration of the system. The lines are overlapping and have very similar slopes. The control mixture had a slower hydration reaction, identified by points

occurring off the grid where little chemical shrinkage occurred prior to any heat release measured. However, once the reaction began the rate of reaction for the mixture was similar to those containing the LSA and HRWR. Strong correlation coefficients were determined for all three mixtures, further characterizing the strong influence of the LF for all three mixtures. Similar to the behavior seen in Figure 104, little conversion or increase in chemical shrinkage was observed between two to three days of hydration. The plain CAC systems had a sharp uptick in the chemical shrinkage behavior that was correlated to the increase in porosity due to conversion. The addition of the LF may mitigate or prevent conversion or at least fill some of the pores which may have prevented the increase in chemical shrinkage therefore preventing the reduction in porosity and strength.

#### *6.2.2.3 Influence of CAC-LF on Autogenous Deformation at 38°C*

The early-age volume deformation of the CAC-LF mixture was investigated at 38°C isothermal testing, and the results are presented in Figure 105.

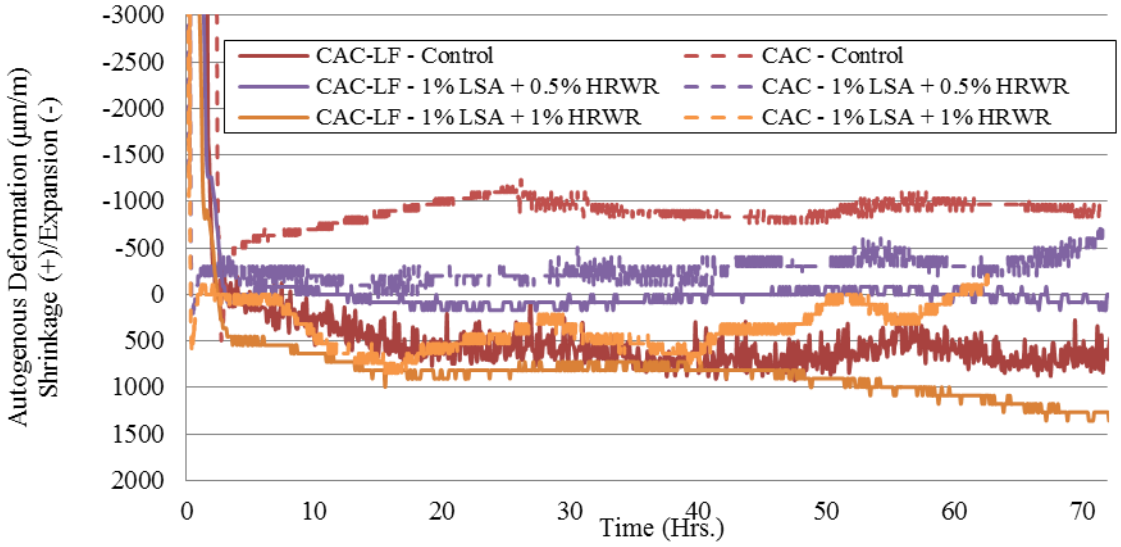


Figure 103: Autogenous deformation of CAC-LF with varying dosages of LSA and HRWR at 20°C

Generally, similar trends in the autogenous deformation of the CAC-LF and plain CAC systems were observed in the 38°C isothermal testing. Some amounts of shrinkage were observed. However, one observation was the behavior in the control mixtures. The plain CAC control mixture clearly experienced an autogenous deformation for the duration of the testing while the CAC-LF control mixture experienced 750 µm/m of shrinkage. The other four mixtures, plain CAC and CAC-LF with varying amounts of LSA and HRWR, had closer similarities in the deformation behavior.

### 6.2.3 Summary

The section presented the characterization of the early-age hydration and volume deformation characteristics of the influence of 20% limestone substitution for CAC at 20°C and 38°C. These key observations and conclusions can be made from the 20°C testing:

- The substitution of the LF accelerated the hydration kinetics with and without the addition of LSA and HRWR. Significant amounts of cumulative heat were measured for these mixtures highlighting the possibility of different microstructural development.
- More chemical shrinkage was observed for the CAC-LF mixtures compared to the plain CAC cement. The addition of LSA and HRWR slightly lowered the total amount of chemical shrinkage compared to the control CAC-LF mixture.
- From the hydration investigations, it appeared that the LF was the controlling factor on the rate of hydration and the addition of the LSA and HRWR had minimal effects after the first 3-4 hours of hydration.
- CAC-LF had similar amount of autogenous shrinkage compared to the plain CAC system with and without chemical admixtures.

The results of the 38°C testing led to these conclusions:

- CAC-LF had varying effects on the hydration reaction at 38°C; however, a higher cumulative heat release was observed for all.
- From chemical shrinkage, a reduction in the secondary ascent of the chemical shrinkage amount was observed, which could be due to the formation of stable hydration products minimizing the amount of conversion that could occur. These results were also observed when the chemical shrinkage was plotted as a function of the cumulative heat release.
- A slight reduction in the autogenous expansion was observed in the CAC-LF control mixture compared to plain CAC. The impact of the LF with the LSA and HRWR had minimal impact on the autogenous deformation.0

## 6.3 Influence of High-Calcium Fly Ash

This section characterizes the influence of 30% high-calcium fly ash substitution on CAC hydration and early-age volume deformation. This fly ash and substitution percentage was chosen based on actual field work done by the Texas Department of Transportation (TxDOT). Currently, TxDOT uses this high-calcium fly ash in all CAC mixtures for repairs of roadways and bridge decks. This section aims to provide a better understanding of the influence of these material combinations.

### 6.3.1 Hydration of CAC-FA at 20°C

#### *6.3.1.1 Influence of CAC-FA on Isothermal Calorimetry at 20°C*

To investigate the influence of this SCM on the hydration kinetics, isothermal calorimetry was performed at 20°C. The results of the testing are presented in Figure 104. The independent influences of the LSA and HRWR on the hydration kinetics are presented in Appendix E.

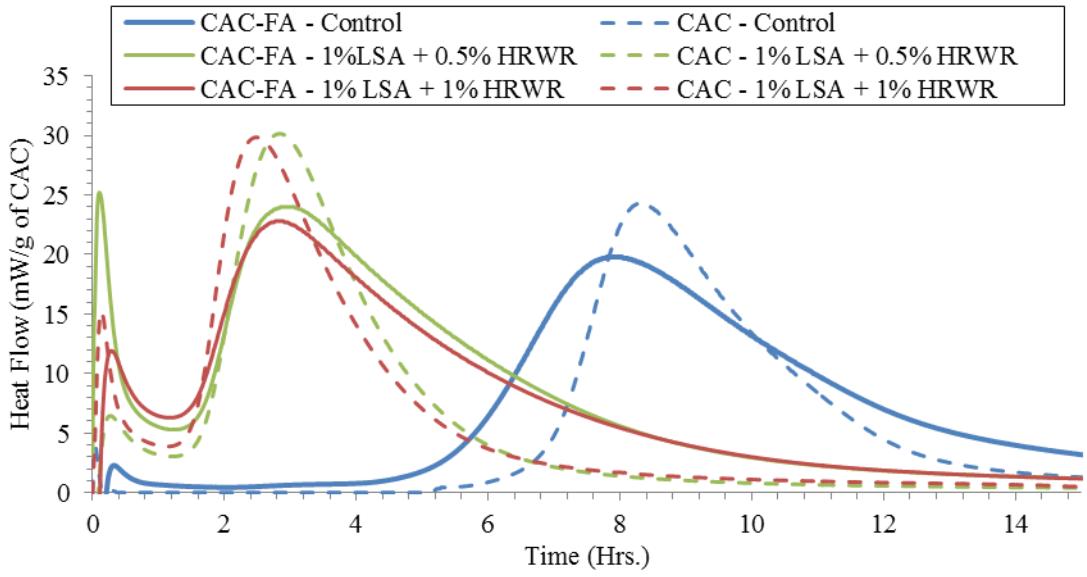


Figure 104: Heat flow of CAC-FA hydrated at 20°C for varying LSA and HRWR dosages

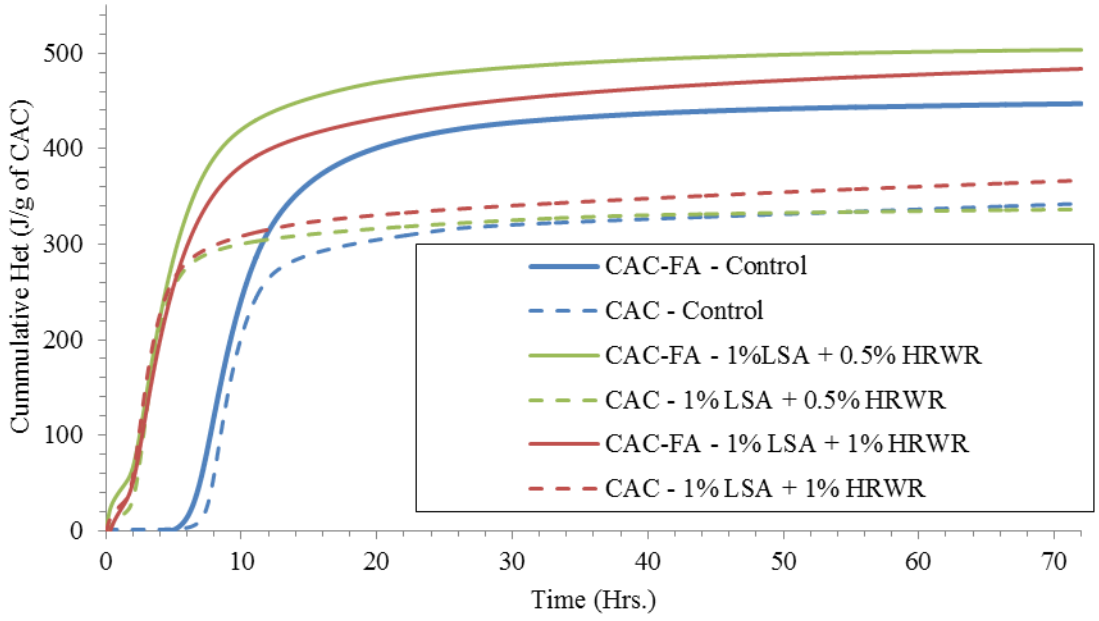


Figure 105: Cumulative heat release of CAC-FA hydrated at 20°C for varying LSA and HRWR dosages

Figure 104 and Figure 105 characterize the influence of the high-calcium fly ash substitution on the hydration kinetics of CAC. From the heat flow curve, a few observations could be made. The addition of FA reduced the peak heat flow of all mixtures with and without the addition of chemical admixtures. The FA substitution generated broader heat flow curves than the plain CAC mixtures. The deceleration of the peak heat flow was especially broader and lasted longer. The addition of the LSA and HRWR had similar effects on the rates of hydration of the CAC-FA and the plain CAC mixture.

From the cumulative heat release curve substantially more cumulative heat release was observed for the CAC-FA mixtures. This figure showed that the FA hydrates and plays a substantial role on the microstructural development and hydration kinetics of the system. The ascent of the cumulative heat flow curves of the CAC-FA mixtures mimic

those of the plain CAC mixtures, further confirming the similarities shown in the heat flow diagram.

### *6.3.1.2 Influence of CAC-FA on Chemical Shrinkage at 20°C*

The CAC-FA mixtures were investigated in chemical shrinkage; the results are presented in Figure 106. The chemical shrinkage was also plotted as bar graph to show the standard deviation of the different mixtures, these results are located in Appendix E.

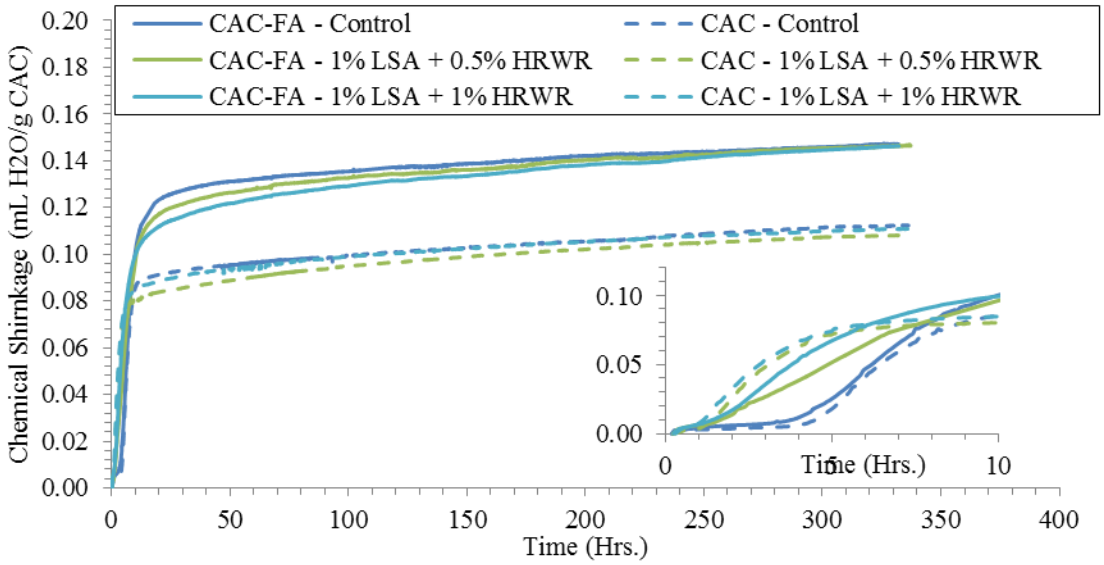


Figure 106: Chemical shrinkage of CAC-FA with varying dosages of LSA and HRWR at 20°C

In Figure 106, the influence of CAC-FA compared to plain CAC with and without the additions of LSA and HRWR at 20°C was shown. The three CAC-FA mixtures had nearly identical amounts of chemical shrinkage at the termination of the experiment. The values had an average of 27% more chemical shrinkage at 14 days than the plain CAC mixtures. Interestingly, this was almost equivalent to the 30% replacement of CAC. Thus, if the graphs were normalized per gram of cementitious material there would be no

distinguishable difference in the behavior of the two systems. The high-calcium fly ash played a substantial role in the total amount of chemical shrinkage and cumulative heat release from isothermal calorimetry. To further look at this comparison, the chemical shrinkage was plotted as a function of the cumulative heat release in Figure 107.

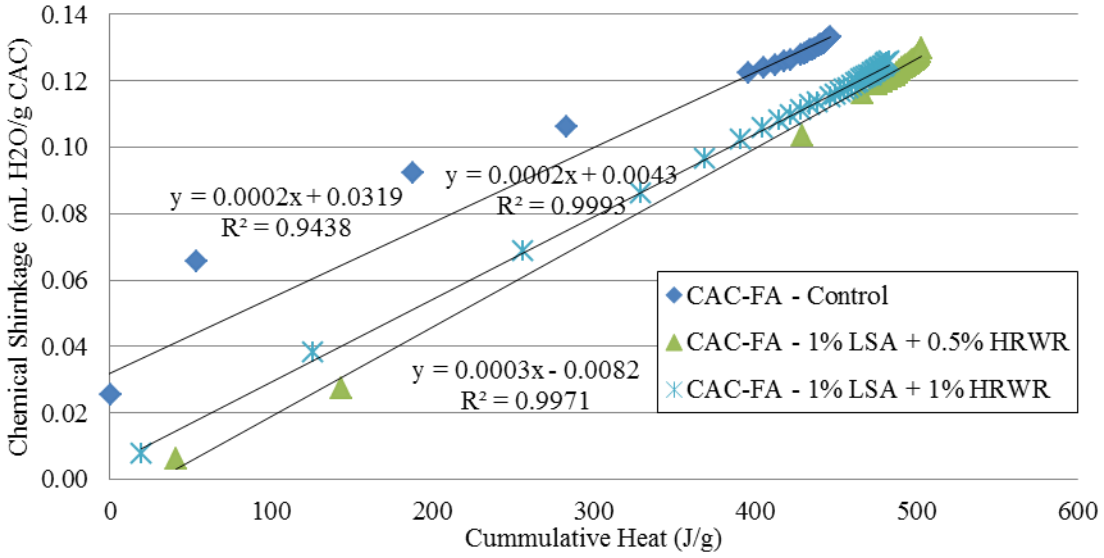


Figure 107: Chemical shrinkage as a function of cumulative heat of CAC-FA with varying LSA dosages at 20°C.

From Figure 107, comparisons on the hydration reactions for the three different CAC-FA mixtures can be made. The mixtures had strong correlation coefficients and similar hydration reaction slopes of the different mixtures. The control mixture reaction was slightly slower than the other mixtures; this can be observed by more data points being presented at the lower chemical shrinkage and cumulative heat release values.

### *6.3.1.3 Influence of CAC-FA on Autogenous Deformation at 20°C*

To investigate the influence of the substitution of FA on the early-age volume deformation, autogenous deformation testing was completed. The results of the 20°C isothermal testing are presented in Figure 108.

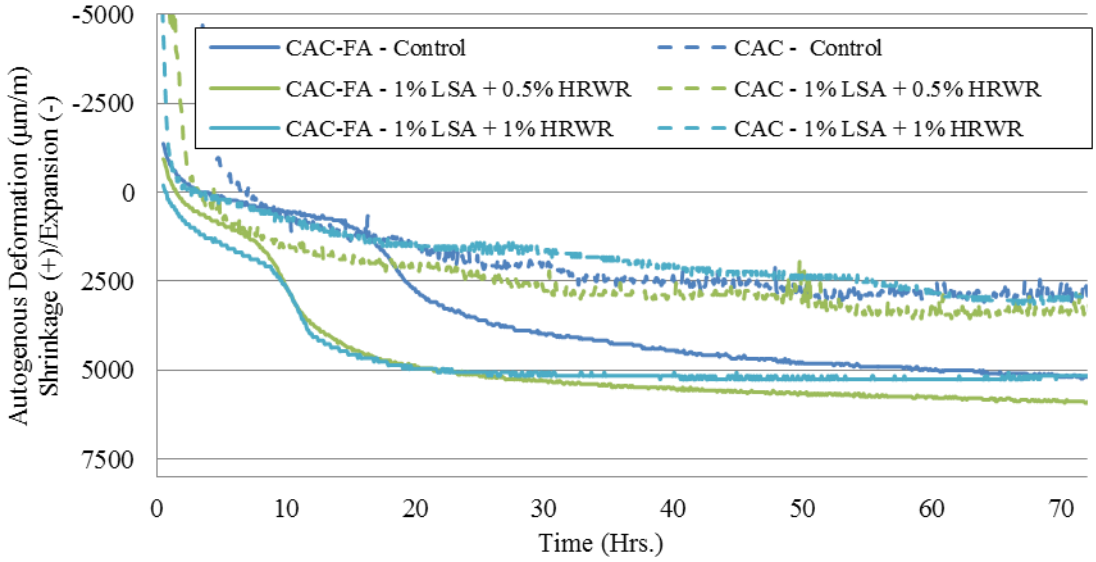


Figure 108: Autogenous deformation of CAC-FA with varying dosages of LSA and HRWR at 20°C

From Figure 108, the autogenous shrinkage of the CAC-FA mixture was clearly evident. Large amounts, over 5000 µm/m, of autogenous shrinkage were observed for all three mixtures at the termination of the test. The very early-age shrinkage patterns of the CAC-FA mixture resembled the shrinkage of the plain CAC systems until 12 hours and 20 hours for the two mixtures containing LSA and the control mixture, respectively. These plots clearly characterize the early-age shrinkage of these material combinations and may indicate the potential for cracking due to early-age shrinkage of this material.

### 6.3.2 Hydration of CAC-FA at 38°C

#### *6.3.2.1 Influence of CAC-FA on Isothermal Calorimetry at 38°C*

Figure 109 and Figure 110 present the isothermal calorimetry results of CAC-FA mixtures with and without LSA and HRWR. The independent influence of these two chemical admixtures on the heat flow and cumulative heat release at 38°C are presented in Appendix E.

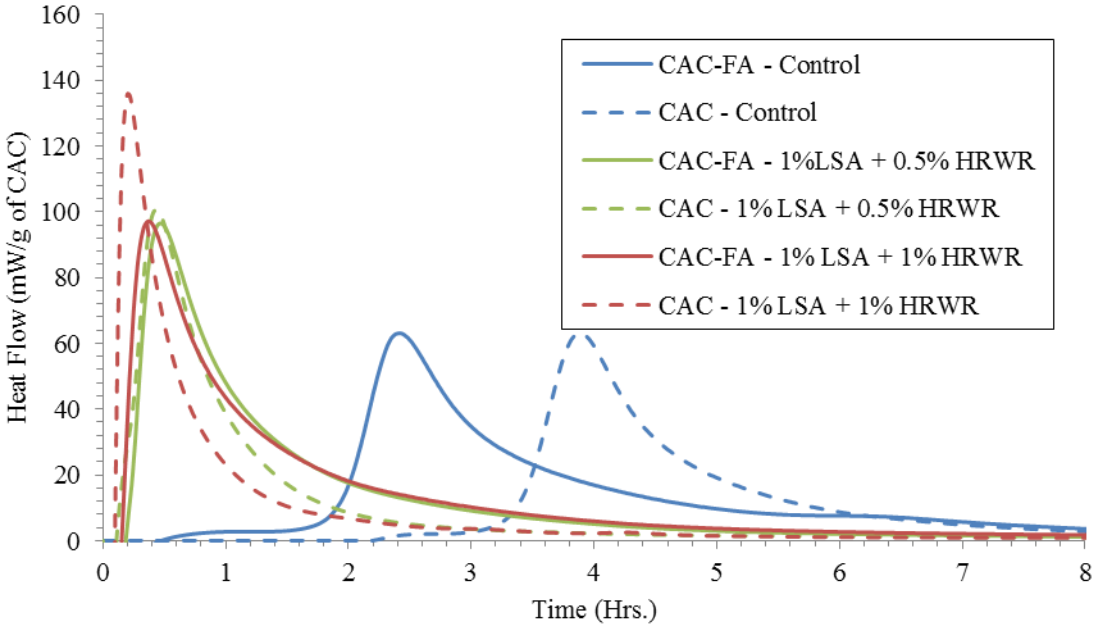


Figure 109: Heat flow of CAC-FA hydrated at 38°C for varying LSA and HRWR dosages

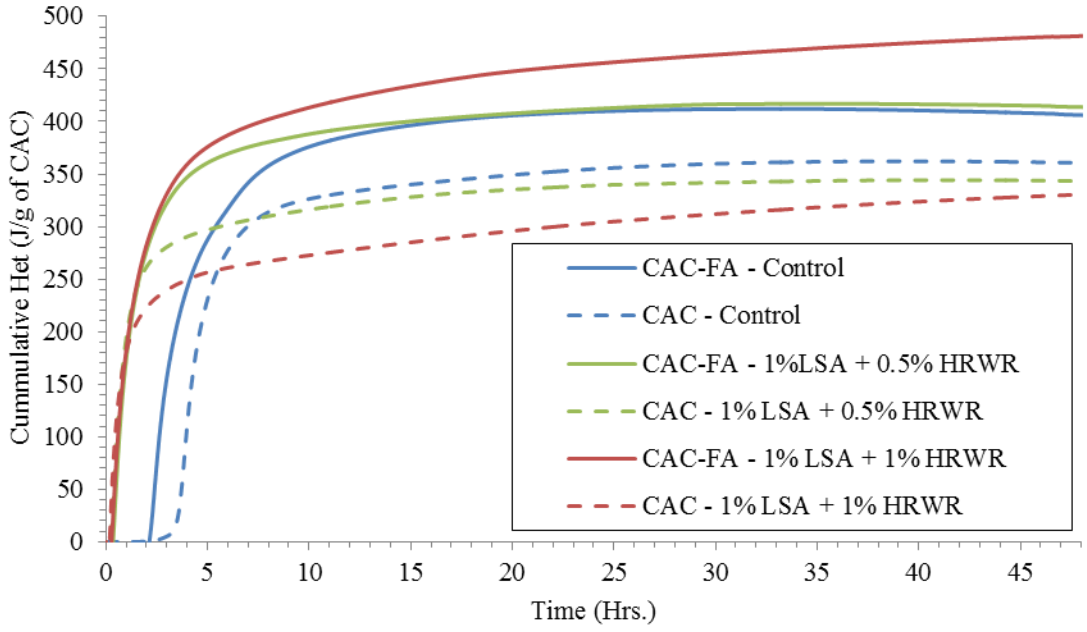


Figure 110: Cumulative heat release of CAC-FA hydrated at 38°C for varying LSA and HRWR dosages

The influence of the FA and chemical admixtures on the hydration kinetics was highlighted in Figure 109. Similar to the results shown with the heat flow of CAC-LF at 38°C, an acceleration of the control mixture was observed with addition of the SCM. However, also similar to the CAC-LF mixtures, the use of the LSA and HRWR slowed the reaction of the CAC-FA mixture compared to plain CAC.

Form Figure 110, an increase in the cumulative heat release was observed for the CAC-FA mixtures compared to the plain CAC systems. Similar quantities of total cumulative heat were observed for these mixtures at both 20°C and 38°C. These graphs were both normalized for the mass of CAC in each mixture. From an obvious increase in the amount of reactivity with the FA substitution it was safe to assume the FA actively participates in the microstructural development of this binder system.

### *6.3.2.2 Influence of CAC-FA on Chemical Shrinkage at 38°C*

The results of the 38°C chemical shrinkage of the CAC-FA mixtures are presented in Figure 111. Also, the chemical shrinkage is plotted in Appendix E to show the standard deviation of the CAC-FA mixtures.

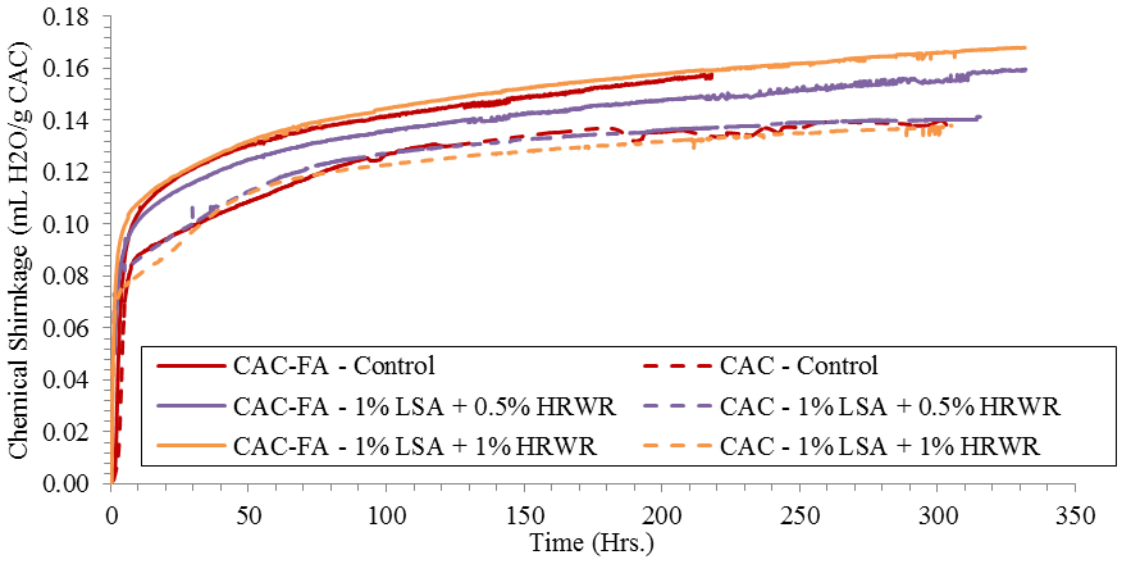


Figure 111: Chemical shrinkage of CAC-FA with varying dosages of LSA and HRWR at 38°C

From Figure 111, an increase in the chemical shrinkage of the mixtures containing FA was observed compared to the plain CAC mixture. The secondary ascent in the chemical shrinkage slope was also observed, which has been found to be correlated to the process of conversion. The addition of the LSA and HRWR had negligible effects on the chemical shrinkage of the CAC-FA mixtures. Figure 112 plots the chemical shrinkage of the CAC-FA mixtures as a function of cumulative heat.

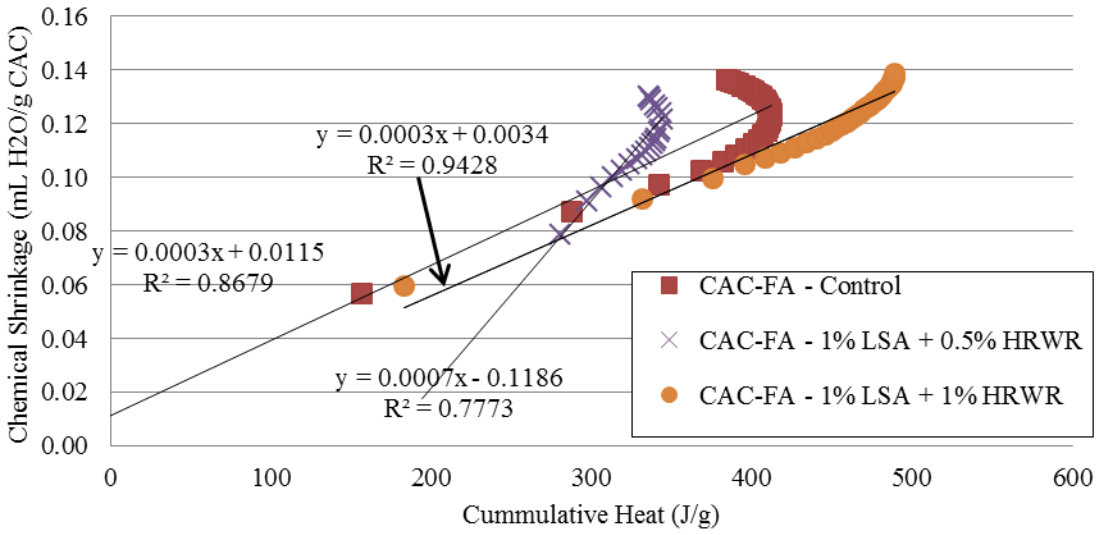


Figure 112: Chemical shrinkage as a function of cumulative heat of CAC-FA with varying LSA dosages at 38°C

Figure 112 shows the best-fit lines for the chemical shrinkage as a function of the cumulative heat release. Lower correlation coefficients were observed with these mixtures compared to other mixtures presented earlier in this chapter and in Chapter 5. This was caused by conversion of the samples when they continued to uptake water once the mixture stopped producing heat. This, again, confirms that the application of chemical shrinkage can be used to identify conversion of CAC samples. A reduction in the cumulative heat was observed in Figure 112. This was from the deviations in the baseline data of the testing. These mixtures were made in the calorimeter prior to finishing all upgrades on the system as described in Chapter 4.

#### *6.3.2.3 Influence of CAC-FA on Autogenous Deformation at 20°C*

The autogenous deformation results of the CAC-FA mixtures are presented in Figure 113.

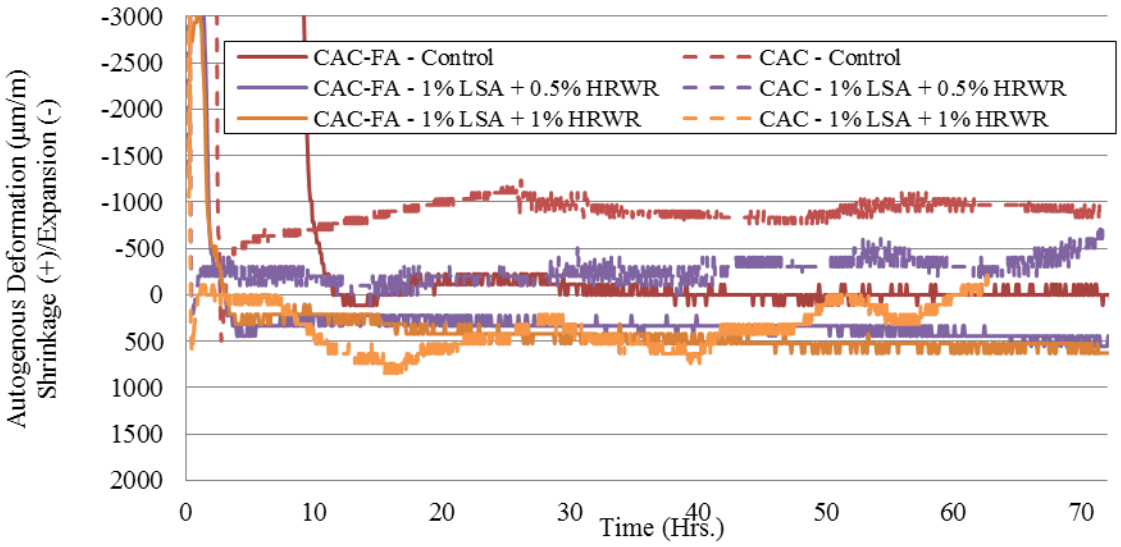


Figure 113: Autogenous deformation of CAC-FA with varying dosages of LSA and HRWR at 38°C

From Figure 113, the early-age autogenous deformation of the CAC-FA mixture was presented. Relatively small amounts of autogenous shrinkage, around 300-550 µm/m, were observed in the two CAC-FA, mixtures containing chemical admixtures. The control mixture experienced little deformation throughout the duration of the test and actually a 0 µm/m reading was recorded as the average of three different mixtures at the termination of the test at 72 hours. This zero strain reading however was a reduction from the expansion values observed by the control CAC mixture at 38°C.

While a large increase in the amount of auto autogenous shrinkage was observed at the 20°C testing due to the addition of FA; the same impact was not measured under the 38°C isothermal testing. The effects of the SCM on the early-age volume change were well documented. More work is necessary to understand the thermal effects of changing temperature and not just isothermal testing.

### 6.3.3 Summary

High-calcium fly ash substitution in CAC was investigated in this chapter due to its use in rapid repair projects by TxDOT. Every CAC mixture used had a 30% replacement and was investigated with the addition of LSA and HRWR. This section investigated the combination of these materials to characterize the influence on the early-age hydration kinetics and deformation. These key conclusions were drawn from this section at 20°C:

- From isothermal calorimetry, a reduction in the peak heat flow and broader more gradual hydration kinetics were observed when FA was used. Substantially more cumulative heat release was measured for all three mixtures containing FA compared to the plain CAC.
- The FA increased the amount of chemical shrinkage by an average of 27% at the termination of the test. This increase was almost proportional to replacement percentage of CAC, which highlights its contribution to the cementitious reactions.
- The CAC-FA mixtures all had over 5000 μm/m shrinkage at the termination of the test. This was about twice the amount of shrinkage observed with the plain CAC systems.

From the 38°C isothermal testing, these observations were made:

- A reduced induction period for the control mixture was observed for the control mixture compared to the plain CAC control mixtures; however, the mixtures containing chemical admixtures had slightly delayed peak heats of hydration. These results are inconsistent with what was observed at 20°C, but are consistent with the effects seen with the addition of LF in the previous section.

- From chemical shrinkage at 38°C, more shrinkage was observed for the FA mixtures compared to the plain CAC mixtures. A secondary ascent in the chemical shrinkage curve was observed, indicating the occurrence of conversion.
- The CAC-FA control mixture had a zero strain state after 72 hours of testing. The addition of FA had minimal effect on the autogenous shrinkage at 38°C and does not appear to have as large of an influence as the 20°C testing.

## 6.4 Influence of Chemical Admixtures

The results of the influence of two additional chemical admixtures, citric acid and styrene butadiene latex, on CAC hydration and early-age volume deformation are presented in this section. These materials were selected for investigation because they were used in a large-scale field trial presented in Chapter 7. First, the influence of citric acid on the hydration kinetics is presented. Then, the influence of latex, citric acid, and LSA on the hydration kinetics and early-age volume deformation is shown.

### 6.4.1 Influence of Citric Acid

Citric acid was a known retarder of CAC hydration (Rodger, 1984). This section investigates the influence of citric acid on the hydration and early-age volume deformation of plain CAC with the combination of LSA.

#### *6.4.1.1 Influence of Citric Acid on Isothermal Calorimetry at 20°C*

The results of the influence of citric acid, individually and combined with LSA, on the hydration kinetics of plain CAC at 20°C are presented in Figure 114 and Figure 115.

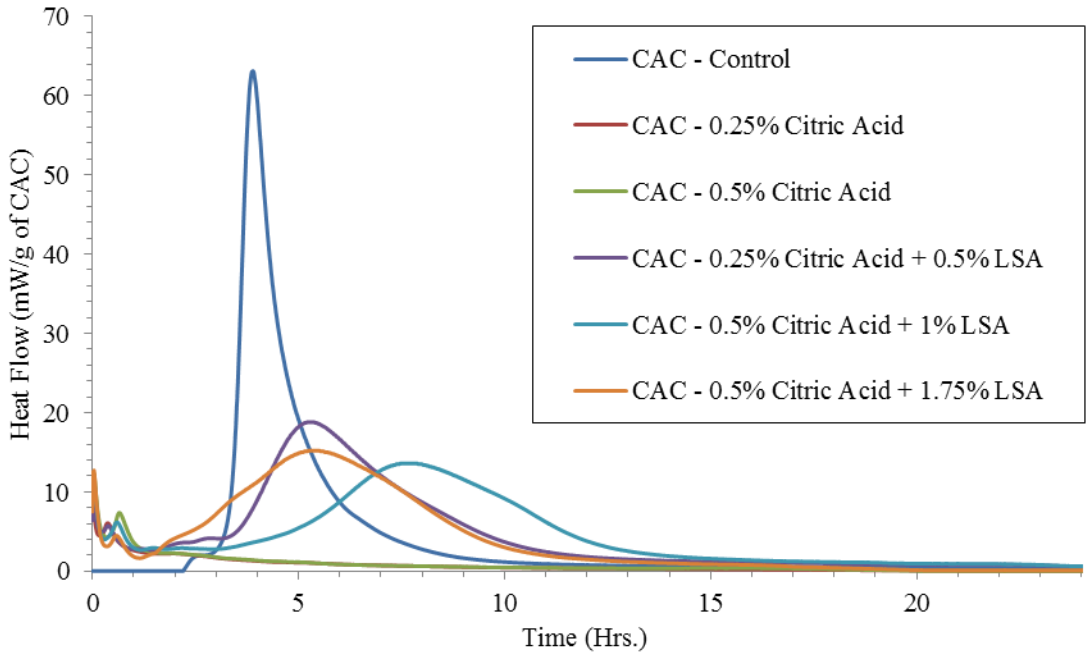


Figure 114: Heat flow of CAC hydrated at 20°C for varying Citric Acid and LSA dosages

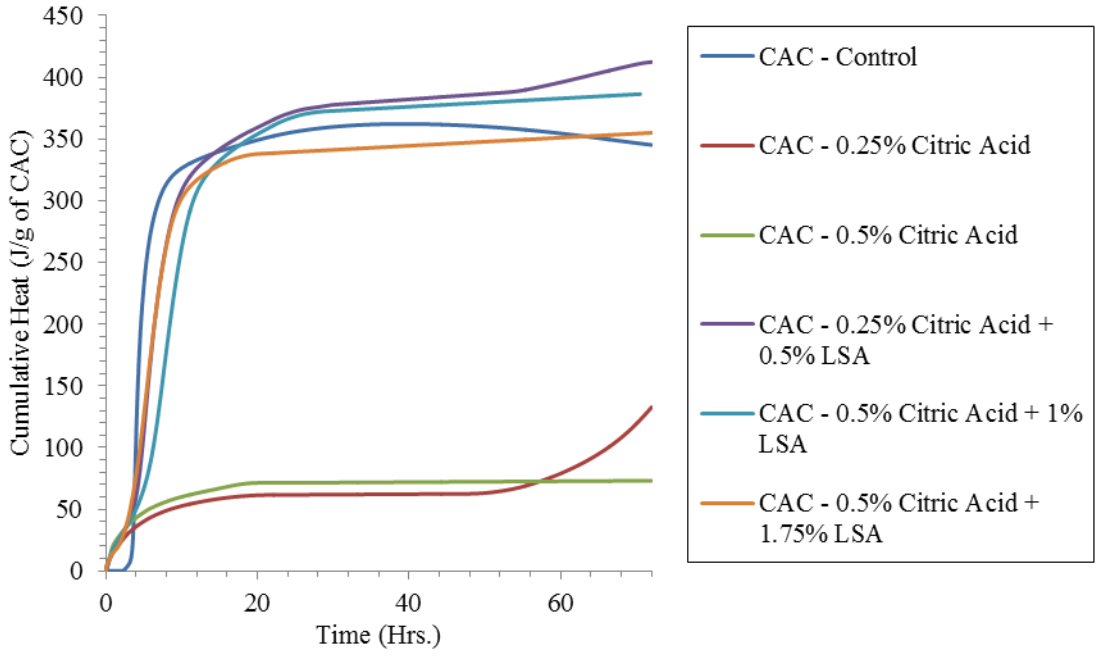


Figure 115: Cumulative heat release of CAC hydrated at 20°C for varying Citric Acid and LSA dosages

From the heat flow curve, the independent influence of the citric acid may not be clear from the graph, but that was because no heat was generated for either mixture for the first 55 hours. These two plots illustrate the retardation effects of citric acid on plain CAC. The mixtures containing citric acid and LSA had much lower peak heat flow curves than the control CAC mixture and the time of the peak heat flow was retarded from the control, even with the addition of 1.75% LSA. It should be noted that the addition of citric acid to control the setting time did not have the negative effects on the workability as did the HRWR did at the higher dosages to control the setting time when LSA was used.

From the cumulative heat flow curve, the retardation of the hydration kinetics was evident. The mixtures containing only citric acid show an initial increase in the amount of heat release over the first 24 hours, this was merely from the heat of dissolution that appears to be extended, but was caused by the error in the experiment. Citric acid had negligible impact on the amount of cumulative heat released compared to control CAC mixture.

#### *6.4.1.2 Influence of Citric Acid on Isothermal Calorimetry at 38°C*

The results of the influence of citric acid on the isothermal calorimetry at 38°C are presented in Figure 116 and Figure 117.

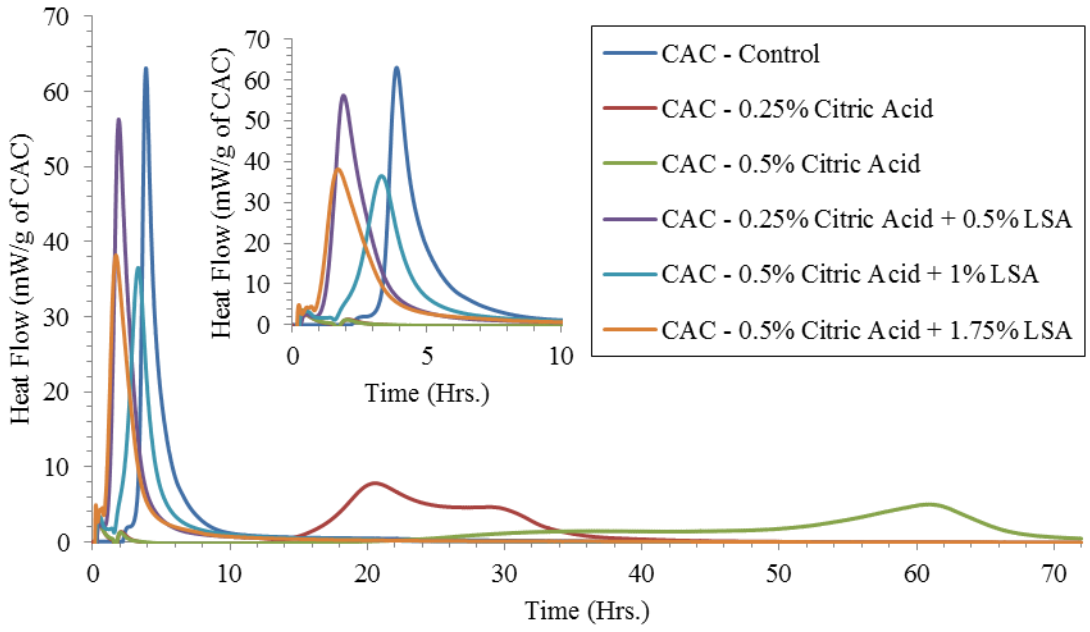


Figure 116: Heat flow of CAC hydrated at 38°C for varying Citric Acid and LSA dosages

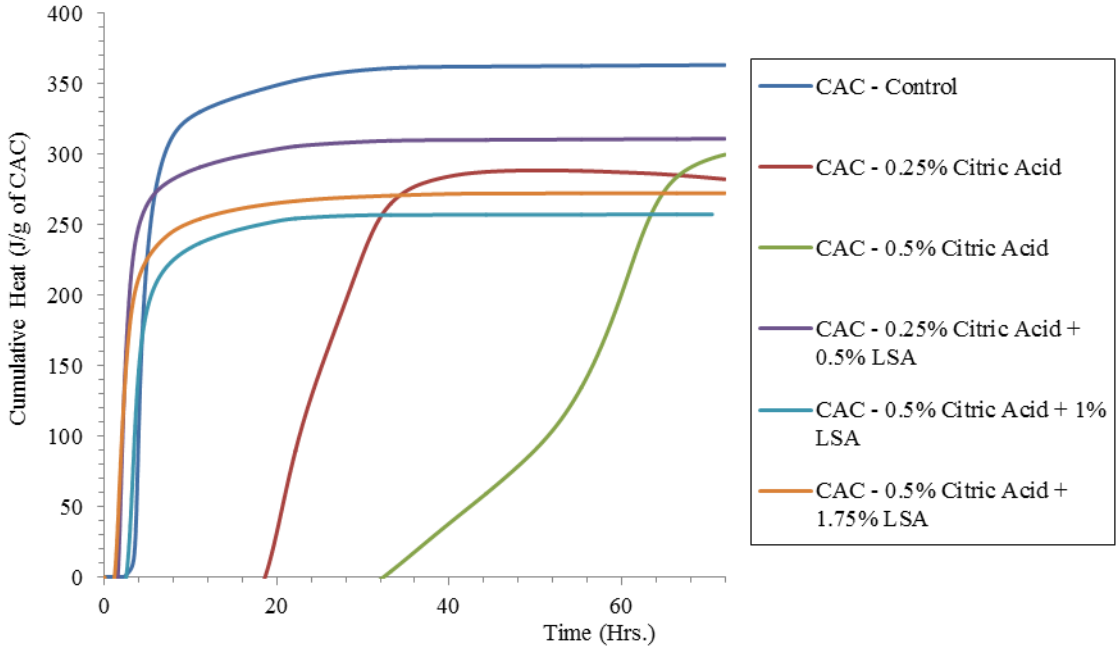


Figure 117: Cumulative heat release of CAC hydrated at 38°C for varying Citric Acid and LSA dosages

From Figure 116, citric acid was still proven to be a potent retarder at 38°C; however, the time until the induction period was shortened significantly compared to the results at 20°C. The addition of 0.25% and 0.50% with CAC drastically reduced the peak heat flow for plain CAC and changed the heat flow pattern. The mixtures containing LSA had completely different heat flow patterns compared to those mixtures and all the mixture tested at 20°C. From the insert in the heat flow diagram, it can be seen that citric acid slowed the hydration reaction of the mixtures with LSA, but it does not have the same effect as when they were combined at 20°C. The heat flow patterns of these mixtures appeared to be similar to plain CAC and the effects of LSA were clearly more pronounced than at 20°C. The other key observation was from Figure 117; a reduction in the cumulative heat was observed with those mixtures containing citric acid. This trend was not observed from the 20°C isothermal testing.

### 6.4.2 Influence of Latex

This section summarizes the influence of 15%, by weight of solids to CAC, addition to plain CAC. This addition was investigated for its use in thin-bonded overlay of bridge decks and roadways. The material combination of CAC with 15% latex, 1.75% LSA, and 0.5% citric acid is a significant mixture design because it was used in the large scale field trial at UT Austin. This section was completed to provide a microscopic understanding to allow for correlation of the results to the macroscopic behavior described in Chapter 7.

#### *6.4.2.1 Influence of Latex on Isothermal Calorimetry at 20°C*

The effect of the combination of CAC with latex, citric acid and LSA on the hydration kinetics at 20°C is presented in Figure 118 and Figure 119.

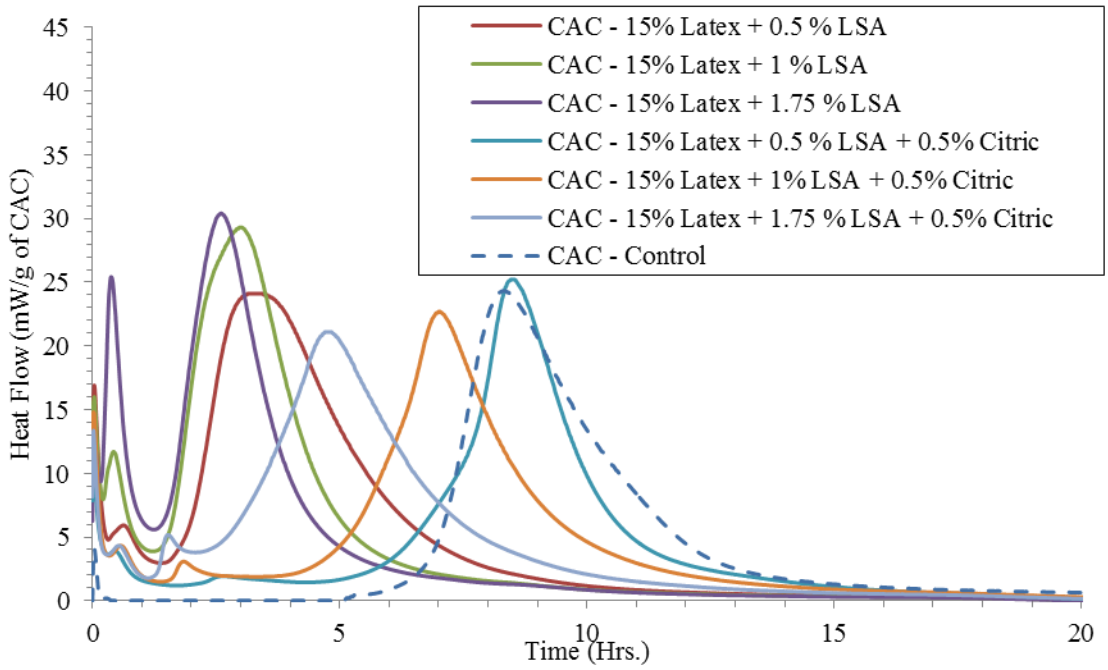


Figure 118: Heat flow of CAC with latex hydrated at 20°C with varying LSA and citric acid

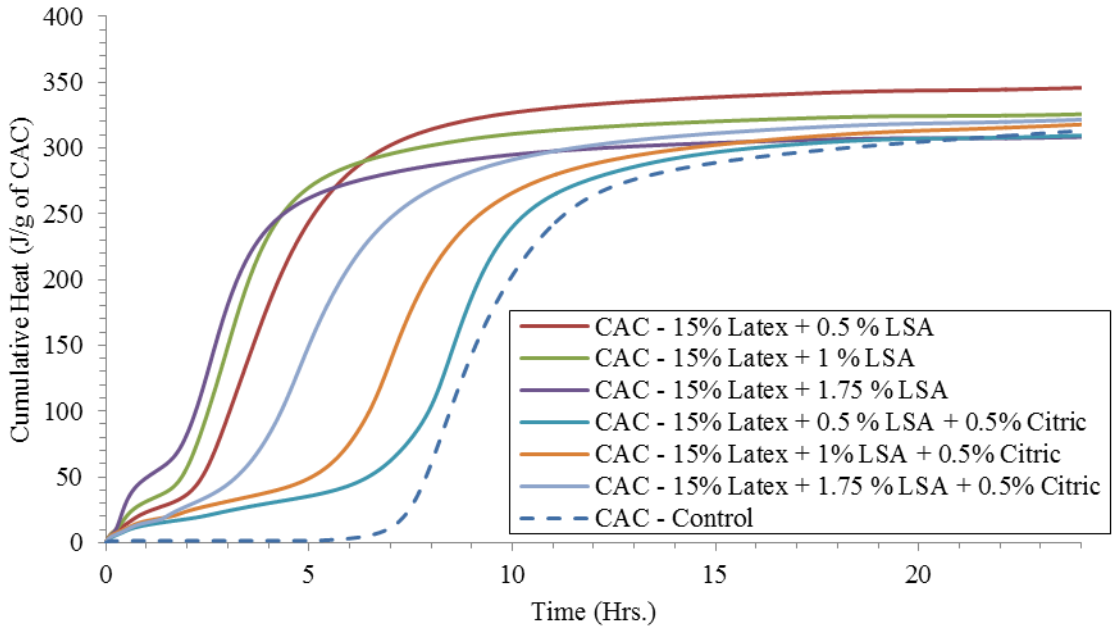


Figure 119: Cumulative heat release of CAC with latex hydrated at 20°C with varying LSA and citric acid

From the isothermal calorimetry results, the addition of latex to CAC with LSA slowed the hydration reaction. The heat flow curves for these mixtures were broader with more gradual acceleration and deceleration of the hydration reaction. The combination of latex with citric acid and LSA had insignificant effects on the heat flow pattern compared to the combinations of plain CAC with citric acid and LSA. The cumulative heat release for all mixtures was similar and the addition of latex did not have an effect on the total amount of heat released at 20°C.

#### *6.4.2.2 Influence of Latex on Chemical Shrinkage at 20°C*

The results of 20°C isothermal testing of plain CAC with Latex and additions of LSA and citric acid are presented in Figure 120; a bar graph of the chemical shrinkage with the standard deviations is shown in Figure 121.

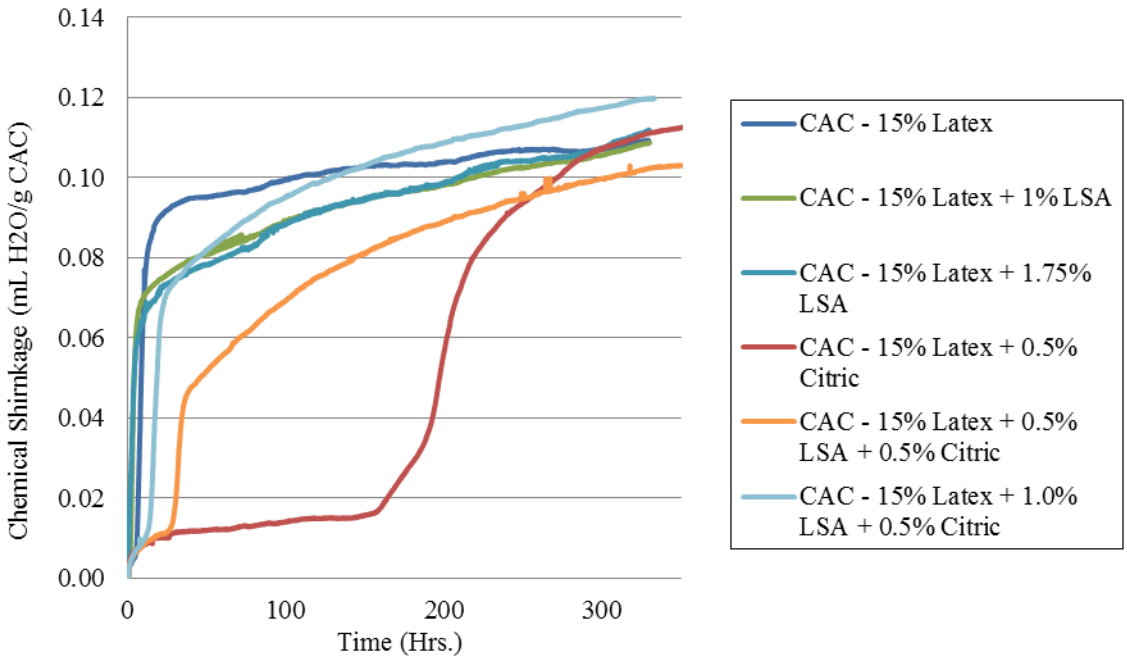


Figure 120: Chemical shrinkage of CAC with latex hydrated at 20°C with varying LSA and citric acid

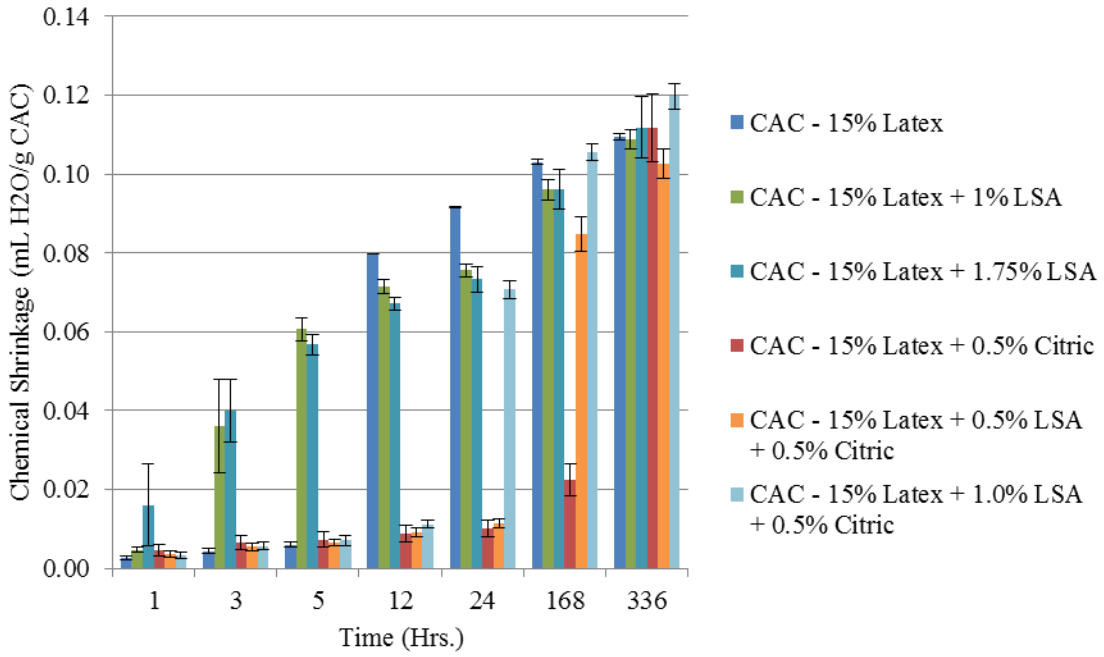


Figure 121: Chemical shrinkage with standard deviation of CAC with latex hydrated at 20°C with varying LSA and citric acid

From Figure 120, two clear ascents in the chemical shrinkage patterns were observed for all mixtures. This was unique to the addition of the latex and citric acid to the systems. This behavior was not observed in any other results at 20°C. After 14 days of testing, similar amounts of total chemical shrinkage was observed for all mixtures. This highlights that the addition of LSA and citric acid had unsubstantial impacts on the total shrinkage when combined with latex.

In Figure 121, standard deviations were presented to highlight that more variability was recorded with specimens containing latex than the other CAC based-systems presented in this chapter and the previous. These large deviations may cause for misinterpretation of some of the data due to the error, especially at earlier ages. The large standard deviations of these mixtures were likely caused by the bleeding of latex to the surface of the specimen and migrating up into the pipette. The latex hardened to the side

of the vials and blocked the camera from taking clear pictures of the red indicator die. These results were attempted to be improved upon numerous times and no resolve was found. To compare the chemical shrinkage and cumulative heat of these mixtures they were plotted in Figure 122.

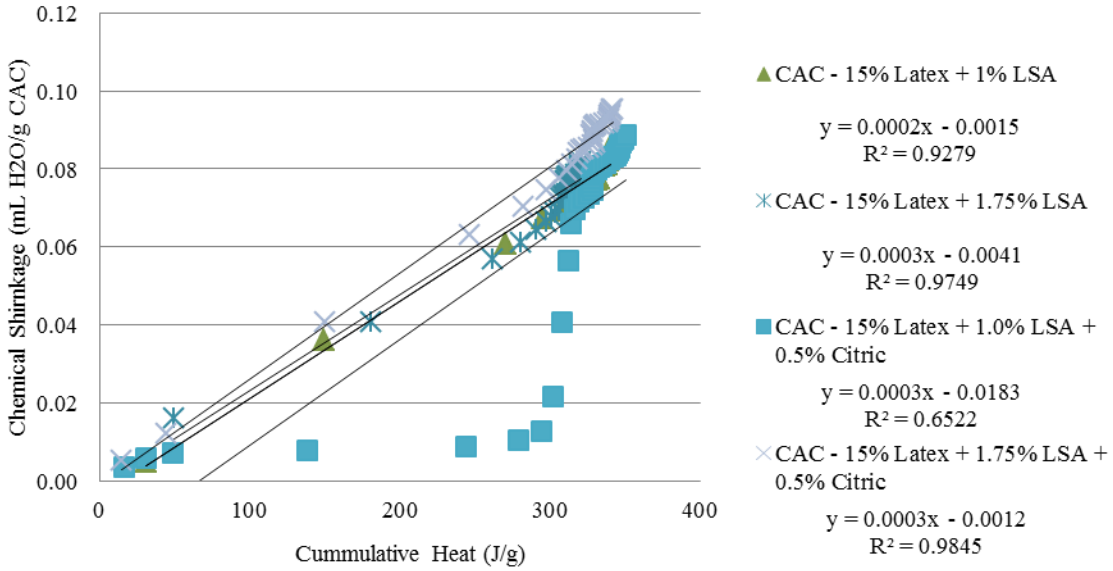


Figure 122: Chemical shrinkage as a function of CAC with latex hydrated at 20°C with varying LSA and citric acid

Chemical shrinkage as a function of cumulative heat release of CAC with latex, LSA and citric acid is shown in Figure 122. This graph does not provide the most telling information about the hydration reaction of these systems. The correlation coefficient of the CAC mixture with 15% latex, 1% LSA, and 0.5% citric acid was weak and the slopes of the lines for all mixtures were approximately the same, meaning that the addition of LSA and citric did not greatly affect the reactions.

### *6.4.2.3 Influence of Latex on Autogenous Deformation at 20°C*

Results from autogenous shrinkage at 20°C are presented in Figure 123.

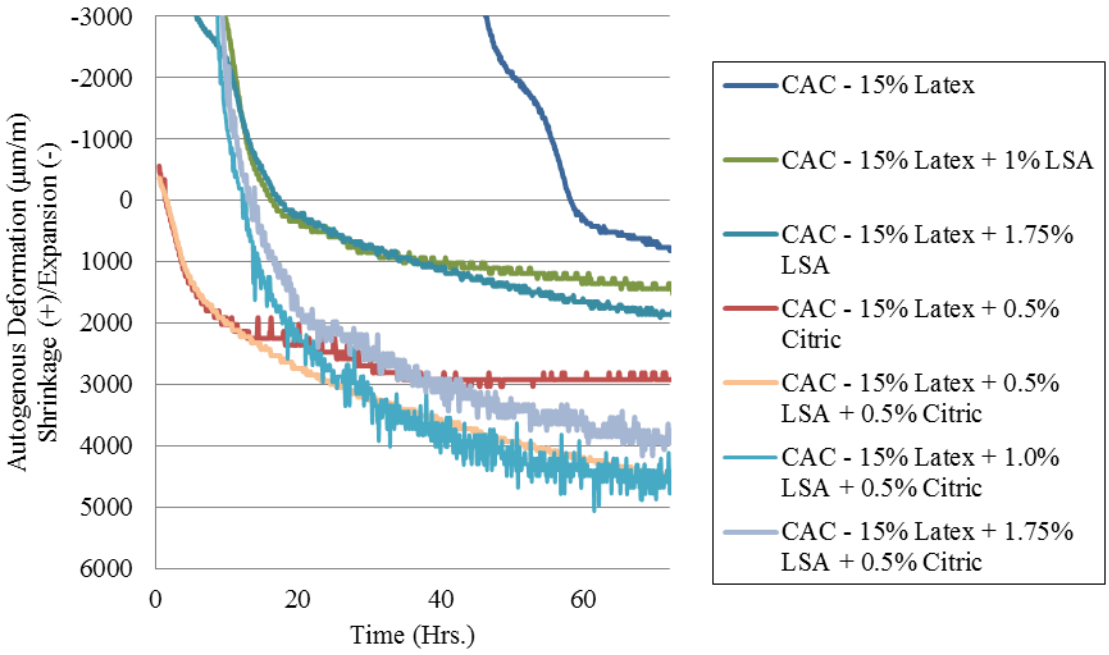


Figure 123: Autogenous deformation of CAC with latex with varying dosages of LSA and citric acid at 20°C

From Figure 123, it was clear that the addition of citric acid increased the total amount of autogenous shrinkage. Mixtures containing more than 1% LSA in combination with citric acid all had greater than 4000 µm/m of chemical shrinkage after 72 hours of hydration. The mixtures containing only latex and LSA had substantially less autogenous shrinkage. This was a key observation that could highlight the potential for early-age cracking if these material combinations were implemented in the field.

#### *6.4.2.4 Influence of Latex on Isothermal Calorimetry at 38°C*

The combinations of these materials were investigated under 38°C isothermal testing. The results of the hydration kinetics of are presented in Figure 124 and Figure 125.

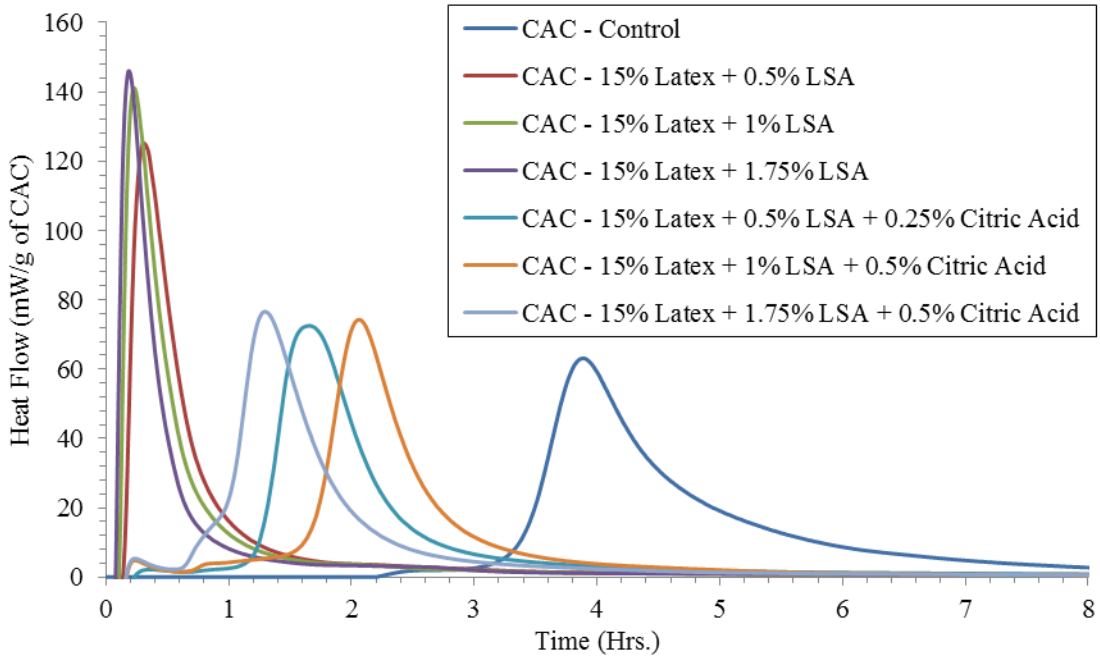


Figure 124: Heat flow of CAC with latex hydrated at 20°C with varying LSA and citric acid

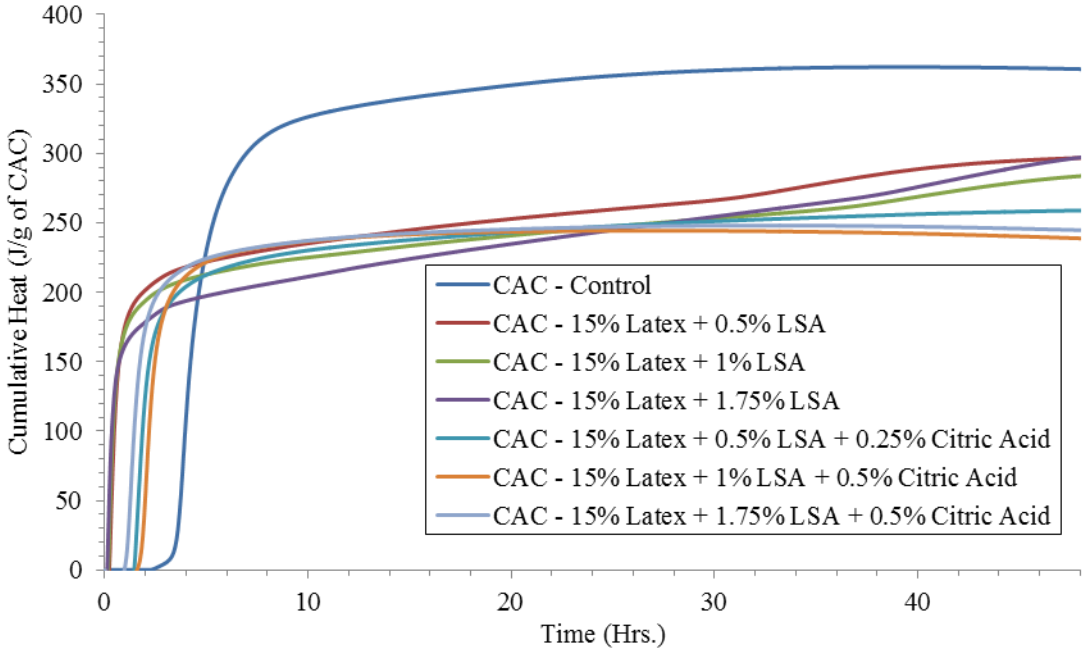


Figure 125: Cumulative heat release of CAC with latex hydrated at 20°C with varying LSA and citric acid

From Figure 124, clear influences of the LSA and citric acid on the hydration kinetics were observed. A decrease in the time of the peak heat flow was observed with the increasing addition of the LSA admixture with and without the addition of the citric acid. In Figure 125, a drastic decrease in the cumulative heat release was observed under the 38°C testing conditions. This reduction in the cumulative heat release was not observed at 20°C.

### *6.4.2.5 Influence of Latex on Chemical Shrinkage at 38°C*

The results of the chemical shrinkage in x-y format and bar graph format are shown in Figure 126 and Figure 127, respectively.

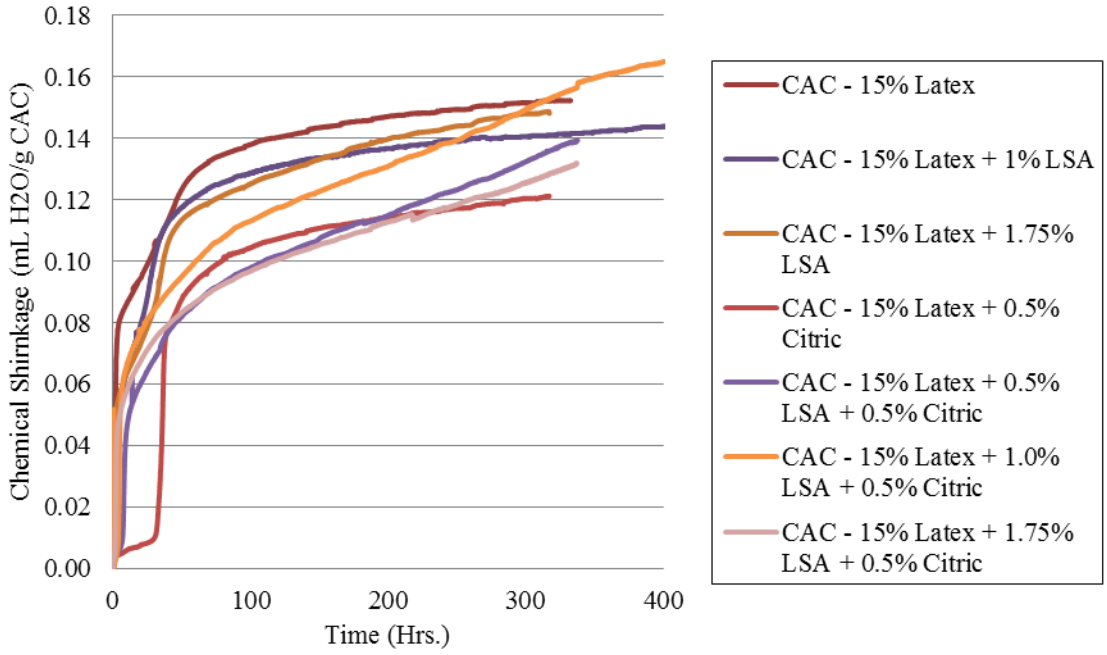


Figure 126: Chemical shrinkage of CAC with latex hydrated at 20°C with varying LSA and citric acid

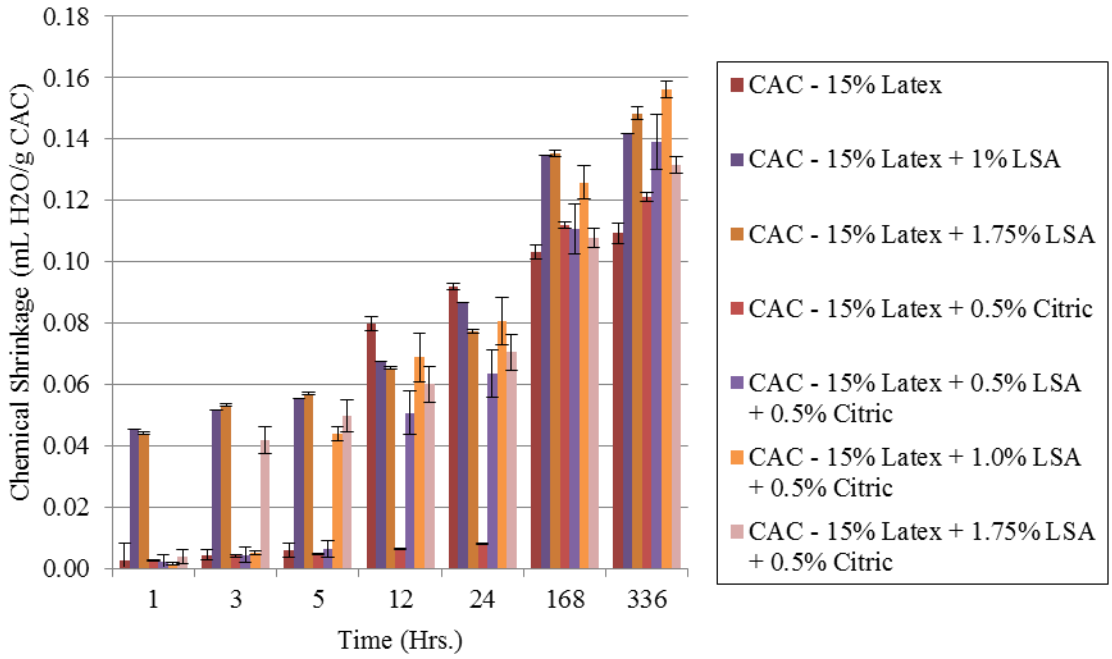


Figure 127: Chemical shrinkage with standard deviation of CAC with latex hydrated at 38°C with varying LSA and citric acid

In Figure 126, clear trends in the data were still observed where the mixtures containing citric acid clearly experienced steep secondary ascents in the total chemical shrinkage. The mixtures without the citric acid had the secondary ascent after the initial ascent that resembled the results from earlier chemical shrinkage testing at 38°C of the other CAC based-systems. The error bars in Figure 127 showed larger than normal variations due to the bleeding of the latex admixture. The chemical shrinkage was plotted as a function of the cumulative heat release in Figure 128.

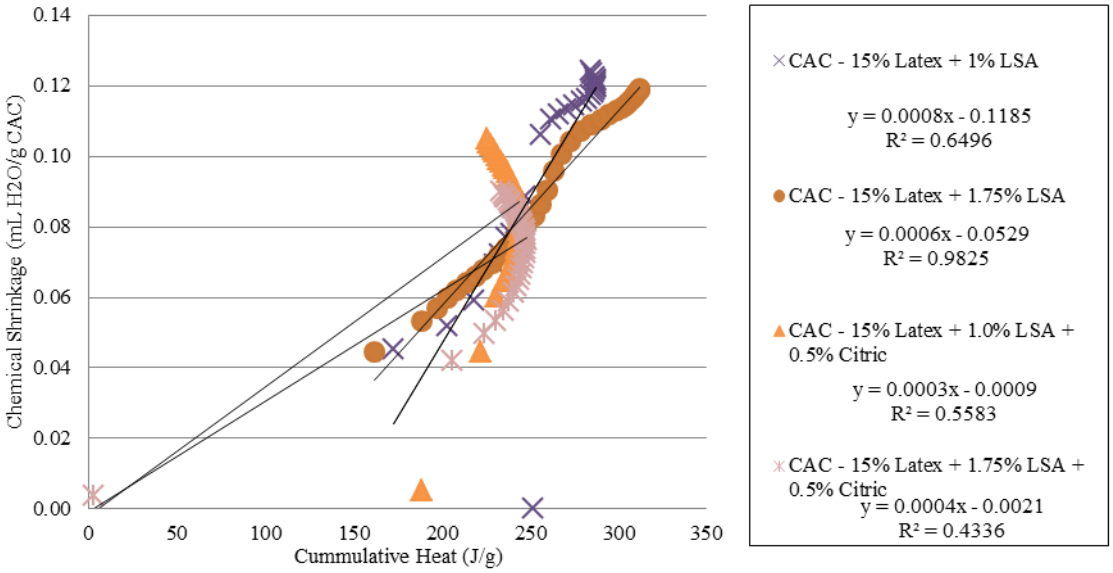


Figure 128: Chemical shrinkage as a function of CAC with latex hydrated at 20°C with varying LSA and citric acid

From Figure 128, poor correlation coefficients were established with the mixtures containing latex, LSA, and citric acid. From the linear best-fit lines not much information can be obtained about the rates of the reaction and ultimate hydration properties.

#### *6.4.2.6 Influence of Latex on Autogenous Deformation at 38°C*

The results of autogenous shrinkage testing of CAC with the addition of latex, citric acid, and LSA are presented in Figure 129.

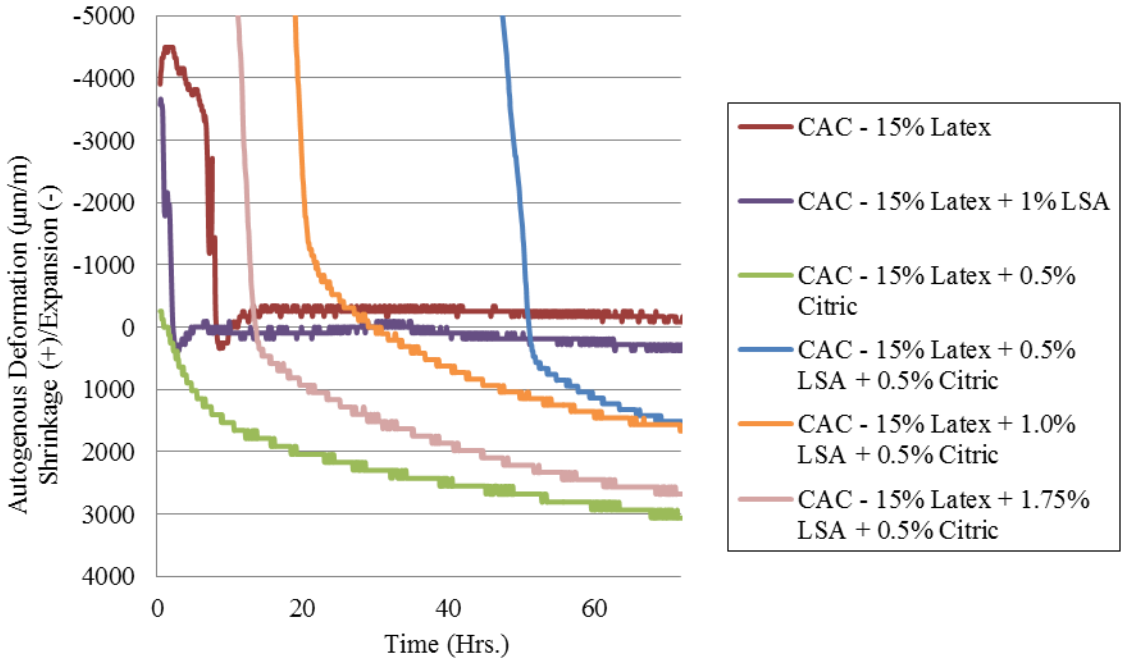


Figure 129: Autogenous deformation of CAC with latex with varying dosages of LSA and citric acid at 38°C

In Figure 129, a large amount of autogenous shrinkage for the mixtures containing latex, citric acid, and LSA at 38°C isothermal testing was shown. These were the first mixtures tested from the CAC based-systems in this dissertation where obvious amounts of autogenous shrinkage were observed at 38°C. This information was relevant for understanding the performance of the large scale testing completed in Chapter 7.

### 6.4.3 Summary

This section investigated the addition of citric acid, latex, and LSA combination to plain CAC. These materials were investigated to provide an understanding of the performance of the same material combination used in the large-scale field trial experiments at UT Austin, described in Chapter 7. The investigations showed:

- Citric acid to be a powerful retarding agent on plain CAC hydration.

- Combinations of LSA and citric acid had similar hydration kinetics to those of plain CAC, noted by similar cumulative heat release.
- Combinations of latex, citric acid, and LSA had substantial amounts of chemical shrinkage, which was increased due to a secondary ascent in the shrinkage curves.
- The most substantial observation was the significant amounts of autogenous shrinkage observed at 38°C isothermal conditions for the mixtures containing LSA, citric acid, and latex. This was an important observation that is valuable to the explanation of field behavior presented in Chapter 7.

## 6.5 RESULTS

Results of over 750 specimens from various experiments were presented in this chapter and in Appendices C, D, and E. This section efficiently summarizes some of the data in a manner that gives the most meaning. The results from hydration and early-age volume deformation are summarized in the following sub-sections.

### 6.5.1 Hydration

Countless variations of SCMs and chemical admixtures were investigated in isothermal calorimetry. The chapter presented the results of the individual influence of each of these addition and the combined effects. The isothermal calorimeter built and calibrated specifically for CAC, described in Chapter 4, was used to characterize the effects these materials have on the hydration kinetics and their potential influence on mechanical properties. These results were also coupled with the results of the automated image analysis recording of chemical shrinkage.

This chapter summarized the results of over 250 chemical shrinkage studies to characterize the influence of the addition of SCMs and chemical admixtures on the early-

age hydration behavior. Figure 130 summarizes the ultimate, 14 day, chemical shrinkage for the control mixtures for various CAC based-systems.

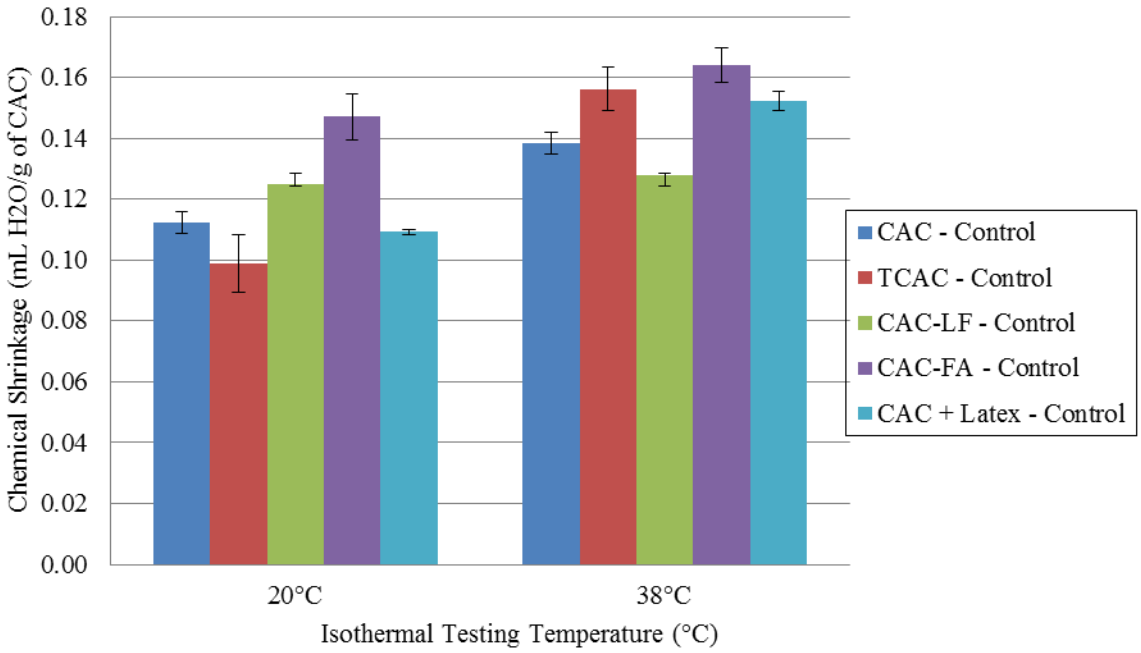


Figure 130: 14 Day chemical shrinkage of CAC control mixtures with various SCMs hydrated at 20°C and 38°C

The 14 day chemical shrinkage values for 4 different CAC based-systems and one latex modified CAC based-system with the standard deviations of each measurement is shown in Figure 130. Overall, an increase in chemical shrinkage was observed from the testing at 38°C compared to the testing at 20°C for all mixtures.

At 20°C, the CAC-LF and CAC-FA mixtures had more chemical shrinkage, 0.125 mL $H_2O$/g and 0.147 mL $H_2O$/g, respectively, than the plain CAC mixture with 0.112 mL $H_2O$/g. These mixtures had 11% and 30% more shrinkage than the plain CAC, which reflected the replacement amounts of 20% and 30%. The TCAC mixture and the

latex modified mixture had 0.099 mL H2O/g and 0.109 mL H2O/g shrinkage, which was less than the plain CAC mixture.

The chemical shrinkage at 38°C isothermal testing had significantly more shrinkage than the specimens at 20°C. The added increase in the reaction was identified as being caused by conversion, and the increase in porosity associated with it. Interestingly, the only mixture to have less chemical shrinkage than the control mixture was the CAC-LF mixtures, which was shown to have very little additional shrinkage in the secondary ascent phase noted during the chemical shrinkage, believed to be prevented by the formation of the mono-carboaluminate phase. Similar to the 20°C testing, the CAC-FA mixture had the most chemical shrinkage at 38°C with a 20% increase over the plain CAC mixture.

For the 20°C isothermal testing, the chemical shrinkage is plotted as a function of the cumulative heat release in Figure 131.

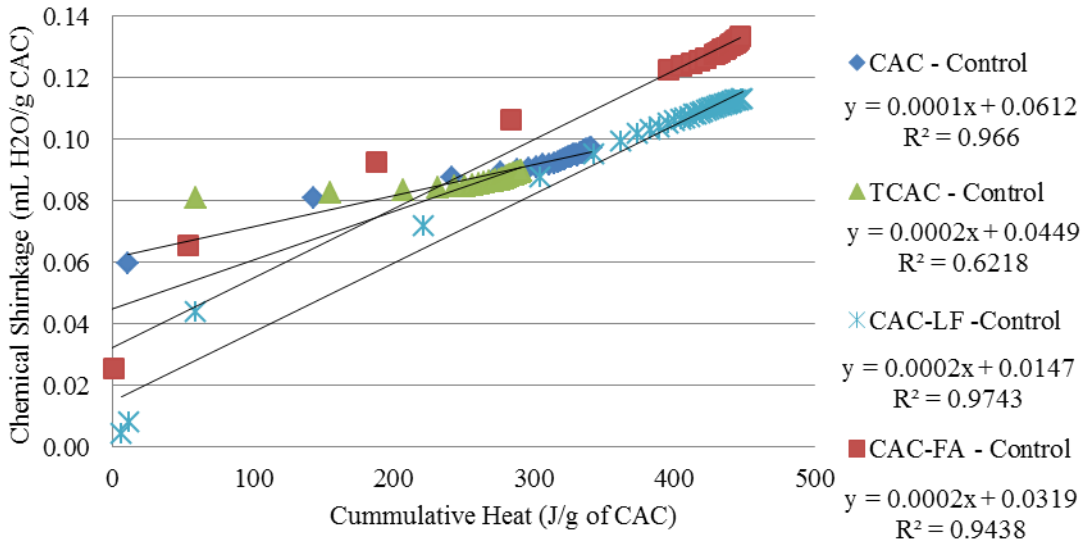


Figure 131: Chemical shrinkage as a function of CAC control mixtures with various SCMs hydrated at 20°C

In Figure 131, the rates of reaction of the four different CAC based-systems at 20°C are shown. From the slopes of the lines, an approximation of the rate of reaction can be made compared to each mixture across a uniform sample of readings for the first three days. All mixtures had a strong correlation coefficient that illustrates a good fit. The mixtures with SCMs clearly had a faster reaction than the plain CAC system. From the graph, it was possible to compare the total cumulative heat release of the different mixtures. The TCAC and plain CAC mixtures clearly had lower cumulative heats than the CAC-LF and CAC-FA mixtures. The chemical shrinkage of these mixtures is plotted as a function of the cumulative heat for the 38°C testing in Figure 132.

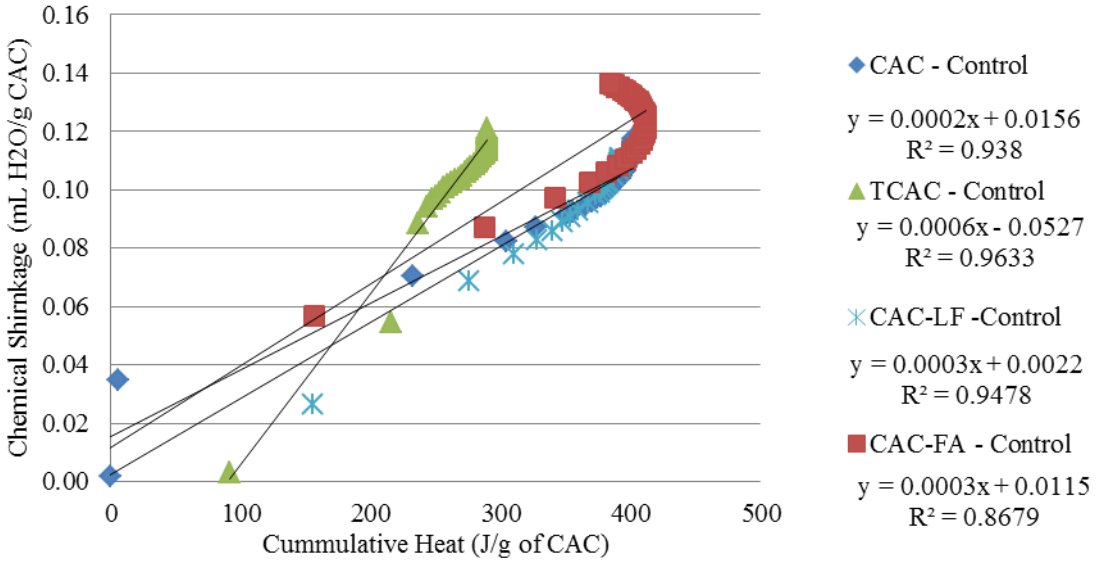


Figure 132: Chemical shrinkage as a function of CAC control mixtures with various SCMs hydrated at 38°C

In Figure 132, distinct differences in the 38°C plot are evident compared to those at 20°C. The increased slope of all mixtures quantifies the increased rate of reaction. Distinct increases in chemical shrinkage from 1-3 days of testing illustrate the conversion of the samples.

### 6.5.2 Early-age Volume Deformation

The results of the autogenous deformation of the control mixtures for 4 CAC based-systems and one latex modified mixture are presented in Figure 133.

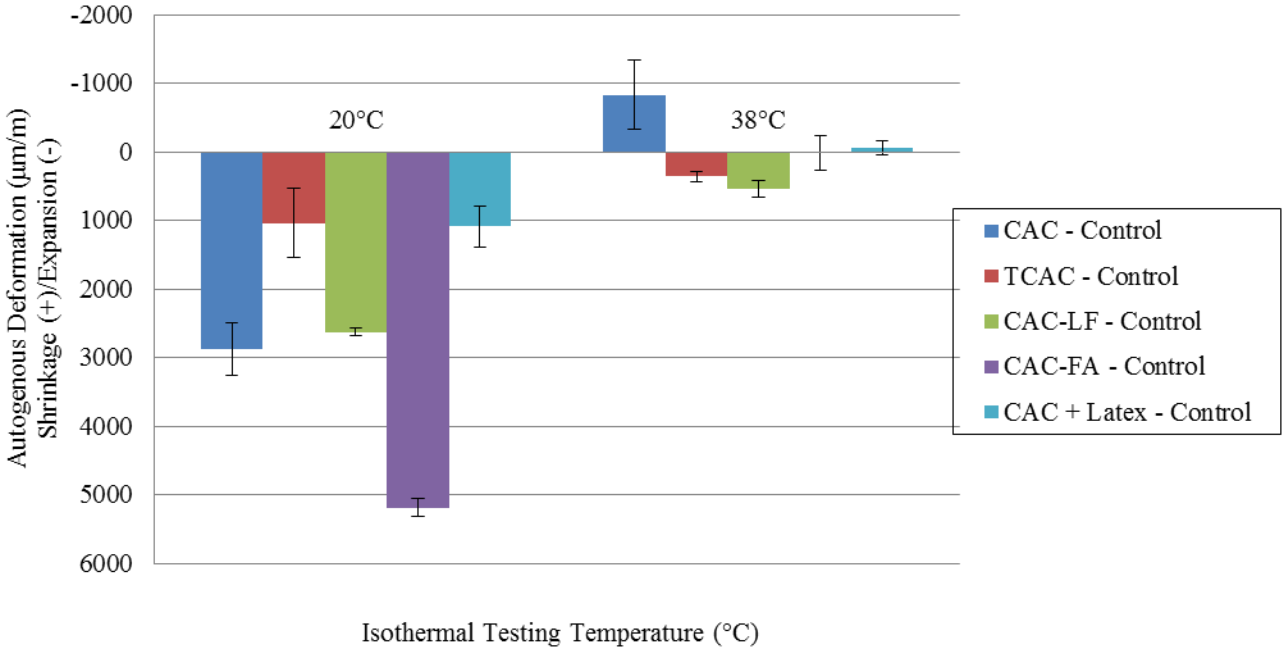


Figure 133: Autogenous deformation of CAC control mixtures with various SCMs and latex hydrated at 20°C and 38°C

In Figure 133, the influences of SCMs and latex modifier on CAC early-age autogenous deformation are presented. The error bars represent the standard deviation of the average of the final ten measurements at 72 hours of testing. At 20°C, early-age autogenous shrinkage was observed for all five mixtures. The CAC-FA mixture had 5200 µm/m, significantly more shrinkage than all others. At 38°C, minimal amounts of shrinkage were observed in the CAC-LF and CAC-FA mixtures. The plain CAC and the CAC with latex had autogenous expansion at the early-ages.

The most significant finding of the material combinations investigated for autogenous deformation, not presented in Figure 133, was the large amounts of

autogenous shrinkage observed by the mixtures containing CAC, LSA, and citric acid at 38°C. From all observations of all the mixtures investigated, this level of expansion noted at 38°C was not observed with any of them. These material combinations were implemented in a large-scale field trail at UT Austin, described in chapter 7, and was a significant contribution to the comprehension of the macroscopic behavior.

The addition of SCMs and latex modifiers were added to CAC to attempt to improve the performance of the plain CAC system. Different advantages and disadvantages of these additions were highlighted in this chapter. Summaries at the end of each section highlight the individual performance of the additions and the supplementary addition of chemical admixtures were presented. This testing aimed to provide a database of results that could be used to link observations in the laboratory to those in the field. The aim is to prevent the implementation of CAC based-materials from having unknown hydration and shrinkage behavior that may jeopardize the long-term performance.

# Chapter 7: Large Scale Field Investigations of Rapid Repair Materials

This chapter summarizes the large-scale field condition surveys of existing rapid repaired roadways, in-situ placement of field rapid repair cements and a large-scale laboratory study. Beyond the limited results presented in Chapter 2, there is a dearth of technical information available discussing specifically the long-term performance of CAC and other rapid hardening cementitious materials (Concrete Society, 1997). The aim of this chapter is to:

- Provide technical background on the applications of rapid hardening cementitious materials
- Present a brief review of bonded overlays and explain why rapid hardening cements are useful for these applications
- Share condition surveys on different field sites for CAC overlays in Chicago, Illinois, USA
- Summarize a field repair from Sunset Beach, North Carolina, USA
- Use the existing information to develop a large scale bonded overlay repair in Austin, Texas, USA
- Present results from laboratory studies and field monitoring of the repair
- Correlate performance of laboratory mixtures to behavior identified in the large-scale study

This chapter was motivated by scientific interest in linking laboratory performance to field performance of rapid hardening materials and from industry-driven demand. This chapter would not be possible without the motivation from industrial sponsor and colleagues including Modified Concrete, Henry Frerk Sons, and Kerneos Aluminates Technologies. This multi-company research was motivated by a demand for

new reliable rapid hardening cements. Due to the demand by industry and the aim of this dissertation this chapter contains a breadth of technical information on bonded overlay condition surveys and actual live repairs that is generally lacking in literature.

## 7.1 Introduction and Background

In 2009, the American Society of Civil Engineers (ASCE) issued a "D-" or a poor evaluation of America's roadways (ASCE, 2009). With an aging infrastructure and limited funding for repair and maintenance, the need exists for the development and placement of durable repair materials on roads and bridges. The use of rapid hardening cements has gained popularity to minimize the impact on America's congested roadways. This chapter provides background on the repair of concrete flatwork, specifically the repairs of roadway and bridge deck driving surfaces through the use of concrete bonded overlays.

Bonded concrete overlays are used to restore structural capacity and improve deteriorated concrete surfaces when the existing "core" concrete is in good structural condition. Bonded concrete overlays provide a cost effective way of extending the service life of existing pavements, often extending it for 30 years or more (McCullough B. F., 1995). Using concrete overlays are cost effective solutions for the maintenance and rehabilitation of existing pavements. These overlays can be constructed quickly and easily because: the existing concrete does not need to be removed, preoverlay repairs are not necessary, concrete overlays can be placed using normal concrete placement techniques, and accelerated construction practices can be used. Bonded concrete overlays provide a sustainable technique for improving the longevity of infrastructure (Harrington, 2008).

Overlays are used to reduce the penetration of water and chloride ions and to improve the drainage, skid resistance, and surface appearance of an existing roadway. In order for overlays to perform well they must be done with proper preparation techniques, material properties, bond strength, surface characteristics, and protection of the base slab.

### 7.1.1 Construction Techniques

Bonded concrete overlays are placed over an existing core concrete whose surface has been roughened (typically by mechanical means) to allow for the two slabs to bond and structurally act as one unit. This bond between the two sections of concrete usually determines success or failure of the rehabilitation (Delatte, 1997). Common techniques for preparing the surface for the overlay are shotblasting, sandblasting, cold milling, and hydro-demolition. Shotblasting is a technique that scarifies the top matrix without damaging the coarse aggregate with compressed air blasts of tiny steel balls (shot). Sandblasting is similar to shotblasting, but instead of shot, sand particles are used. Cold milling is the most widespread method for removing large areas of concrete by removing the top substrate with a rotating mandrel that chips away at the surface. Hydro-demolition is removes damaged or deteriorated concrete through the use of a high pressure water stream. These techniques may be combined to remove patches of severe deterioration and remove all weak or loose concrete prior to placement of the overlay. After scarifying the top surface, extremely thorough surface cleaning is done. This is to remove all dust and debris that may act as bond breakers at the interface of the two concrete layers (Lenz, 2011).

### 7.1.2 Materials

A variety of cementitious materials and chemical admixtures have been used to cast bonded concrete overlays. Typical mixture proportions for different cementitious systems for bonded overlays are shown in Table 25.

Table 25: Typical bonded overlay concrete mixture proportions (Sprinkel, 2008)

| Mixture | LMC | Silica Fume | Fly Ash | Slag | LMC-HE | LMC-VE |
|---|---|---|---|---|---|---|
| Type I/II cement (lb/yd$^3$) | 658 | 658 | 526 | 395 | 815 | 658 |
| Type cement | I/II | I/II | I/II | I/II | III | Rapid-set |
| Silica fume (lb/yd$^3$) | — | 46 | 33 | 33 | — | — |
| Fly ash (lb/yd$^3$) | — | — | 99 | — | — | — |
| Slag (lb/yd$^3$) | — | — | — | 230 | — | — |
| Fine aggregates (lb/yd$^3$) | 1552 | 1269 | 1351 | 1369 | 1402 | 1552 |
| Coarse aggregates (lb/yd$^3$) | 1187 | 1516 | 1510 | 1510 | 1142 | 1187 |
| Water (lb/yd$^3$) | 146 | 282 | 254 | 254 | 164 | 146 |
| Air (%) | 5 | 7 | 7 | 7 | 5 | 5 |
| Admixtures | Latex | HRWR | HRWR | HRWR | Latex | Latex |

Typically, these mixtures are designed to have low permeability and provide good bond to the existing concrete base slab. Mixtures often used include: PC with 15% styrene-butadiene latex by weight of cement (referred to as latex modified concrete (LMC)), low w/c concrete mixtures with HRWRs, and PC concrete mixtures containing SCMs such as silica fume, fly ash, and slag.

When high early strength (HE) is needed to open a repair to traffic within 24 hours of placing a repair Type III PC can be used. Repairs that require the least minimal interruption to traffic can have a repaired section open to traffic after only three hours of curing. These repairs are call very-high early strength or (VE) and often used calcium sulfoaluminate (CSA) cements (Sprinkel, 2008). This chapter discusses in much more detail different material combinations that can be used for VE type mixtures.

For a bonded overlay to be successful, it is imperative that the aggregates should be compatible with those of the existing pavement. Generally, the rule of thumb for the

maximum aggregate size is one-third the overlay thickness, but other rules exist where it is not recommended to use an aggregate greater than No. 8 sieve. These aggregate should meet the requirements of ASTM C 33 (2007). These aggregates should have similar modulus of elasticity and coefficients of thermal expansion (CTE) as those used in the existing base slab. However, having lower moduli and CTE lower the stresses at the interface and minimize the potential for cracking (Sprinkel, 2008) and (Lenz, 2011).

### 7.1.3 Shrinkage

A crucial piece to the long-term success of a concrete overlay is related to volume change, particularly shrinkage. Cracking in these bonded overlays is often caused by the combination of plastic, autogenous, and drying shrinkage. Limits are placed on overlay materials that require them to meet a maximum shrinkage requirement in order to prevent cracking. Often times these values are dictated by a limit of 0.04% maximum shrinkage limit for combined shrinkage mechanisms (Lenz, 2011). The use of Type K (expansive cement additive) and CSA cements is beneficial due to the early-age expansive properties. In the field, the expansive cements initially place concrete slabs in a compressive state that attempt to offset the tensile forces of the shrinkage mechanisms.

### 7.1.4 Summary

Bonded concrete overlays are an economical technique for extending the service life of bridges and pavements. This section provided a general overview to bonded concrete overlays and was aimed to provide the reader with a understanding of the different techniques and materials used. The use of rapid hardening cementitious materials for bonded concrete overlays allows for expedited repair; however, care must be taken to ensure a durable long-lasting repair.

## 7.2 EXISTING CAC FIELD REPAIRS

Beyond the studies published in the 1997 Concrete Society Report, little information exists on the long-term field performance of CAC (Concrete Society, 1997). Beyond the studies published in the 1997 Concrete Society Report, little information exists on the long-term field performance of CAC (Concrete Society, 1997). To attempt to generate some additional field data on CAC performance, specifically related to road/bridge repair, visual inspections of various CAC concrete repairs were performed on May 12 and 13, 2009.

Several different sites were evaluated in the metropolitan Chicago, Illinois, USA area. All the sites were comprised of rapid hardening concrete cast by Henry Frerk Sons, a local mobile concrete repair company. Frerk began using CAC for rapid repairs in 2006 because they were looking for alternatives to CSA cements. The company was having difficulty regulating the setting times with CSA and was interested in CAC for a more controlled setting time under all weather conditions. Henry Frerk Sons has an open contract with the city of Chicago to repair potholes and other immediate repairs in the city. Every day, they receive a communication from the city on locations where repairs need to be made. The trucks deploy to these different locations and work with other contractors to remove the old concrete and have the new materials placed and open to traffic with minimal interruptions.

### 7.2.1 Full-depth CAC Repair

CAC was used to place a full-depth CAC repair on a major arterial road as shown in Figure 134.

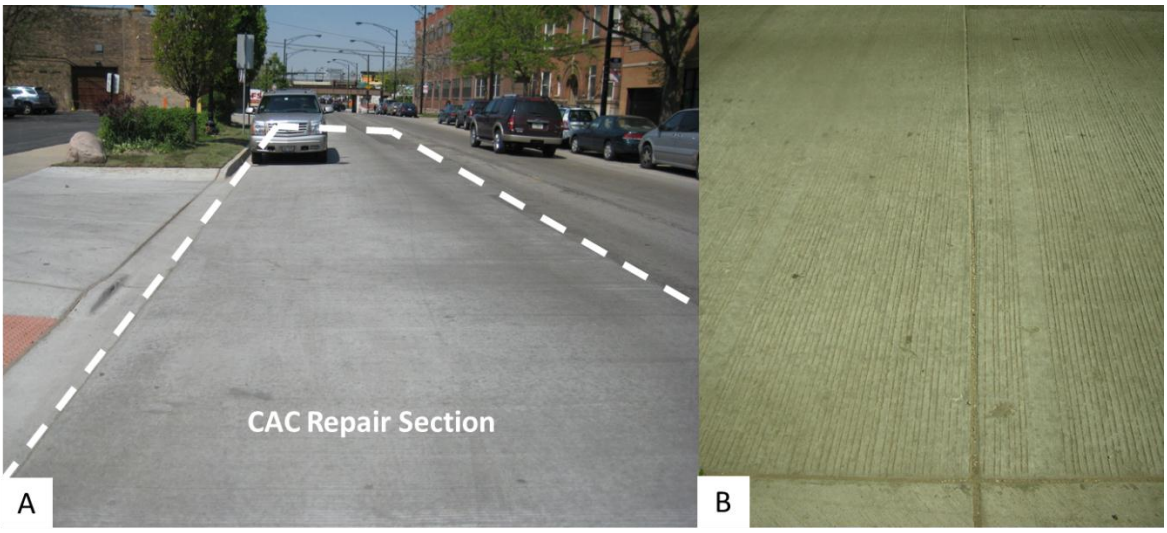


Figure 134: Full-depth CAC repair in downtown Chicago

The full-depth repair, shown in

Figure 134a, was located near the corner of Hermitage Avenue and Montrose Avenue on the northside of Chicago, IL. This was a full-depth 0.22 m (9 in.) repair that was approximately 30 x 4.5 m (100 x 15 ft.). This roadway serves as a major thoroughfare to Wrigley Field, a major league baseball stadium. An emergency repair of the roadway was needed during the baseball season due to the rupture of a water main underneath the roadway. A timely repair was necessary to minimize the impact on traffic to and from the stadium. The slab was cast using CAC with 1% LSA accelerator. No curing was performed on the repair. The site visit occurred approximately 3 years after placement and no signs of cracking or deterioration were evident in this repair. The repair was placed with control joints at 15 ft. intervals and a tined surface as shown in Figure 134b.

### 7.2.2 Bonded Concrete Overlay

Another repair that was investigated was the emergency entrance ramp to the Children's Memorial Hospital of Chicago. Figure 135 shows a few images of the entrance ramp.

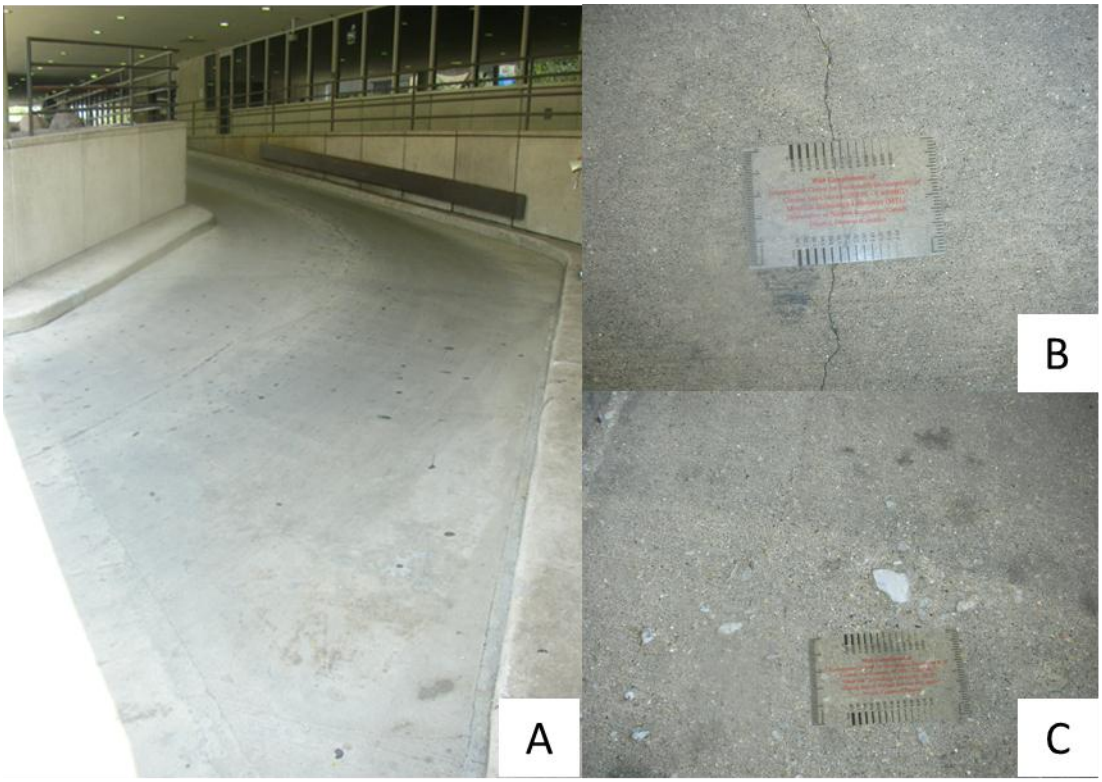


Figure 135: a) Emergency entrance ramp to Children's Memorial Hospital, b) cracking, c) scaling

Being the only entrance to the hospital for emergency vehicles, this ramp could not be replaced using ordinary cementitious materials. The ramp could only be closed for a very short window of time and needed to be re-opened as quickly as possible. CAC with 1% LSA accelerator was used to cast a 100 mm (4 in.) replacement slab over the existing PC concrete. The site visit occurred approximately three years after placement.

Cracking was seen extending out from the radial curves in the geometry. There were no control joints placed in the topping slap to regulate the cracking locations. In addition to cracking, popouts and scaling were seen on the ramp and the entrance to the building. This was caused by the heavy salt and deicing methods used to prevent accidents from occurring on the steep entrance ramp.

### 7.2.3 Interstate 290: Full-depth Repair

A full-depth CAC repair was performed in 2007 on Interstate 290 in downtown Chicago, IL. The repair section can be seen in Figure 136.

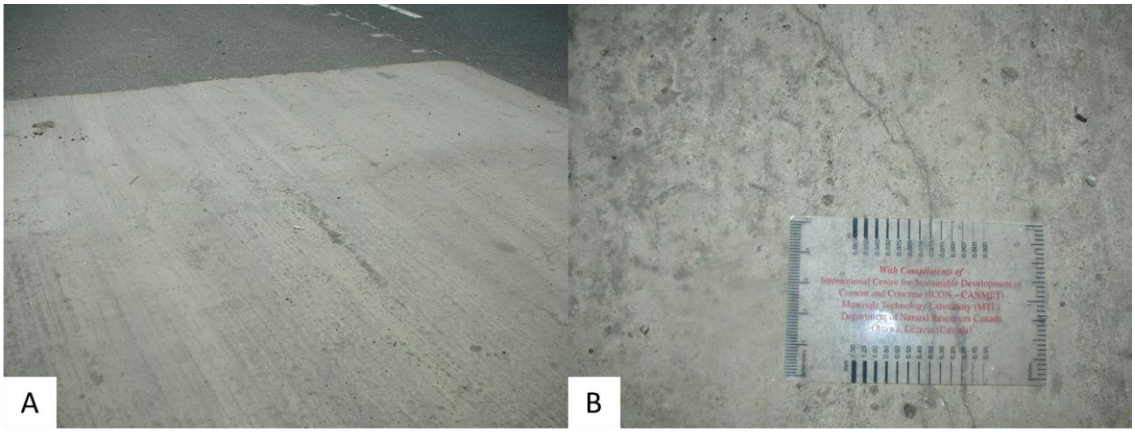


Figure 136: a) Full-depth CAC repair on Interstate 290 in downtown Chicago, IL, b) cracking

CAC with 1% LSA was used to construct this full-depth repair on a major interstate in downtown Chicago. The existing roadway section was removed due to the rupture of a water main beneath the shoulder of the highway. The repair section was approximately 300 mm (12 in.) deep with a tined driving surface. Slight cracking was noticed in the surface of the repair, however no other signs of deterioration were observed and the repair appeared to be in good condition.

### 7.2.4 Bridge Thin-bonded Concrete Overlay

A thin-bonded latex modified CAC concrete overlay was used to repair a private concrete bridge to the entrance of a water treatment plant near Chicago, Illinois. Figure 137 shows the bridge with the repaired surface.

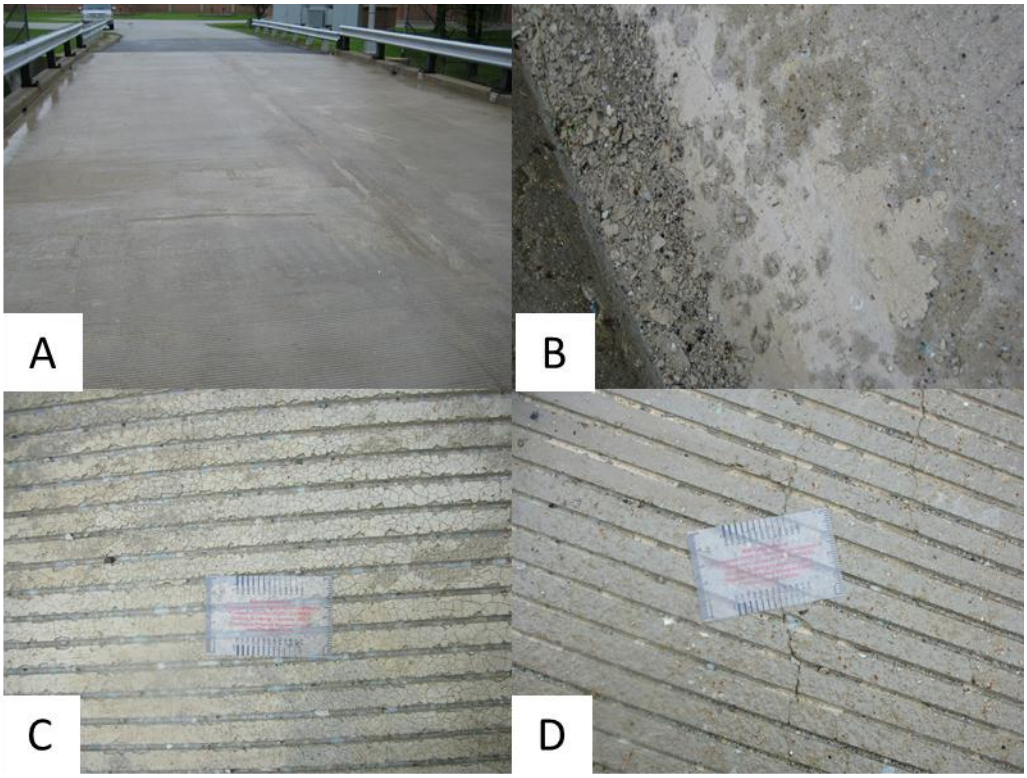


Figure 137: a) Latex modified CAC bridge deck, b) surface scaling, c) crazing, and d) cracking

This thin-bonded latex modified CAC bridge deck is the first one known to exist in service in the United States. Frerk Sons prepared this material combination based of previous experience with latex modified CSA. They used mixture proportions with 15% latex and 1% LSA. The bridge had only experienced one full winter prior to the site visit. A heavily tined surface was used to finish the bridge. Figure 70b illustrates the heavy

amount of salt scaling for the newly repaired bridge after only one full winter. Figure 70c showed the crazing of the surface, possibly due to excessive bleeding caused by extra latex in the mixture or other unknown problems. Figure 70d illustrates the cracking seen throughout the bridge deck surface. This newly placed repair showed many signs of premature deterioration that may be a cause for concern the future of the bridge. With very little known about the exact mixture proportions it was difficult to pinpoint the exact cause of distress. However, more research and continued monitoring is needed at this site. It is not clear how the addition of latex to CAC affects strength development, microstructure or durability.

### 7.2.5 Partial Depth Bridge Deck Repair

In addition to evaluating existing repairs, the research team was able to monitor the live repair of a bridge deck on the Roosevelt Bridge in downtown Chicago. Pictures of the repair placement and preparation are shown in Figure 138.

Figure 138: Repair of the Roosevelt Bridge in downtown Chicago, IL

CAC was used to repair a small 0.9 x 0.9 m (3 x 3 ft.) section on the bridge deck. The existing concrete was sawn cut approximately 76 mm (3 in.) deep then removed with a jackhammer. The section was cleaned with a pressure washer. Welded wire mesh was

placed in the repair section and the repair material was mixed using a volumetric mix truck. The mixture had good flow and was rough finished with a lumber screed and final finished with hand trowels. The surface was tinned and the bridge was opened to traffic approximately three hours after placement.

### 7.2.6 Summary

These examples were aimed to provide understanding of the demands of rapid repair materials as well as to provide qualitative assessments of their field condition. Little information exists in literature on the actual use of these materials and their long-term performance. In general, the CAC concrete repairs that were inspected were performing well. A few concerns with durability and cracking were highlighted from these site visits, however without knowing the exact material compositions and age of the repairs it was difficult to identify exact causes. The latex modified CAC thin-bonded overlays showed the worst signs of deterioration, most likely due to scaling.

## 7.3 CSA Bonded Overlay Repair

To fully grasp the repair strategy and techniques used to repair bridge decks for bonded overlays, the research team visited an actual rapid repair of a bridge deck. This site evaluation was essential to ensure that proper techniques would be used on a planned large-scale field trial at UT Austin, presented later in this chapter. From the site visit, the research team aimed to:

- Grasp strategies for preparing bridge deck surface for overlays.
- Understand the strategies used in the field for placement and curing of rapid hardening cementitious materials.
- Fully document techniques for rapid repair of infrastructure.

### 7.3.1 Project Background

The research team traveled to Sunset Beach, North Carolina to monitor the resurfacing of a causeway bridge, which connected costal barrier islands to the mainland. A thin-bonded latex modified CSA cement was selected by the contractor for use. An overview of the site and a photograph of the bridge are shown in Figure 139 and Figure 140, respectively.

Figure 139: Site location

Figure 140: Sunset Beach bridge

The structure being repaired was a two lane prestressed concrete bridge with a reinforced concrete bridge deck cast on stay-in-place corrugated metal formwork. This bridge was the only connection between the barrier island and the mainland for 20 miles. The bridge was not capable of being closed for extended periods of time due to the impact on commuters and in case emergency vehicles needed to get on or off of the island. Due to these limitations, the North Carolina Department of Transportation (NCDOT) decided to use a nighttime repair strategy that would only close one traffic lane and facilitate the use of rapid hardening cementitious materials.

The repair plan was to close one lane at nighttime and remove and replace small sections of concrete each night. With only one lane closed, cars could cross safely with proper traffic control. The use of rapid hardening cements would allow for section of concrete to be repaired during the night and allow both lanes of traffic to be opened in the morning before the commuter rush-hour.

One lane of the bridge was to be closed at 7:00 PM and re-opened by 6:00 AM the next morning. If the bridge was not to be re-opened by 6:00 AM the contractors faced a $1500 penalty for every 15 minutes that bridge was delayed. This agreement in the contract was written to stress the timeliness of the repair and encourage the contractors to minimize disturbance to daily commuter traffic. The contractors planned to remove and place 55 m (180 ft.) each night. Before the bridge could be opened, the concrete was required to reach 20.7 MPa (3000 psi) compressive strength.

### 7.3.2 Bridge Deck Preparation and Concrete Removal

The research team monitored the construction of this overlay on September 15, 2010. This was the first night of repairs on the bridge and the first night of these teams of contractors working together. One lane of roadway was closed at 7:00 PM and

temporary traffic control lights were placed on either of the bridge to allow for cars to safely cross the bridge one direction at a time. By 8:00 PM all traffic control cones and barriers were in place and allowed for the milling of the concrete surface to begin. Figure 141 shows the milling machine used to remove the top surface of the concrete.

Figure 141: Milling of bridge deck

The first stage of concrete removal was milling of the existing concrete bridge deck. The milling machine was used to remove the top 6.4 mm (¼ in.) of the concrete surface. It took approximately 50 minutes to complete four passes that were 1.2 m (4 ft.) wide to remove the top surface. Once the top surface was milled, the hydro-demolition robot was moved into place as shown in Figure 142.

Figure 142: Setup and calibration of hydro-demolition robot

The hydro-demolition robot was driven into position on the bridge deck. The robot was connected to a large engine that pressurizes the water used remove the concrete surface. Milling the concrete surface before the hydro-demolition provided a deformed surface for the water jet to more easily remove the top layer of the concrete surface. The water was supplied from a fire hydrant that was located at the beginning of the bridge and fed to the truck with long fire hoses.

Once the machine was moved in position, an initial calibration was needed determine the proper water pressure to remove the top concrete layer. The designed

overlay was estimated to be 31-44 mm (1.25-1.75 in.). The calibration started at 9:15 PM and took approximately 45 minutes to complete. On that night, the time of the calibration took longer than normal due to being the first time working on the bridge deck and a repair that needed to be completed on the equipment.

To prevent pollution of the intercostal waterway, below the bridge, all the water from the hydro-demolition process was required to be collected. The drains of the bridge were sealed shut and a dike system was built with plastic sheeting incasing the debris from the milling process. This dike contained the water from the hydro-demolition and forced it to flow down the slope of the bridge where a large vacuum truck was waiting to collect the water and pump it off the bridge to offsite storage containers. The water would then be processed and eventually released back into the waterway.

The hydro-demolition began at 10:00 PM and took two hours to complete. Next, the hydro-demolition equipment was mobilized and moved to a staging area near the beginning of the bridge. A large vacuum truck was then used to clean the debris from the concrete surface. This truck has two large nozzles that were the width of a truck were used to vacuum the debris from the concrete surface. It took many passes for all the sand and loose concrete to be removed from the newly abraded concrete surface.

### 7.3.3 Repair Placement and Curing

The cleaning of the concrete surface took over four hours to complete. During this time, the volumetric mix trucks were loaded with aggregates and water at an offsite batch yard. Once the two trucks were loaded, a quality control and calibration of the trucks was completed. A field engineer from the NCDOT was present to verify proper procedures and appropriate mixture proportions were used.

After the trucks were calibrated and sampling was done for testing at the NCDOT's laboratory, the trucks were moved to the repair slab. A plastic sheet was laid over the cleaned surface, to prevent oil or other debris from falling into the cleaned surface. The truck was backed directly into position at the beginning of the repair area. A gas powered vibrating screed was used to provide the initial finishing of the concrete surface. The placement and finishing of the latex modified CSA overlay is shown in Figure 143.

Figure 143: Placement and finishing of repair materials

Concrete was initially cast at 4:45 AM; this was delayed from the typical starting times of placing concrete due various factors. The concrete pour was completed by 5:50 AM. Wet burlap was progressively placed on the surface 10 minutes after casting. After the entire slab was placed, plastic sheeting was laid over the surface to mitigate the amount of moisture loss due to evaporation.

The concrete was wet cured for three hours; after that time the burlap and sheeting were removed and the concrete and the bridge was opened to traffic. On this day, the

bridge was not opened until 10:00 AM and the contractors faced $24,000 in penalties due to the delay of opening the bridge to traffic. The completed section is shown in Figure 144.

Figure 144: Completed repair section

After removing the curing blankets, the slab appeared to be free of cracking and ready for driving. Follow-up communications with the contractors verified that the crews were able to improve their efficiency and meet the strict time demands set forth by the requirements of the project.

### 7.3.4 Summary

Section 7.3 documents the actual repair strategies and requirements for completing rapid repairs on bridge decks in the field. This example field trail highlighted the time demands on the concrete removal and the requirements for strength development of freshly placed concrete. This section was written to provide a thorough understanding

of procedures used in the field and provide documentation for full-scale laboratory field trials. These repair strategies were followed in the next section for the repair of laboratory created specimens at the University of Texas at Austin Pickle Research Campus.

## 7.4 UT AUSTIN BONDED CAC AND CSA REPAIR

This section summarizes the construction, evaluation, and results of the large-scale field performance of two full-scale pavements constructed at the University of Texas at Austin. The main purpose of the construction of these two full-scale test specimens was to characterize the field performance of latex modified rapid repair materials. Calcium aluminate and calcium sulfoaluminate cements were selected for comparison. This criterion was motivated by industry to allow for a side-by-side comparison of two potential materials for repair of actual structures in the field. The evaluations of the material included the resistance to early-age cracking, strength development, drying shrinkage, and long-term durability.

### 7.4.1 Introduction

To evaluate the large-scale performance of thin bonded concrete overlays at UT Austin three options for repair were evaluated. The selection criteria for the best option was based on the most realistic (field representative) concrete elements, ease of access, and lowest cost.

Figure 145 illustrates repair option no. 1 an existing on-grade concrete pavement. This option consisted of two existing on-grade reinforced concrete slabs located at the University of Texas at Austin Pickel Research Campus. These slabs were 0.25 x 3.66 x 17.68 m (0.83 x 12 x 58 ft.). The slabs were perched atop a small hill in the middle of a field, making it difficult for access by concrete mix trucks and for power as well as other

essenitals needed to conduct the experiments. Also, the slabs had large amounts of cracking and deterioration that would make the use of thin-bonded concrete overlays difficult. Due to the limited access and damage, these slabs were not selected.

Figure 145: Repair option No. 1 an existing on grade concrete pavement

Figure 146 illustrates the second option evaluated, which consisted of elevated bridge decks located behind the Concrete Durability Center at the Pickel Research Campus at the University of Texas at Austin. These bridge decks were built according to Texas Department of Transportation standards where a cast-in-place reinforced slab is placed over a prestressed concrete panel. These slabs were left-over from previous research projects. The slabs were 0.20 x 2.74 x 5.49 m (0.67 x 9 x 18 ft.). The slabs were elevated 1.22 m (4 ft.) above the ground, which would prevent the use of typical volumetric mix trucks. These slabs were not selected because of the limited access for the concrete mix trucks.

Figure 146: Repair option no. 2 existing elevated bridge decks

Figure 147 illustrates the third option evaluated for the field trial repairs at UT Austin. This option was to construct on-grade slabs that replicated slabs that would be seen in the field. These were to be built directly across from the Concrete Durability Center at the University of Texas at Austin in a large open flat field that would allow access for concrete trucks and any other equipment necessary. The site was over-grown with vegetation as shown in Figure 147. This option allowed for the construction of on-grade slabs built specifically for this project that would have a known history and known material properties. This third option was selected for the field trial, based on meeting the key technical and practical criteria described herein.

Figure 147: Repair option no. 3 develop continously reinforced slabs on grade

### 7.4.2 Base Slab Construction

Design and Site-layout

The base slabs were constructed directly across from the Concrete Durability Center in Austin, Texas, USA. The layout and design of the slabs can be seen in Figure 148.

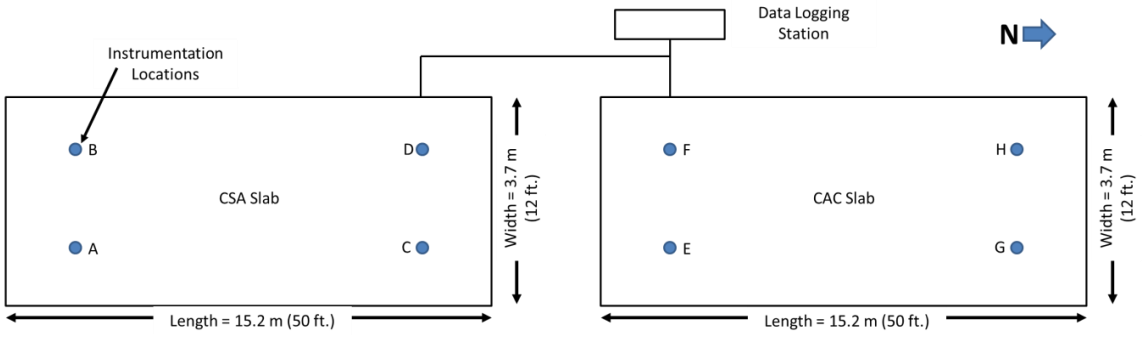


Figure 148: Site layout and elevation of on-grade slabs

In Figure 148, the slabs are identified by the type of repair cement that would be used on each. These slabs were aligned adjacent to each other to allow for the ease of

grading the site and casting the concrete. The criteria for construction of the bases slabs were designed for a typical car lane width 3.66 m (12 ft.) and have a length- to-width aspect ratio greater than 3.0. The thickness of the base slab was also required to be 3X greater thickness than the overlay that would be cast at a later date.

Grading and Sub-base

All site preparation, grading, and construction was completed by the research team. A Bobcat S130 skid-steer loader was rented to clear all vegetation and level the site. Figure 149 shows the cleared field and initial stages of leveling.

Figure 149: Initial site grading

The site was leveled and graded with 2% gradation across the width of the slab. This grade was used to match the typical crown seen in roadways to prevent the ponding of water on the surface. A walk behind sheep's foot drum roller was used to compact the ground after the initial grading.

Formwork and steel reinforcement

After the ground preparation was complete, the next step was to complete final grading and construction of the formwork. Typical no. 2 yellow pine 50.8 x 203 mm (2 x 8 in.) wood formwork was used to form the sides of the slabs. The wood was held in place by 0.61 m (24 in.) formwork spikes driven into the ground using a 6.80 kg (15 lb.) sledge hammer and attached using formwork duplex nails. Figure 150 shows the construction of the base slab formwork.

Figure 150: Construction of the base slab formwork

The formwork was installed and checked for gradation and slope across the slab. A fine aggregate crushed stone base was compacted and placed inside of the formwork to further prepare the ground for the concrete placement. The formwork had 0.91 m (3 ft.) extension built on the far ends to allow for the vibrating screed to be used to continue to the end of the slabs.

Steel reinforcement was used to provide a rigid base slab that would mimic typical continuously reinforced concrete pavements and bridge decks. No. 5 steel reinforcement bars were used in both directions on the slab. The steel reinforcement was spaced at 152 mm (6 in.) in the transverse direction and 203 mm (8 in.) in the longitudinal direction. To ensure proper placement of the steel reinforcement each of the bars were marked with a thin white line at the appropriate spacing. Over 4000 reinforcement connections were marked and tied by the research team in temperatures exceeding 38°C as shown in Figure 151.

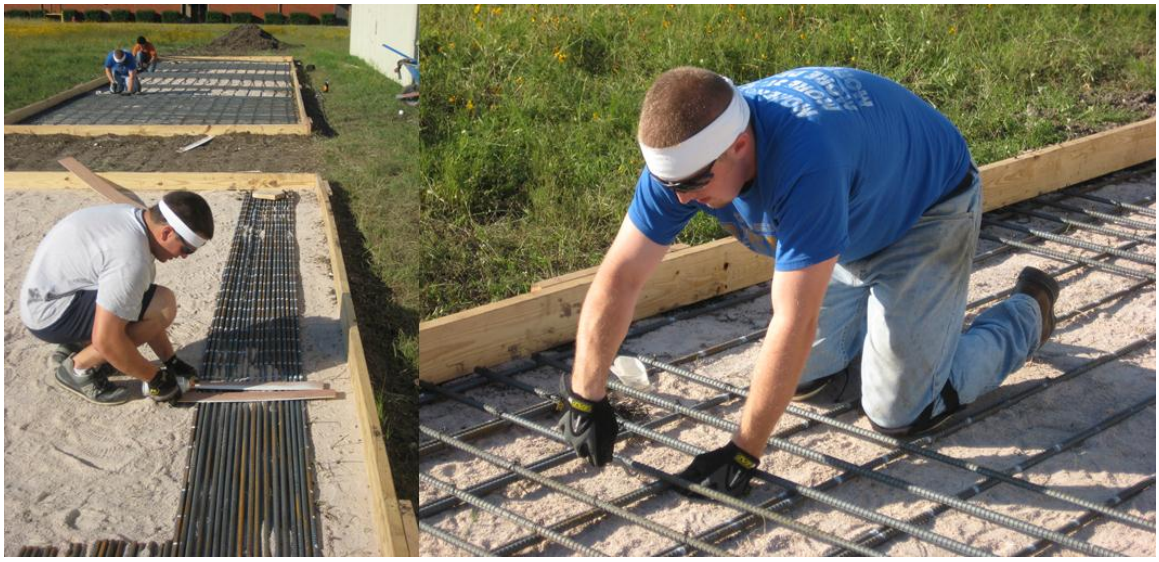

Figure 151: Students marking and placing the steel reinforcement

For the ease of tying, layout, and construction the steel reinforcement was tied on the ground and later be raised to the proper height through the use of the laboratories forklift. The steel reinforcement mat was placed approximately 102 mm (4 in.) from the edge of the slabs. The steel mat was raised by using a chain hoist to lift the mat and place on metal reinforcement chairs. The final placement and pictures of the steel mat can be seen in Figure 152.

Figure 152: Final steel reinforcement location

Casting of base slab and curing

The grading, compacting, formwork, and reinforcement placement was completed in approximately one week. Next, the research team cast the PC base slab on May 8, 2010 as shown in Figure 153.

.

Figure 153: Casting of the PC concrete base slab

Approximately 20 $m^3$ (26 $yd^3$) of portland cement concrete were cast using three ready-mix concrete trucks from Transit Mix Concrete & Materials Company. The mixtures contained a coarse river gravel from the Colorado River basin, locally dredged river sand, 25% replacement of portland cement with class F fly ash and had a 0.45 w/c. The slabs were moist cured with wet burlap sheets and plastic for 7 days after casting.

After moist curing the slab, the blankets were removed and the slab was allowed to dry for 128 days. The research team aimed to maximize the amount of time between the casting of the base slab and the overlay. This interval was to allow for the base slab

to dry and prevent differential shrinkage from occurring between the two slabs that would be cast in the future.

### 7.4.3 Surface Preparation

To prepare for the overlay of the previously cast slabs, hydro-demolition was chosen to abrade the surface. The hydro-demolition services were completed and donated by Hydro-Technologies Incorporated (Hydro-Tech). The team from hydro-tech donated two operators and one remotely controlled hydro demolition robot and one 18 wheel power house shown in Figure 154.

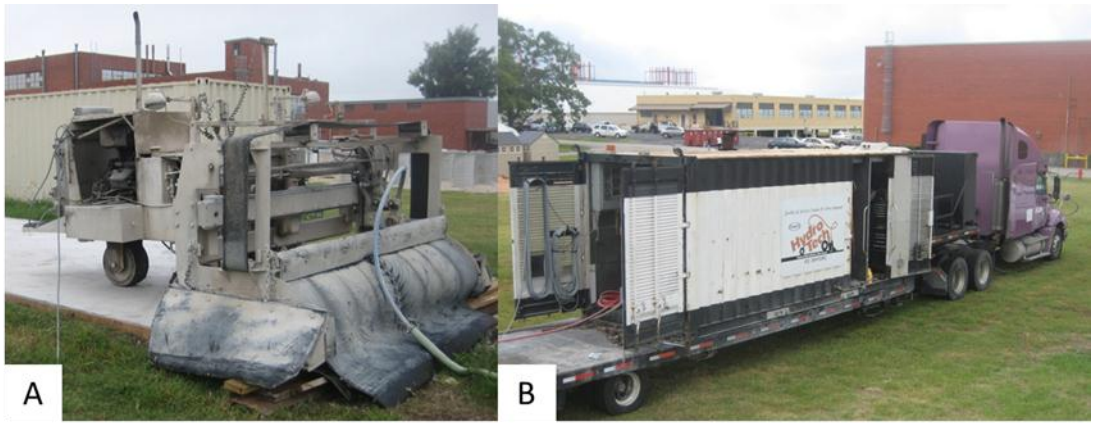


Figure 154 a) Remotely controlled hydro-demolition robot, b) water supply power house

As seen in Figure 154, the remotely controlled robot was responsible for removing the top layer of concrete. This machine had a single nozzle water hose that moves back and forth across the front of the machine to remove a 1.83 m (6 ft.) wide strip with each pass. In addition to moving across the machine, the nozzle is actuated in a diamond pattern. This allowed for the application of a water stream from multiple directions to find the weakest plane of concrete to scarify the surface. The water jet pressure was supplied from within the storage unit on the back of the transportation truck.

Figure 155 shows the hydro-demolition robot in the process of removing the concrete surface and the remaining debris.

Figure 155: Hydro-demolition robot in use scarifying the concrete surface

The hydro-demolition of the two base slabs took approximately two hours to calibrate and remove the top-layer of the concrete slabs. The hydro-demolition removed approximately 50-64 mm (2-2.5 in.) off the top of the concrete surface. The exposed coarse aggregates appeared to be in good condition with minimal signs of wear, which was essential for creating a good bond between the two concrete layers. The final concrete surface after washing using a high pressure water hose is shown in Figure 156.

Figure 156: Freshly washed concrete surface after hydro-demolition.

### 7.4.4 Overlay Formwork and Instrumentation

After casting the base slab and completing the hydro-demolition, the next stage of construction was to prepare for the overlay placement. This included the construction of the formwork and data logging station shown in Figure 157.

Figure 157: Overlay formwork and data logging station

The formwork for the overlay was 50.8 mm (2 in.) strips placed on top of the existing formwork used to build the base slab. A Campbell Scientific Protective box and solar panel were mounted on a stainless steel fence post between the two slabs. This protective unit would be used to house the data logging station.

A Campbell Scientific CR10X data logger, AM 16/32 Multiplexer, 4-120 ohm Terminal Input Modules, and battery supply were housed in the protective unit. The Campbell Scientific hardware was used to record data from the Vishay concrete embedment strain gauges. The product specifications on each of these pieces of the data logging system and wiring diagram can be found in Appendix F. The wires were run through 50.8 mm (2 in.) PVC pipe from the data logging station to a T-splitter and then to each slab. The data logging station is shown in Figure 158 and the concrete embedment strain gauges are shown in Figure 159.

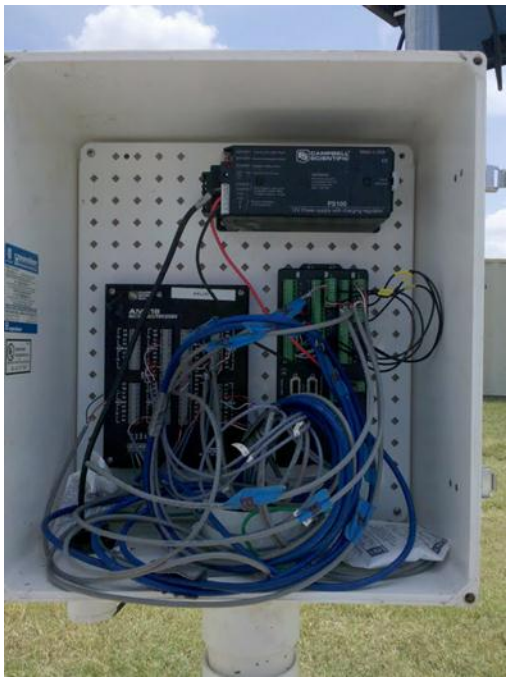

Figure 158: Data logging system

Figure 159: Concrete embedment strain gages

The concrete embedment strain gages were specifically designed for measuring the strains inside of concrete. The gages are made of polymer concrete resin to protect the gages from moisture and corrosion. The gages have a 102 mm (4 in.) gage length and are constructed with a 3.04 m (10 ft.) wire connection built into each gage. The gages

were epoxied on one end to a PVC pipe that was mounted in the base slab approximately 25.4 m (1 in.) from the surface (or near mid-depth) of where the overlay would be. To measure the temperature in the overlay Thermochron iButtons were used as shown in Figure 160.

Figure 160: Thermochron i-Button temperature sensor and data loggers

The iButtons were used to measure the time and temperature history of the concrete during the casting of the overlay and hydration. The iButtons have a built in data recording and logging device. To allow for the iButtons to be read wires were sautered to each of them and run to the edge of the slab. Two iButtons were installed at each of the points identified in the project schematic. One measured the temperature at the interface between the base slab and the new overlay and the other was suspended at the mid-depth of the overlay. They were attached to a plastic rod that was mounted into the concrete. Before the iButtons were installed on the slab, they were dipped in a two

part epoxy to prevent the ingress of moisture and corrosion of the iButtons (not shown in the figure). The specification on the Thermochron iButtons can be found in Appendix F.

Each of the slabs contained 2 concrete embedment strain gauges and 8 temperature recording iButtons. The strain gages and 4 iButtons located at the beginning of the slab were permanently mounted into the concrete surface. The four remaining iButtons on each slab would be placed on the day of casting once the concrete truck cleared their location.

A Campbell Scientific weather station was deployed near the slab to monitor the impact of the environment on the hydration and curing. The weather station was configured to record: temperature, wind speed, wind direction, rain fall, relative humidity, dew point, time, and date. A picture of the weather station is shown in Figure 161.

Figure 161: Campbell scientific weather station setup near repair slabs

### 7.4.5 CSA Overlay Placement

The placement of the two overlays was to be completed in two days in October 2010. First, the CSA slab would be cast followed by the CAC slab. A volumetric mixture truck was graciously made available by Modified Concrete for use on the pour days. This procedure was chosen for placement of the overlay to simulate real-world repair of a roadway or bridge. The truck arrived from Indianapolis, Indiana pre-charged with Rapid Set calcium sulfoaluminate based cement. A local dolomitic limestone coarse aggregate with a maximum 9.5 mm (3/8 in.) gradation was used as the coarse aggregate and sand from the Colorado River was used for the fine aggregate. The aggregates were loaded in the truck using a front end loader. The mixture design of the CSA slab is presented in Table 26.

Table 26: CSA overlay mixture design

| | lbs./yd$^3$ | kg/m$^3$ |
|---|---|---|
| Cement | 658 | 390 |
| Coarse Aggregate | 1416 | 840 |
| Fine Aggregate | 1282 | 761 |
| Water | 120 | 71 |
| Latex* | 209 | 124 |
| Citric Acid | 1.6 | 1.0 |

* Latex was added at 15% latex solids/cement weight
the latex contains 47.2% solids

The originally cast slabs were left to cure and dry for 165 days after completion of the moist curing. Prior to the casting of the slab, the base slab was thoroughly washed with a high-pressure hose the night before and covered with plastic sheets to prevent condensation and debris from gathering on the slab from the wind. The volumetric mix truck and slab preparation can be seen in Figure 162.

Figure 162: a) Slab cleaning, b) volumetric mix truck

Prior to casting the overlays, a small pour ejecting concrete into wheel barrows was done to allow for the casting of small specimens for follow-up testing (strength gain, durability, etc.). This was done in the parking lot of the Concrete Durability Center at 7:00 AM on October 20, 2010. The pour started early in the morning to prevent exposure of direct sunlight and high temperatures during hydration. This pour required 15 students to make approximately 100 specimens for compression testing and various durability tests. After all the specimens were cast and finished, they were moist cured with soaked and ringed wet burlap blankets. While the specimens were being cast and finished, the mix truck was washed the chute and auger. This was to prevent the concrete from

hardening during the 45 minutes it took to prepare everything for the slab overlay. Next, the concrete truck drove onto the slab and backed into place to prepare for casting the CSA bonded overlay as shown in Figure 163.

Figure 163: Volumetric mixture truck prior to casting

From Figure 163, it was shown that the volumetric truck was backed into place on the slab and would be driven off as the concrete was cast. The truck was driven on top of the plastic sheeting to prevent debris or oil from the truck from getting on the slab to act as a bond breaker and causing future delamination. The two sets of Thermochron iButtons placed at the beginning of the slab were removed and placed to the side. They would later be installed once the truck had cleared them. A vibrating screed was to be used to provide the initial screeding and finish on the concrete overlay. The placement of the thin-bonded concrete overlay is shown in Figure 164.

Figure 164: Placement of the latex-modified CSA overlay

The concrete was leveled through the use of a vibrating screed, operated by two members of the research team. The truck operator swung the chute back and forth keeping a consistent flow of concrete in front of the vibrating screed. The vibrating screed followed closely behind the placement of the concrete due to the short working time with this rapid hardening cement, approximately 20 mins. As the concrete was placed and began to set, the presoaked and ringed burlap sheets were placed on the surface. A plastic sheet was placed over the burlap to minimize the drying of the sheets. To mimic the placement of the rapid repair cements in the field, a three hour wet-cure

time was used. This was identical to what was done in the field at the North Carolina field trial. The slabs with the wet cure are shown in Figure 165.

Figure 165: Three hour wet-cure

The wet cure time was dictated by the placement of the last part of concrete. After three hours, the blankets were removed. A few small cracks were observed in the surface after placement of concrete. These cracks are believed to be from plastic settlement cracking due to the settling of the concrete into deeper uneven pockets of the hydro-demolished concrete surface. The small cracks are shown in Figure 166.

Figure 166: Plastic settlement cracking of the concrete surface

All the follow-up testing and results are presented in Section 7.4.6

### 7.4.6 CAC Toppling Slab Placement

After casting the CSA slab, the modified concrete mix truck was charged with CAC materials that afternoon for preparation of placement the next morning. The same coarse and fine aggregates were used to load the truck with aggregates. The CAC was loaded into the truck at Ferguson Structural Engineering Laboratory. The CAC was in super sacks containing 900 kg (2000 lbs) of cement and were loaded through the use of the overhead crane.

That afternoon trial mixtures were performed to finalize the mixture design used for use on the CAC slab. The CAC mixture was designed to use the LSA to promote the rapid strength gain, however, the open working time when these materials were combined was less than 10 minutes and would not provide enough time for the research team to place and finish the concrete. Thus, it was decided to use 0.5% citric acid to delay the hydration. A secondary liquid admixture container was built on site with the use of a fish pond pump to circulate and a 5 gallon bucket to introduce the admixture to the concrete mixture. The final mixture design is presented in Table 27.

Table 27: Final mixture design for CAC overlay

| | lbs./yd$^3$ | kg/m$^3$ |
|---|---|---|
| Cement | 658 | 390 |
| Coarse Aggregate | 1416 | 840 |
| Fine Aggregate | 1282 | 761 |
| Water | 120 | 71 |
| Latex* | 209 | 124 |
| LSA | 11.5 | 6.8 |
| Citric Acid | 3.3 | 2.0 |

* Latex was added at 15% latex solids/cement weight the latex contains 47.2% solids

The pour started at 7:00 AM on October 21, 2010. Two separate pours were completed just as the day before with the CSA slab. First, the laboratory specimens were cast, then the truck's auger and chute were cleaned and washed followed by the truck moving into position to cast the slab. The pour began at 8:23 AM there was a slight delay compared to the day prior due to the casting of more specimens. The placement, finishing, and curing of the CAC is shown in Figure 167.Figure 167: Placement of the CAC overlay

Figure 167: Placement of the CAC overlay

The casting and curing of the CAC overlay were completed identically to that of the CSA slab. However, one key observation from the fresh concrete was an excessive amount of bleeding from the slabs surface. A thick white latex film formed on the top of the slab that was not seen from in CSA slab. After three hours of moist curing the burlap blankets were removed off the slab. Small transverse cracks were observed almost immediately. These cracks were difficult to see due to the thick layer of latex covering them. The crack widths grew and cracking developed in the both the transverse and longitudinal direction as the day progressed. More data is presented in later sections on the cracking and cracking patterns.

### 7.4.7 Slab Performance

#### *7.4.7.1 Hydration/Curing Temperatures*

As stated earlier both of these rapid hardening cementitious materials are known to generate significant heat compared to PC. Each slab was equipped with eight Thermochron iButtons, four at mid-depth and four at the interface between the overlay and the base slab. The pouring direction and time when concrete contacted the iButtons is identified in Figure 168.

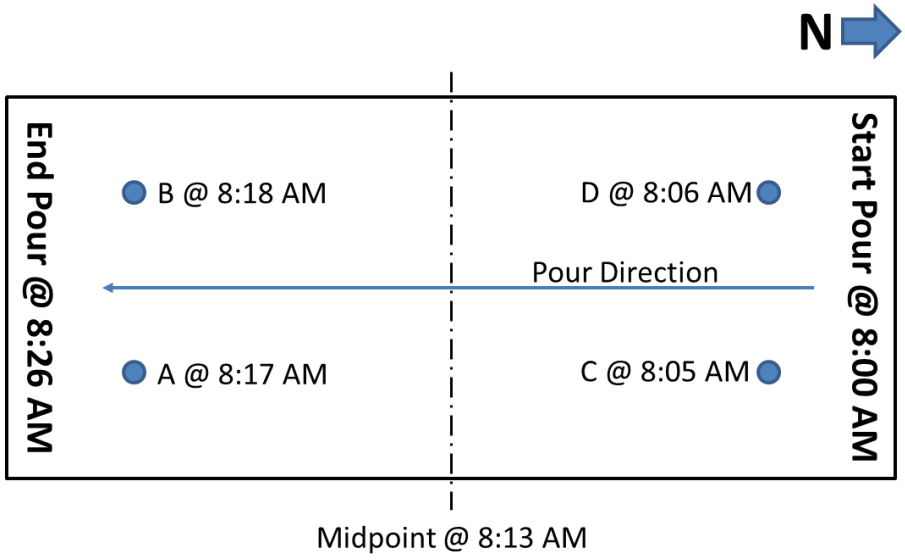


Figure 168: CSA concrete slab schematic and time of concrete pour details

The pour started at 8:00 AM on October 20, 2010 and was completed by 8:26 AM. The time when the concrete contacted the different iButtons was identified in Figure 168. This timing information was presented to highlight any difference that may have occurred from the beginning to the end. The mid-depth and interface temperatures of the CSA overlay are shown in Figure 169 and Figure 170, respectively.

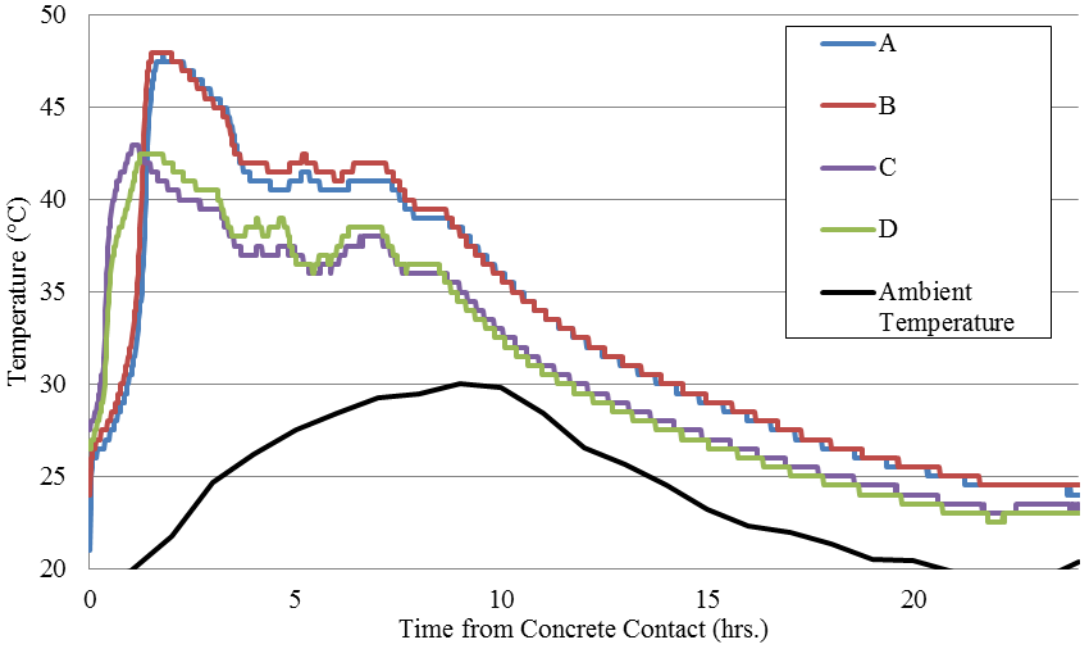


Figure 169: Mid-depth CSA 24 hour curing temperatures

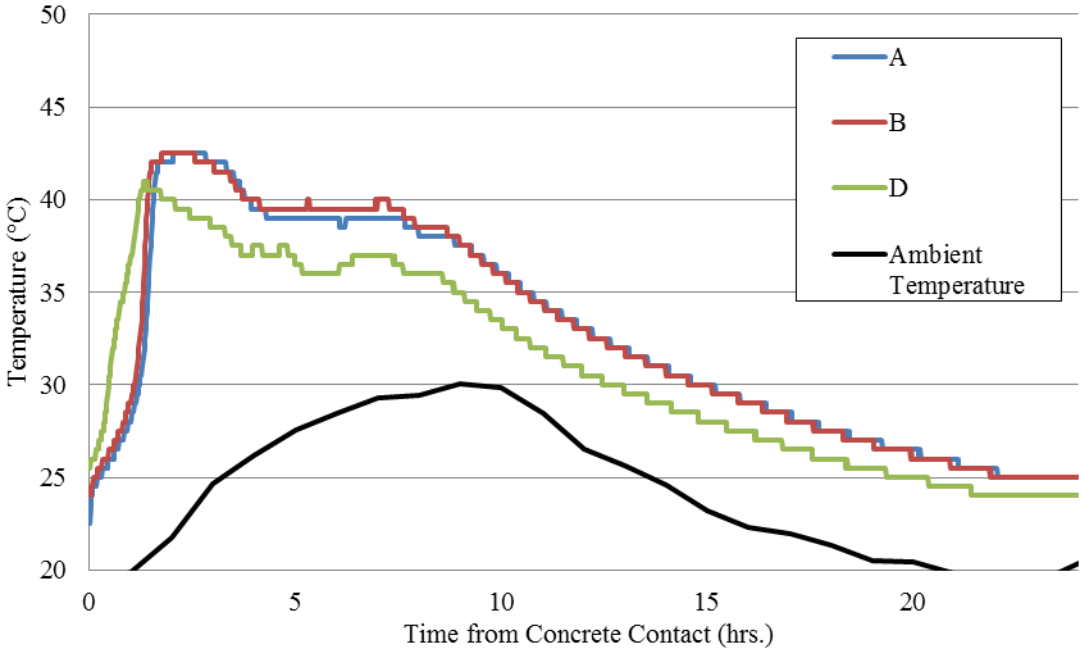


Figure 170: Interface of repair slab and base slab 24 hour curing temperatures

From the two temperature profiles presented, it was evident that the slabs rapidly hydrated. The peak temperatures during curing occurred three to four hours after placement. After these peak temperatures, a sharp drop in temperature was evident. This was caused by the removal of curing blankets three hours after pouring the concrete. Again, this was done to mimic exactly how curing was done in the field in the North Carolina field trial. Then, the slab cooled gradually until it began to change temperatures with the change in ambient temperature at approximately 25-30 hrs.

Higher temperatures were observed on the iButtons embedded mid-depth in the repair material. The CSA slab reached a maximum recorded temperature of 48°C which was almost twice as high as the highest ambient temperature recorded at 23.4°C. The iButton at Location C at the interface failed during the casting due to moisture ingress into the iButton. From the graphs, it was evident that the iButtons at locations C and D had lower temperatures compared to the others

As with the CSA slab, the CAC slab was equipped with eight iButtons. The schematic of the pouring direction and time for the CAC slab are shown in Figure 171.

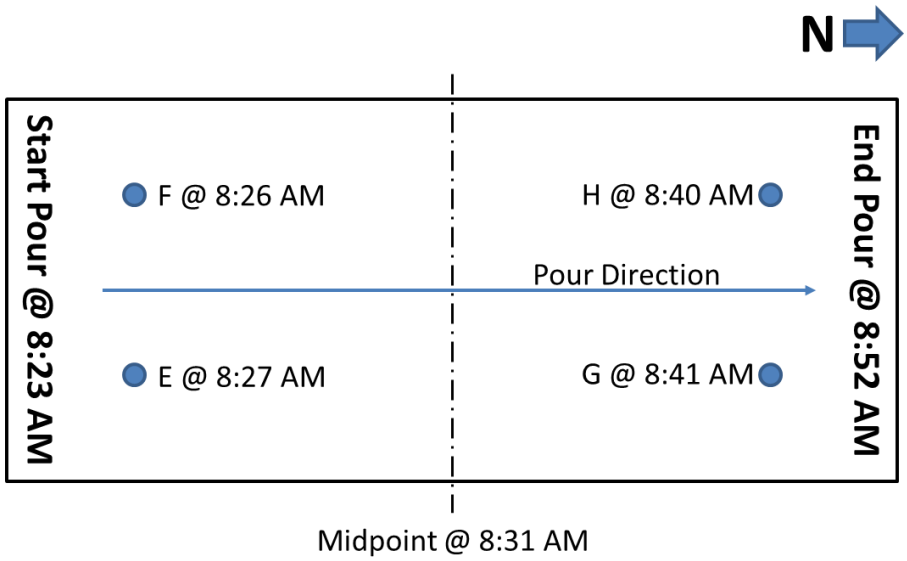


Figure 171: CAC concrete slab schematic and time of concrete pour details

The next day the pour started later than the day before due to more specimens being made by hand ahead of time for follow-up laboratory testing. The truck was backed into place and began pouring at 8:23 AM on October 21, 2010. The temperatures of the mid-depth and interface iButtons are presented in Figure 172 and Figure 173, respectively.

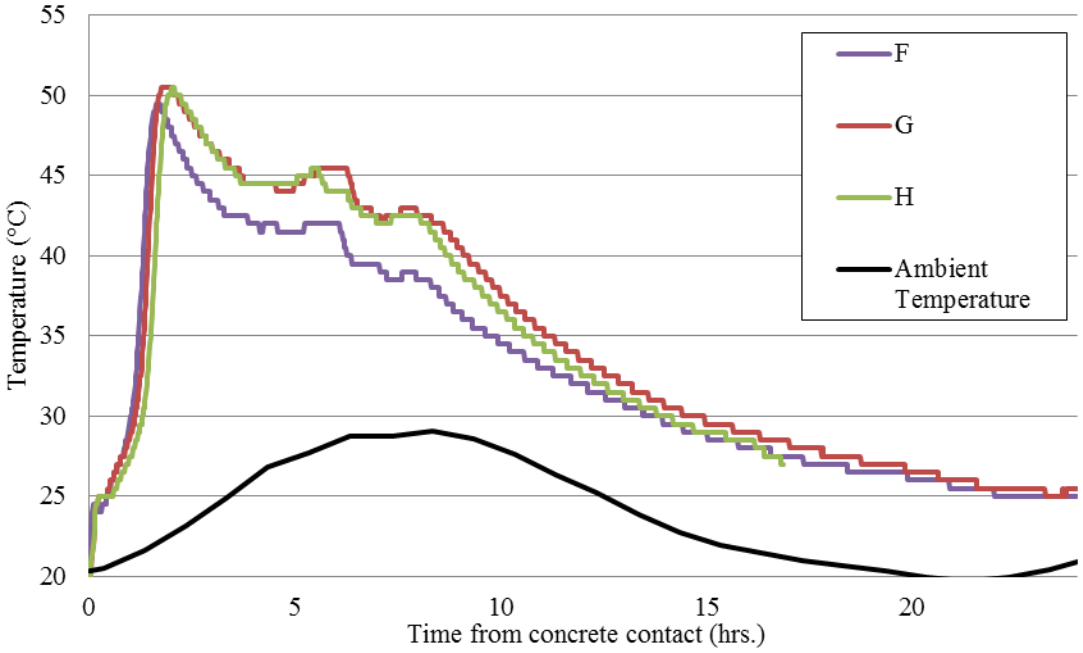


Figure 172: Mid-depth CAC 24 hour curing temperatures

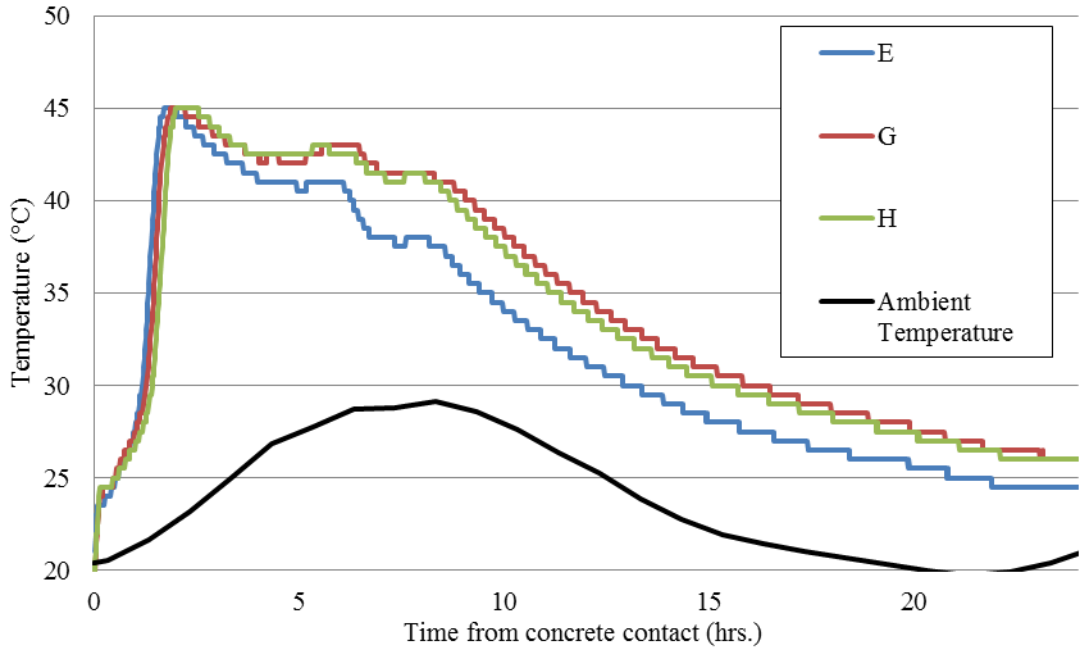


Figure 173: Interface of repair slab and base slab 24 hour curing temperatures

The temperature profiles of the CAC slab show similar general trends as with the CSA slab. A sharp acceleration of the amount of heat generated was evident over the first two hours followed by a brief sharp drop when the curing blankets were removed. Then, a similar gradual cooling trend was observed for the rest of the first day. Later, the slab temperature changed with the temperatures of the ambient temperature.

The CAC slab reached a peak temperature of 50.5°C during hydration. The mid-depth temperature was higher than the interface iButton temperatures similar to the trends seen with CSA. Two of the iButtons failed during the pour and were not able to record any data. Similar to CSA, the second set of buttons (Locations G and H) experienced higher ultimate temperatures than those that were cast earlier at Locations E and F.

#### *7.4.7.2 Strength Development*

Specimens for compression testing were cast each day prior to casting the large-scale slab. The specimens were cured outside near the slabs, but kept in the shade to prevent direct sunlight. The specimens were kept moist with wet burlap blankets for the first 24 hours. After 24 hours, the specimens were demolded and cured in a moist cure room which is kept at 23°C ± 0.5°C and 100% relative humidity. The results of the early first six hours of testing are shown in Figure 174.

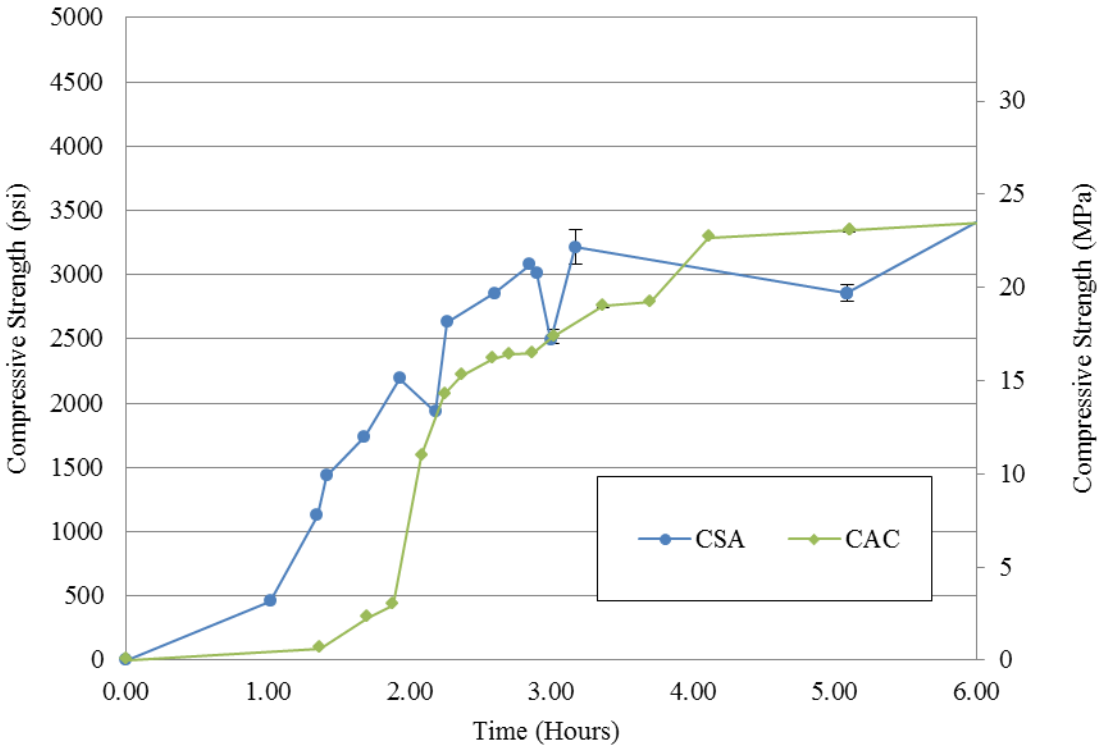


Figure 174: Six hour strength development of CSA and CAC

In Figure 174, error bars were only displayed on the data points where three cylinders were broken. For all other data points, only one or two cylinders were tested. These very early-age compression test were completed to characterize the strength development soon after casting.

The first three to five hours are the most critical for these rapid hardening materials. Often, projects require these rapid hardening materials to reach 20 MPa (3000 psi) compressive strength in three hours after casting such as the field trials mentioned earlier in Chicago and North Carolina. The CSA mixture reached 17.17 MPa (2490 psi) compressive strength at three hours and eclipsed the 20 MPa (3000 psi) mark at 5.09 hours. The CAC mixture achieved 16.16 MPa (2520 psi) compressive strength at three hours and passed the critical threshold at 4.11 hours.

In addition to curing specimens with wet burlap, sixteen 100 x 200 mm (4 x 8 in.) specimens were placed in a semi-adiabatic box immediately after casting. An image of the box can be seen in Figure 175.

Figure 175: Semi-adiabatic box

The image shows the box with the lid removed in Figure 175. When specimens are in the box, a heavy foam lid, 150 mm (6 in.) thick, is lowered on the top of the specimens. The box is constructed to hold 16 - 100 x 200 mm (4 x 8 in.) specimens and minimize the amount of heat released during curing. This box was designed to force CAC specimens to convert from the meta-stable hydrates to the stable hydrates in a few days after curing for 24 hours in the box. Thermocouples were inserted into the specimens to monitor the heat gain as shown Figure 176.

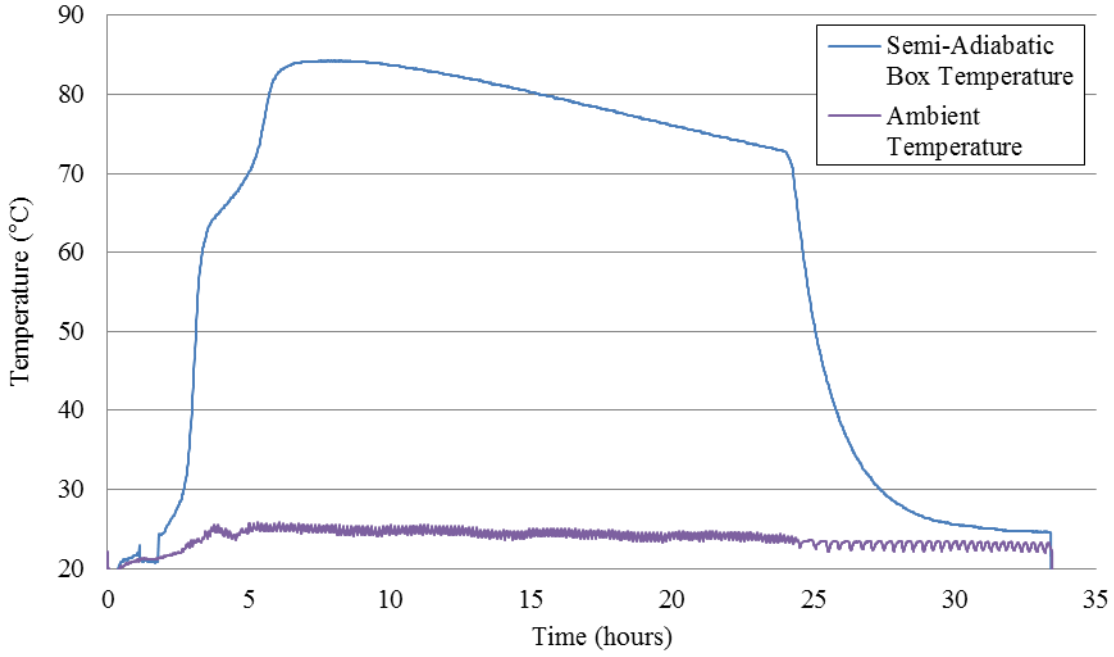


Figure 176: Semi-adiabatic curing temperatures for CAC mixture

CAC cylinders reached a maximum temperature of 82.7°C. The specimens were removed from the box at 24 hours; then cured in the moist cure room. The specimens were not tested prior to 24 hours because this would allow the heat to escape the box and allow for cooling of the specimens. The strength development of the cylinders on a logarithmic time scale is shown in Figure 177.

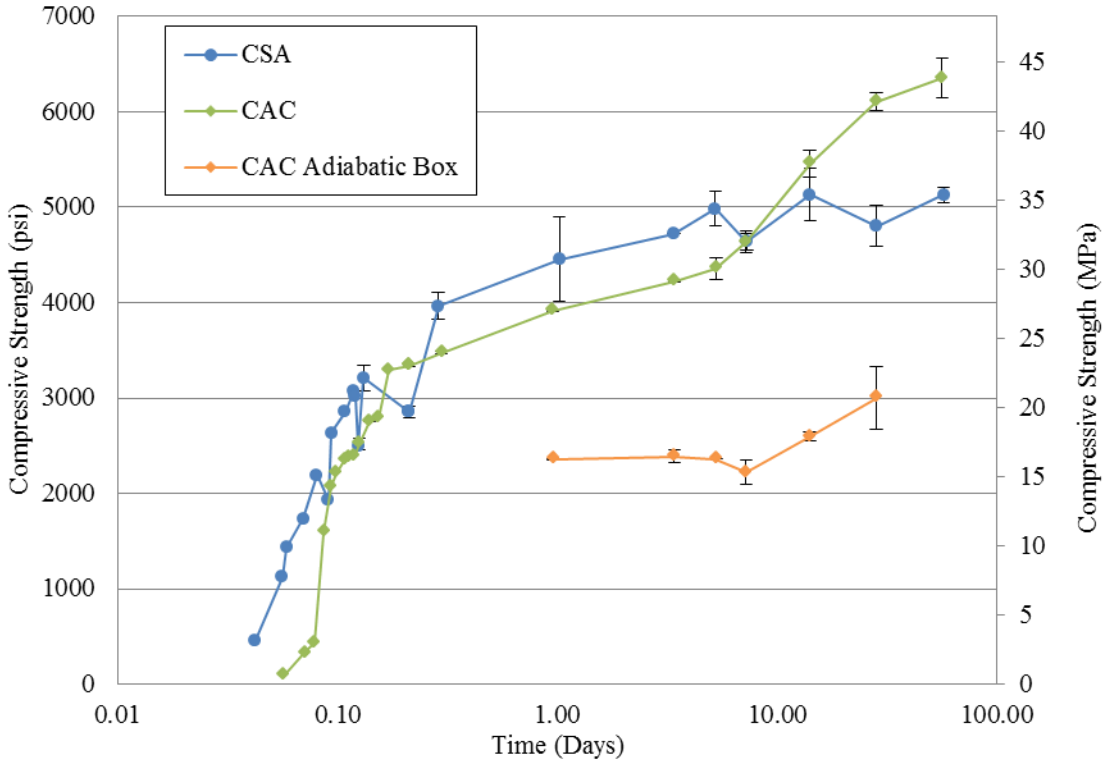


Figure 177: Long-term strength development

From Figure 177, the compressive strength development was; error bars were shown on the data points where three cylinders were tested. The ambient, moist cured CSA and CAC specimens maintained a monotonic strength gain up the age tested. Conversion was not detected during the time scale in which the CAC cylinders were monitored. The impact of latex on conversion is not established at this time. The ultimate strength gain of the CSA mixtures was 35.9 MPa (5210 psi) and the CAC mixture was 43.8 MPa (6350 psi). Two specimens cured in ambient temperatures were equipped with thermocouples; however, failure of the equipment prevented the recording of the information. The semi-adiabatic cylinders had a low ultimate strength and barely surpassed the 20 MPa (3000 psi). A slight reduction in strength was observed at 7 days, possibly due to conversion.

Overall, the ambient compressive strengths of the CAC and CSA cylinders did not achieve the 20 MPa (3000 psi) in 3 hours. The CAC cylinders did not achieve the target strength until 4 hours and for CSA the time was 5 hours.

### *7.4.7.3 Volume Change*

Two concrete embedment strain gages were installed on each of the slabs. These gages were used to monitor the shrinkage/expansion of the concrete repair. The shrinkage/expansion of the two slabs is shown in Figure 178.

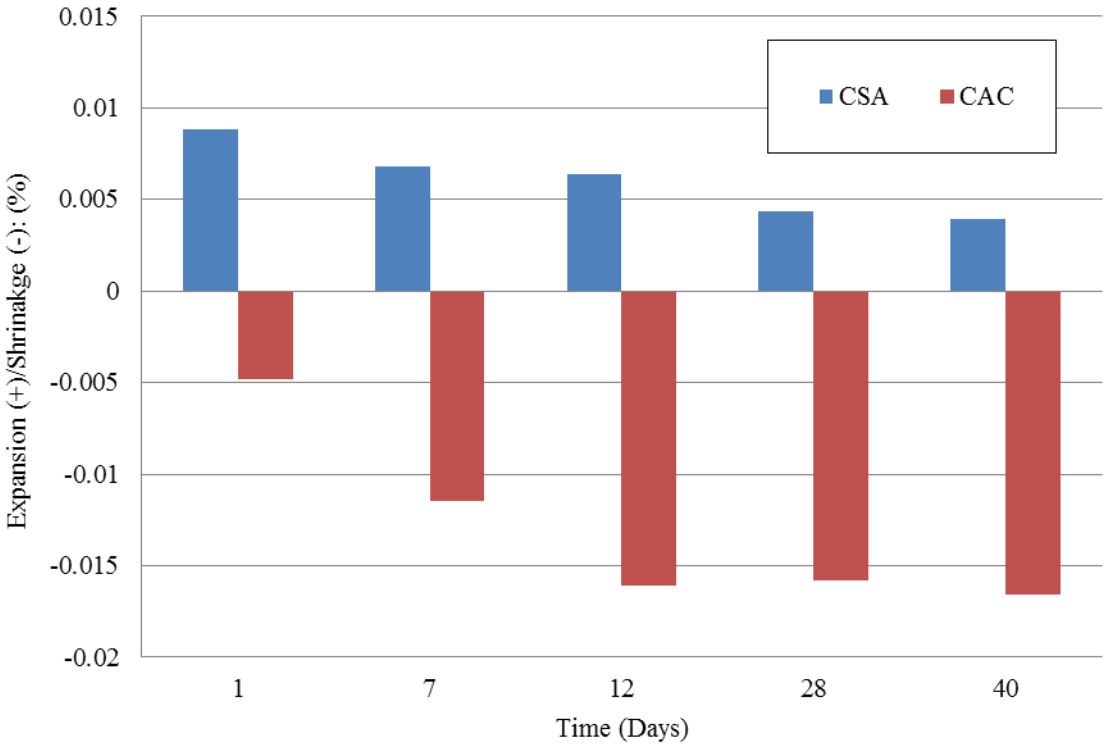


Figure 178: Shrinkage/expansion of rapid hardening cementitious materials in –situ

The deformation of the CAC and CSA overlays for the first 40 days is shown in Figure 178. On the graph, expansion is shown in the positive direction and in the negative direction. The measurements presented are the average of five measurements

taken at 1:00 AM in the morning at each of the time intervals. The measurements were taken at these times to minimize the temperature and weather effects from one measurement to the next. A linear plot was not used to represent the data for this due to problems with the data logging equipment during the testing. Intermittent recording occurred in between the key intervals presented in the graph, thus this presentation of data was chosen.

The data highlights the expansive properties of the CSA cement and is reflected in the quality of the slab. The CSA overlay has a 0.0085% expansion that is gradually reduced during the monitoring. The CAC data illustrated the early-age shrinkage of the system and the continued shrinkage throughout the duration of the monitoring. This continued shrinkage was reflected in the crack mapping and propagation of cracks shown in Section 7.4.6.5.

Due to the errors with the data logging equipment, the true validity of all measurements is subject to question. The author hopes to use this data to highlight the general trends in the data, which showed early-age expansion with the CSA cement and shrinkage with CAC. The CSA slab began to shrink during the monitoring however, the slab never went into tension. The CAC slab shrank immediately and continued to experience shrinkage. Further implementation of these strain gages on other slabs would be beneficial for the monitoring of the early-age volume deformation.

#### *7.4.7.4 Visual Observations and Crack Mapping*

As mentioned earlier, few cracks or deformities were visible immediately after placement of the CSA overlay. Later, small hairline cracks were visible when the observer was very close to the slab. Figure 179 illustrates the cracking pattern of these

hairline cracks; these cracks are highlighted with a permanent marker to make them visible for imaging.

Figure 179: CSA slab cracking overview

The CAC slab cracked immediately (after removal of the curing, or just immediately) and the cracks were visible by the naked eye. An overview picture of the cracking pattern and slab are shown in Figure 180, again, these cracks were highlighted with a permanent marker for the photograph.

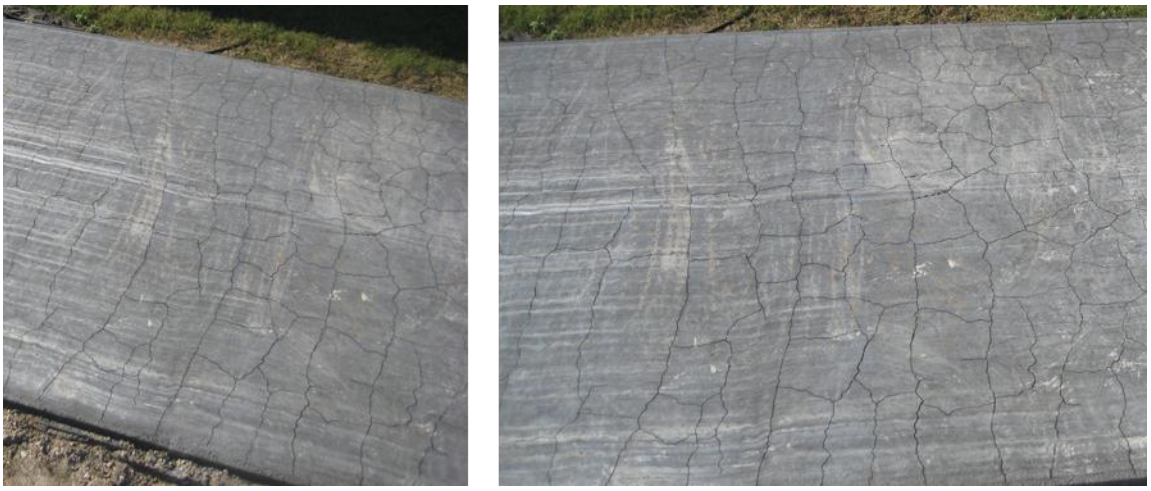

Figure 180: CAC slab cracking overview

In addition to displaying signs of cracking the CAC slab showed signs of crazing. Figure 181 shows a small portion of the crazing that occurred throughout the surface of the slab.

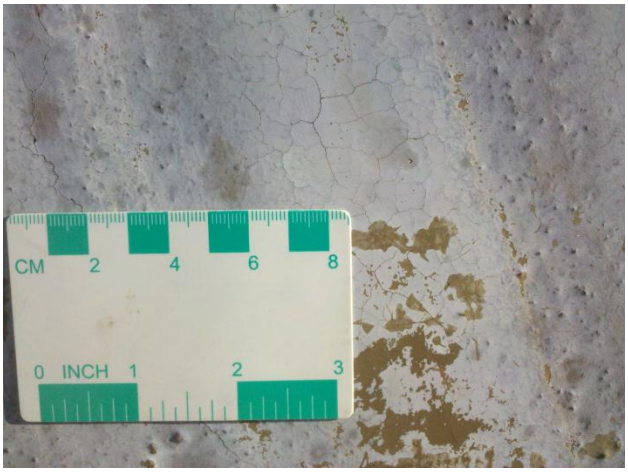


Figure 181: Crazing of CAC slab

Example cracking patterns and spacing for the CAC and CSA slab are shown in Figure 182; however, it is important to note that the cracks have been highlighted through the use of permanent marker and are not as large as they appear in the image below.

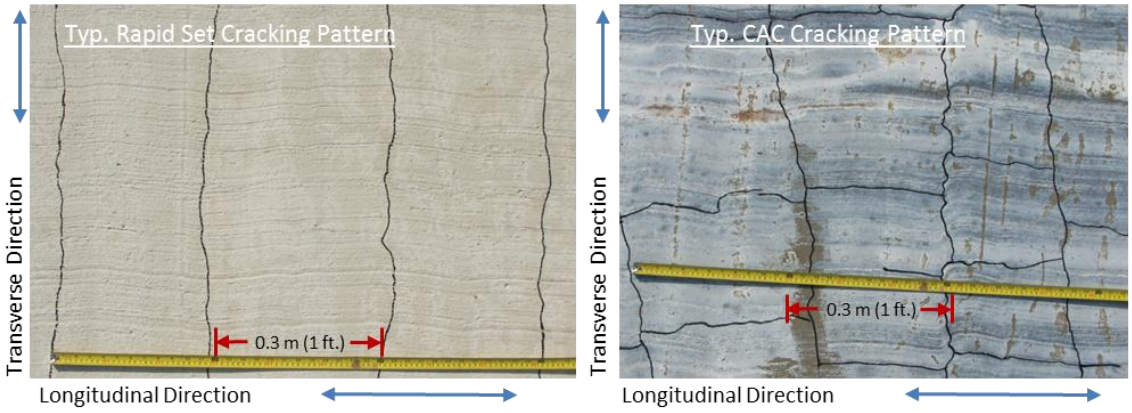


Figure 182: a) Typical cracking patter in the CSA slab, b) CAC slab

From Figure 182, the cracking pattern in the CSA slab is regular with transverse cracks occurring at every 0.3 m (1 ft.) across the length of the slab. While in the CAC slab, the regular transverse cracking is evident there are many cracks in the longitudinal direction. Also, from the image of the CAC slab, a thick white layer of latex is evident on the surface of the slab. This was likely caused by the excessive bleeding of the concrete during the fresh state of the repair.

To evaluate the cracking of the different slabs, a quantitative crack mapping technique was developed specifically for this slab. The layout of the crack mapping grid is shown in Figure 183.

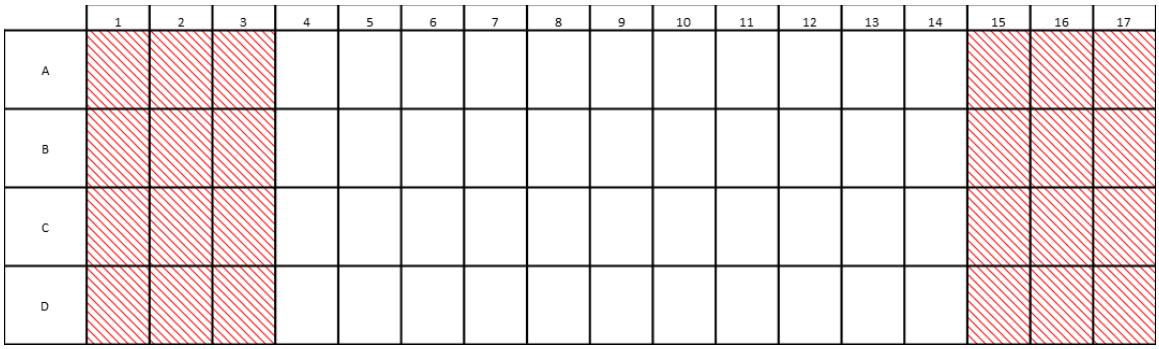


Figure 183: Crack mapping grid

A 0.9 x 0.9 m (3 x 3 ft.) grid was placed on the surface of the slab using a construction chalk line. A crack card with a minimum crack width of 0.10 mm and a 10x eye loupe was used to measure width of the cracks. If a crack was observed, but smaller than 0.10 mm the crack was recorded as 0.05 mm to allow for it to be added into the total crack widths. The cracks were measured where they intersected the chalk lines on the grid. This allowed for the number of cracks to be quantified and the average width of their openings to be monitored in both the transverse and longitudinal direction. From

Figure 183, large end regions are distinguished at the end 2.7 m (9 ft.) of each slab; in these regions cracking was neglected due to the edge effects. The research team felt that there may be a potential for debonding and slippage between the two slabs and would affect the bond therefore potentially affecting the cracking. The quantified results of the cracking are presented in the Table 28.

Table 28: Quantified cracking results

| | Slab | CSA | | CAC | |
|---|---|---|---|---|---|
| | Age (days) | 21 | 118 | 18 | 117 |
| No. Cracks | Transverse | 82 | 91 | 134 | 128 |
| | Longitudinal | 10 | 14 | 136 | 130 |
| | Total | 92 | 105 | 270 | 258 |
| Avg. Crack Width (mm) | Transverse | 0.05 | 0.05 | 0.12 | 0.13 |
| | Longitudinal | 0.05 | 0.05 | 0.06 | 0.10 |
| | Total | 0.05 | 0.05 | 0.09 | 0.11 |

The cracks were measured by a team of three researchers. With this technique there is always a degree of variability between users that could affect the number of cracks measured each time and the measurement of the width of each crack. A general observation is the number of cracks measured on the CAC slab; 270 cracks were measured the first time after crack mapping and 258 cracks the second time. This reduction in the number of cracks measured from the first time to the second time is assumed to be within the error of the technique.

From Table 28, it is evident that the number of cracks and size of the cracks were much less for the CSA slab than the CAC slab. While the CSA slab displayed many cracks in the transverse direction, these cracks were microscopic and did not penetrate

deeply into the surface. The CSA slab had no signs of longitudinal cracking, the cracks identified were merely transverse cracks that were at a slight angle and intersected the transverse chalk lines drawn by the research team. The largest crack recorded on the CSA slab was 0.2 mm and average crack width was 0.05 mm.

The CAC slab experienced significant cracking compared to the CSA slab. Over 250 cracks were measured each time the slab was crack mapped. Unlike the CSA slab, the CAC slab did have cracking in the transverse and longitudinal directions. A similar number of cracks were measure in both directions. When the slab was initially investigated the average crack width opening in the transverse direction was almost two times greater than the longitudinal cracking. Over time, these longitudinal crack widths continued to open and have similar average crack widths in both directions. The largest crack width measured on the CAC slab was 0.85 mm and an overall average crack width opening of 0.11 mm. This shows that the CAC has very large crack openings compared to the CSA slab. Cores were taken through the cracks in the end region of the slab to evaluate the depth of cracking as shown in Figure 184.

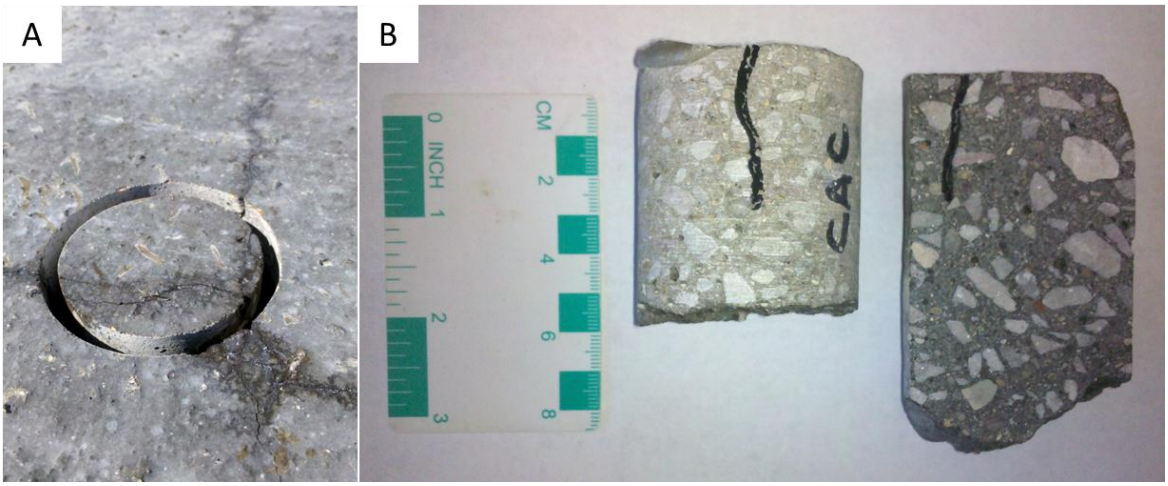


Figure 184: a) Core location taken to determine depth of cracking, b) Cores with cracks highlighted

Cores were taken from the end region to minimize effects on stress concentrations and potential for worsening cracking near the holes. Intentionally, these 50 mm (2 in.) diameter cores were taken through the center of cracks. From image Figure 184 b), the observations from the edge of the slabs where the cracks penetrated from 38 mm (1.5 in.) to the base slab of the repair were also confirmed from the cores. This again would highlight concern with the application of this material in the field.

### *7.4.7.5 Drying Shrinkage*

Specimens were cast on the days of the pour to monitor the drying shrinkage according to a modified ASTM C 157. Changes to the ASTM standard procedure were implemented due to the rapid hydration of these specimens. The specimens were cast and wet cured for 24 hours as required by the standard, but instead of moving them into lime baths, they were moved directly into the environmental chamber. This was done because of the rapid hydration of these systems and to match what was done in the field. The environmental chamber was kept at 23°C±0.5°C and 50%±5% RH. The results of

the length change and mass change of three specimens cast from each mixture are shown in Figure 185 and Figure 186, respectively.

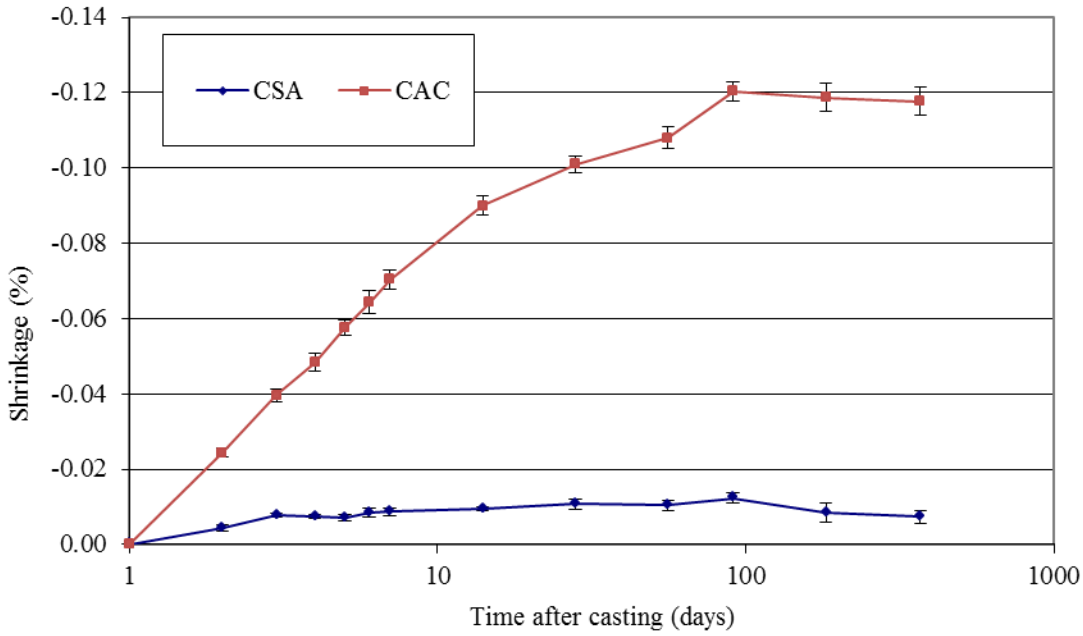


Figure 185: Drying shrinkage

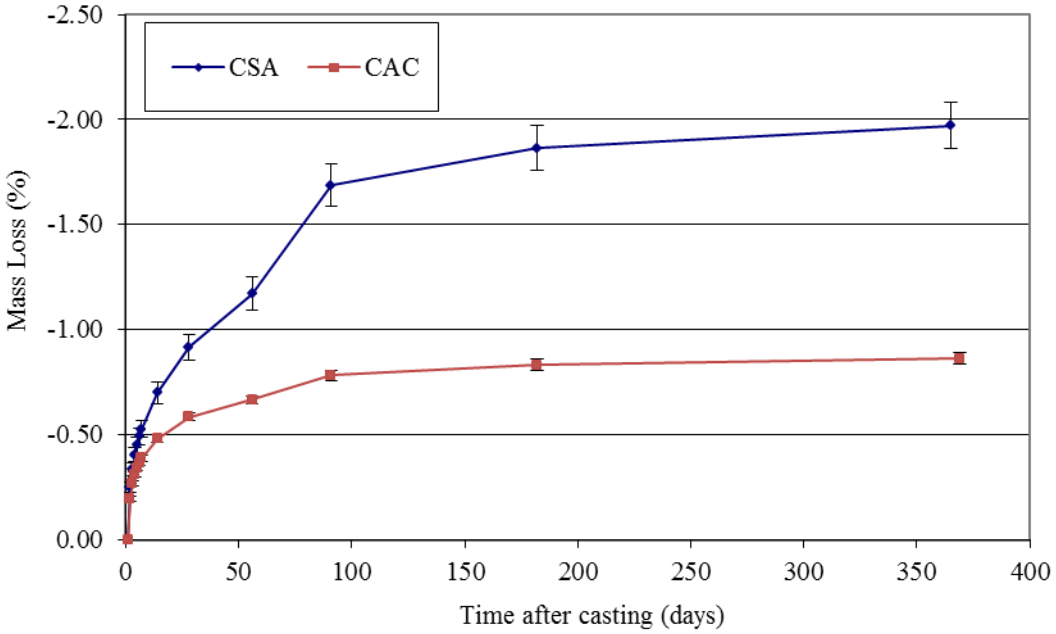


Figure 186: Mass change of drying shrinkage specimens

The drying shrinkage of the CAC is much greater than that of the CSA. The CAC has an ultimate drying shrinkage of 0.1177 microstrain and the CSA of 0.0073 microstrain. This is inversely related to the mass change of these specimens where the CSA mixture lost 1.97% and the CAC lost 0.87%.

### 7.4.8 Discussion

The laboratory field trial completed at the Pickle Research Campus simulated the field the repair of a concrete pavement with a thin-bonded concrete overlay with the scrutiny and precision of laboratory conditions. This research aimed to characterize the hydration and early-age strength development as well as investigate the potential for cracking of truly large-scale specimens.

The hydration of the two different binders resulted in excessive heat release and rapid strength gain; however, neither of these mixtures achieved the desired compressive

strength of 20 MPa (3000 psi) in 3 hours. The research team felt the desired strength could be achieved by reducing the amount of citric acid in each of the mixtures. The CSA mixture achieved 17.17 MPA (2490 psi) and the CAC concrete reached 16.16 MPa (2520 psi) in the first three hours after casting. The ultimate strength of the CAC slab was greater than the CSA where the mixtures had 43.8 MPa (6350 psi) and 35.9 MPa (5210 psi), respectively.

The heat generated due to hydration of the different slabs was significant and facilitated the rapid strength development, but it may have also influenced the excessive cracking in the CAC slab due to thermal shock or thermal gradients. Both the CSA and CSA slabs reached internal temperatures near 50°C, which was around 30°C greater than the ambient conditions. The cracking was thought to be caused due to the possibility of thermal shock, which may have been caused when the curing blankets were removed. A drastic change in temperature was observed when these blankets were taken off; however, both slabs experienced similar thermal histories and the CSA slab did not have the cracking.

Also, the thermal gradients observed from the slab interfaces and the slab mid-depth had a 5°C thermal gradient across a 25 mm (1 in.) depth, which could potentially cause cracking due to the strain across such a small distance. This gradient was observed in both slabs; thus, from the thermal monitoring of the repair section it is believed that temperature was not the cause of the excessive cracking seen in the CAC slabs.

The concrete embedment strain gauges showed the pre-compression of the CSA slab that helped prevent early-age cracking. The slab expands initially and as it began to cure and to dry the amount of expansion was reduced due to the different shrinkage mechanisms. During the monitoring of the shrinkage the slab did not go into tension and

maintained the compression preventing the cracking. From testing completed in this dissertation and by work completed by Ideker and Fu, which showed an early-age expansion at higher temperatures, the CAC slab was expected to undergo a similar pre-compression Ideker (2008) and Fu (2011). With the maximum temperature experiencing temperatures above 50°C this behavior was expected. Instead, the slab went immediately into tension and continued to shrink throughout the monitoring period.

The CSA slab had minimal cracking that occurred in the very top surface of the slab that were measured smaller than 0.10 mm these cracks were deemed to have no influence on the long-term performance of the slabs. The CAC slabs had significant amounts of cracking that penetrated from 1.5 in. to through the depth of the overlay. These cracks continued to propagate during the monitoring and open in width.

In Chapter 6 laboratory investigations of the hydration and early-age volume deformation were presented on the influence of the CAC with latex, LSA, and citric acid. The results from the autogenous deformation are presented in Figure 187.

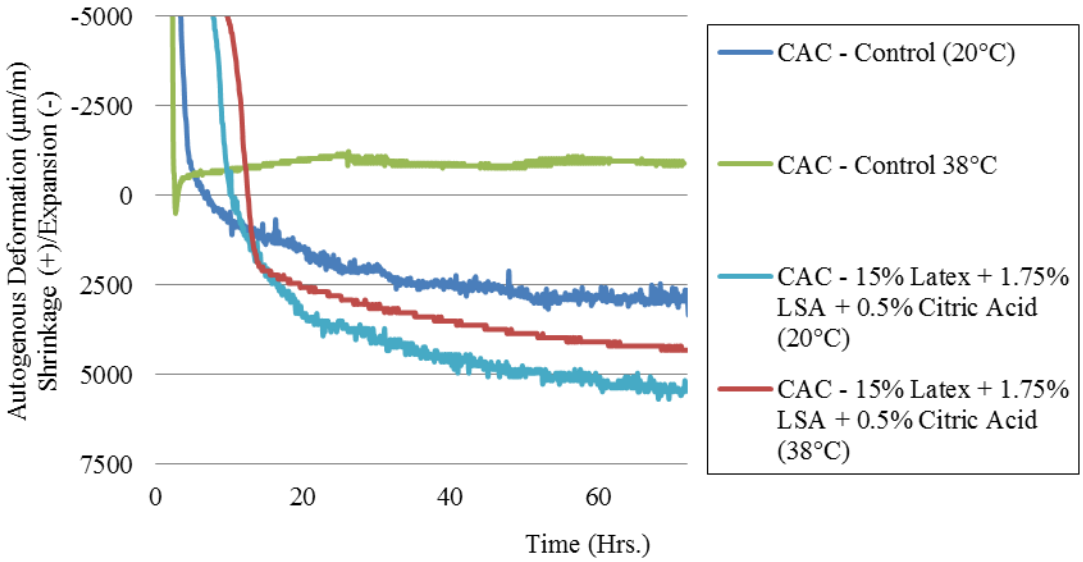


Figure 187: Autogenous deformation of CAC at 20°C and 38°C

From Figure 187, it was evident that the addition of the citric acid to the CAC with latex and LSA caused a substantial amount of shrinkage at 20°C and 38°C. From all the material combinations investigated in chapters 5 and 6, the mixtures containing CAC, latex, LSA, and citric acid were the only ones to experience autogenous shrinkage at 38°C. It is possible that autogenous shrinkage initially caused the cracking the CAC slab and the drying shrinkage continued to increase the crack width and cause more cracking at later ages.

From the field trial, it was evident that these materials have potential use for rapid repair situations. The cracking observed with the latex modified CAC pours was believed to be caused by the addition of citric acid with latex and LSA. The CSA performed well with insignificant surface cracking and rapid strength gain.

## 7.5 SUMMARY

A wide array of topics was covered in this chapter; the overall aim was to provide a summary of field performance of different rapid repair materials. With continuing

growth in demand for these materials it is essential to develop a database of the long-term performance from the Chicago site visits, document application techniques from the North Carolina field trial, and summarize through laboratory investigations at UT Austin field trial.

From the site visits in Chicago, the research team investigated the application of CAC in true field conditions. The material was regularly cast in this market using a volumetric mix truck and has had success achieving the rapid strength requirements. All the sites visited in the Chicago field trial were different ages and provided a database of the long-term performance of different combinations of materials.

The site visit of the North Carolina field visit was essential for documenting the proper techniques used in the field trial at UT Austin. This site visit provided an extremely through comprehension of techniques used to prepare and cast these rapid repair materials on bridge decks. The research team gained a tremendous amount of knowledge on novel hydro-demolition technique and debris removal. Observing the placement of the rapid repair materials highlighted the urgency and techniques that were demanded for the placement, vibration, finishing, and curing of these rapid repair materials.

The field trial at UT Austin allowed for the implementation of techniques observed in the other field trials as well as a side-by-side comparison of two different rapid hardening cementitious materials, CAC and CSA. These studies allowed for the characterization of the large scale performance of the different materials. The repairs highlighted the rapid strength development and the potential for early-age cracking.

## 7.6 CONCLUSIONS

CAC was shown to be an effective repair material when used in the field in Chicago, Illinois. However, the field trial in Austin, TX resulted in significant cracking, possibly due to excessive volume changes triggered by a combination of using CAC, Latex, LSA, and Citric Acid. Additional research is needed to better understand the underlying mechanisms of the cracking observed in the CAC overlay cast in Austin. The CAC generated significant amount of heat during the hydration process that resulted in 20 MPA (3000 psi) four hours after placement.

The CSA mixtures used in Austin is consistent to similar thin-bonded overlays throughout the country. The material was shown to gain strength rapidly and provide good bond to the base slab. A pre-compression of the overlay was shown to be beneficial to prevent cracking due to drying and autogenous shrinkage. The CSA mixtures generated similar heat to the CAC during hydration and experienced similar levels of early-age strength development.

Compared to PC, very little is known about these materials especially on the characterization of the field performance. This chapter provided information related to the application of these materials for thin-bonded concrete overlays. Continued work is needed in the laboratory and field to fully characterize the field performance of these complex cementitious systems.

# Chapter 8: Conclusions and Recommendations

This chapter summarizes the key observations and conclusions of the multi-scale characterization of the hydration and early-age properties of CAC based-systems.

## 8.1 CONCLUSIONS

This dissertation summarizes the results of testing of the hydration kinetics and microstructural development, early-age volume deformation and large-scale behavior of CAC based-systems.

### 8.1.1 HYDRATION AND MICRO-STRUCTURAL DEVELOPMENT

From the work completed with isothermal calorimetry, qualitative XRD, and chemical shrinkage, the key findings include:

- All isothermal calorimeters may not be able to handle the excessive heat release associated with the hydration of CAC paste and mortars.
- The new isothermal calorimeter, designed and built, for this dissertation was proven to be repeatable for identifying the time and peak heat of hydration at 5°C, 23°C, and 38°C. However, more error was observed at 60°C for identifying the peak heat of hydration, but the repeatability of the time of the peak heat was acceptable.
- The addition of 0.5% and1.0% LSA with plain CAC and TCAC led to the direct formation of $C_2AH_8$ at 20°C, when both metastable hydrates, $CAH_{10}$ and $C_2AH_8$, would be expected to form.
- Conversion was identified in 38°C isothermal chemical shrinkage testing for all plain CAC, TCAC, and CAC-FA mixtures. This behavior was identified by a secondary ascent in the chemical shrinkage plots previously identified Fu (2011). This behavior was not observed in the CAC-LF mixtures.

- Plotting chemical shrinkage as a function of the total cumulative heat release clearly identified conversion for 38°C isothermal testing. These plots also served as a tool for comparing the rates of reaction of different mixtures.
- From the qualitative XRD patterns of 38°C isothermal hydration, $C_2ASH_8$ and $C_3AH_6$ stable hydration products were found. However, in the mixture containing LSA and HRWR, no stable hydration products were found. Conversion was assumed to have occurred from observations of the chemical shrinkage plot as a function of cumulative heat.
- The substitution of the LF accelerated the hydration kinetics with and without the addition of LSA and HRWR. It also increased the amount of cumulative heat released and chemical shrinkage compared to plain CAC.
- From isothermal calorimetry, a reduction in the peak heat flow and broader more gradual hydration kinetics were observed when FA was used. Substantially more cumulative heat release was measured for all three mixtures containing FA compared to the plain CAC.
- The FA increased the amount of chemical shrinkage by an average of 27% at the termination of the test. This increase was almost proportional to replacement percentage of CAC, which highlights its contribution to the cementitious reactions.
- From chemical shrinkage at 38°C, more shrinkage was observed for the FA mixtures compared to the plain CAC mixtures.
- Combinations of LSA and citric acid had similar cumulative heat release compared to those of plain CAC.

- Combinations of latex, citric acid, and LSA had substantial amounts of chemical shrinkage, which was increased due to a secondary ascent in the shrinkage curves.

### 8.1.2 Early-age Volume Deformation and Large Scale Field Performance

- Plain CAC, TCAC, CAC-FA, and CAC-LF mixtures with and without the addition of LSA and HRWR experienced shrinkage at 20°C and expansion or minimal amounts of shrinkage at 38°C from autogenous deformation testing.
- A substantial amount of autogenous shrinkage observed at 38°C isothermal conditions for the mixtures containing plain CAC, LSA, citric acid, and latex.
- From the Chicago field visits, CAC concrete installations have generally performed well to date, although severe scaling was observed on a bridge deck that included a combination of CAC and latex.
- From the large-scale field trial at UT-Austin:
    - CSA performed well in a thin-bonded concrete overlay. It exhibited rapid strength gain, with a compressive strength of 20 MPa (3000 psi) in 3 hours. The overlay had minimal amount of cracking.
    - A thin-bonded overlay using CAC (in place of CSA) exhibited substantial amounts of cracking, starting within a few hours of placement. Although the exact mechanism underlying this early-age cracking may not be fully understood, it appears that the cracking was triggered by the combined use of plain CAC, LSA, citric acid and latex, which led to excessive autogenous and drying shrinkage.

## 8.2 FUTURE WORK

This dissertation focused on the characterization of the hydration, microstructural development, and large-scale performance of CAC based-systems. Although significant progress was made in these areas, future research is needed that focuses on:

- Long-term isothermal calorimetry and chemical shrinkage at 38°C to further characterize the identification of conversion on the plots of chemical shrinkage as a function of cumulative heat release.
- Microstructural characterization and early-age volume deformation of the effect of citric acid.
- Investigations of the effect of realistic time-temperature histories on the autogenous deformation and chemical shrinkage behavior of CAC-based systems.
- Characterizing the drying shrinkage of various CAC based-systems, with particular focus on the impact of chemical admixtures and alternative binders or fillers.
- The microstructural characterization and mechanical strength development of LF substitutions of CAC.
- Additional large-scale testing to allow for further correlation the behavior of actual field repairs to that seen in the laboratory.
- Long-term characterization of CAC repairs in the field.
- The effect of SCMs and chemical admixtures on the long-term durability of these mixtures, especially with regard to sulfate resistance, corrosion resistance, and carbonation.

# Appendix A: Material Certificates

WYOMING ANALYTICAL LABORATORIES, INC.
14335 W. 44th Avenue
Golden, CO 80403
www.wal-lab.com
Email: walxray@aol.com
(303) 278-2446
Fax: (303) 278-2439

April 19, 2012

Katy Aughenbaugh
University of Texas at Austin-Construction
Materials Research Group
10100 Burnet Rd, Bldg. 18-B
Austin, TX 78758

Denver Division #: 120261-1
Sample ID: Fondu 1
PO#: 2012A20329

CHEMICAL ANALYSIS
WT%, AS RECEIVED

| | |
|---|---|
| Silicon Dioxide, $SiO_2$ | 5.93 |
| Aluminum Oxide, $Al_2O_3$ | 39.15 |
| Iron Oxide, $Fe_2O_3$ | 14.23 |
| Total ($SiO_2 + Al_2O_3 + Fe_2O_3$) | 59.30 |
| Calcium Oxide, CaO | 35.34 |
| Magnesium Oxide, MgO | 0.70 |
| Sodium Oxide, $Na_2O$ | 0.08 |
| Potassium Oxide, $K_2O$ | 0.19 |
| Titanium Dioxide, $TiO_2$ | 1.75 |
| Manganese Dioxide, $Mn_2O_3$ | 0.48 |
| Phosphorus Pentoxide, $P_2O_5$ | 0.17 |
| Strontium Oxide, SrO | 0.03 |
| Barium Oxide, BaO | 0.01 |
| Sulfur Trioxide, $SO_3$ | 0.16 |
| Loss on Ignition (950°C) | 1.81 |
| Total | 100.00 |

Analysis per ASTM C 311

Charles R. Wilson
Division Manager

MEMBER ACIL

Figure 188: Fondu Material Certificate

WYOMING ANALYTICAL LABORATORIES, INC.
14335 W. 44th Avenue
Golden, CO 80403
www.wal-lab.com
Email: wabray@aol.com
(303) 278-2446
Fax: (303) 278-2439

April 19, 2012

Katy Aughenbaugh
University of Texas at Austin-Construction
Materials Research Group
10100 Burnet Rd, Bldg. 18-B
Austin, TX 78758

Denver Division #: 120261-4
Sample ID: LBC
PO#: 2012A20329

CHEMICAL ANALYSIS
WT%, AS RECEIVED

| | |
|---|---|
| Silicon Dioxide, $SiO_2$ | 14.44 |
| Aluminum Oxide, $Al_2O_3$ | 34.29 |
| Iron Oxide, $Fe_2O_3$ | 11.18 |
| Total ($SiO_2 + Al_2O_3 + Fe_2O_3$) | 59.92 |
| Calcium Oxide, CaO | 35.06 |
| Magnesium Oxide, MgO | 2.07 |
| Sodium Oxide, $Na_2O$ | 0.07 |
| Potassium Oxide, $K_2O$ | 0.18 |
| Titanium Dioxide, $TiO_2$ | 1.55 |
| Manganese Dioxide, $Mn_2O_3$ | 0.20 |
| Phosphorus Pentoxide, $P_2O_5$ | 0.06 |
| Strontium Oxide, SrO | 0.03 |
| Barium Oxide, BaO | 0.03 |
| Sulfur Trioxide, $SO_3$ | 0.62 |
| Loss on Ignition (950°C) | 0.22 |
| Total | 100.00 |

Analysis per ASTM C 311

Charles R. Wilson
Division Manager

MEMBER ACIL

Figure 189: TCAC Material Certificate

WYOMING ANALYTICAL LABORATORIES, INC.
14335 W. 44th Avenue
Golden, CO 80403
www.wal-lab.com
Email: walxray@aol.com
(303) 278-2446
Fax: (303) 278-2439

April 19, 2012

Katy Aughenbaugh
University of Texas at Austin-Construction
Materials Research Group
10100 Burnet Rd, Bldg. 18-B
Austin, TX 78758

Denver Division #: 120261-5
Sample ID: Limestone
PO#: 2012A20329

CHEMICAL ANALYSIS
WT%, AS RECEIVED

| | |
|---|---|
| Silicon Dioxide, SiO2 | 0.16 |
| Aluminum Oxide, Al2O3 | 0.10 |
| Iron Oxide, Fe2O3 | 0.12 |
| Total (SiO2 + Al2O3 + Fe2O3) | 0.37 |
| Calcium Oxide, CaO | 55.93 |
| Magnesium Oxide, MgO | 0.31 |
| Sodium Oxide, Na2O | 0.00 |
| Potassium Oxide, K2O | 0.01 |
| Titanium Dioxide, TiO2 | 0.00 |
| Manganese Dioxide, Mn2O3 | 0.01 |
| Phosphorus Pentoxide, P2O5 | 0.01 |
| Strontium Oxide, SrO | 0.01 |
| Barium Oxide, BaO | 0.00 |
| Sulfur Trioxide, SO3 | 0.03 |
| Loss on Ignition (950°C) | 43.32 |
| Total | 100.00 |

Analysis per ASTM C 311

Charles R. Wilson
Division Manager

MEMBER ACIL

Figure 190: LF Material Certificate

WYOMING ANALYTICAL LABORATORIES, INC.
14335 W. 44th Avenue
Golden, CO 80403
www.wal-lab.com
Email: walxray@aol.com
(303) 278-2446
Fax: (303) 278-2439

April 19, 2012

Katy Aughenbaugh
University of Texas at Austin-Construction
Materials Research Group
10100 Burnet Rd, Bldg. 18-B
Austin, TX 78758

Denver Division #: 120261-6
Sample ID: Welsch
PO#: 2012A20329

CHEMICAL ANALYSIS
WT%, AS RECEIVED

| | |
|---|---|
| Silicon Dioxide, SiO2 | 30.78 |
| Aluminum Oxide, Al2O3 | 17.44 |
| Iron Oxide, Fe2O3 | 5.89 |
| Total (SiO2 + Al2O3 + Fe2O3) | 54.12 |
| Calcium Oxide, CaO | 29.00 |
| Magnesium Oxide, MgO | 6.47 |
| Sodium Oxide, Na2O | 2.19 |
| Potassium Oxide, K2O | 0.34 |
| Titanium Dioxide, TiO2 | 1.37 |
| Manganese Dioxide, Mn2O3 | 0.05 |
| Phosphorus Pentoxide, P2O5 | 0.86 |
| Strontium Oxide, SrO | 0.47 |
| Barium Oxide, BaO | 0.71 |
| Sulfur Trioxide, SO3 | 3.83 |
| Loss on Ignition (950°C) | 0.60 |
| Total | 100.00 |

Analysis per ASTM C 311

Charles R. Wilson
Division Manager

MEMBER ACIL

Figure 191: FA Material Certificate

WYOMING ANALYTICAL LABORATORIES, INC.
14335 W. 44th Avenue
Golden, CO 80403
www.wal-lab.com
Email: walkray@aol.com
(303) 278-2446
Fax: (303) 278-2439

April 19, 2012

Katy Aughenbaugh
University of Texas at Austin-Construction
Materials Research Group
10100 Burnet Rd, Bldg. 18-B
Austin, TX 78758

Denver Division #: 120261-3
Sample ID: Rapid Set
PO#: 2012A20329

CHEMICAL ANALYSIS
WT%, AS RECEIVED

| | |
|---|---|
| Silicon Dioxide, SiO2 | 14.22 |
| Aluminum Oxide, Al2O3 | 15.58 |
| Iron Oxide, Fe2O3 | 0.98 |
| Total (SiO2 + Al2O3 + Fe2O3) | 30.78 |
| Calcium Oxide, CaO | 49.84 |
| Magnesium Oxide, MgO | 1.46 |
| Sodium Oxide, Na2O | 0.16 |
| Potassium Oxide, K2O | 0.47 |
| Titanium Dioxide, TiO2 | 0.57 |
| Manganese Dioxide, Mn2O3 | 0.07 |
| Phosphorus Pentoxide, P2O5 | 0.11 |
| Strontium Oxide, SrO | 0.16 |
| Barium Oxide, BaO | 0.02 |
| Sulfur Trioxide, SO3 | 14.73 |
| Loss on Ignition (950°C) | 1.64 |
| Total | 100.00 |

Analysis per ASTM C 311

Charles R. Wilson
Division Manager

MEMBER ACIL

Figure 192: CSA Material Certificate

# Appendix B: Characterization of Grace AdiaCal Isothermal Calorimeter

## APPENDIX B.1: REPEATABILITY OF PC MORTAR

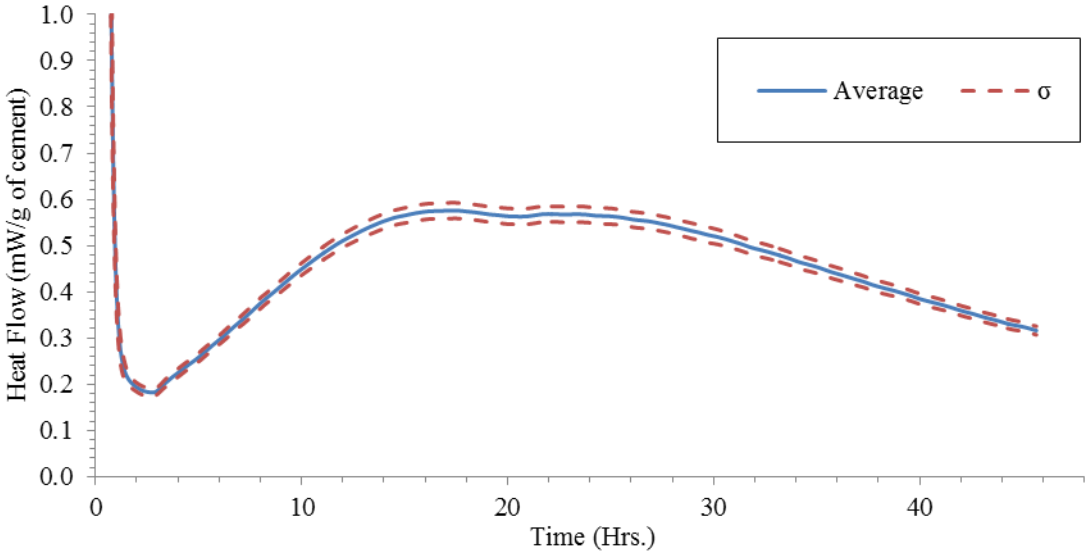


Figure 193: Heat flow of portland cement mortar at 5°C isothermal

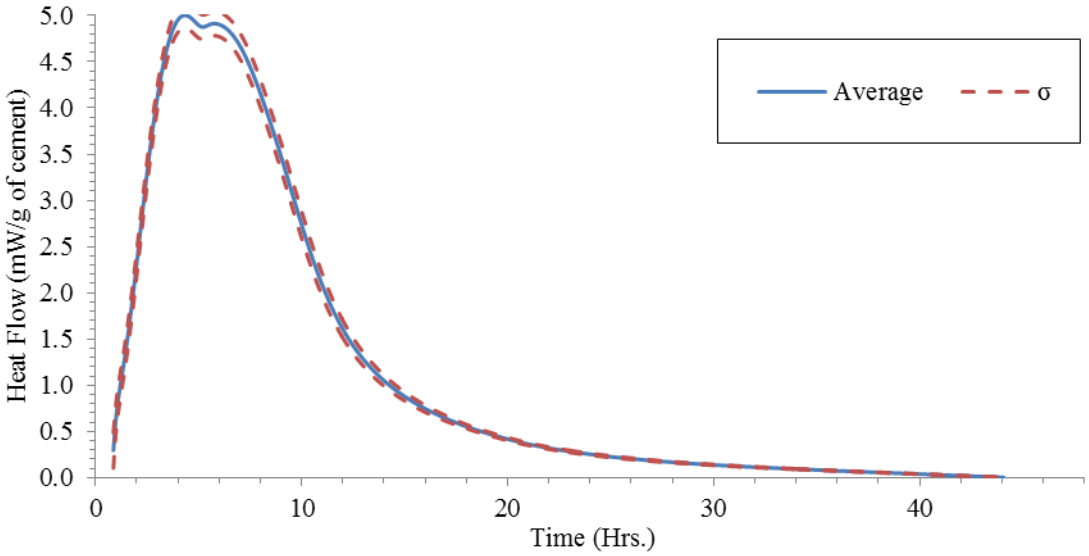

Figure 194: Heat flow of portland cement mortar at 23°C isothermal

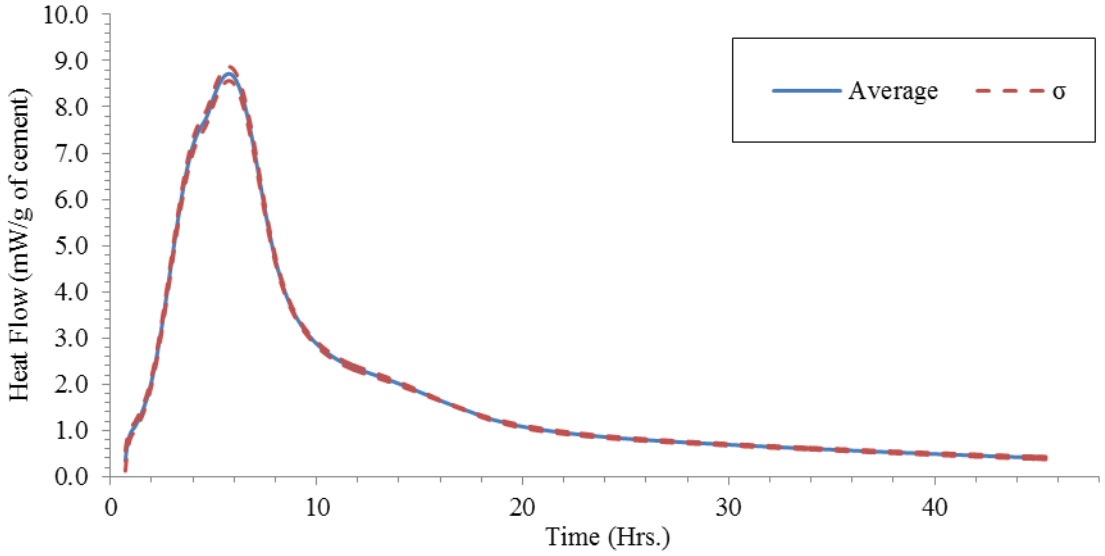


Figure 195: Heat flow of portland cement mortar at 38°C isothermal

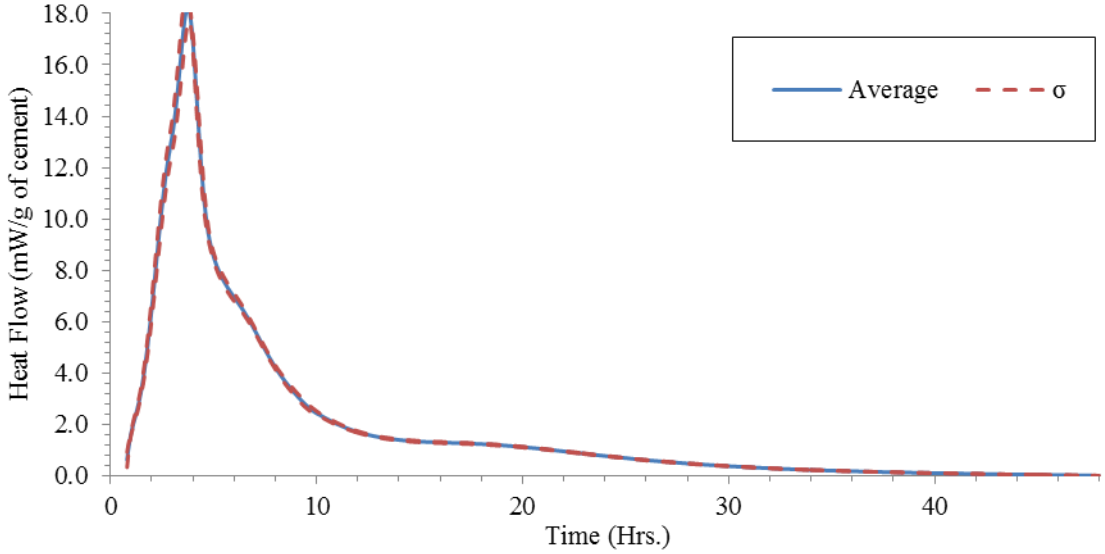


Figure 196: Heat flow of portland cement mortar at 60°C isothermal

## APPENDIX B.2: REPEATABILITY OF PC PASTE

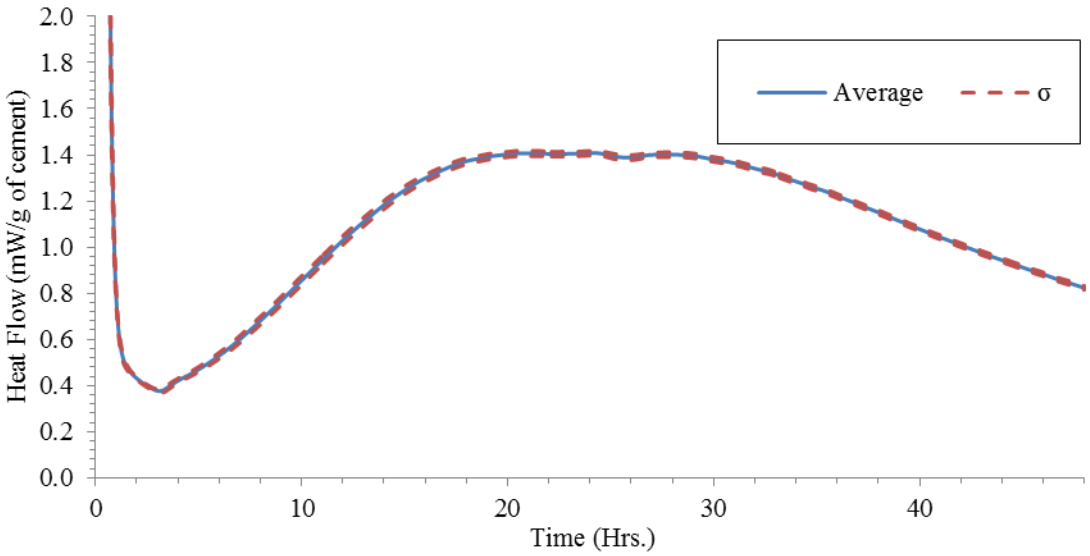


Figure 197: Heat flow of portland cement paste at 5°C isothermal

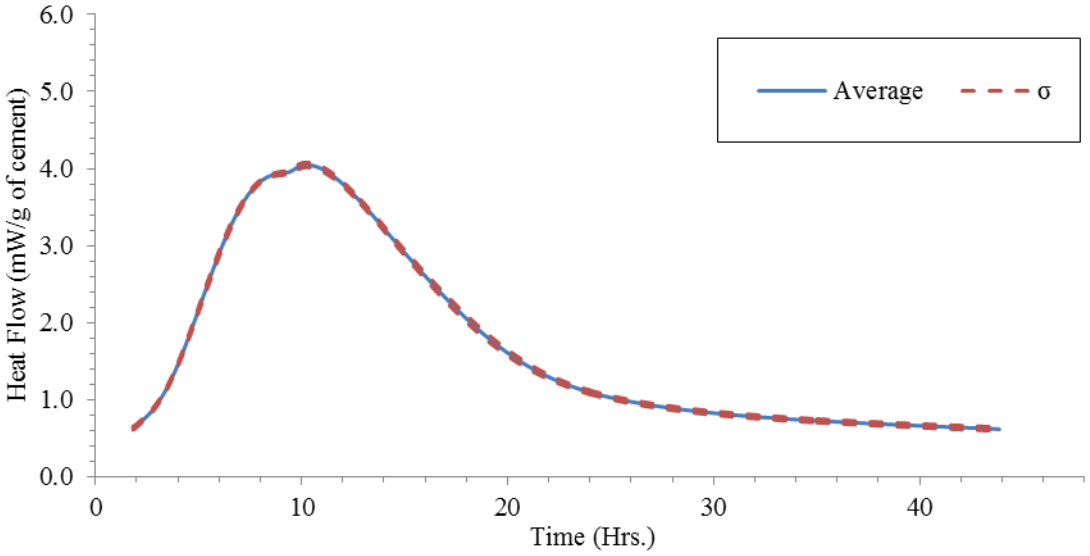


Figure 198: Heat flow of portland cement paste at 23°C isothermal

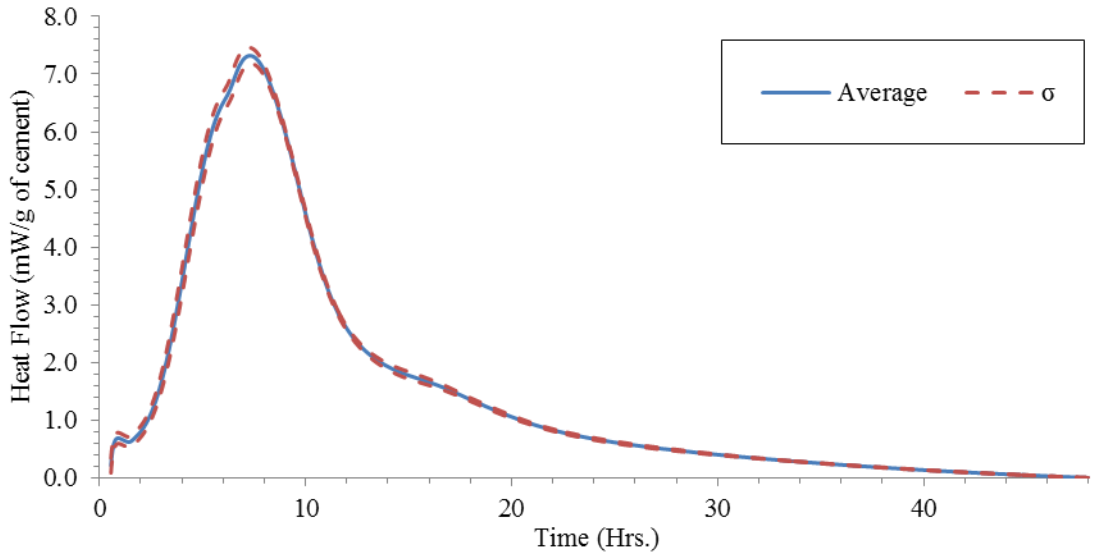


Figure 199: Heat flow of portland cement paste at 38°C isothermal

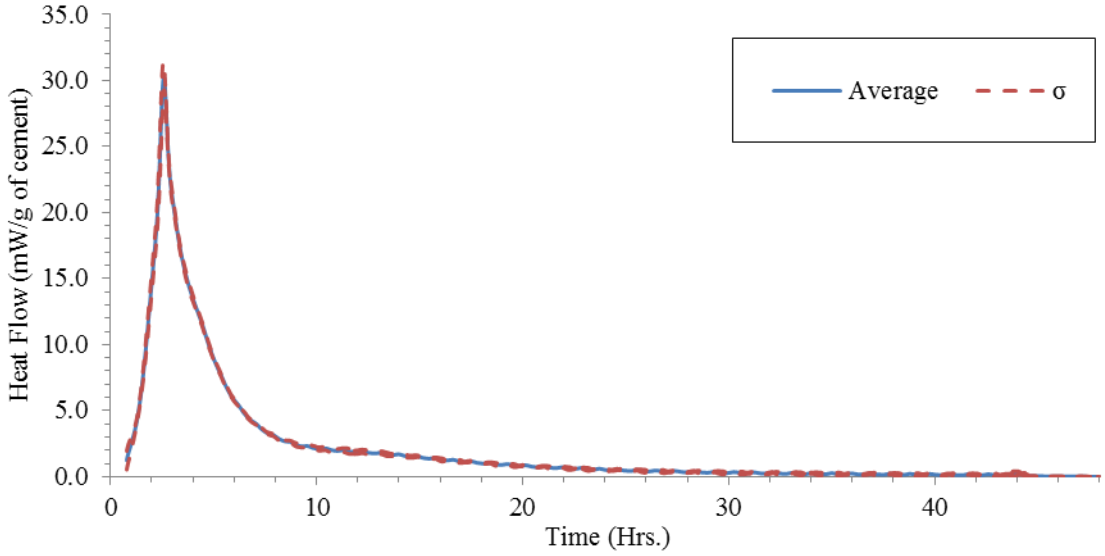


Figure 200: Heat flow of portland cement paste at 60°C isothermal

## APPENDIX B.3: INFLUENCE OF SAMPLE SIZE VARIABILITY ON PC MORTAR

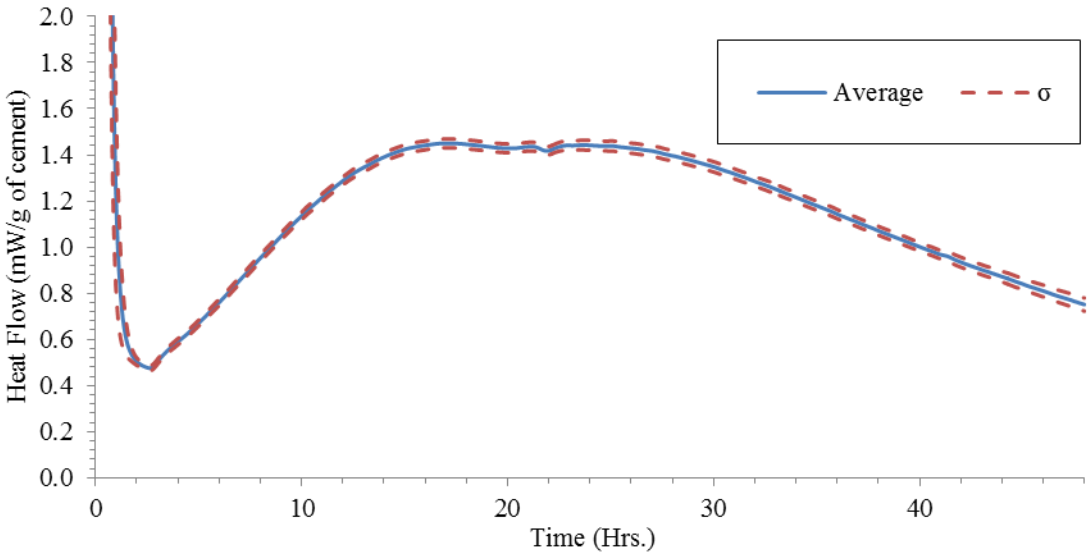


Figure 201: Heat flow of various PC mortar sample size at 5°C isothermal

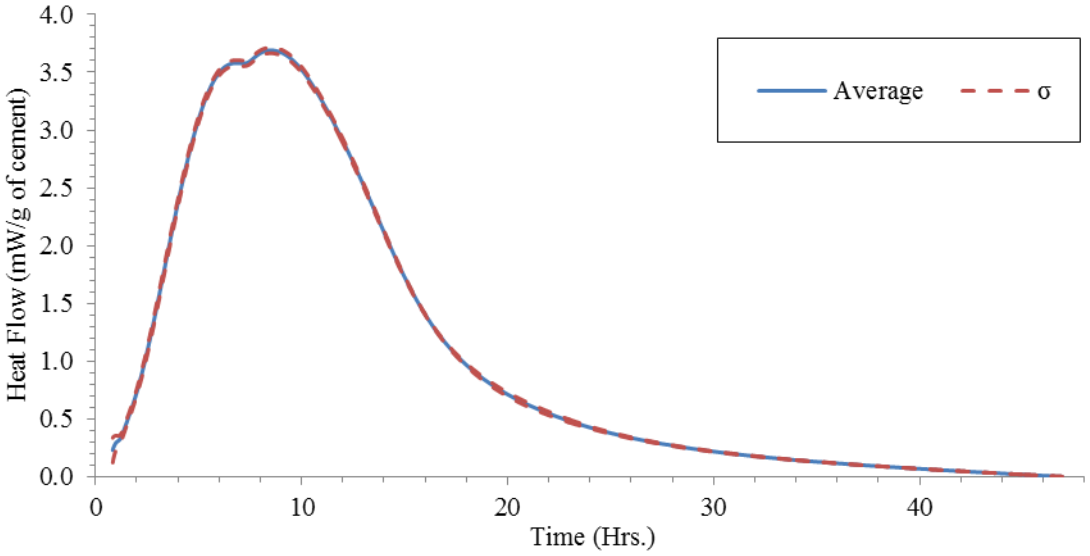


Figure 202: Heat flow of various PC mortar sample size at 23°C isothermal

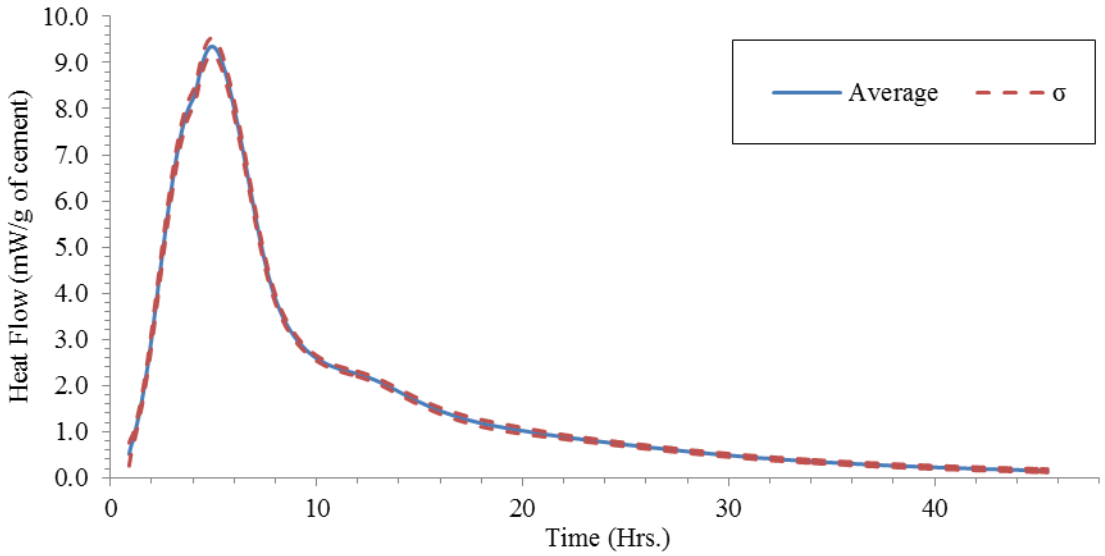


Figure 203: Heat flow of various PC mortar sample size at 38°C isothermal

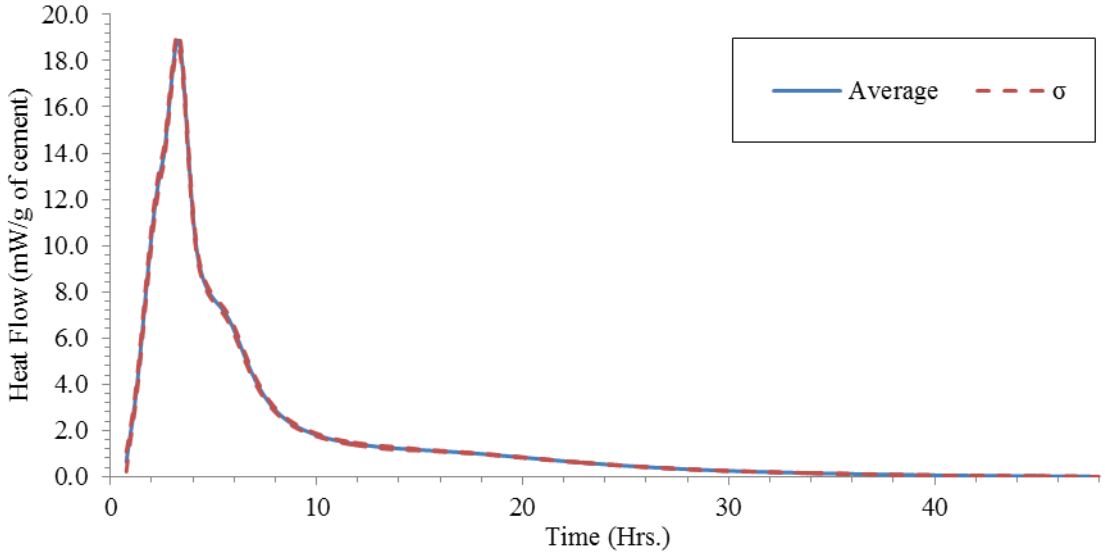


Figure 204: Heat flow of various PC mortar sample size at 60°C isothermal

## APPENDIX B.4: INFLUENCE OF SAMPLE SIZE VARIABILITY ON PC PASTE

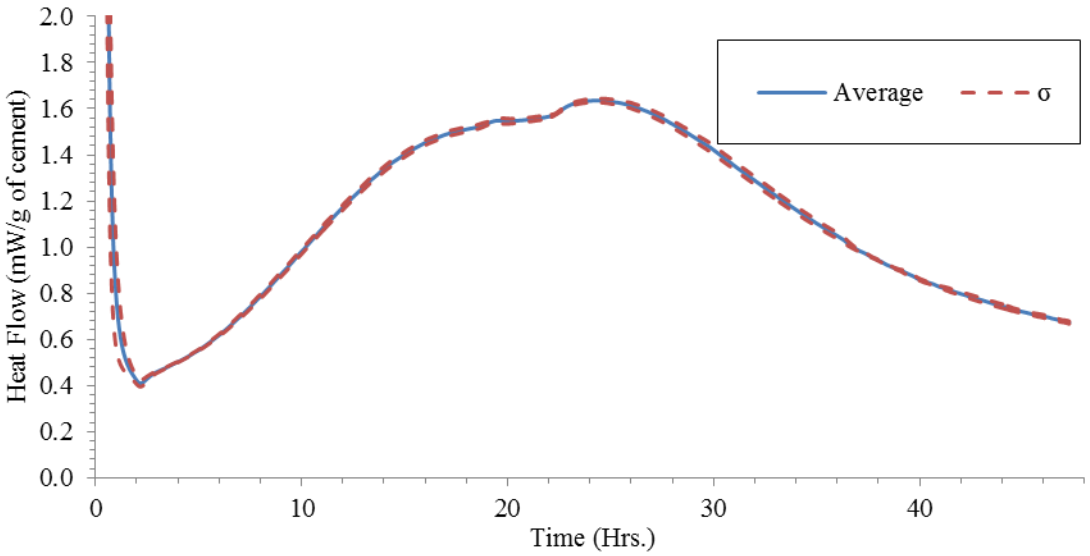


Figure 205: Heat flow of various PC paste sample size at 5°C isothermal

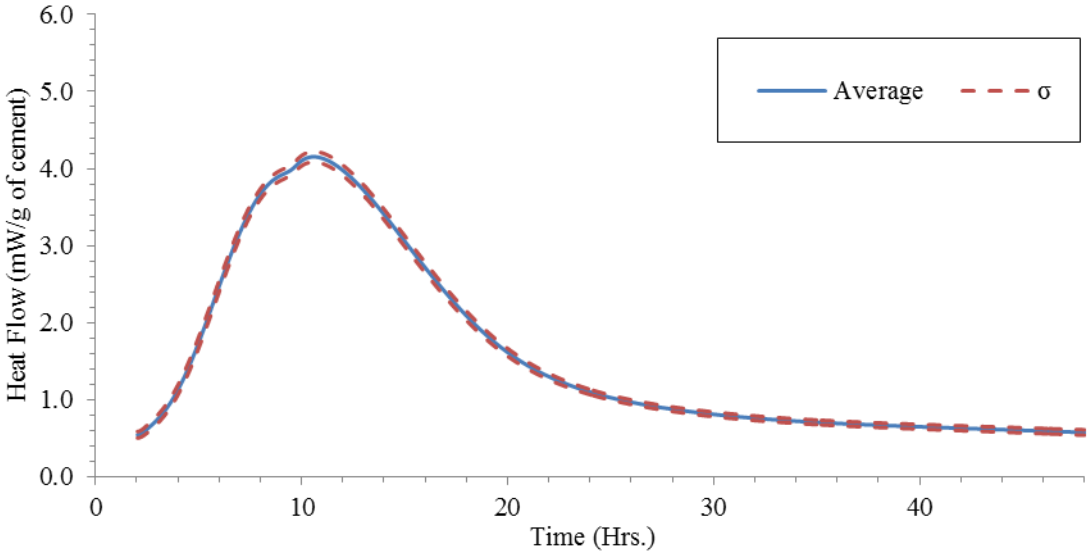


Figure 206: Heat flow of various PC paste sample size at 23°C isothermal

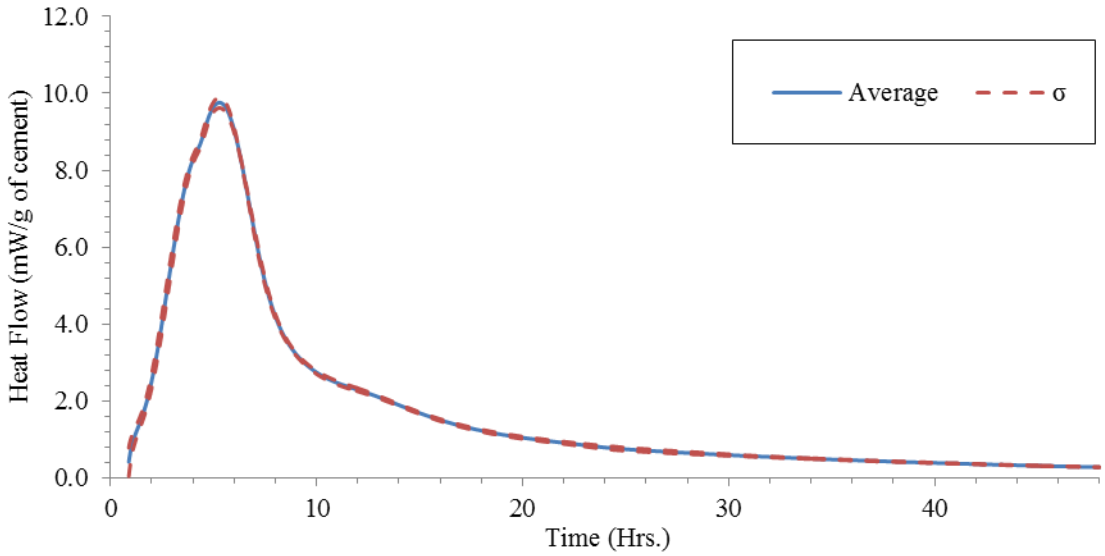


Figure 207: Heat flow of various PC paste sample size at 38°C isothermal

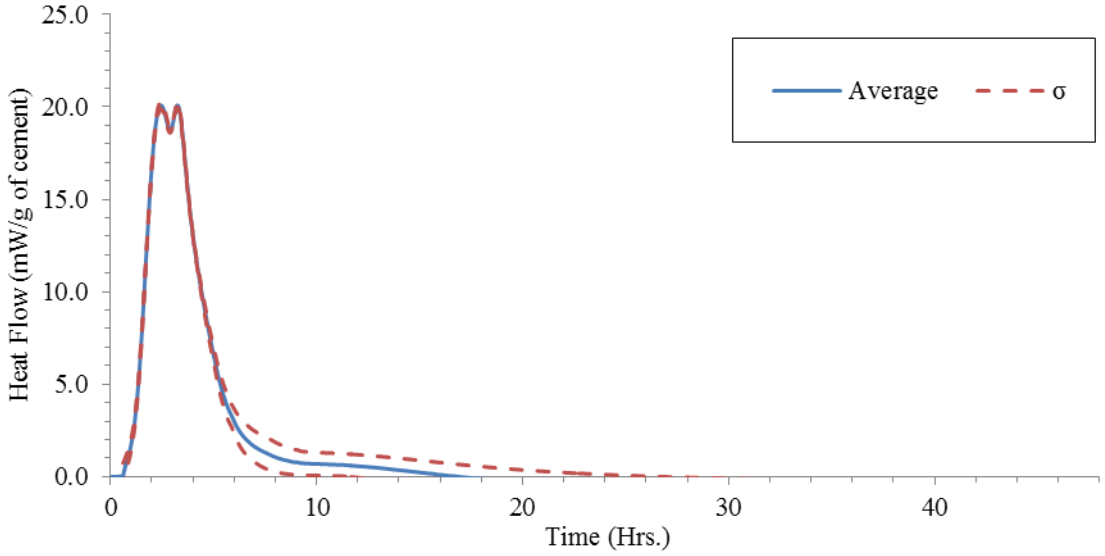


Figure 208: Heat flow of various PC paste sample size at 60°C isothermal

## APPENDIX B.5: PR-59 TEMPERATURE CONTROLLER SPECIFICATIONS

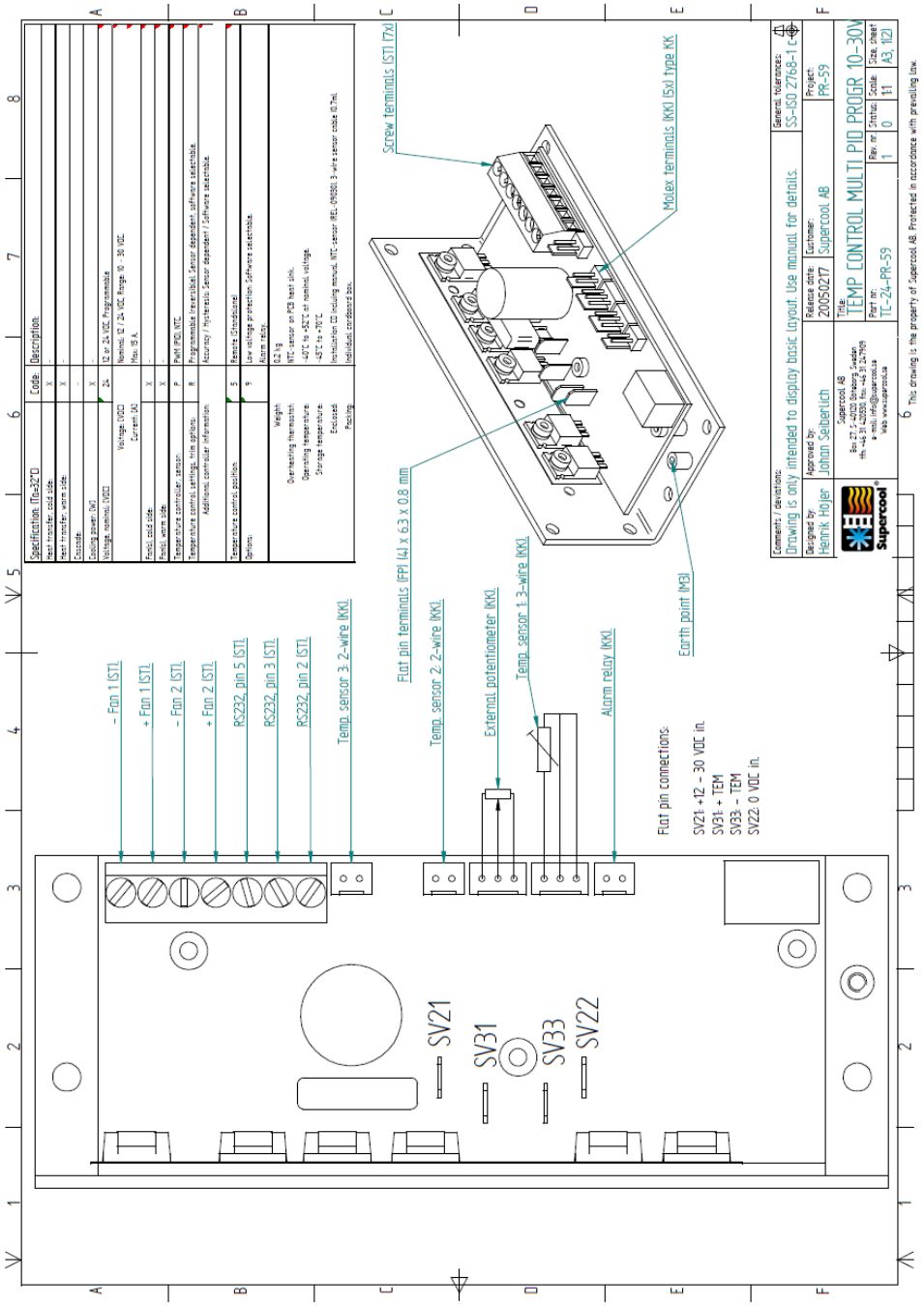


## APPENDIX B.6: THERMOELECTRIC HEATER-COOLER SPECIFICATIONS

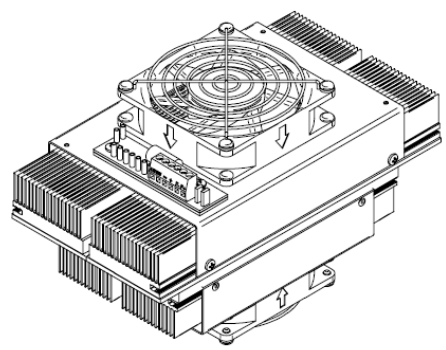

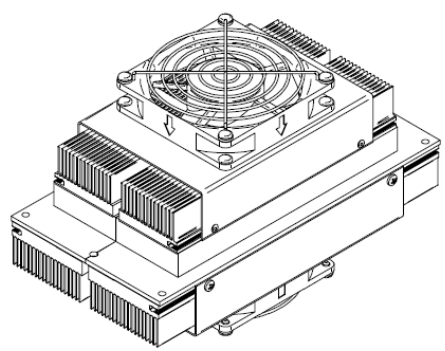

| Specification: (Ta=32°C) | Code: | Description: |
|---|---|---|
| Heat transfer, cold side: | A | Air |
| Heat transfer, warm side: | A | Air |
| Cascade: | - | |
| Cooling power: [W] | 060 | 58 W at dT=0°C. Tolerance: ±10%. |
| Voltage, nominal: [VDC] | 24 | 24 VDC. |
| TEM Voltage: [VDC] | | Nominal: 24 VDC, Max: 30 VDC. |
| TEM Current: [A] | | Nominal: 3.1 A, Initial: 3.9 A. All at dT=0°C. Tolerance: ±10%. |
| Fan(s), cold side: | 2 | MTBF: 52,000 hrs. L10 at 25°C. Nominal current: 0.14 A. Voltage: 24 VDC ±10%. |
| Fan(s), warm side: | 2 | MTBF: 50,000 hrs. L10 at 25°C. Nominal current: 0.21 A. Voltage: 24 VDC ±10%. |
| Temperature controller, sensor: | 0 | None. |
| Temperature control settings, trim options: | 0 | - |
| Additional controller information: | | - |
| Temperature control position: | 0 | - |
| Options: | 0 | - |
| Weight: | | 2.5 kg |
| Overheating thermostat: | | 75°C ±5°C on hot side heat sink surface. |
| Operating temperature: | | -10°C to +51°C at nominal voltage. |
| TE-Module(s) temperature specification: | | Max. surface temperature: 80°C. |
| Enclosed: | | - |
| Packing: | | Individual cardboard box. |

Mounting hole print: 182x105

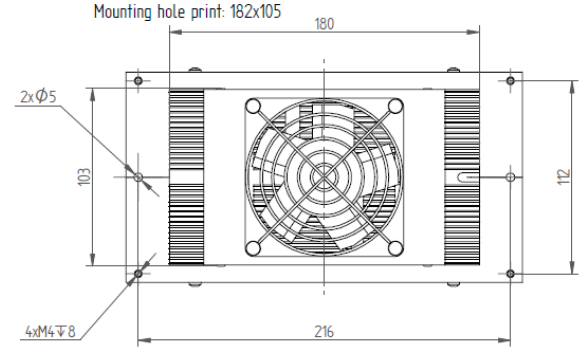


| | | | | |
|---|---|---|---|---|
| Comments / deviations: Heat sinks and, if applicable, D-plates and shrouds in anodised aluminium. | | | | General tolerances: SS-ISO 2768-1 c |
| Designed by: Pavel Cech | Approved by: Henrik Höjer | Release date: 20041028 | Customer: Supercool AB | Project: HDPC |
| Supercool® | Supercool AB<br>Box 27, S-40120 Göteborg, Sweden<br>tfn. +46 31 420530, fax. +46 31 247909<br>e-mail: info@supercool.se<br>Web: www.supercool.se | Title: TE ASSEMBLY 24VDC AIR – AIR | | |
| | | Part nr: AA-060-24-22-00-00 | Rev. nr: 4 | Status: 0 | Scale: 1:2 | Size, sheet A3, 1(3) |

This drawing is the property of Supercool AB. Protected in accordance with prevailing law.

## APPENDIX B.7: INFLUENCE OF SAMPLE SIZE VARIABILITY ON CAC MORTAR

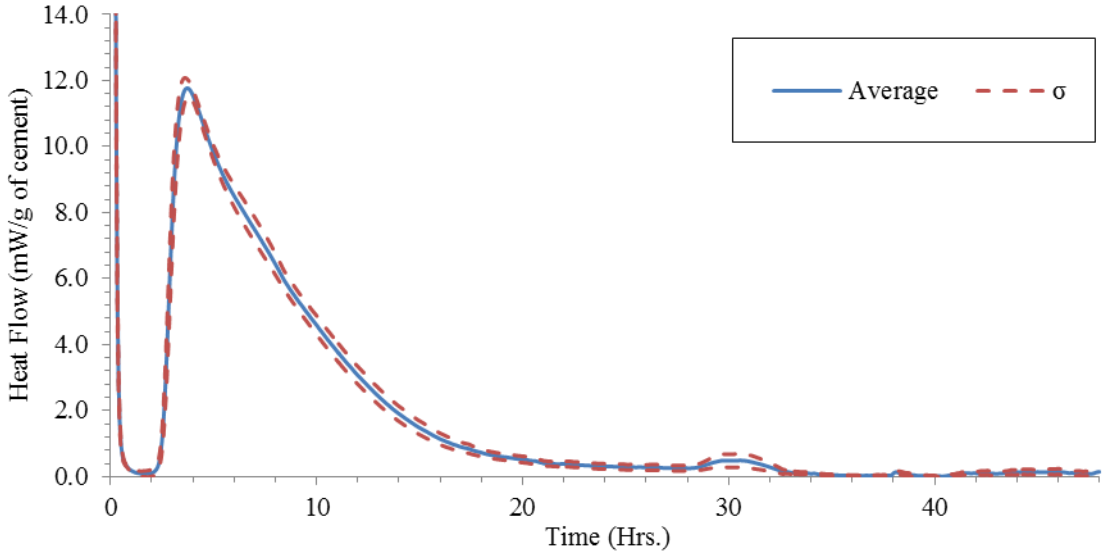


Figure 209: Heat flow of various CAC mortar sample size at 5°C isothermal

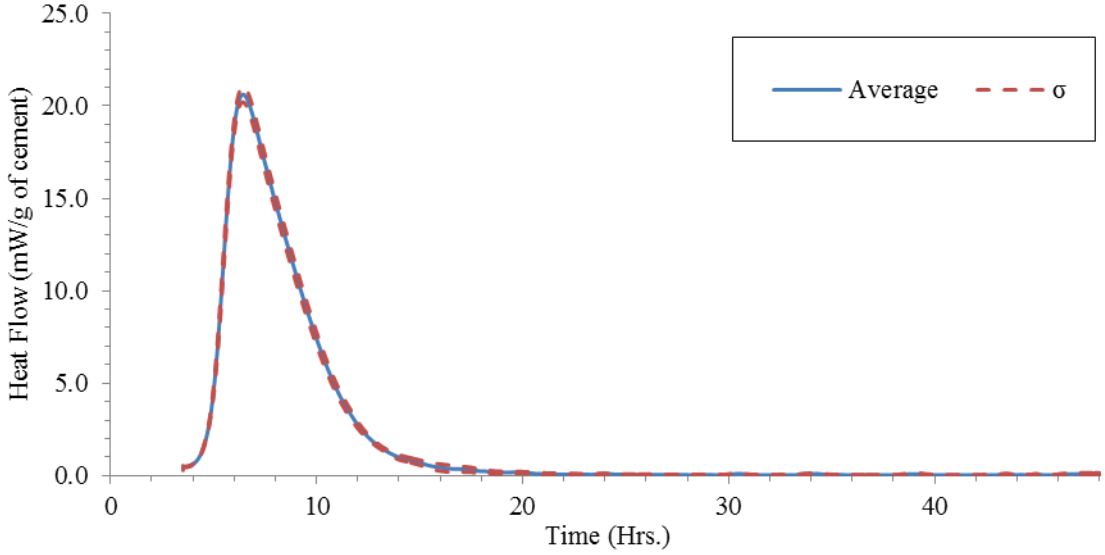


Figure 210: Heat flow of various CAC mortar sample size at 23°C isothermal

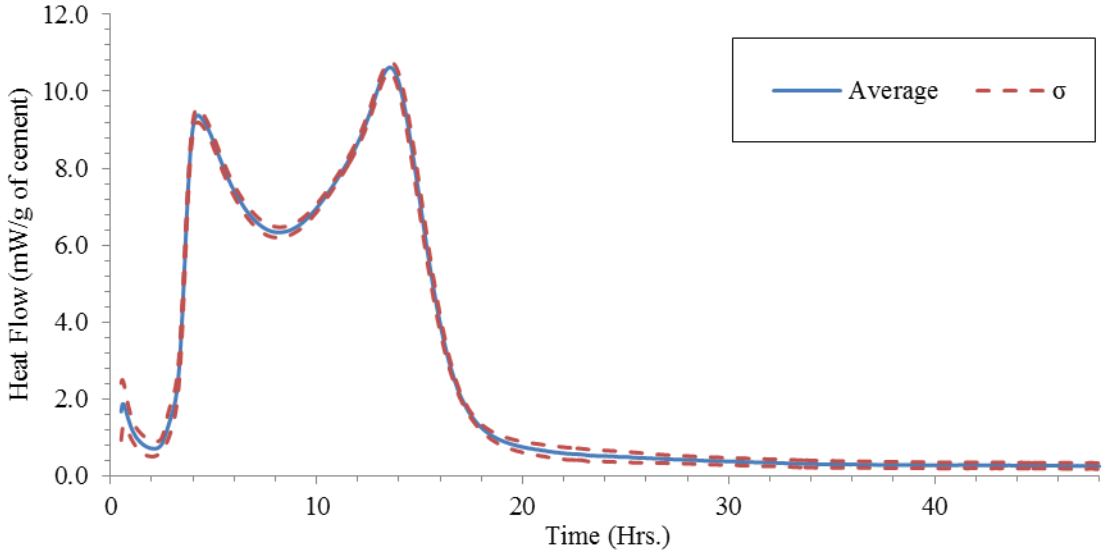


Figure 211: Heat flow of various CAC mortar sample size at 38°C isothermal

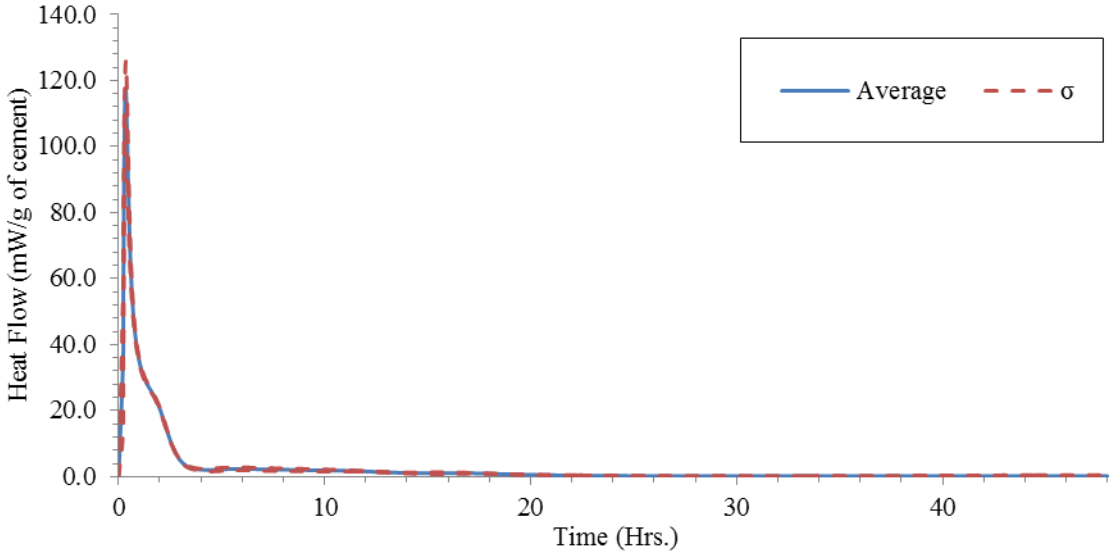


Figure 212: Heat flow of various CAC mortar sample size at 60°C isothermal

## APPENDIX B.8: INFLUENCE OF SAMPLE SIZE VARIABILITY ON CAC PASTE

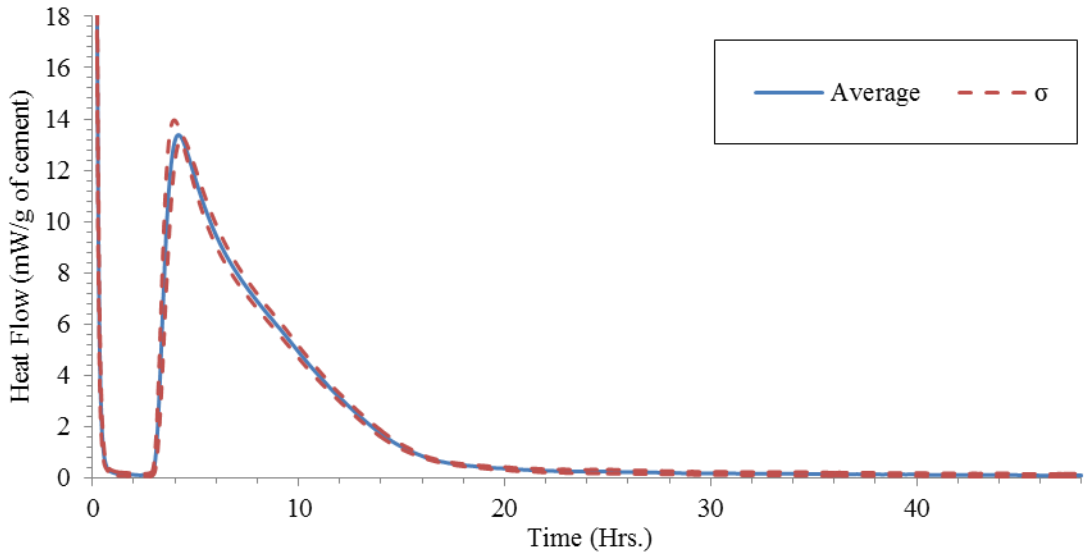


Figure 213: Heat flow of various CAC paste sample size at 5°C isothermal

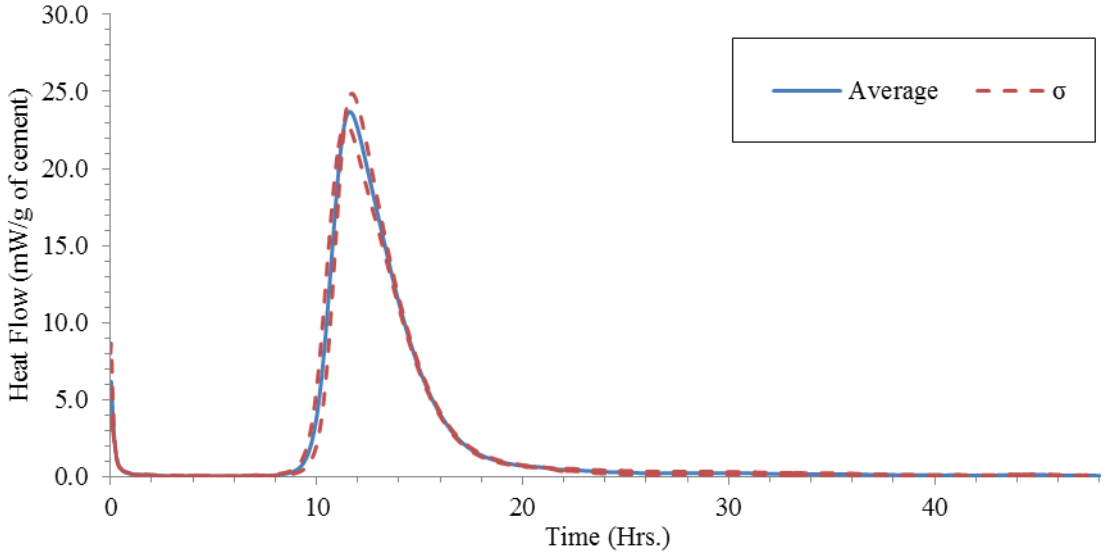


Figure 214: Heat flow of various CAC paste sample size at 23°C isothermal

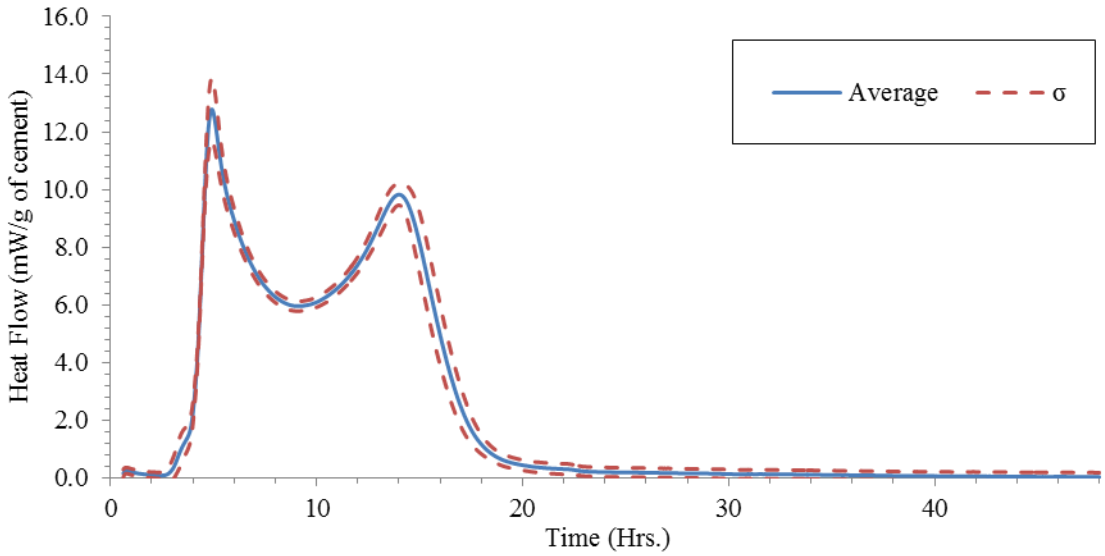


Figure 215: Heat flow of various CAC paste sample size at 38°C isothermal

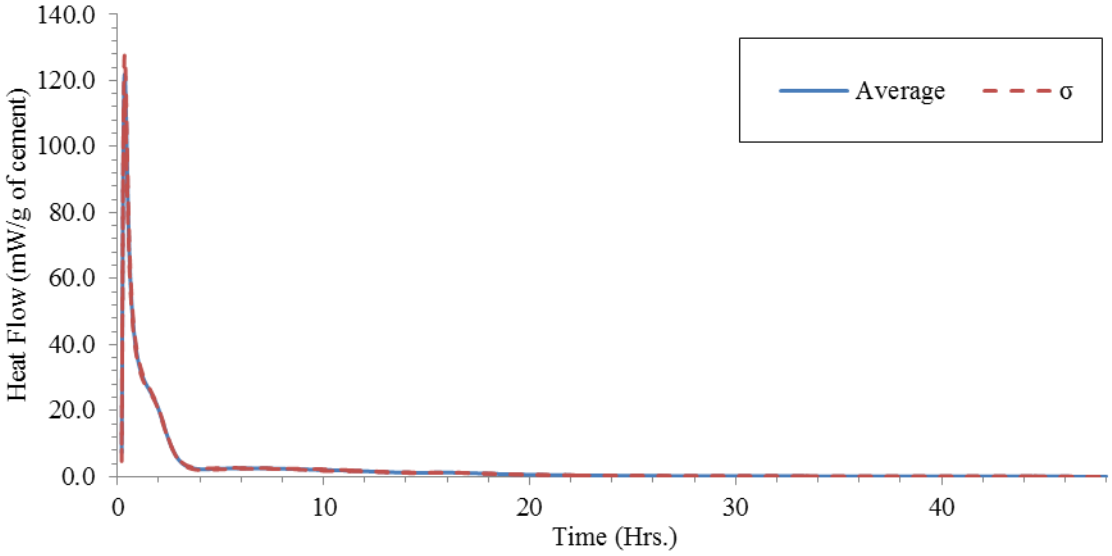


Figure 216: Heat flow of various CAC paste sample size at 60°C isothermal

## APPENDIX B.9: REPEATABILITY OF CAC MORTAR

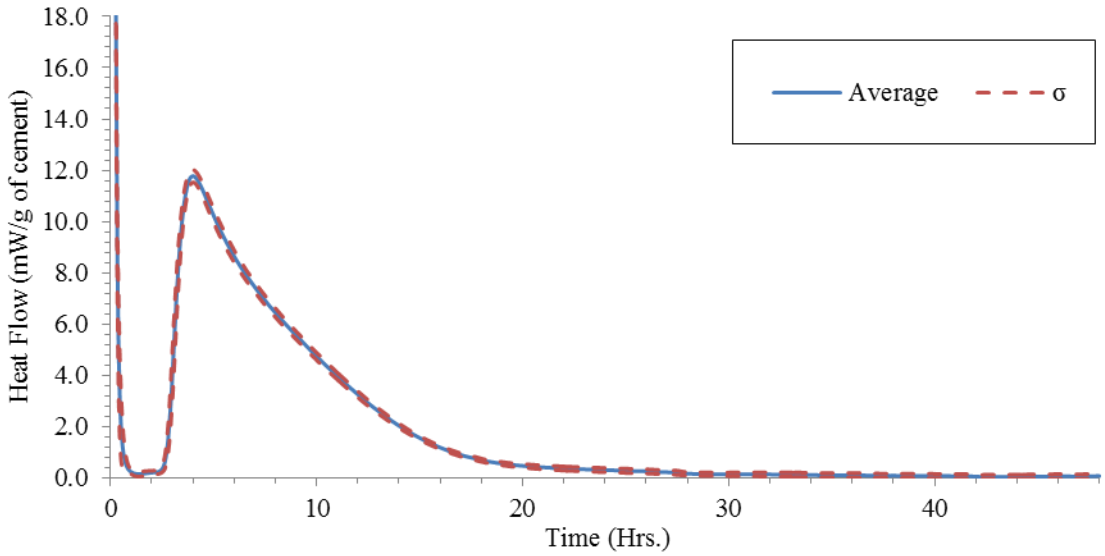


Figure 217: Heat flow of CAC mortar size at 5°C isothermal

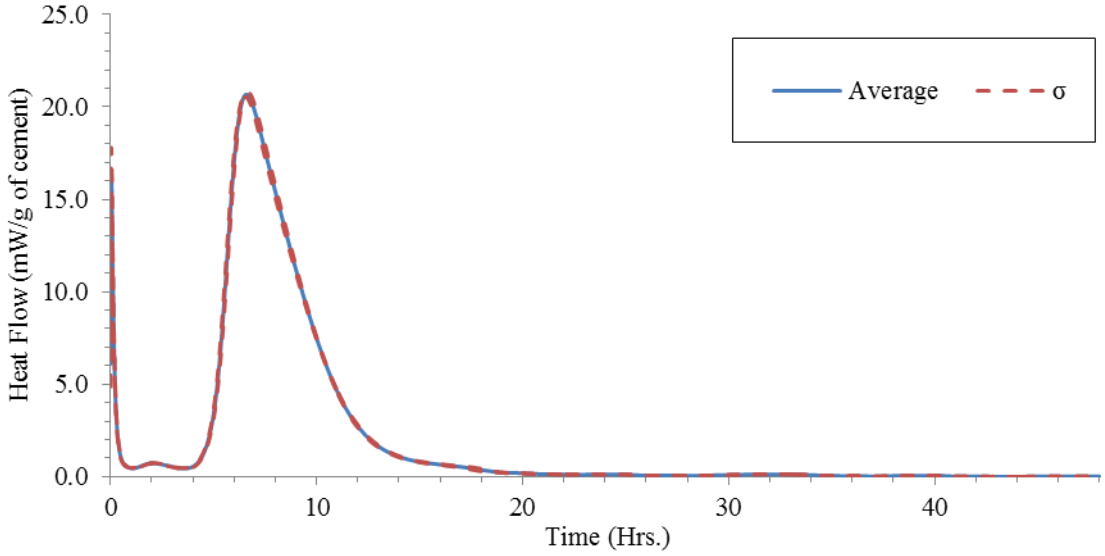


Figure 218: Heat flow of CAC mortar size at 23°C isothermal

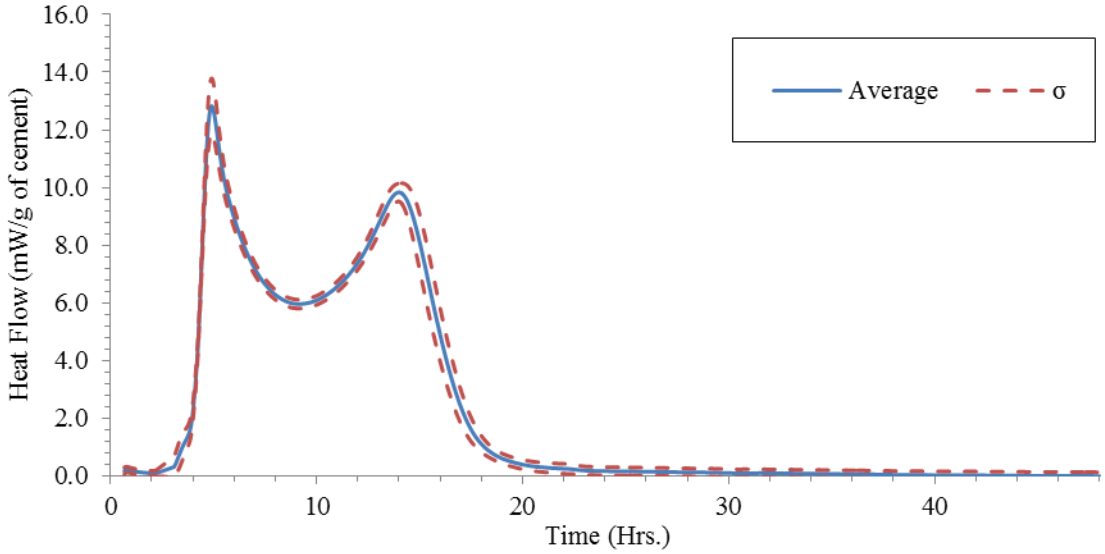


Figure 219: Heat flow of CAC mortar size at 38°C isothermal

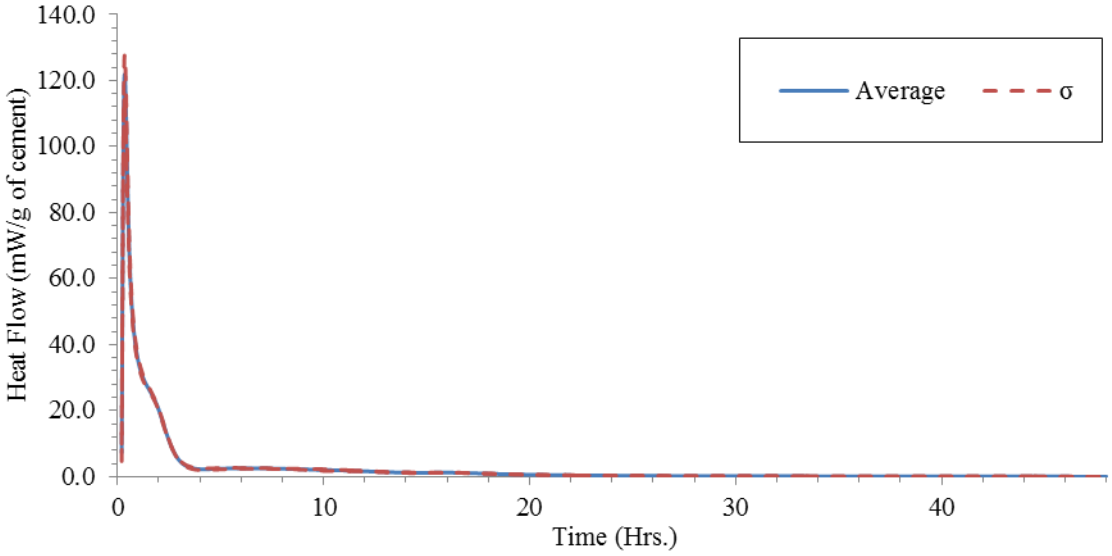


Figure 220: Heat flow of CAC mortar size at 60°C isothermal

## APPENDIX B.10: REPEATABILITY OF CAC PASTE

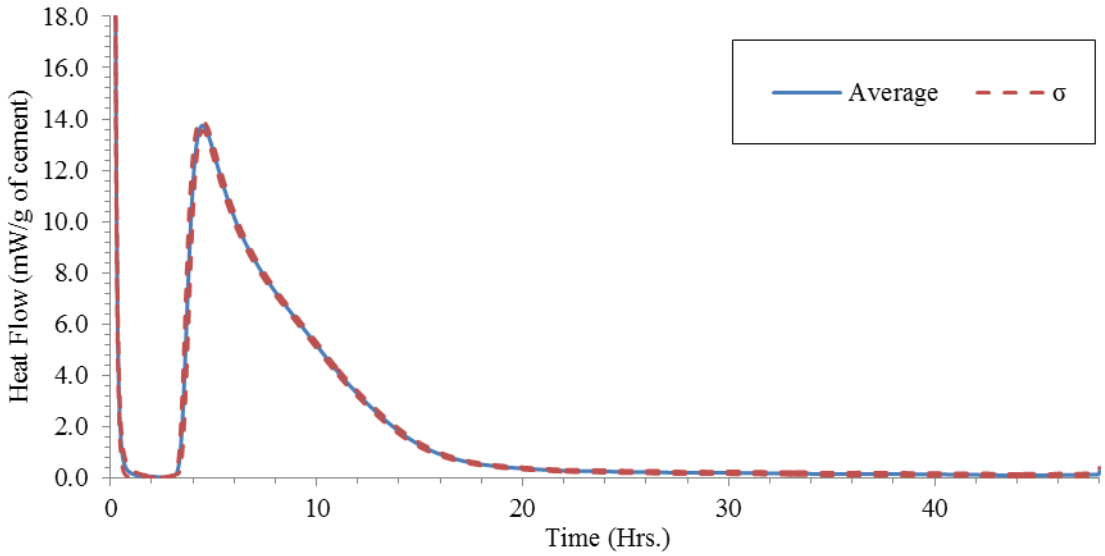


Figure 221: Heat flow of CAC paste size at 5°C isothermal

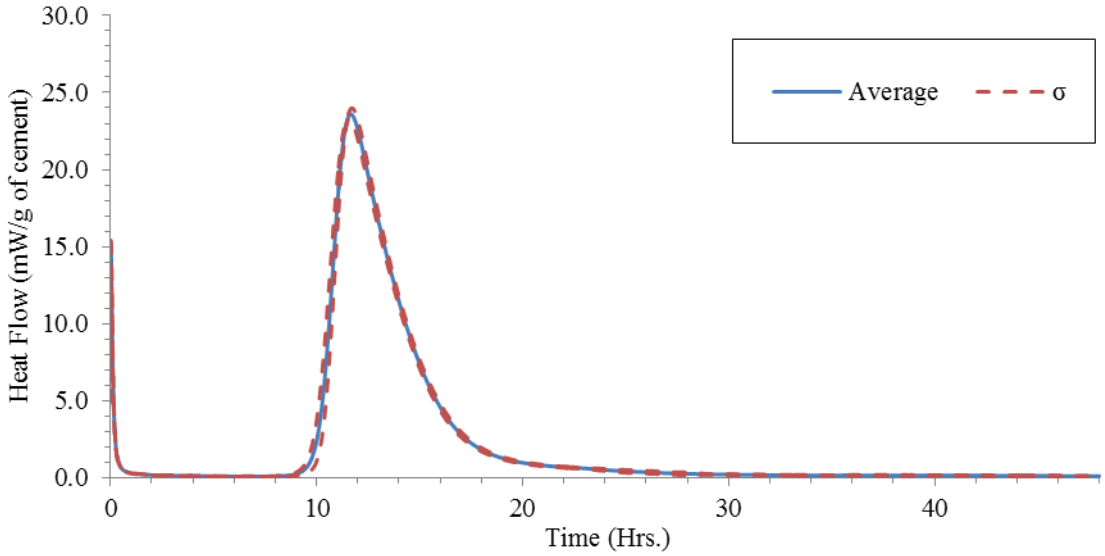


Figure 222: Heat flow of CAC paste size at 23°C isothermal

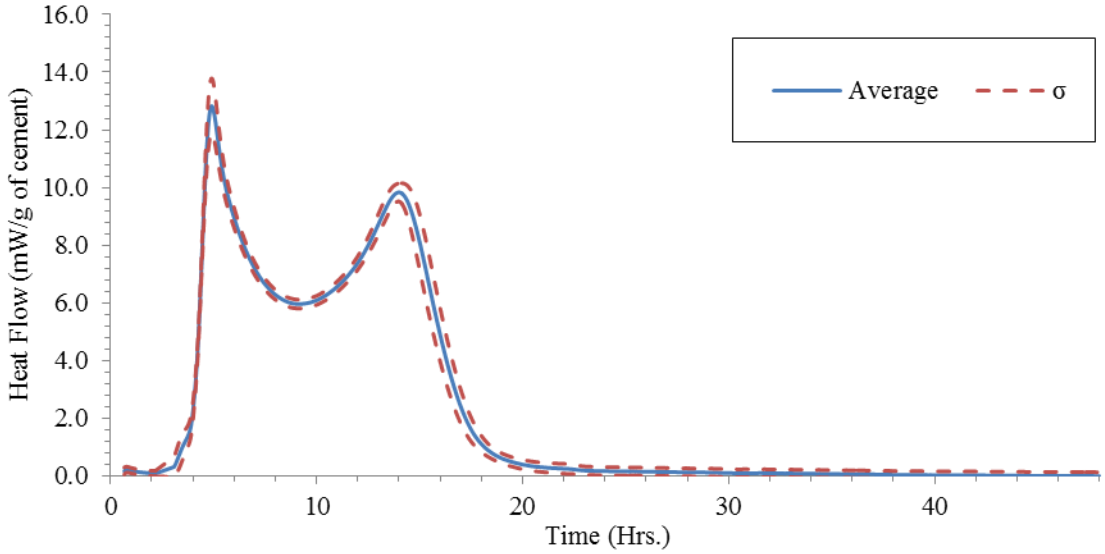


Figure 223: Heat flow of CAC paste size at 38°C isothermal

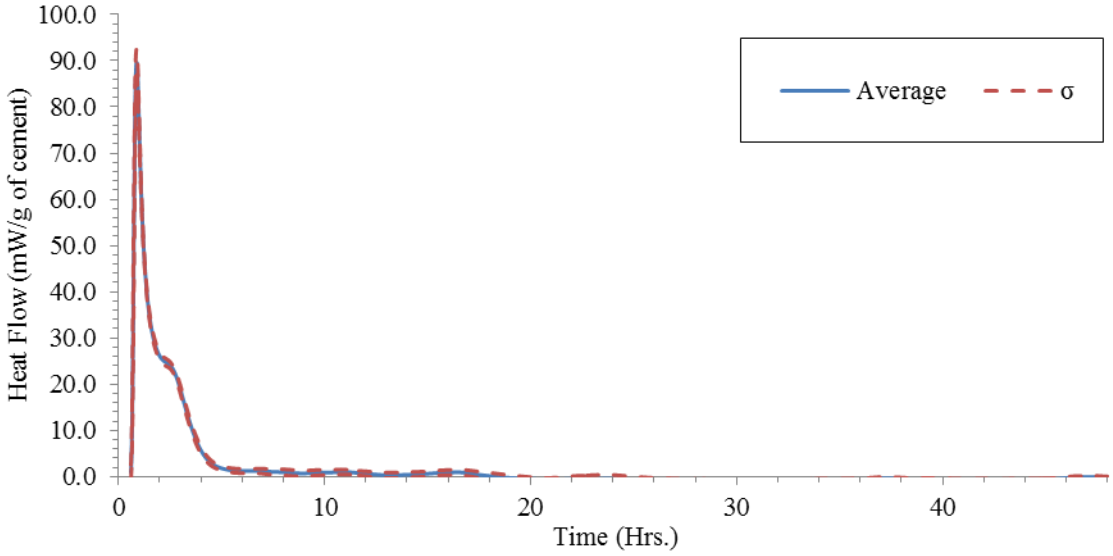


Figure 224: Heat flow of CAC paste size at 60°C isothermal

# Appendix C: Hydration and Early-age Volume Deformation of TCAC systems

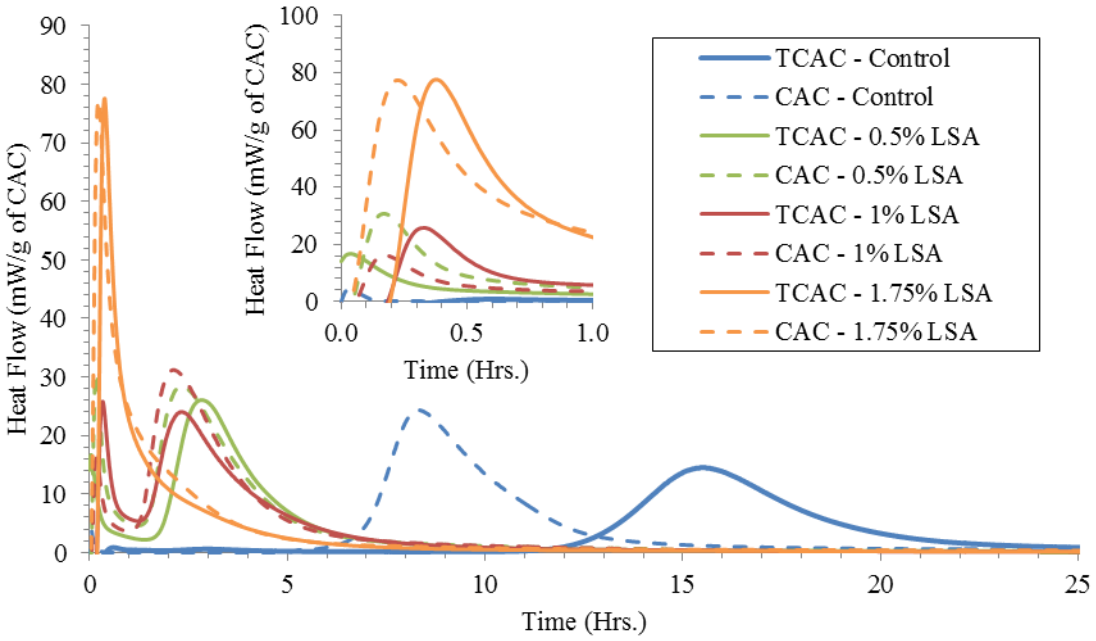


Figure 225: Heat flow of TCAC hydrated at 20°C for varying LSA dosages

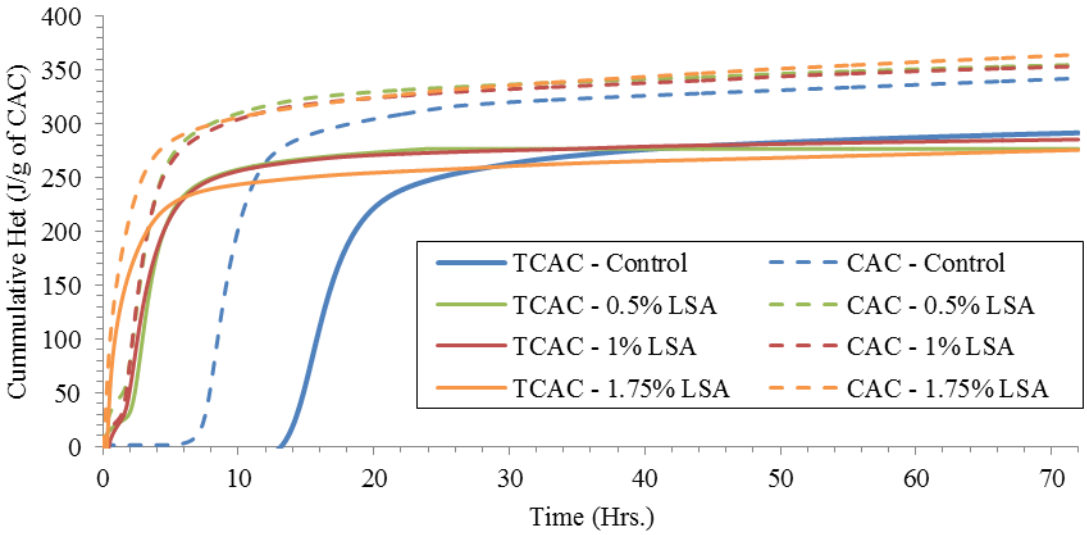


Figure 226: Cumulative heat release of TCAC hydrated at 20°C for varying LSA dosages

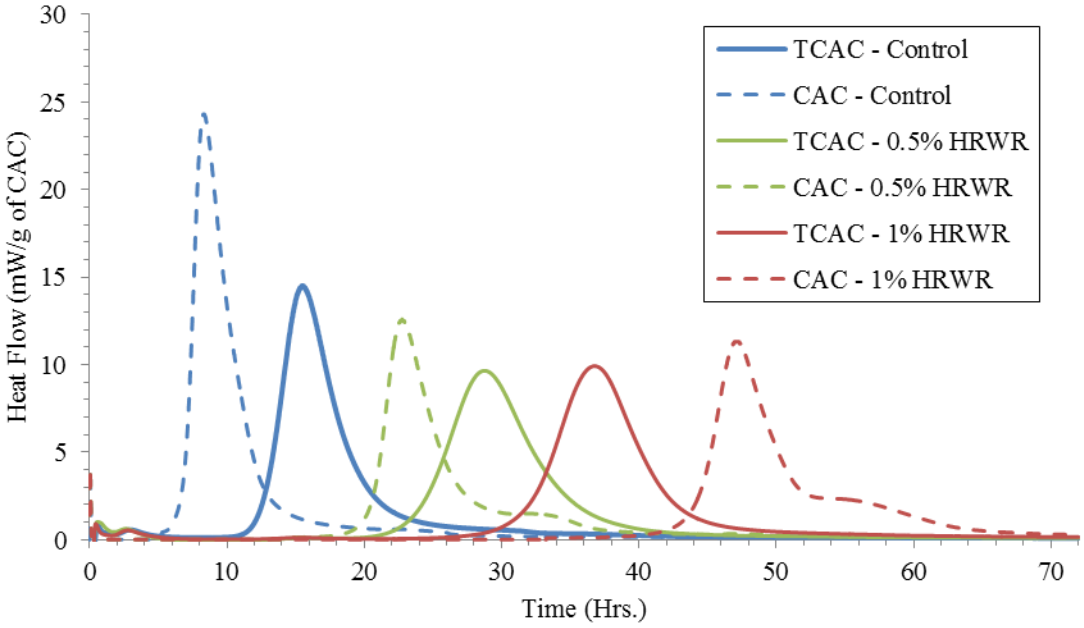


Figure 227: Heat flow of TCAC hydrated at 20°C for varying HRWR dosages

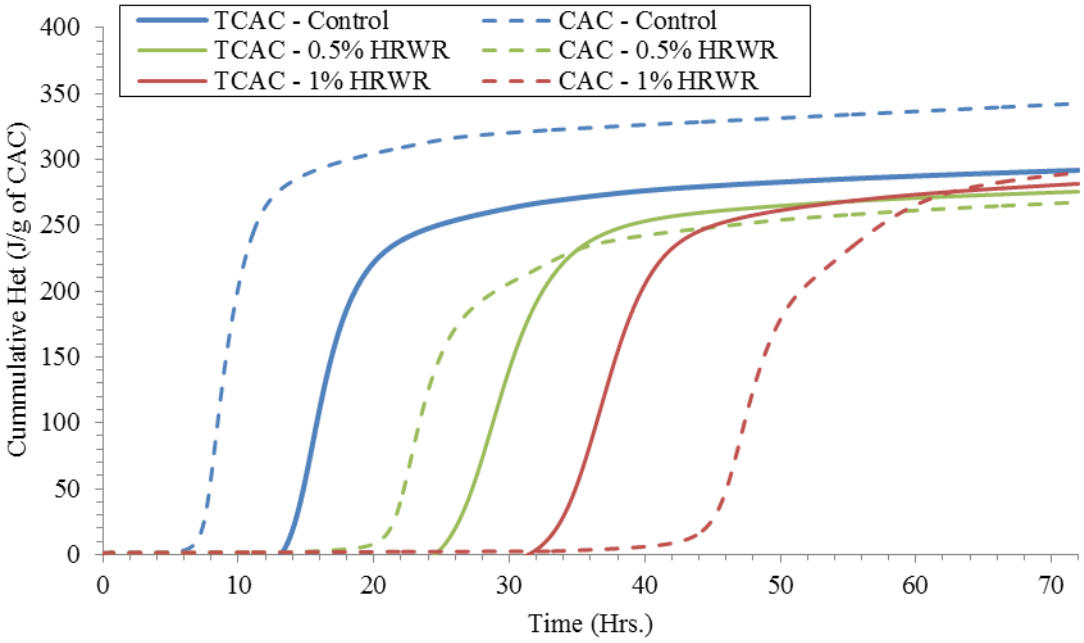


Figure 228: Cumulative heat release of TCAC hydrated at 20°C for varying HRWR dosages

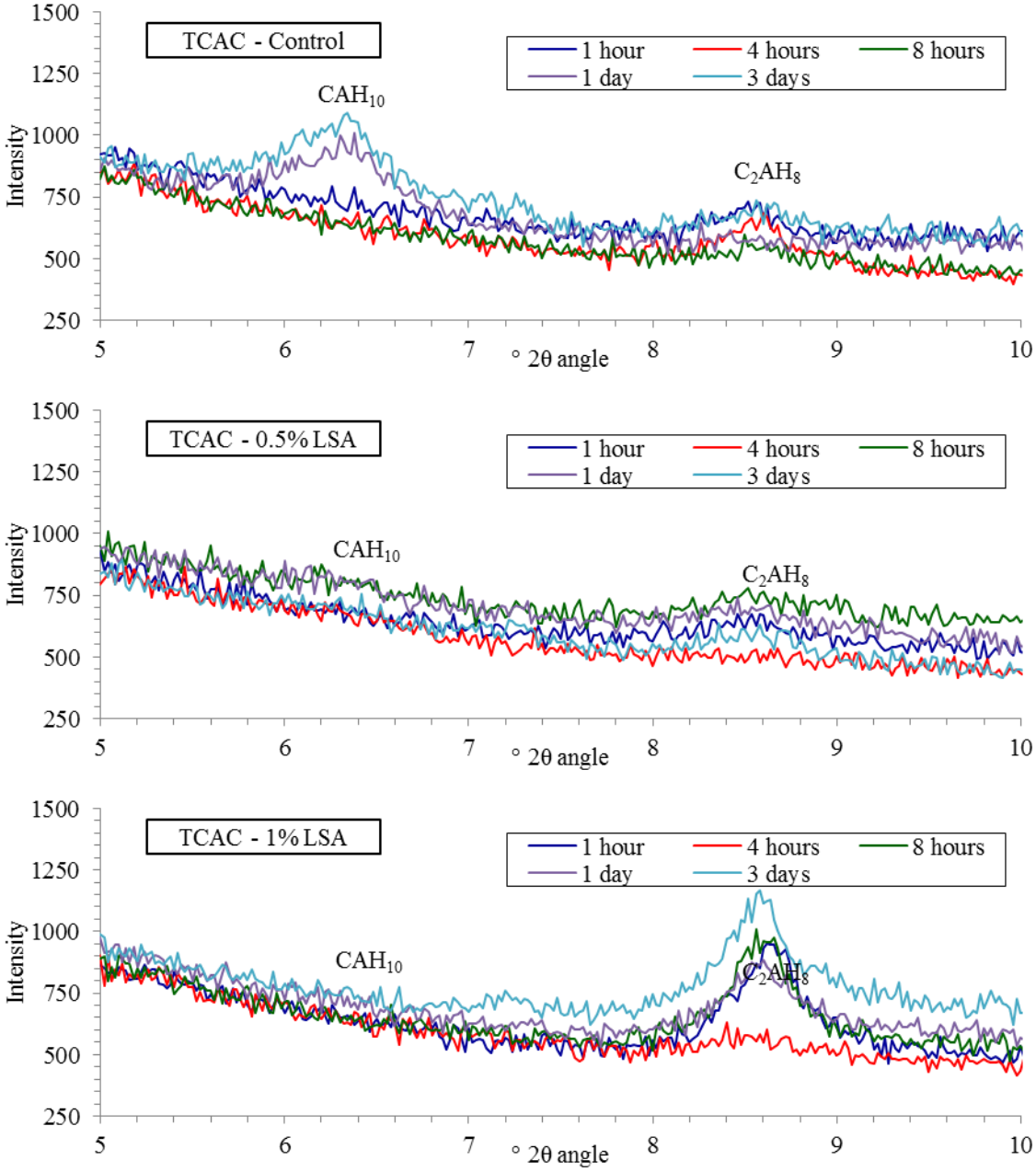


Figure 229: Qualitative XRD of TCAC with LSA hydrated at 20°C, illustrating the formation of $CAH_{10}$ and $C_2AH_8$

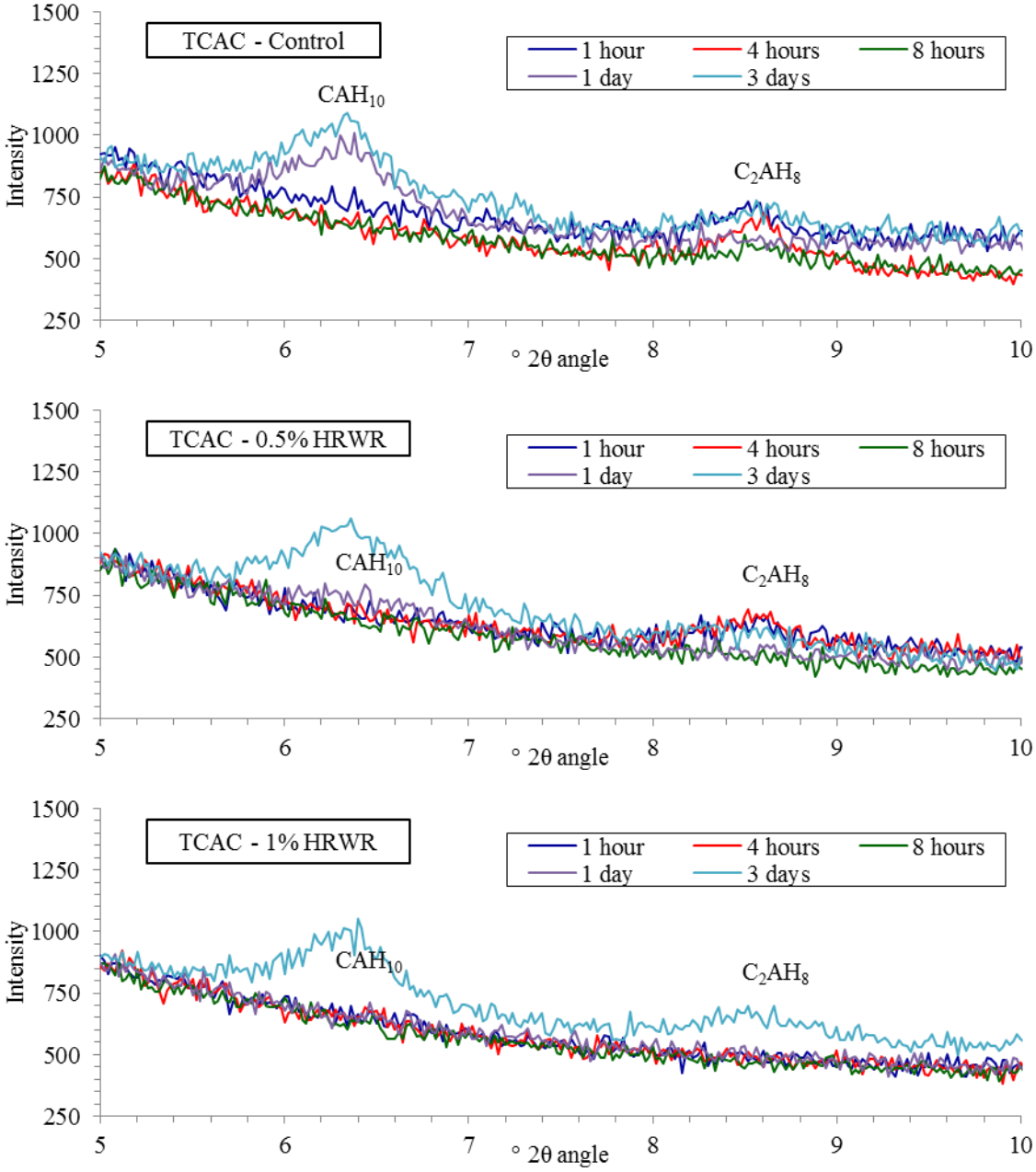


Figure 230: Qualitative XRD of TCAC with HRWR hydrated at 20°C, illustrating the formation of $CAH_{10}$ and $C_2AH_8$

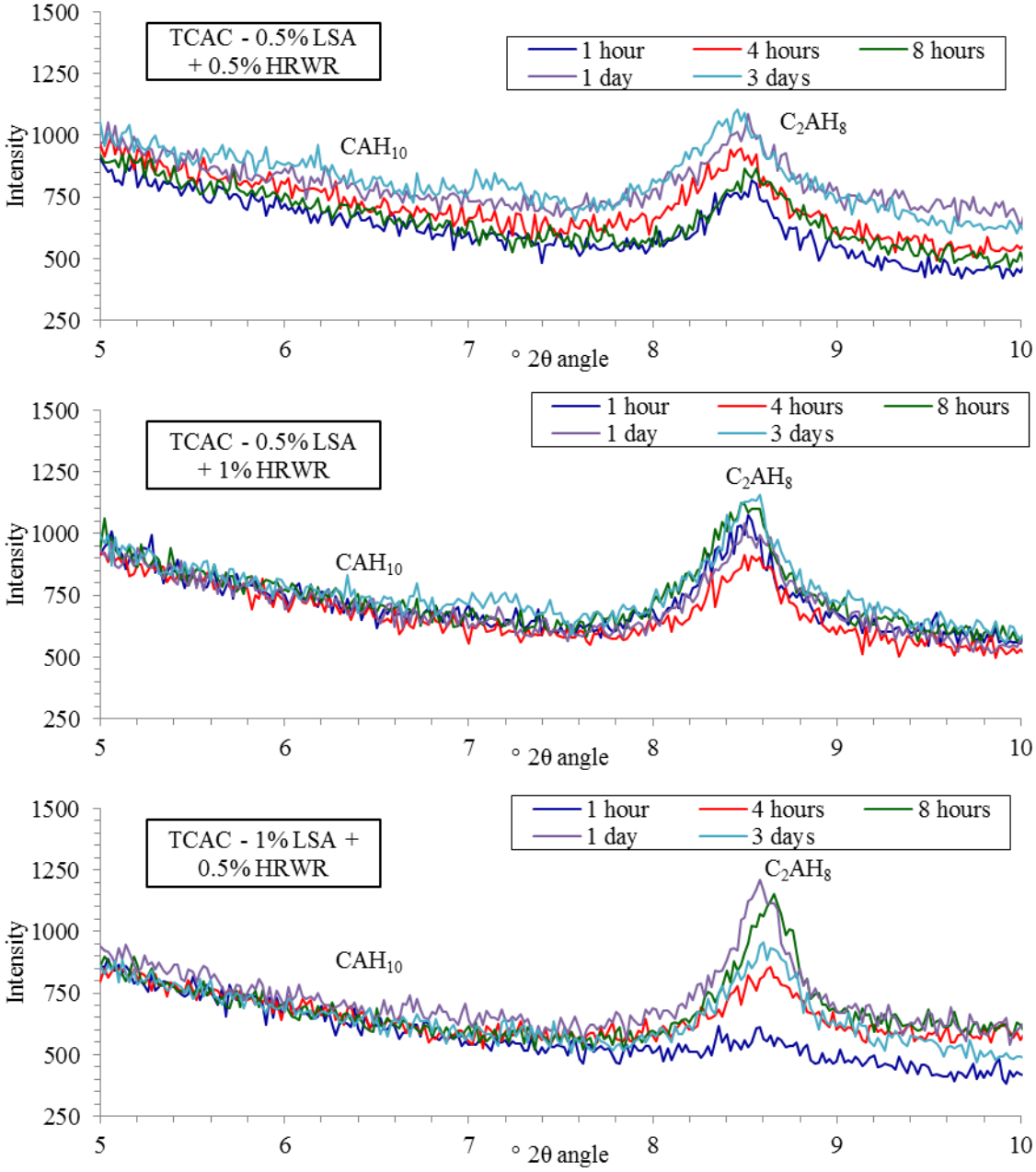


Figure 231: Qualitative XRD of TCAC with LSA and HRWR hydrated at 20°C, illustrating the formation of $CAH_{10}$ and $C_2AH_8$

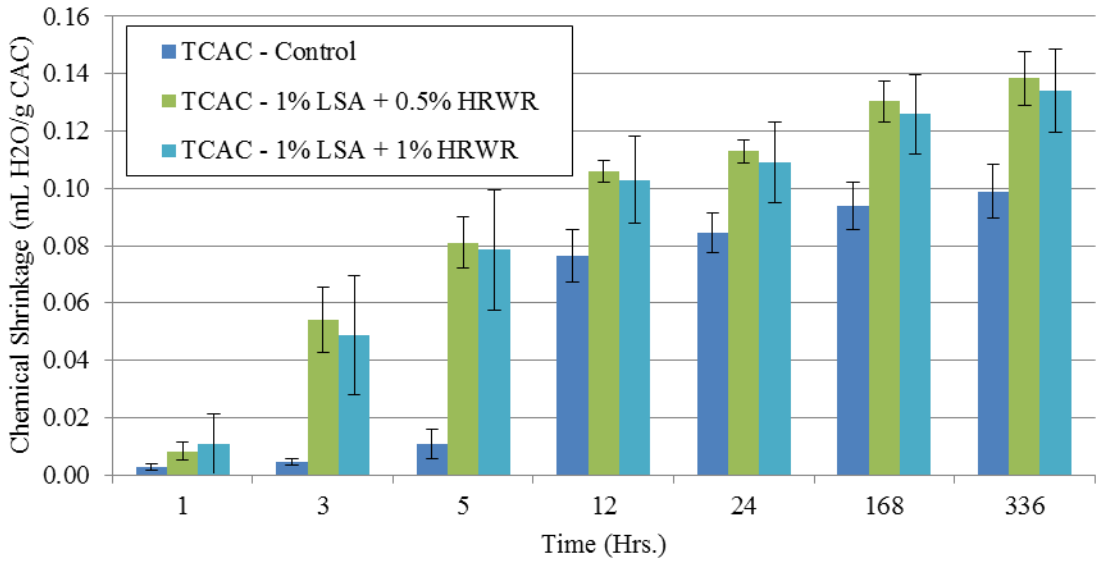


Figure 232: Chemical shrinkage with standard deviation for TCAC with varying dosages of LSA and HRWR at 20°C

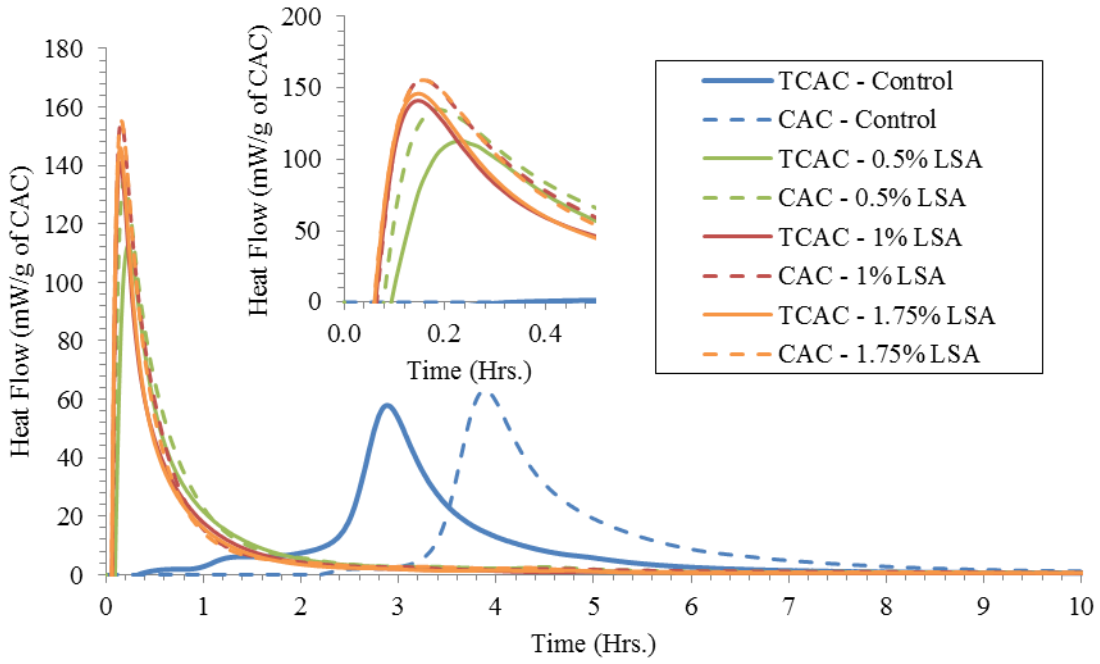


Figure 233: Heat flow of TCAC hydrated at 38°C for varying LSA dosages

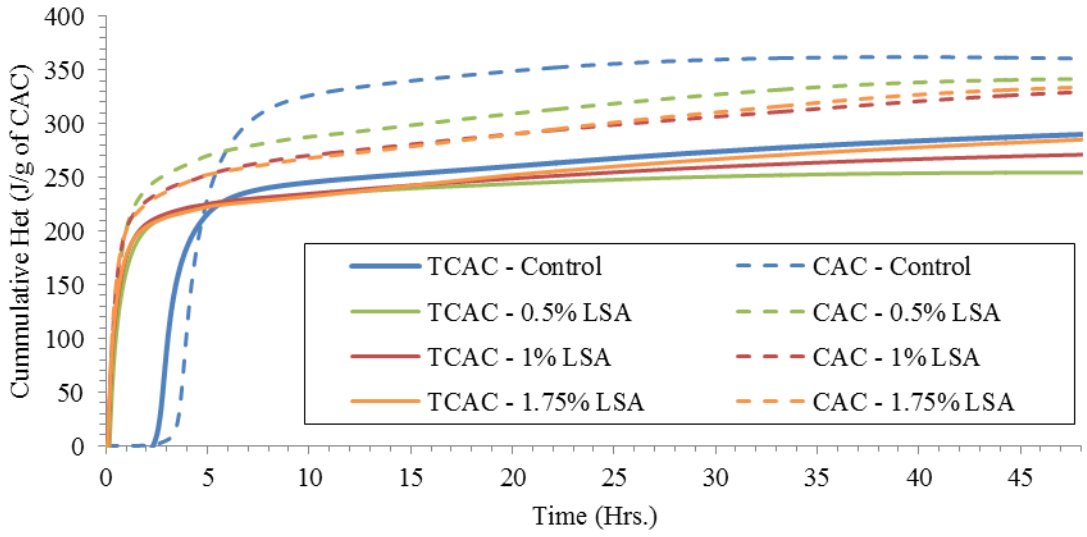


Figure 234: Cumulative heat release of TCAC hydrated at 38°C for varying LSA dosages

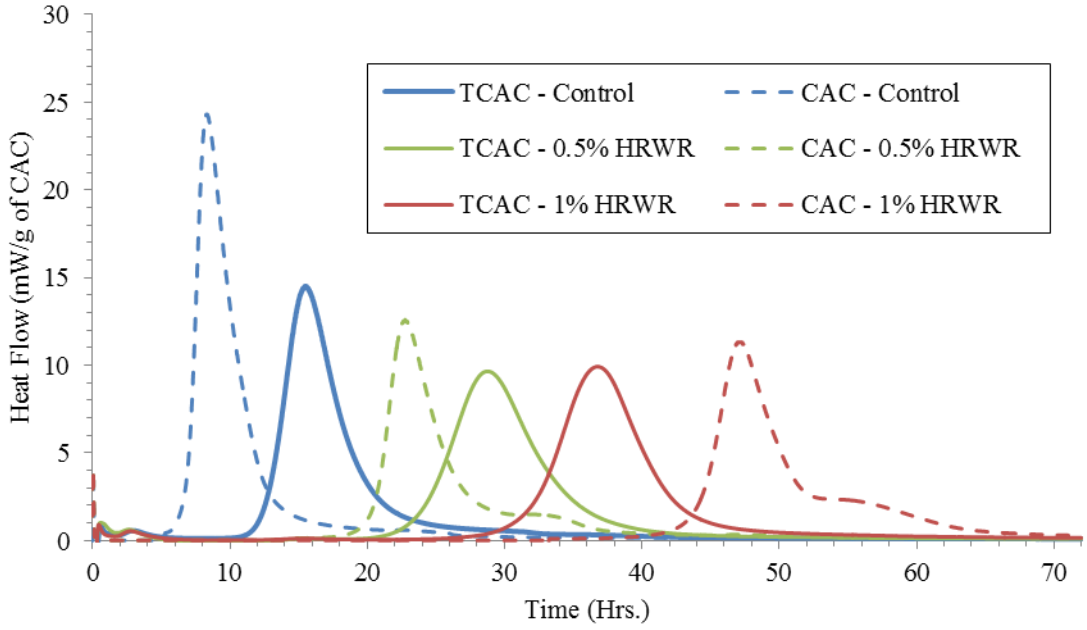


Figure 235: Heat flow of TCAC hydrated at 38°C for varying HRWR dosages

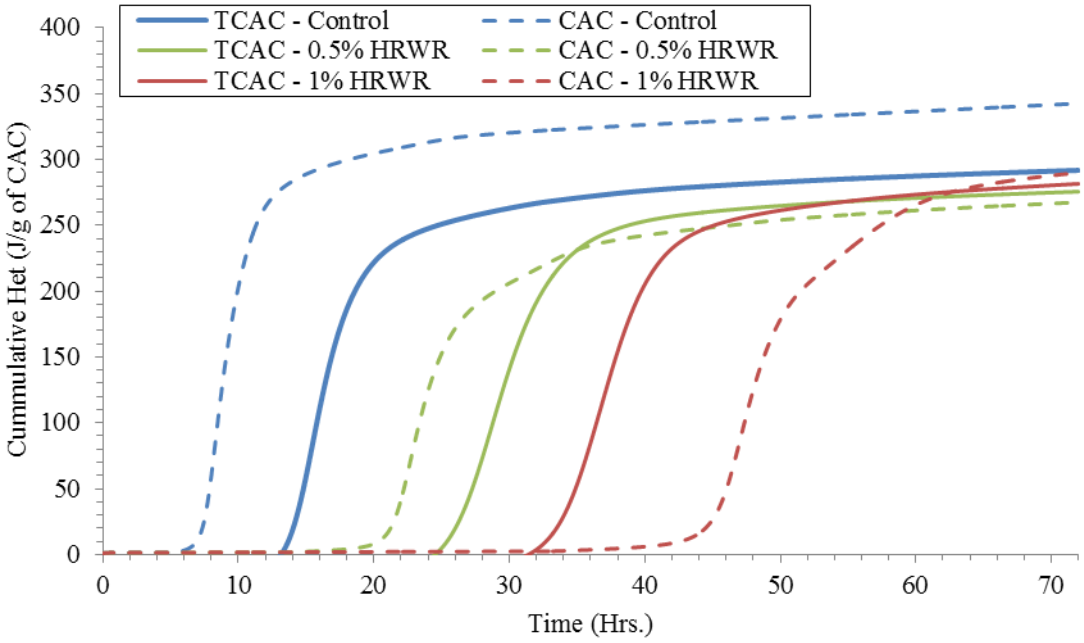


Figure 236: Cumulative heat release of TCAC hydrated at 38°C for varying HRWR dosages

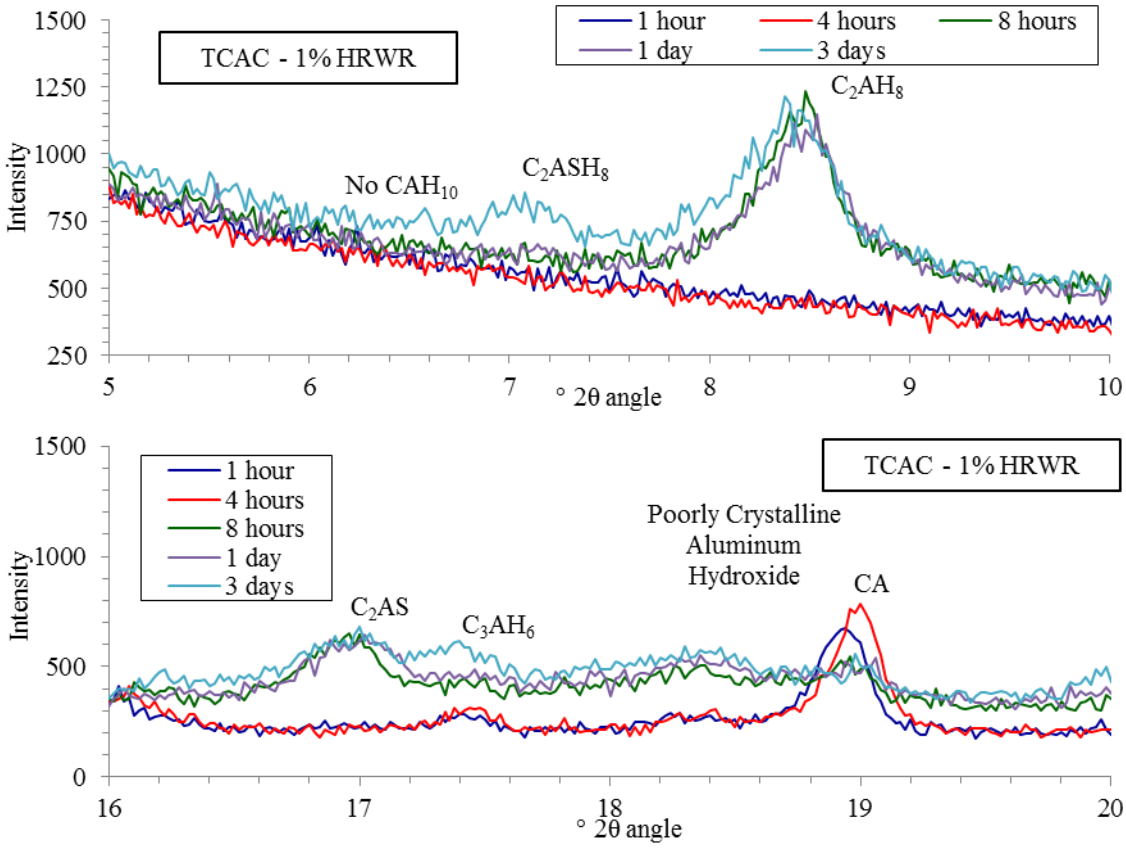


Figure 237: Qualitative XRD of TCAC with 1% HRWR hydrated at 38°C, illustrating the formation of $C_2AH_8$ and some $C_3AH_6$

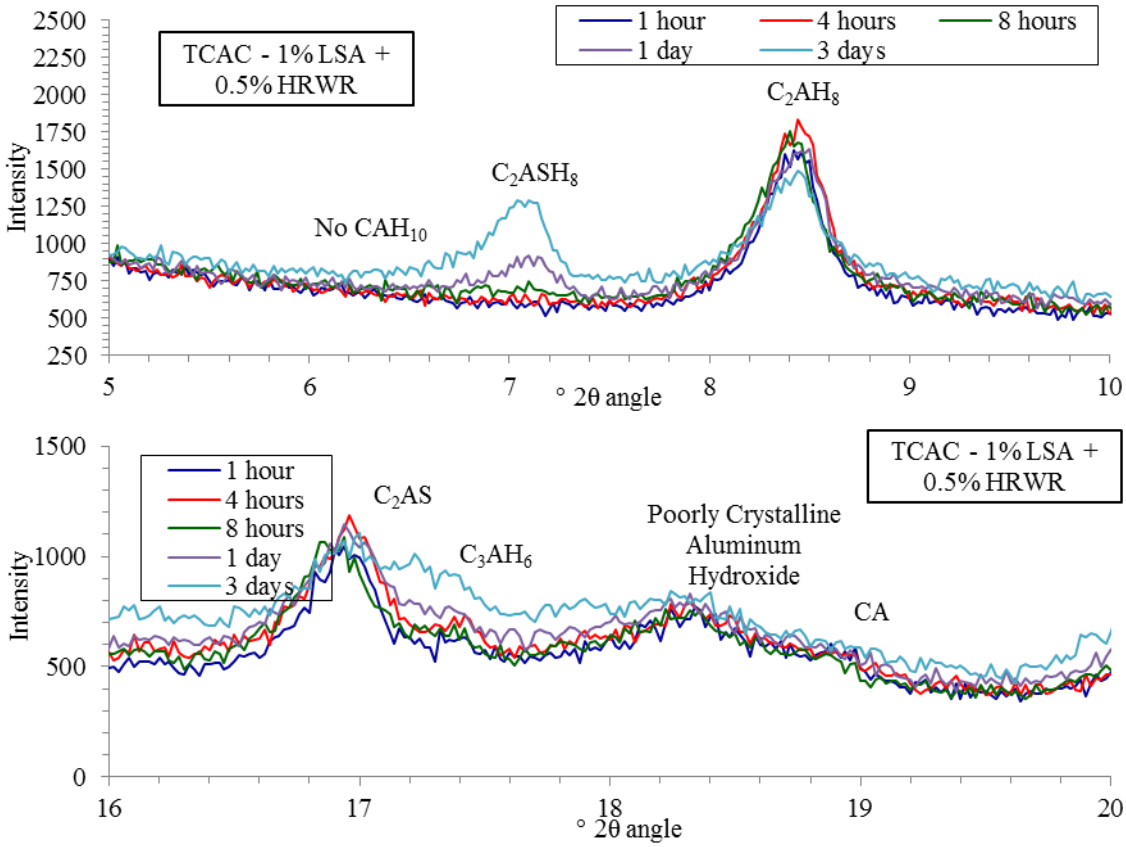


Figure 238: Qualitative XRD of TCAC with 1% LSA and 0.5% HRWR hydrated at 38°C, illustrating the formation of $C_2ASH_8$, $C_2AH_8$ and some $C_3AH_6$

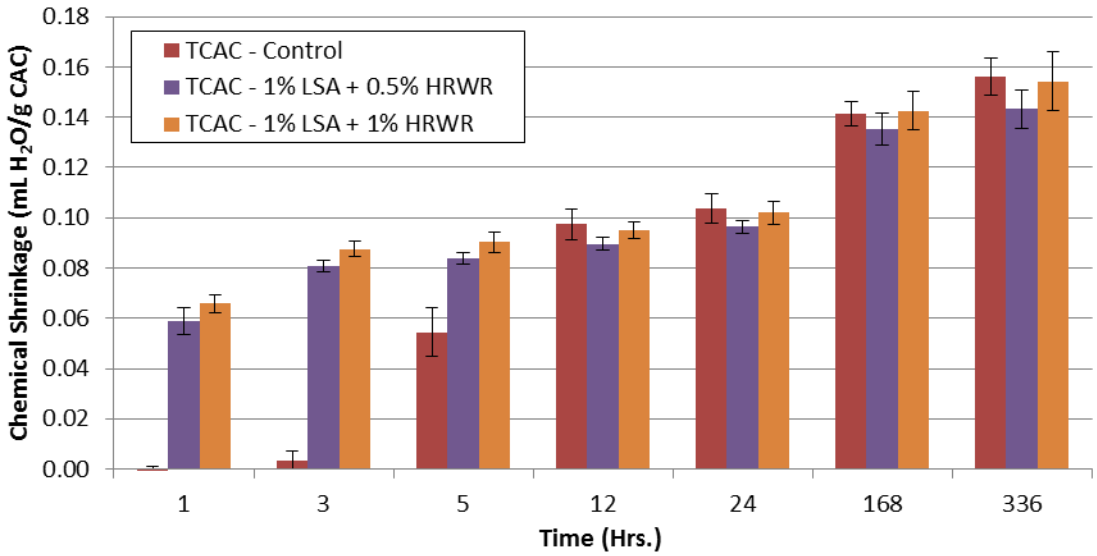


Figure 239: Chemical shrinkage with standard deviation for TCAC with varying dosages of LSA and HRWR at 38°C

# Appendix D: Hydration and Early-age Volume Deformation of CAC-LF systems

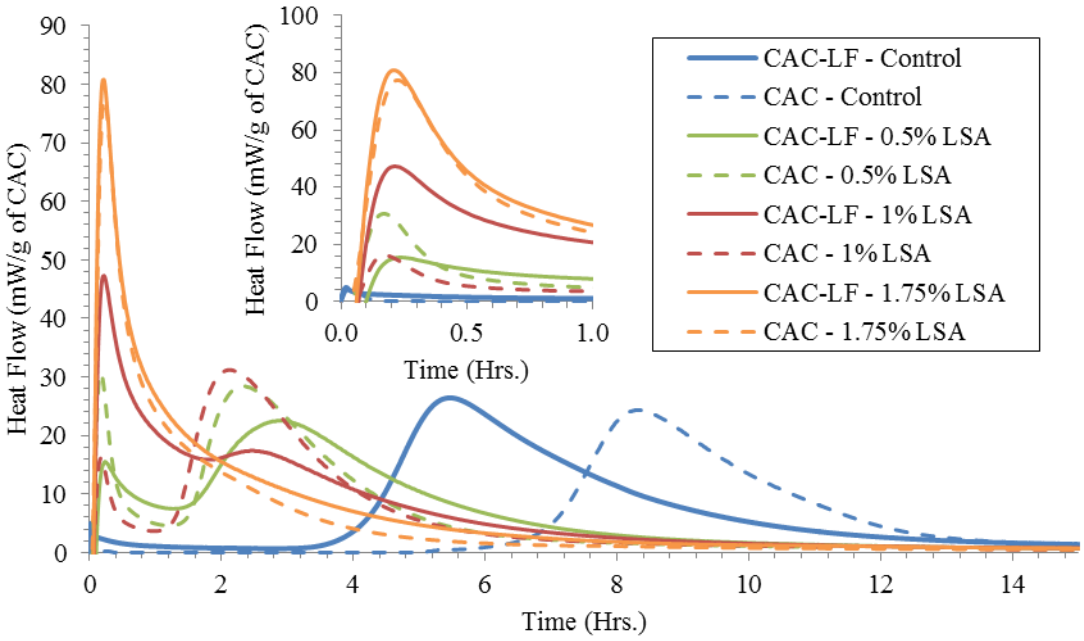


Figure 240: Heat flow of CAC-LF hydrated at 20°C for varying LSA dosages

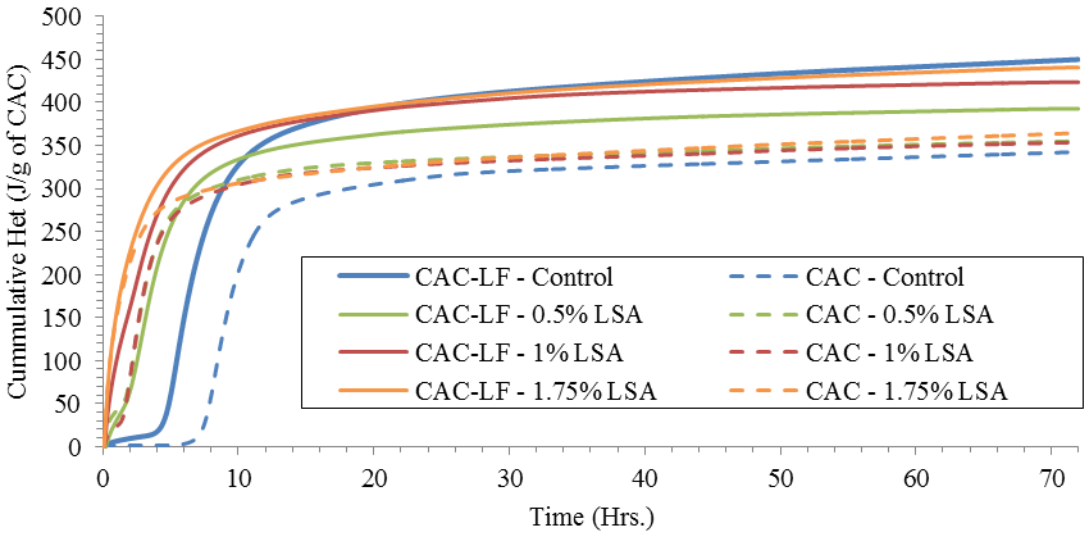


Figure 241: Cumulative heat release of CAC-LF hydrated at 20°C for varying LSA dosages

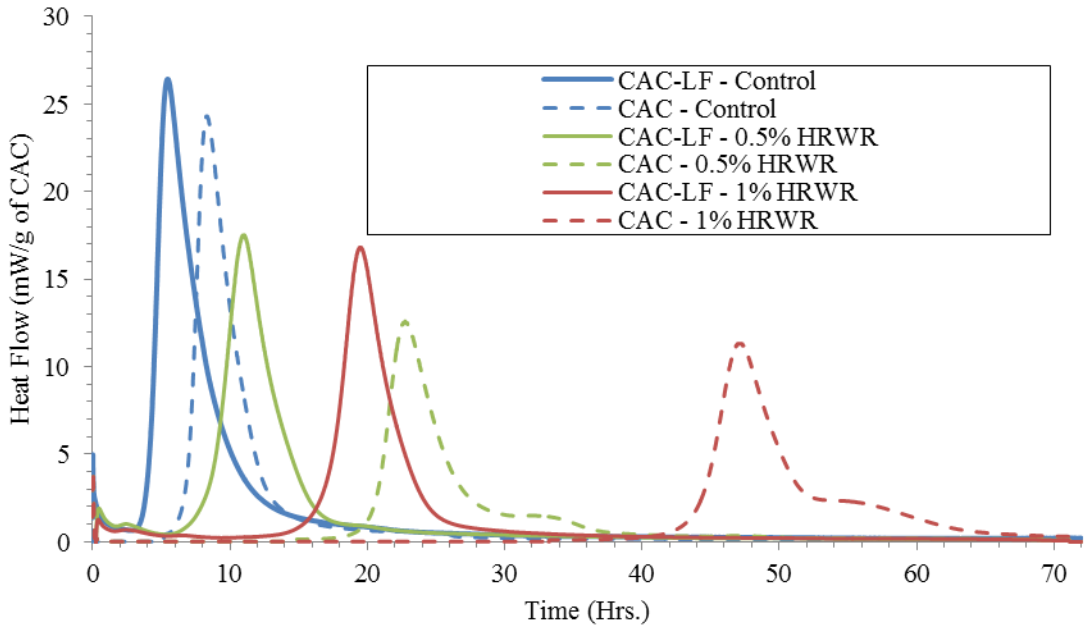


Figure 242: Heat flow of CAC-LF hydrated at 20°C for varying HRWR dosages

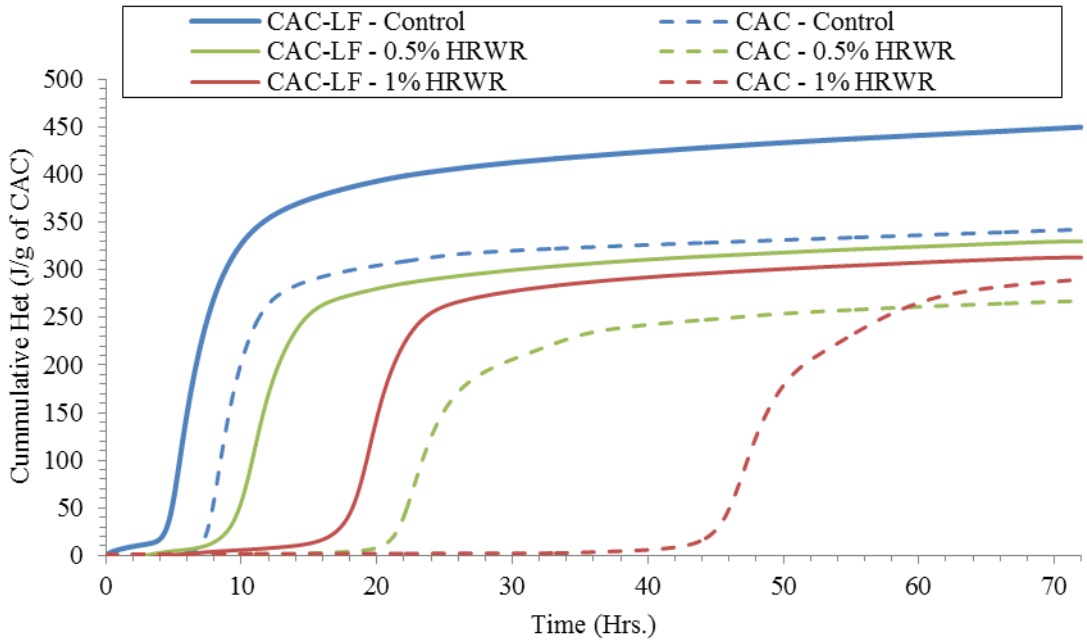


Figure 243: Cumulative heat release of CAC-LF hydrated at 20°C for varying HRWR dosages

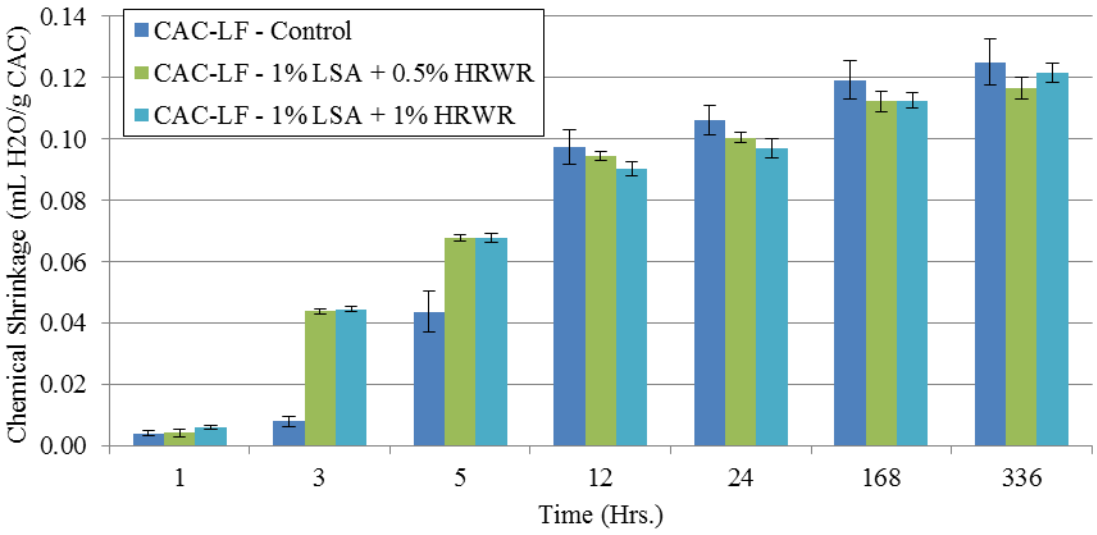


Figure 244: Chemical shrinkage with standard deviation for CAC-LF with varying dosages of LSA and HRWR at 20°C

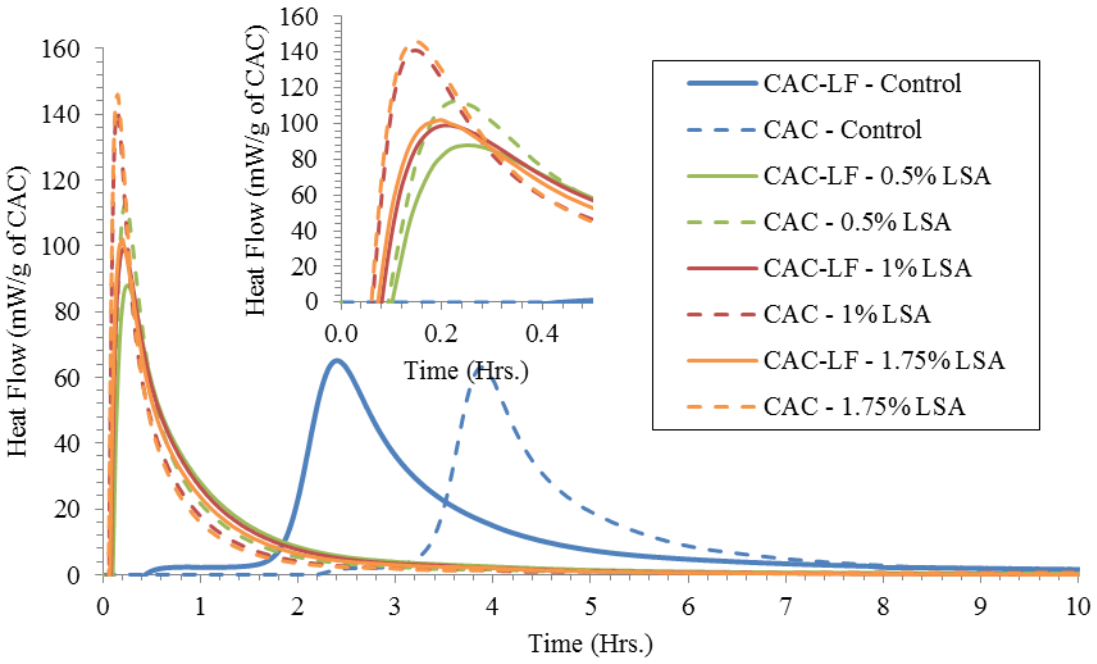


Figure 245: Heat flow of CAC-LF hydrated at 38°C for varying LSA dosages

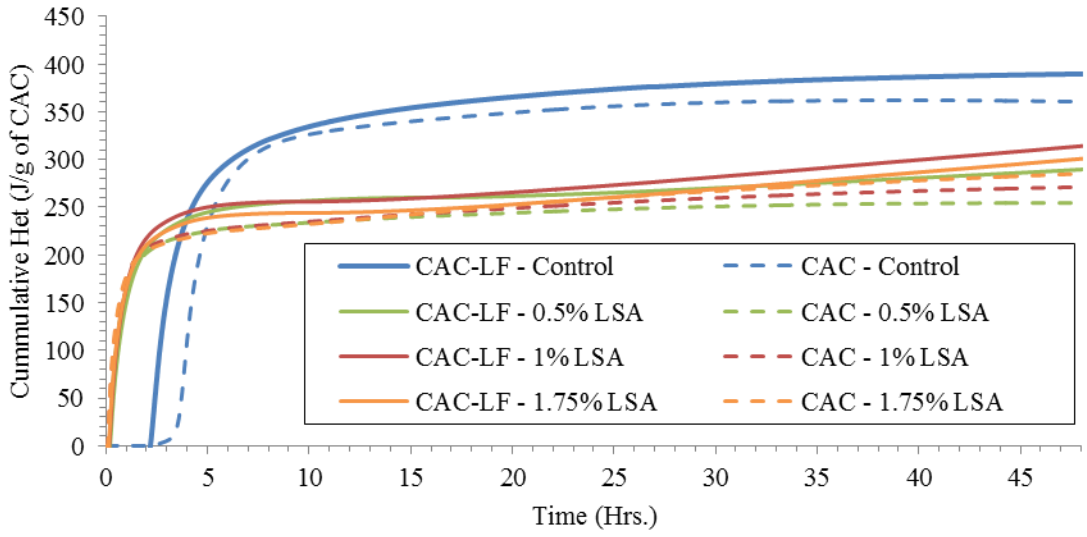


Figure 246: Cumulative heat release of CAC-LF hydrated at 38°C for varying LSA dosages

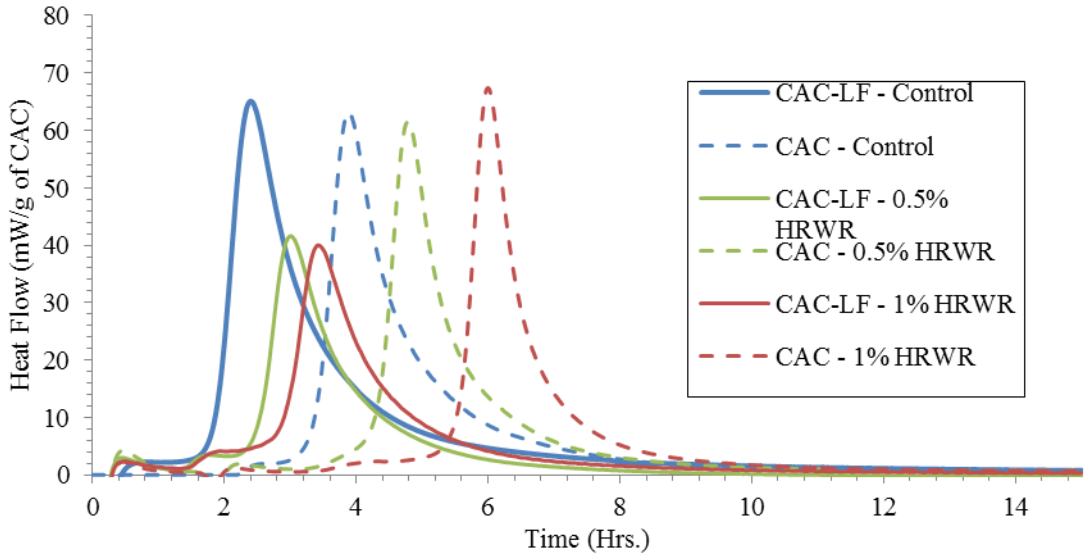


Figure 247: Heat flow of TCAC hydrated at 38°C for varying HRWR dosages

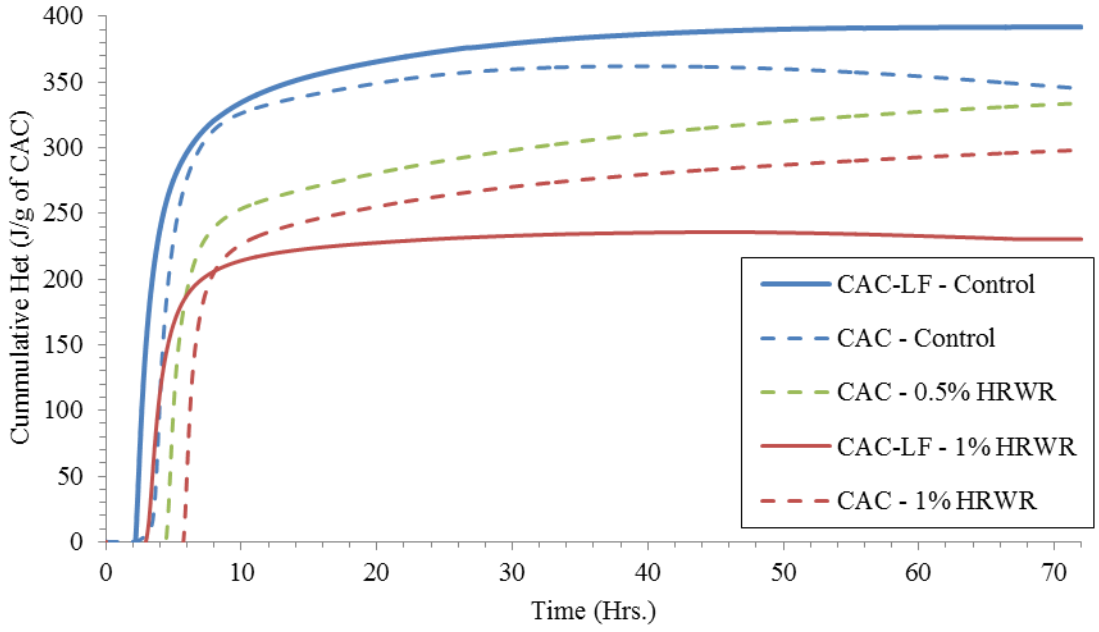


Figure 248: Cumulative heat release of CAC-LF hydrated at 38°C for varying HRWR dosages

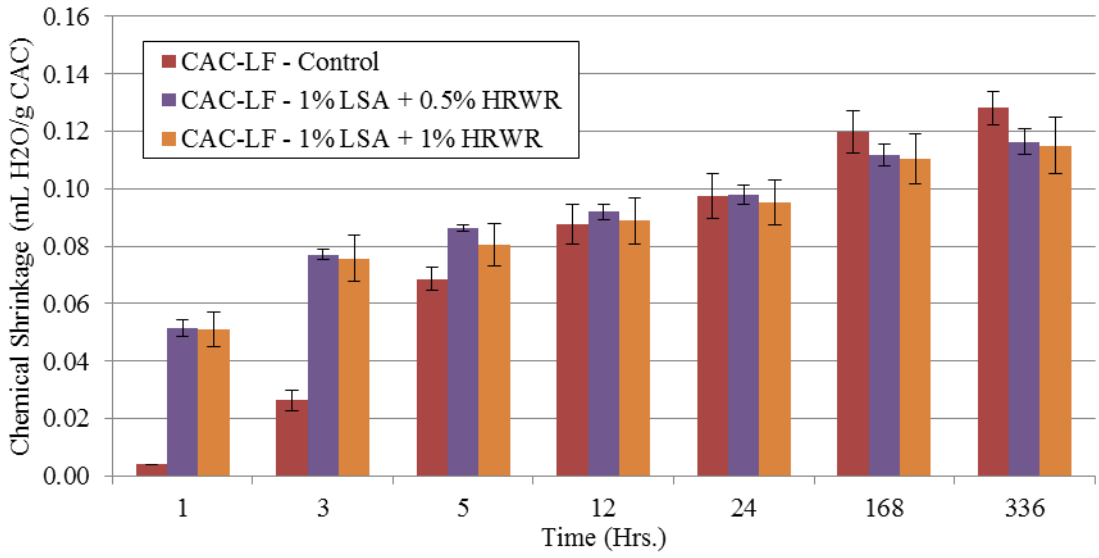


Figure 249: Chemical shrinkage with standard deviation for CAC-LF with varying dosages of LSA and HRWR at 38°C

# Appendix E: Hydration and Early-age Volume Deformation of CAC-FA Systems

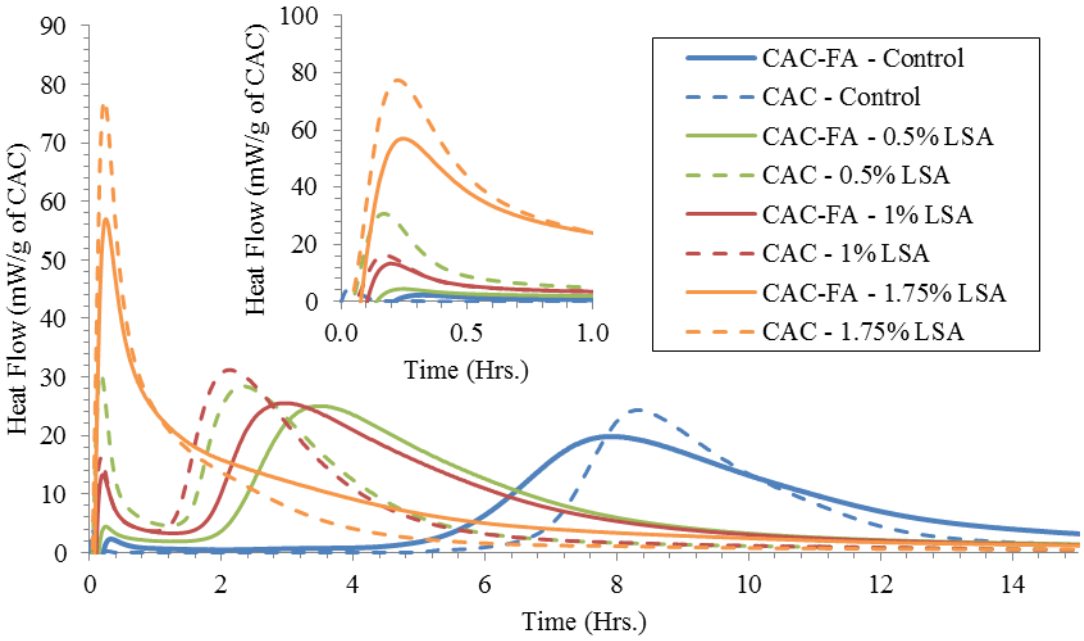


Figure 250: Heat flow of CAC-FA hydrated at 20°C for varying LSA dosages

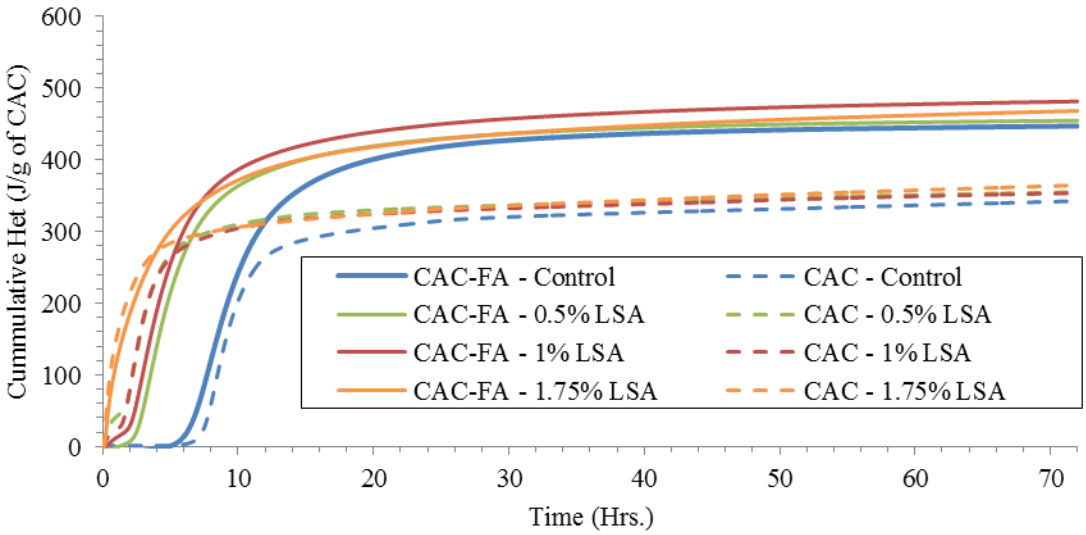


Figure 251: Cumulative heat release of CAC-FA hydrated at 20°C for varying LSA dosages

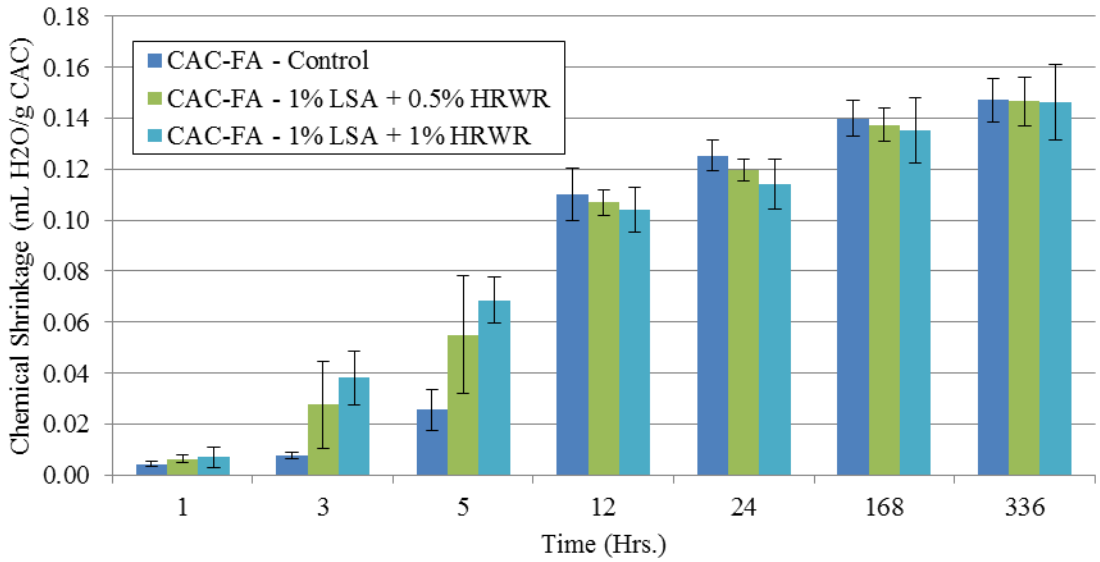


Figure 252: Chemical shrinkage with standard deviation for CAC-FA with varying dosages of LSA and HRWR at 20°C

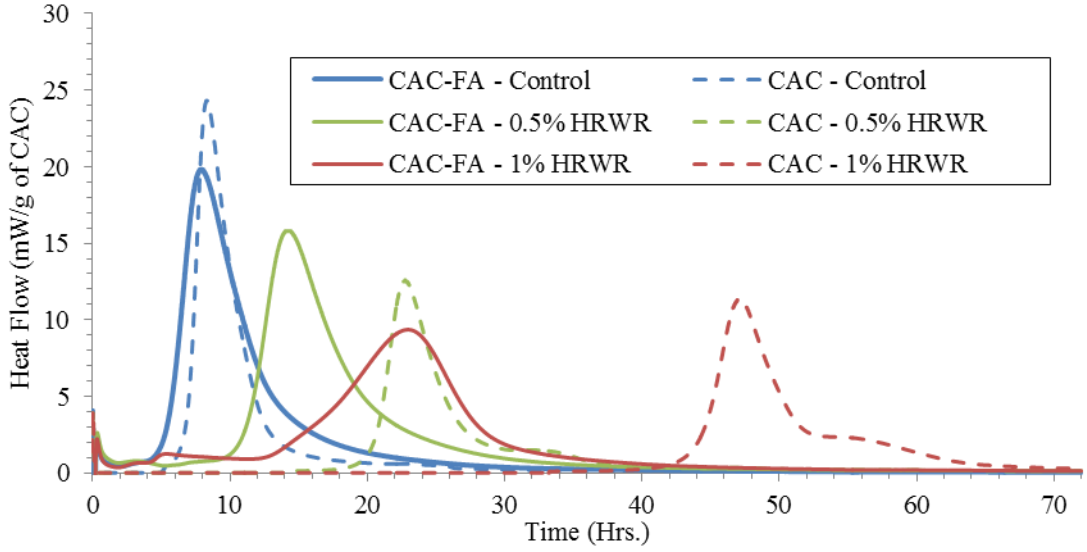


Figure 253: Heat flow of CAC-FA hydrated at 20°C for varying HRWR dosages

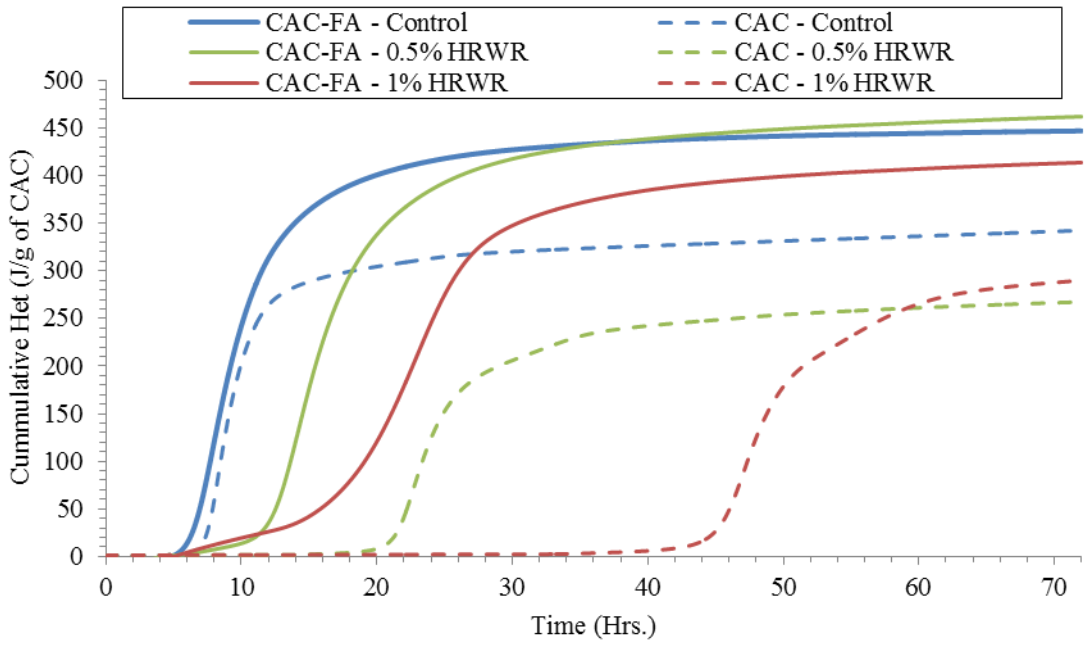


Figure 254: Cumulative heat release of CAC-FA hydrated at 20°C for varying HRWR dosages

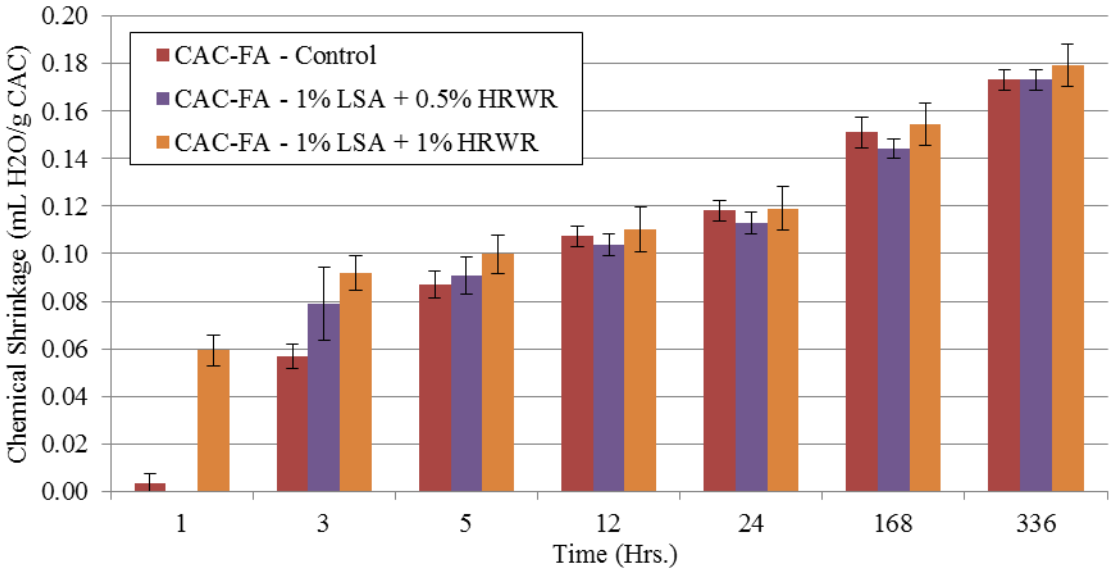


Figure 255: Chemical shrinkage with standard deviation for CAC-FA with varying dosages of LSA and HRWR at 38°C

# Appendix F: Strain and Temperature Data Logging Equipment Specifications

## CR10X Specifications

*Electrical specifications are valid over a -25° to +50°C range unless otherwise specified; non-condensing environment required. To maintain electrical specifications, Campbell Scientific recommends recalibrating dataloggers every two years.*

### PROGRAM EXECUTION RATE

Program is synchronized with real-time up to 64 Hz. One channel can be measured at this rate with uninterrupted data transfer. Burst measurements up to 750 Hz are possible over short intervals.

### ANALOG INPUTS

NUMBER OF CHANNELS: 6 differential or 12 single-ended, individually configured. Channel expansion provided by AM16/32 or AM416 Relay Multiplexers and AM25T Thermocouple Multiplexers.

ACCURACY: ±0.1% of FSR (-25° to 50°C); ±0.05% of FSR (0° to 40°C); e.g., ±0.1% FSR = ±5.0 mV for ±2500 mV range

RANGE AND RESOLUTION:

| Full Scale Input Range (mV) | Resolution (µV) Differential | Single-Ended |
|---|---|---|
| ±2500 | 333 | 666 |
| ±250 | 33.3 | 66.6 |
| ±25 | 3.33 | 6.66 |
| ±7.5 | 1.00 | 2.00 |
| ±2.5 | 0.33 | 0.66 |

INPUT SAMPLE RATES: Includes the measurement time and conversion to engineering units. The fast and slow measurements integrate the signal for 0.25 and 2.72 ms, respectively. Differential measurements incorporate two integrations with reversed input polarities to reduce thermal offset and common mode errors.

| | |
|---|---|
| Fast single-ended voltage: | 2.6 ms |
| Fast differential voltage: | 4.2 ms |
| Slow single-ended voltage: | 5.1 ms |
| Slow differential voltage: | 9.2 ms |
| Differential with 60 Hz rejection: | 25.9 ms |
| Fast differential thermocouple: | 8.6 ms |

INPUT NOISE VOLTAGE (for ±2.5 mV range):
Fast differential: 0.82 µV rms
Slow differential: 0.25 µV rms
Differential with 60 Hz rejection: 0.18 µV rms

COMMON MODE RANGE: ±2.5 V

DC COMMON MODE REJECTION: >140 dB

NORMAL MODE REJECTION: 70 dB (60 Hz with slow differential measurement)

INPUT CURRENT: ±9 nA maximum

INPUT RESISTANCE: 20 Gohms typical

### ANALOG OUTPUTS

DESCRIPTION: 3 switched, active only during measurement, one at a time.

RANGE: ±2.5 V

RESOLUTION: 0.67 mV

ACCURACY: ±5 mV; ±2.5 mV (0° to 40°C)

CURRENT SOURCING: 25 mA

CURRENT SINKING: 25 mA

FREQUENCY SWEEP FUNCTION: The switched outputs provide a programmable swept frequency, 0 to 2.5 V square wave for exciting vibrating wire transducers.

### RESISTANCE MEASUREMENTS

MEASUREMENT TYPES: The CR10X provides ratiometric bridge measurements of 4- and 6-wire full bridge, and 2-, 3-, and 4-wire half bridges. Precise dual polarity excitation using any of the switched outputs eliminates dc errors. Conductivity measurements use a dual polarity 0.75 ms excitation to minimize polarization errors.

ACCURACY: ±0.02% of FSR plus bridge resistor error.

### PERIOD AVERAGING MEASUREMENTS

The average period for a single cycle is determined by measuring the duration of a specified number of cycles. Any of the 12 single-ended analog input channels can be used. Signal attentuation and ac coupling are typically required.

INPUT FREQUENCY RANGE:

| Signal peak-to-peak[1] Min. | Max. | Min. Pulse w. | Max Freq.[2] |
|---|---|---|---|
| 500 mV | 5.0 V | 2.5 µs | 200 kHz |
| 10 mV | 2.0 V | 10 µs | 50 kHz |
| 5 mV | 2.0 V | 62 µs | 8 kHz |
| 2 mV | 2.0 V | 100 µs | 5 kHz |

[1]Signals centered around datalogger ground
[2]Assuming 50% duty cycle

RESOLUTION: 35 ns divided by the number of cycles measured

ACCURACY: ±0.01% of reading (number of cycles ≥100) ±0.03% of reading (number of cycles <100)

TIME REQUIRED FOR MEASUREMENT: Signal period times the number of cycles measured plus 1.5 cycles + 2 ms

### PULSE COUNTERS

NUMBER OF PULSE COUNTER CHANNELS: 2 eight-bit or 1 sixteen-bit; software selectable as switch closure, high frequency pulse, and low level ac.

MAXIMUM COUNT RATE: 16 kHz, eight-bit counter; 400 kHz, sixteen-bit counter. Channels are scanned at 8 or 64 Hz (software selectable).

SWITCH CLOSURE MODE
Minimum Switch Closed Time: 5 ms
Minimum Switch Open Time: 6 ms
Maximum Bounce Time: 1 ms open without being counted

HIGH FREQUENCY PULSE MODE
Minimum Pulse Width: 1.2 µs
Maximum Input Frequency: 400 kHz
Voltage Thresholds: Count upon transition from below 1.5 V to above 3.5 V at low frequencies. Larger input transitions are required at high frequencies because of input filter with 1.2 µs time constant. Signals up to 400 kHz will be counted if centered around +2.5 V with deviations ≥ ±2.5 V for ≥ 1.2 µs.
Maximum Input Voltage: ±20 V

LOW LEVEL AC MODE
(Typical of magnetic pulse flow transducers or other low voltage, sine wave outputs.)
Input Hysteresis: 14 mV
Maximum ac Input Voltage: ±20 V
Minimum ac Input Voltage:

| (Sine wave mV RMS) | Range (Hz) |
|---|---|
| 20 | 1.0 to 1000 |
| 200 | 0.5 to 10,000 |
| 1000 | 0.3 to 16,000 |

### DIGITAL I/O PORTS

8 ports, software selectable as binary inputs or control outputs. 3 ports can be configured to count switch closures up to 40 Hz.

OUTPUT VOLTAGES (no load): high 5.0 V ±0.1 V; low < 0.1 V

OUTPUT RESISTANCE: 500 ohms

INPUT STATE: high 3.0 to 5.5 V; low -0.5 to 0.8 V

INPUT RESISTANCE: 100 kohms

### SDI-12 INTERFACE STANDARD

Digital I/O Ports C1-C8 support SDI-12 asynchronous communication; up to ten SDI-12 sensors can be connected to each port. Meets SDI-12 Standard version 1.2 for datalogger and sensor modes.

### CR10XTCR THERMOCOUPLE REFERENCE

POLYNOMIAL LINEARIZATION ERROR: Typically <±0.5°C (-35° to +50°C), <±0.1°C (-24° to +45°C).

INTERCHANGEABILITY ERROR: Typically <±0.2°C (0° to +60°C) increasing to ±0.4°C (at -35°C).

### CE COMPLIANCE (as of 09/01)

STANDARD(S) TO WHICH CONFORMITY IS DECLARED:
EN55022: 1995 and EN61326: 1998

### EMI and ESD PROTECTION

IMMUNITY: Meets or exceeds following standards:
ESD: per IEC 1000-4-2; ±8 kV air, ±4 kV contact discharge
RF: per IEC 1000-4-3; 3 V/m, 80-1000 MHz
EFT: per IEC 1000-4-4; 1 kV power, 500 V I/O
Surge: per IEC 1000-4-5; 1 kV power and I/O
Conducted: per IEC 1000-4-6; 3 V 150 kHz-80 MHz

Emissions and immunity performance criteria available on request.

### CPU AND INTERFACE

PROCESSOR: Hitachi 6303

PROGRAM STORAGE: Up to 16 kbytes for active program; additional 16 kbytes for alternate programs. Operating system stored in 128 kbytes Flash memory.

DATA STORAGE: 128 kbytes SRAM standard (approximately 60,000 data values). Additional 2 Mbytes Flash available as an option.

OPTIONAL KEYBOARD DISPLAY: 8-digit LCD (0.5" digits)

PERIPHERAL INTERFACE: 9 pin D-type connector for keyboard display, storage module, modem, printer, card storage module, and RS-232 adapter.

BAUD RATES: Selectable at 300, 1200, 9600 and 76,800 bps for synchronous devices. ASCII communication protocol is one start bit, one stop bit, eight data bits (no parity).

CLOCK ACCURACY: ±1 minute per month

### SYSTEM POWER REQUIREMENTS

VOLTAGE: 9.6 to 16 Vdc

TYPICAL CURRENT DRAIN: 1.3 mA quiescent, 13 mA during processing, and 46 mA during analog measurement.

BATTERIES: Any 12 V battery can be connected as a primary power source. Several power supply options are available from Campbell Scientific. The Model CR2430 lithium battery for clock and SRAM backup has a capacity of 270 mAhr.

### PHYSICAL SPECIFICATIONS

SIZE: 7.8" x 3.5" x 1.5" - Measurement & Control Module; 9" x 3.5" x 2.9" - with CR10WP Wiring Panel. Additional clearance required for serial cable and sensor leads.

WEIGHT: 2 lbs

### WARRANTY

Three years against defects in materials and workmanship.

We recommend that you confirm system configuration and critical specifications with Campbell Scientific before purchase.

CAMPBELL SCIENTIFIC, INC.
815 W. 1800 N. • Logan, Utah 84321-1784 • (435) 753-2342 • FAX (435) 750-9540
Offices also located in: Australia • Brazil • Canada • England • France • South Africa • Spain

Copyright © 1986, 2004
Campbell Scientific, Inc.
Printed March 2004

Figure 256: CR-10X data logger specifications

# AM16/32B

## Relay Multiplexer

CAMPBELL SCIENTIFIC
WHEN MEASUREMENTS MATTER

The AM16/32B Relay Multiplexer increases the number of sensors that can be measured by a datalogger. It multiplexes 16 groups of four lines (a total of 64 lines) through four common (COM) terminals. Alternatively, a manual switch setting allows the AM16/32B to multiplex 32 groups of two lines (also a total of 64 lines) through two COM terminals.

The AM16/32B supports two clocking modes. Clocking mode A sequentially advances through each channel. Whereas clocking mode B uses a relay address to go directly to a specific channel, which reduces power consumption and wear on the relay switches.

The AM16/32B is compatible with most of our dataloggers (not compatible with the CR200(X) series or CR510). The maximum distance between the datalogger and the AM16/32B is determined by the sensors used, the datalogger's scan rate, and the cable used in the application.

### Features/Benefits

- Increases system channel capacity
- Decreases the cost of cabling individual sensors on long wire runs
- Reduces power consumption and wear on the relay switches by using a relay address to go directly to a specific channel.
- Contains gas tubes on all of the inputs and a ground lug for better surge protection
- Includes strain relief for sensor leads and independent routing for sensor shield lines
- Compatible with thermistors, potentiometers, load cells, strain gages, vibrating wires, water content reflectometers, and gypsum soil moisture blocks; AM25T is recommended for multiplexing thermocouples

When multiple sensor types are connected to the AM16/32B, Mode B allows one sensor type to be measured more frequently than the other sensor type.

### Maximum Number of Sensor Connections

The maximum number of sensors multiplexed through one AM16/32B depends on the type(s) of sensors measured. For example, assuming identical sensors, the AM16/32B can multiplex:

- Up to 32 single-ended or differential sensors that require two wires (e.g., thermistors, half bridges)
- Up to 16 single-ended or differential sensors that require four wires (e.g., full bridges, four-wire half bridges)
- Up to 32 vibrating wire sensors (16 with temperature) in conjunction with a AVW1, AVW4, AVW100, or AVW200-series Vibrating Wire Interface
- Up to 48 half-bridge measurements (assumes common excitation and completion resistors at the datalogger)
- Up to 48 CS616 Water Content Reflectometers (assumes common excitation)
- Up to 32 gypsum soil moisture blocks (model 223 or 253). The AM16/32B eliminates the requirement for dc blocking capacitors, significantly reducing sensor cost

### Environmental Enclosures

The AM16/32B operates in most field conditions but requires a non-condensing environment. A weather-resistant enclosure equipped with desiccant is required for field use. The ENC10/12 is the enclosure of choice for multiplexers housed at a distance from the datalogger.

If the AM16/32B is to be housed in the datalogger's enclosure, one AM16/32B, a CR800, CR850, CR1000, CR3000, or CR10X datalogger, and a PS100 power supply will fit in an ENC12/14. For convenience in wiring, a larger enclosure (e.g., ENC16/18) is recommended.

Figure 257: AM16/32 multiplexer specifications

# TIMs

## Terminal Input Modules

CAMPBELL SCIENTIFIC
WHEN MEASUREMENTS MATTER

Terminal input modules (TIMs) are small peripherals that provide completion resistors for resistive bridge measurements, or act as voltage dividers or precision current shunts. The modules attach directly to the datalogger's input terminals. Each module provides circuitry to connect one sensor, except for the voltage dividers which allow connection of two single-ended sensors. Please note that the legs of our TIMs do not fit on the CR7 datalogger's connectors.

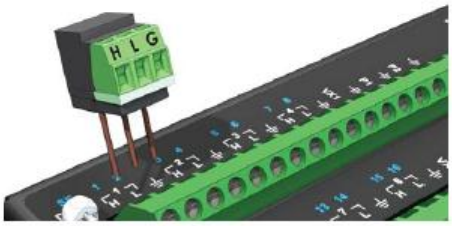


### 3-Wire Half Bridge Module (3WHB10K)

Typically used with 100 Ω and 1 kΩ PRTs, the 3WHB10K is designed for 3-wire half-bridge measurements.

*Specifications*

**10 kΩ Completion Resistor (Rf) (bulk metal foil)**

| | |
|---|---|
| **Tolerance @ 25°C:** | ±0.01% |
| **Maximum Temperature Coefficient:** | ±0.8 ppm °C$^{-1}$ |
| **Power Rating:** | 0.25 W @ 70°C |

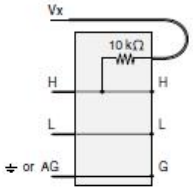


3WHB10K Schematic

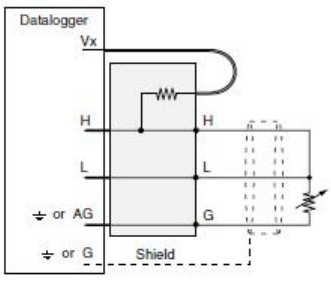


3WHB10K-to-Sensor Hookup

### 4-Wire Half Bridge Module (4WHB10K)

The 4WHB10K provides a completion resistor for 4-wire half bridge measurements. This module should be used with sensors that have a 10 kΩ resistance.

*Specifications*

**10 kΩ Completion Resistor (Rf) (bulk metal foil)**

| | |
|---|---|
| **Tolerance @ 25°C:** | ±0.01% |
| **Maximum Temperature Coefficient:** | ±0.8 ppm °C$^{-1}$ |
| **Power Rating:** | 0.25 W @ 70°C |

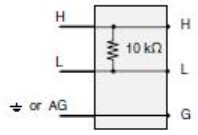


4WHB10K Schematic

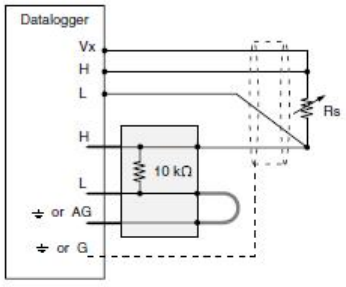


4WHB10K-to-Sensor Hookup

Figure 258: 120 ohm terminal input modules

# Special Purpose Sensors - Embedment Gages

The EGP-Series Embedment Strain Gage is specially designed for measuring mechanical strains inside concrete structures. The sensing grid, constructed of a nickel-chromium alloy (similar to Karma), has an active gage length of 4 in (100 mm) for averaging strains in aggregate materials. A rugged 5-in (130-mm) outer body of proprietary polymer concrete resists mechanical damage during pouring, minimizes reinforcement of the structure, and provides protection from moisture and corrosive attack. The grid, cast within the polymer concrete to ensure maximum strain sensitivity, is self-temperature-compensated to minimize thermal output when installed in concrete structures. Each gage incorporates a heavy-duty 10-ft (3-m) cable with 22-AWG (0.643-mm dia.) leadwires; a three-wire construction to the sensing grid helps minimize temperature effects in the instrumentation leads. Special lengths of preattached cable will be quoted upon request. Vishay Micro-Measurements M-LINE accessory cable 322-DJV is available for adding cable length in the field.

Rugged and reliable, EGP-Series Strain Gages are available in both 120-ohm (EGP-5-120) and 350-ohm (EGP-5-350) resistances.

## SPECIFICATIONS

- **Construction.** Strain sensing grid cast in a sturdy, water-resistant material.
- **Sensing Grid.** Nickel-chromium alloy on polyimide backing. Active gage length of 4 in (100 mm) nominal. Grid resistance of 120 or 350 ohms, ±0.8%.
- **Outer Body.** Proprietary polymer concrete. 5 x 0.7 x 0.4 in (130 x 17 x 10 mm) nominal.
- **Cable.** Three 10-ft (3-m) leads of 22-AWG (0.643-mm dia.) stranded tinned copper in 0.015-in (0.4-mm) thick PVC insulation. Nominal cable diameter of 0.2 in (5 mm). (Other lengths quoted upon request.)
- **Temperature Range.** The normal usage range is +25° to +125°F (–5° to +50°C). Extended range is –25° to +150°F (–30° to +60°C).

## EMBEDMENT GAGE SELECTION

| GAGE DESIGNATION | RES. IN OHMS | DIMENSIONS | | | |
|---|---|---|---|---|---|
| | | ACTIVE GAGE LENGTH | OUTER BODY WIDTH | OUTER BODY LENGTH | OUTER BODY THICKNESS |
| EGP-5-120 | 120 ±0.8% | 4 | 0.7 | 5 | 0.4 |
| | | 100 | 17 | 130 | 10 |
| EGP-5-350 | 350 ±0.8% | 4 | 0.7 | 5 | 0.4 |
| | | 100 | 17 | 130 | 10 |



Figure 259: Vishay concrete embedment strain gage

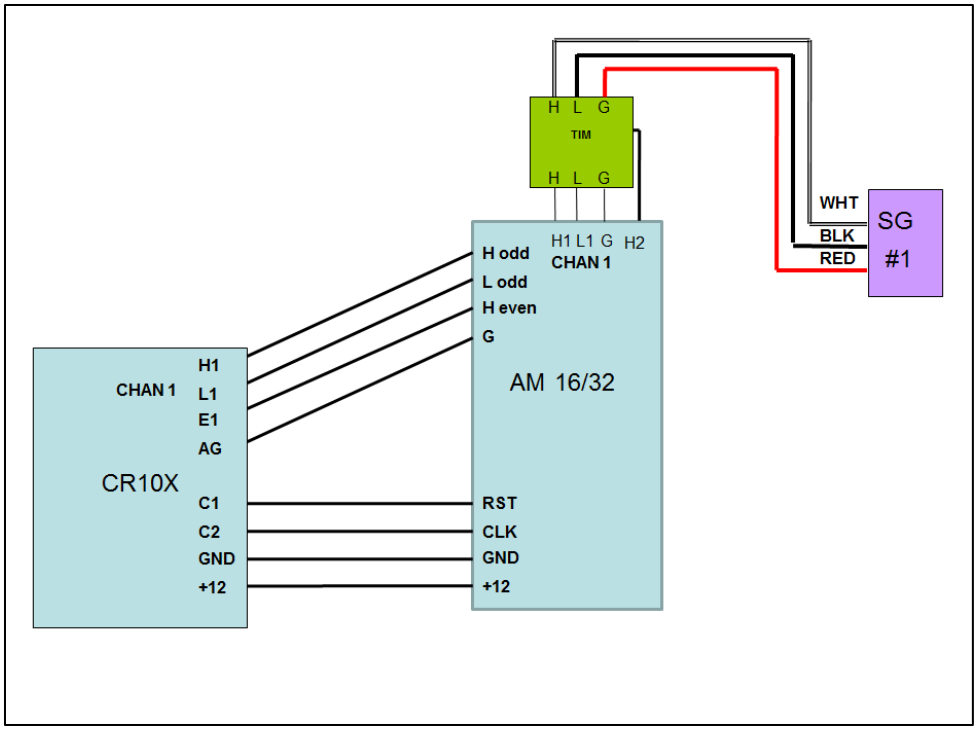


Figure 260: Wiring diagram for concrete embedment strain gages

```
};CR10X
;BentiGauge.dld
;$
;:mVperV_1 :mVperV_2 :mVperV_3
:mVperV_4 :V_1
;:_2V_1    :_1_2V_1
:Denominat:_4e6     :Numerator
;:uE_1      :uE_2      :uE_3
:uE_4      :Vr_1_2V_1
;:Mult      :uStrain
;$

;%
;Final Storage Label File for:
BentiGauge.csi
;Date:  10/4/2010
;Time:  10:53:21
;
;1 Output_Table   1.00 Min
;1 1 L
;2 Year_RTM  L
;3 Day_RTM  L
;4 Hour_Minute_RTM  L
;5 mVperV_1  L
;6 mVperV_2  L
;7 mVperV_3  L
;8 mVperV_4  L
;9 uE_1  L
;10 uE_2  L
;11 uE_3  L
;12 uE_4  L
;
;
;Estimated Total Final Storage
Locations used per day 17280
;%

MODE 1
SCAN RATE 60

1:P86
1:41

2:P87
1:0000
2:4

3:P86
1:72

4:P22
1:1
2:0000
3:20
4:0000

5:P6
1:1
2:2
3:1
4:1
5:2000
6:1--
7:1.0
8:0.0

6:P95

7:P86
1:51

8:P92
1:0
2:1
3:10

9:P80
1:1
2:1

10:P77
1:1110

11:P70
1:4
2:1

12:P70
1:4
2:11

MODE 2
SCAN RATE 0.0000

MODE 3

MODE 10
1:28
2:64
3:0

MODE 12
1:0000
2:0000
```

Figure 261: Strain gage control program written PC 400

19-5101; Rev 5; 9/11

MAXIM

# Thermochron iButton

DS1921G

## General Description

The DS1921G Thermochron® iButton® is a rugged, self-sufficient system that measures temperature and records the result in a protected memory section. The recording is done at a user-defined rate, both as a direct storage of temperature values as well as in the form of a histogram. Up to 2048 temperature values taken at equidistant intervals ranging from 1 to 255min can be stored. The histogram provides 63 data bins with a resolution of 2.0°C. If the temperature leaves a user-programmable range, the DS1921G also records when this happened, for how long the temperature stayed outside the permitted range, and if the temperature was too high or too low. An additional 512 bytes of read/write nonvolatile (NV) memory allows storing information pertaining to the object to which the DS1921G is associated. Data is transferred serially through the 1-Wire® protocol, which requires only a single data lead and a ground return. Every DS1921G is factory lasered with a guaranteed unique, electrically readable, 64-bit registration number that allows for absolute traceability. The durable stainless steel package is highly resistant to environmental hazards such as dirt, moisture, and shock. Accessories permit the DS1921G to be mounted on almost any object including containers, pallets, and bags.

## Applications

Temperature Logging in Cold Chain, Food Safety, Pharmaceutical, and Medical Products

## Ordering Information

| PART | TEMP RANGE | PIN-PACKAGE |
|---|---|---|
| DS1921G-F5# | -40°C to +85°C | F5 iButton |
| DS1921G-F5N# | -40°C to +85°C | F5 iButton |

*#Denotes a RoHS-compliant device that may include lead(Pb) that is exempt under the RoHS requirements.*
*A NIST traceability certificate is available for the DS1921G-F5N. See Application Note 4629 for details.*

## Examples of Accessories

| PART | ACCESSORY |
|---|---|
| DS9096P | Self-Stick Adhesive Pad |
| DS9101 | Multipurpose Clip |
| DS9093RA | Mounting Lock Ring |
| DS9093A | Snap-In Fob |
| DS9092 | iButton Probe |

***Pin Configuration appears at end of data sheet.***

*Thermochron, iButton, and 1-Wire are registered trademarks of Maxim Integrated Products, Inc.*

## Features

- **Digital Thermometer Measures Temperature in 0.5°C Increments**
- **Accuracy ±1°C from -30°C to +70°C (See the *Electrical Characteristics* for Accuracy Specification)**
- **Built-In Real-Time Clock (RTC) and Timer Has Accuracy of ±2 Minutes per Month from 0°C to +45°C**
- **Water Resistant or Waterproof if Placed Inside DS9107 iButton Capsule (Exceeds Water Resistant 3 ATM Requirements)**
- **Automatically Wakes Up and Measures Temperature at User-Programmable Intervals from 1 Minute to 255 Minutes**
- **Logs Up to 2048 Consecutive Temperature Measurements in Protected NV RAM**
- **Records a Long-Term Temperature Histogram with 2.0°C Resolution**
- **Programmable Temperature High and Temperature Low Alarm Trip Points**
- **Records Up to 24 Timestamps and Durations When Temperature Leaves the Range Specified by the Trip Points**
- **512 Bytes of General-Purpose Read/Write NV RAM**
- **Communicates to Host with a Single Digital Signal at 15.4kbps or 125kbps Using 1-Wire Protocol**

## Common iButton Features

- **Digital Identification and Information by Momentary Contact**
- **Unique, Factory-Lasered, and Tested 64-Bit Registration Number (8-Bit Family Code + 48-Bit Serial Number + 8-Bit CRC Tester) Assures Absolute Traceability Because No Two Parts are Alike**
- **Multidrop Controller for 1-Wire Net**
- **Chip-Based Data Carrier Compactly Stores Information**
- **Data Can Be Accessed While Affixed to Object**
- **Button Shape is Self-Aligning with Cup-Shaped Probes**
- **Durable Stainless-Steel Case Engraved with Registration Number Withstands Harsh Environments**
- **Easily Affixed with Self-Stick Adhesive Backing, Latched by Its Flange, or Locked with a Ring Pressed Onto Its Rim**
- **Presence Detector Acknowledges When Reader First Applies Voltage**
- **Meets UL 913, 5th Ed., Rev. 1997-02-24; Intrinsically Safe Apparatus: Approved Under Entity Concept for Use in Class I, Division 1, Group A, B, C, and D Locations**



***For pricing, delivery, and ordering information, please contact Maxim Direct at 1-888-629-4642, or visit Maxim's website at www.maxim-ic.com.***

Figure 262: Thermochron  iButton specifications

# References


116, A. C. (2000). *Cement and Concrete Terminology.* Farmington Hills, MI: American Concrete Institute.

231R-10, A. (2010). *Report on Early-age Cracking: Causes, Measurement, and Mitigation.* Farmington Hills, MI: American Concrete Institute.

Alonso, M. V. (2011). Compatibility between PCE admixtures and calcium aluminate cement. *13th International Congress on the Chemisty of Cement* (pp. 1-7). Madrid: BRE Press.

Amathieu, L. B. (2000). Mechanisms of Set Acceleration of Portland Cement Through CAC Addition. *Calcium Aluminate Cements* (pp. 303-317). Ediburgh Scotland: The University Press.

Anatychuk, L. (1979). Thermoelements and Thermoeletrical Devices. 151.

Andion, L. G. (2001). Metallic Corrosion of Steels Embedded in Calclium Aluminate Cement Mortars. *Calcium Aluminate Cements* (pp. 405-421). Edinburgh: The University Press.

Andrade, C. S. (2001). Effect of Humidity in the Natural Carbonation of CAC. *Calcium Aluminate Cements* (pp. 361-369). Edinburgh, Scotland: The University Press.

ASCE. (2009). *Report Card for America's Infrastructure*. Retrieved 2011, from American Society of Civil Engineers: http://www.asce.org/reportcard/2009/grades.cfm

Association, A. C. (1998). *Concrete Paving Technology: Guidelines for Partial-Depth Spall Repair.* Skokie, IL: American Concrete Pavement Association.

ASTM C 157. (2008). *Standard Test Method for Length Change of Hardened Hydraulic-Cement Mortar and Concrete.* Conshochocken, PA: ASTM International.

ASTM C 1600. (2011). *Standard Specification for Rapid Hardening Cement.* West Conshohocken, PA: ASTM International.

ASTM C 1608. (2007). *Standard Test Method for Chemical Shrinkage of Hydraulic Cement Paste.* West Conshohocken, PA: ASTM International.

ASTM C 1679. (2009). Standard Practice fore Measuring Hydration Kinetics of Hydraulic Cementitious Mixtures Using Isothermal Calorimetry. *ASTM*.

ASTM C 1698. (2009). Standard Test Method for Autogenous Strain of Cement Paste and Mortar. *American Society for Testing and Materials*, 8.

ASTM C 305. (2006). *Standard Practice for Mechanical Mixing of Hydraulic Cement Pastes and Mortars of Plastic Consistency.* Conshohocken, PA: ASTM International.

ASTM C 33. (2007). Standard Specifications for Concrete Aggregates. *American Society for Testing and Materials*, 11.

ASTM C 494. (2011). Standard Specification for Chemical Admixtures for Concrete. *American Society for Testing and Materials*, 10.

ASTM C 596. (2007). Standard Test Method for Drying Shrinkage of Mortar Containing Hydraulic Cement. *ASTM*.

Bachiorrini, A. a. (1986). Alumina cement hydration in pure water and in sulfate solution in the presence of siliceous or calcareous aggregate. *8th International Congress on Chemistry of Cement*, (pp. 383-388). Rio De Janeiro.

Banfill, P. a. (1993). Superplasticizers for Ciment Fondu. Part 1: Effects on rheological properties of fresh paste and mortar. *Advances in Cement Research*, 131-138.

Barborak, R. (2010). *TxDOT SS-4491 Class CAC Concrete.* Austin, Texas: Texas Department of Transportation.

Barborak, R. a. (2010). *Calcium Aluminate Cement Concrete (Class CAC Concrete) TxDOT Special Specification SS-4491 Tip Sheet.* Austin, TX: TxDOT Construction and Bridge Divisions.

Barenberg, E. (1980). Rehabilitation of Concrete Pavements by Using Portland Cement Concrete. *Transportation Research Board*, 29-34.

Bennett, S. (1993). *A history of control engineering 1930-1955.* London: Institution of Engineering and Technology.

Bensted. (1996). A Dissucsiion of the Paper: The Influence of Pozzolanic Materials on the mechanical Stability of Aluminous Cement. *Cement and Concrete Research*, 649-650.

Bensten, S. S. (1990). Effect of Microsilica on Conversion of High Alumina Cement. *Calcium Aluminate Cements: Proceedings of the International Symposium R.J. Mangabhai* (pp. 294-334). London: E. & F.N. Spon.

Bhatty, J. (1991). A Review of the Application of Thermal Analysis to Cement-Admixture Systems. *Thermochimica Acta*, 313-350.

Bishnoi, S. (2009). *Automated Chemical Shrinakge Test and Shrinakge Suite Software.* Lausanne.

Bushnell-Watson, S. a. (1986). The Effect of Temperature Upon the Setting Behaviour of Refractory Calcium Aluminate Cemetns. *Cement and Concrete Research*, 875-884.

Campas, S. a. (1998). Calcium Aluminate Cements. In Hewlett, *Lea's Chemistry of Cement and Concrete - 4th Edition* (pp. 711-770). Woburn: Butterworth-Heinemann.

Collepardi, M. M. (1995). The Influence of Pozzolanic Materials on the Mechanical Stability of Aluminous Cement. *Cement and Concrete Research*, 961-968.

Concrete Society. (1997). *Calcium Aluminate Cements in Construction - A Re-assessment: Technical Report 46.* Berkshire: Concrete Society.

Concrete Society. (1997). *Calcium Aluminate Cements in Construction a Re-assessment: Technical Report No. 46.* London: Concrete Society.

Crammond, N. (1990). Long-term performance of high alumina cement in sulfate-bearing eviroments. In R. Mangabhai, *Calcium aluminate cements* (pp. 208-221). London: E & FN Spon.

Davey, T. a. (1929). *The effect of temperature on the setting time of cements and on mortars and concretes.* London: Building Research Report No. 13.

Delatte, N. W. (1997). Bond Strength Development with Maturity of High-early-strength Bonded Concrete Overlays. *ACI Mateials Journal*, 201 - 207.

Digng, J. F. (1995). Stratlingite Formation in High Alumina Cement - Silica Fume Systems: Significance of Sodium Ions. *Cement and Concrete Research*, 1311-1319.

Ding, J. F. (1996). Effect of Different Inorganic Salts/Alkali on Conversion-Prevention in High Alumina Cement Products. *Advanced Cement Based Materials*, 43-47.

Dunster, A. (2008). Carbonation and Reinforcement Corrosion in CAC Concrete. *Proceedings of the Centenary Conference* (pp. 221-233). Avignon, France: BRE Press.

Dunster, A. a. (2001). A Laboratory Study of the Resistance of CAC Concretes to Chemcial Attack by Sulphate and Alkali Carbonate Solutions. *Calcium Aluminate Cements 2001* (pp. 333-359). Edinburgh, Scotland: The University Press.

Fentiman, C. (1985). Hydration of carbo-aluminous cement at different temperatures. *Cement and Concrete Research*, 622-630.

Fernandez-Carrasco, L. a. (2008). Calcium Aluminate Cement with Supplementary Cementitious Materials: Fly Ashes. *Calcium Aluminate Cements* (pp. 475-483). Avignon, France: BRE Press.

Fisher, R. a.-J. (1982). Reinvestigation of the System C4AnH2O-C4ACO2nH20. *Cement and Concrete Research*, 517-526.

Folliard, K. P. (2009). *Phase 1 Report on the Development of Predictive Model for Bridge Deck Cracking and Strength Development.* Austin, TX: FHWA.

Fryda, H. G. (2000). Interaction of Superplasticizers with Calcium Aluminate Cements. *American Concrete Institute - Special Publication SP 195-7*, 91-101.

Fryda, H. L. (2008). Calcium Aluminate Cement Concrete in an Old Marine Structure. *Calcium Aluminate Cements* (pp. 209-220). Avignon, France: BRE Press.

Fu, T. (2011). *Master Thesis: Autogenous Deformation and Chemical Shrinkage of High Performance Cementitious Systems.* Corvallis, Oregon: Oregon State University.

Gaztanaga, M. G. (2001). Accelerated Carbonation of Calcium Aluminate Cement Paste. *Calcium Aluminate Cements* (pp. 349-259). Edinburgh, Scotland: The University Press.

Goni, S. A. (1991). Corrosion Behavior of Steel in High Alumina Cement Pastes. *Cement and Concrete Research*, 635-646.

Gosselin, C. (2009). *Microstructural Development of Calcium Aluminate Cement Based-Systems With and Without Supplementary Cementing Materials.* Laussane, Switzerland: Ecole Polytechnique Federale De Lausanne.

Gosselin, C. a. (2008). Microstructure Development of Calcium Aluminate Cements Accelerated by Lithium Sulphate. *Calcium Aluminate Cements: Proceedings of the Centenary Conference* (pp. 109-122). Avignon: IHS BRE Press.

Harrington, D. (2008). *Guide to Concrete Overlays: Suistanable Solutions for Resurfacing and Rehabilitating Existing Pavements: Second Edition.* Ames: National Concrete Pavement Technology Center.

Helmuth, V. a. (1968). Structure and physical properties of cement paste. *5th International Symposium on the Chemistry of Cement*, (pp. 1-32). Tokyo.

Ideker, J. (2008). *Dissertation: Early-age Behavior of Caclium Aluminate Cement Systems.* Austin, Texas: The University of Texas at Austin.

Ideker, J. (2008). *Early-age Behaviour of Calcium Aluminate Cements.* Austin, TX: The University of Texas at Austin.

Jensen, O. a. (1995). A dilatomoeter for measuring autogenous deformation in hardening Portland cement paste. *Experimental Methods and Devices Methods*, 406-409.

Jensen, O. a. (2001). Autogenous derormation and RH-change in perspective. *Cement and Concrete Research*, 1859-1865.

Jolin, M. a. (2008). De-icer Salt Scaling Resistance of CAC Concretes Exposed to Various De-icer Salts. *Calcium Aluminate Cements* (pp. 259-277). Avignon, France: BRE Press.

Justines, H. (2008). Rapid Repair of Airfield Runway in Cold Weather Using CAC Mortar. *Calcium Alumiante Cements* (pp. 365-372). Avignon, France: BRE Press.

Kirca, O. Y. (2008). Strength Development of Calcium Aluminate Cement-Portland Cement Blends at Different Temperatures. *Calcium Aluminate Cements* (pp. 487-497). Avignon, France: BRE Press.

Kosmatka, S. K. (2008). *Design and Control of Concrete Mixtures.* Skokie, IL: Portland Cement Association.

Kuzel, H.-J. a. (1996). Hydration of calcium aluminate cements in the presence of calcium carbonate. *European Journal of Minerology*, 129-141.

Kyong-Ku Yun, P.-G. C.-H. (2007). Thermal and Autogenous Shrinkages of Very Early Strength Latex-Modified Concrete. *Transportation Research Record*, 30-39.

Lamberet, S. A. (2008). Microstructure Development of Binders Based on Calcium Aluminate Cement, Calcium Sulfate, and Portland Cement. *Calcium Aluminate Cements* (pp. 501-510). Avignon, France: BRE Press.

Lamberet, S. F. (2008). Drying and Shrinkage of CAC-Based Concrete. *Calcium Aluminate Cements* (pp. 171-180). Avignon, France: BRE Press.

Lenz, R. (2011). *Pavement Design Manual.* Austin: Texas Department of Transportation.

Lura, P. a. (2007). Measuring Techniques for Autogenous Strain. *Materials and Structures*, 431-440.

Lura, P. a. (2007). Measuring Techniques for Autogenous Strain of Cement Paste. *Materials and Structures*, 431-440.

McCullough, B. a. (1995). *Fast-Track Paving Concrete Temperature Control and Traffic Opening Critera for Bonded Concrete Overlays.* Washington D.C.: Federal Highway Administration (FHWA).

McCullough, B. F. (1995). *Fast-Track Paving: Concrete Temperature Control and Traffic Opening Criteria for Bonded Concrete Overlays.* Washington D.C.: FHWA Publication No. Concrete Temperature Control and Traffic Opening Criteria for Bonded.

Microsystems, T. (2011). *THERMOELECTRIC COOLERS BASICS.* Berlin: TEC Mircrosystems.

Midgley, H. (1990). High Alumina Cement in Construction - A Future Based on Experience. In R. Mangabhai, *Calcium Aluminate Cements* (pp. 1-26). London: E. & F.N. Spon.

Miller, D. a. (1933). *Technical Bulletin 358.* Washington D.C.: United States Department of Agriculture.

Muller. (2010). *Thesis: Conversion & résistance en compression des ciments cT a lu m in a tes de calcium.* Quebec City, Canada: Laval University.

Newman, K. (1960). Design of concrete mixes with high alumina cement. *Reinforced Concrete Rev.*, 269-294.

Nurse, R. (1949). Steam Curing Concrete. *Magazine of Concrete Research*, 79-88.

Parrott, L. G. (1990). Monitoring Portland cement Hydration: Comparison of Methods. *Cement and Concrete Research*, 919-926.

Poole, J. (2007). *Modeling Temperature Sensitivity and Heat Evolution of Concrete.* Austin: The University of Texas at Austin.

Poole, J. R. (2007). Methods of Activation Energy Calculation for Portland Cement. *ACI Materials Journal*, 303-311.

Rastrup, E. (1954). Heat of hydration in concrete. *Magazine of Concrete Research*, 79-92.

Riding, K. (2007). *Early-age Concrete Thermal Stress Measurement and Modeling.* Austin: The University of Texas at Austin.

Robson, T. (1962). *High-Alumina Cements and Concretes.* New York: Contractors Record Limited.

Rodger, S. a. (1984). The Chemistry of Hydration of High Alumina Cement in the Presence of Accelerating and Retarding Admixtures. *Cement and Concrete Research*, 73-82.

Sant, G. D. (2009). Detecting the Fluid-to-Solid Transistion in Cement Pastes. *Concrete International*, 53-58.

Sant, G. L. (2006). A Discusssion of Analysis Approaches for Determining 'Time-zero' from Chemical Shrinakge and Autogenous Strain Measurments in Cement Paste. *International Rilem Conference on Volume Changes of Hardening Concrete: Testing and Mitigation* (p. 9). Lyngby, Denmark: RILEM.

Sant, G. L. (2006). Measurement of Volume Change in Cementitious Materials at Early Ages. *Transportation Research Record*, 21-29.

Sant, L. a. (2006). Measurement of Volume Change in Cementitious Materials at Early-ages Review of Testing Protocols and Interpretation of Results. *Transportation Research Record: Journal of the Transportation Research Board*, 21-29.

Schindler. (2004). Effect of Temperature on Hydration of Cementitious Materials. *ACI Materials Journal*, 72-81.

Scrivener. (2003). Calcium Aluminate Cements. In J. a. Newman, *Advanced Concrete Technology* (pp. 2/1-2/30). Oxford: Butterworth-Heinemann.

Sprinkel. (2008). Bonded Concrete Overlays. In E. Nawy, *Concrete Costruction Engineering* (pp. 23-1 - 23-18). Boca Raton: CRC Press.

Touche. (1926). *Note sur l' emploi du ciment, Fondu sur la Ligne de Nice a Com.*

Transportation, S. o. (2008). Isolated Partial Depth Concrete Repair. In S. o. Transportation, *Maintenance Technical Advisory Guide Volume II - Rigid Pavement Preservation Second Edition* (pp. 7-1 - 7-20). Sacrmento, CA: State of California Deparment of Transportation.

Trivino. (1986). Aluminous cement: How to avoid degrading of mechanical resistance. *8th Internal Congress on Chemistry of Cement*, (pp. 417-422). Rio de Janeiro.

Viviani, G. a. (2006). System for monitoring the evolution of the thermal expansion coefficent and autogenous deformation of hardening materials. *Smart Materials and Structures*, 137-146.